Exchange of Colloidal Kaolinite between Stream and Sand Bed in a Laboratory Flume

thesis by

Aaron I. Packman

In Partial Fulfillment of the Requirements for the Degree of

Doctor of Philosophy

California Institute of Technology

Pasadena, California

1997

(Submitted May 19, 1997)

Disclaimer

This material is based upon work supported by the National Science Foundation under grants BES-9421491 and BCS-9105965. The Government has certain rights in this material.

Any opinions, findings, conclusions, or recommendations expressed in this publication are those of the author and do not necessarily reflect the views of the National Science Foundation.

Dedication

To my wife, Jennifer, for all your love and support. Thanks for putting up with me.

"Love is not love which alters when it alteration finds,
or bends with the remover to remove:
O no! it is an ever-fixed mark
that looks on tempests and is never shaken."
-Shakespeare

Also to my parents, for making it possible for me to accomplish what I have.

Acknowledgments

Innumerable thanks to Norman Brooks, my advisor, for teaching me just about everything. I will think about you every time I walk by a stream. I hope you enjoy your retirement. Thanks also to Jim Morgan, my co-advisor, for many productive discussions. Thanks to John List, Janet Hering, and Geoff Blake for serving as members of my thesis examining committee, and to Bruce Murray for serving as a member of my candidacy committee. I would also like to thank Menachem Elimelech and Marcelo Garcia for the helpful comments and advice provided during their tenure as visiting professors.

I greatly appreciate the financial support provided for the first three years of my graduate study by the Office of Naval Research through the DOD/NDSEG fellowship program, and the research funding provided by the National Science Foundation through grants BES-9421491 and BCS-9105965.

Thanks to Fran Matzen for making sure everything always ran smoothly, and for being a friend as well. Thanks also to the other support staff in the building, Linda Scott, Andrea Wilson, Carmen Lopez, and Elaine Granger, and the librarians Rayma Harrison and Susan Leising.

Thanks to Tad Fujioka and Nathan Lee for assisting with the laboratory work. Thanks most especially for washing all that sand. Thanks to Rich Eastvedt for providing

excellent support in the lab and for helping clean up all the spills. Thanks to Joe Fontana and Russ Green for able craftsmanship in the construction of laboratory equipment, and to Hai Vu for help with electronic equipment.

Thanks go to many of my fellow graduate students for helping make my stay at Caltech much more pleasant. Thanks especially to Hinrich Eylers and Bruce Nairn for their help in the lab and for many productive discussions. I also greatly appreciate the help with chemical techniques provided by Jeff Noelte and Tom Lloyd, and to Jeff again for allowing the use of some of his unpublished data. On a more personal note, thanks go to Bruce for ice-skating, to Matt Fraser for dim sum, to Susan Paulsen for good cheer, to Andrea Marion and Fabrizio d'Auria for just being Italian, to John Malady for barbecues, to Jeremy Semrau for softball, to Catherine Petroff for being especially nice, and to just about every other EES graduate student for being friendly and generally helpful. Thanks also to some non-Caltech friends, notably Carlos Gordon and J.J. Wolf, for making my weekends more fun and profitable.

Abstract

Experiments were conducted in a recirculating flume to study the exchange of colloids between a stream and sand bed. Observations of the net transport of kaolinite clay from the stream to the bed were used to validate models for colloid exchange which include the hydraulics of water exchange along with the particle-specific effects of filtration and settling.

The flume allowed extensive control of the stream conditions (slope, depth, velocity) and bed parameters (bed depth, bedform height, wavelength, and velocity). All experiments had steady, uniform stream flow and well-developed bedforms. To define the chemistry of the system, the composition of the flume water was controlled, the clay was reproducibly prepared, and the sand was cleaned prior to every experiment.

Experiments involved observing the exchange of both a conservative lithium chloride tracer and the kaolinite tracer. Net exchange was determined by measuring the change of tracer concentration in the stream water. Vertical profiles of the tracer distribution in the bed were also measured.

Column experiments were performed to measure kaolinite filtration by the bed sediment. The pH and ionic strength of both the flume and column water were controlled to vary the extent of filtration.

Two mechanisms are responsible for exchange between the stream and stream bed--an advective pore-water flow driven by bedform-induced pressure variations at the surface of the bed (pumping), and the burial and release of water due to bedform motion

(turnover). Pumping causes kaolinite to be carried deep in the bed where it is trapped due to filtration and settling. Turnover causes continuous mixing of the uppermost portion of the bed which hinders penetration of clay to the deeper bed.

Models incorporating the relevant physical and chemical processes controlling colloid transport were developed to predict the net exchange of kaolinite between the stream and sand bed. Model parameters were nondimensionalized so the models can be applied to problems of any scale. Models for conservative solutes were developed to predict the exchange with a finite bed and exchange due to fast-moving bedforms. Models for colloid transport were developed which are based on the solute transport models, but include the impact of settling on particle flow paths and filtration along path lines. When input data were taken from laboratory experiments, the models generally predicted the flume results well with no calibration. In all flume experiments, filtration and settling of colloids in the bed were sufficiently high so that it could be assumed that all colloid which entered the bed was irreversibly trapped.

Additional model simulations were performed to demonstrate the effect of major input variables on exchange. These simulations cover cases not examined in experiments and provide a sensitivity analysis for the model inputs.

Contents

List of Tables

List of Figures

Notation

a_c	radius of collector particle
a_p	radius of filtered particle
A	Hamaker constant
A_c	surface area of collector grains
A_s	parameter for flow through a packed bed, taken from the Happel model
C	concentration
C*	normalized concentration, $C^* = C/C_0$
C_0	initial concentration
C_{01}	concentration at the start of the main experiment, identical to C_0
C_{02}	concentration at the start of the secondary experiment
C_f	final concentration of conservative tracer in stream after dilution with pore water
C_s	surface concentration of particles, with units of mass/area
d	stream depth
d'	effective stream depth, i.e., the total stream volume (including return pipe, etc.) per unit bed area
d'*	dimensionless effective stream depth, $d'^* = 2\pi k d'/\theta$
d_b	bed depth
d_b^*	dimensionless bed depth, $d_b^* = kd_b$
d_c	diameter of collector particle
D	sand diameter
D_{ms}	depth of maximum scour
d_p	diameter of filtered particle
D_∞	particle diffusion coefficient given by the Stokes-Einstein equation

f	Darcy-Weisbach friction factor, $f = 8(U^*/V)^2$
f_i	relative frequency of occurrence of each bedform size class
F	Froude Number, $F=\frac{V}{\sqrt{gd}}$
g	acceleration due to gravity
h	dynamic pressure head
h_m	amplitude of dynamic pressure head at bed surface
H	bedform height (crest-to-trough)
H_i	height of each bedform size class
I	ionic strength
k	bedform wavenumber ($2\pi/\lambda$)
k	Boltsmann's constant
K	coefficient of permeability of bed sediment
L	column length
m'_{ap}	mass flux through the projected collector area
m'_{at}	rate of attachment to a collector
M	equivalent penetration depth into the bed
M^*	dimensionless equivalent penetration depth, $M^* = 2\pi kM$
M_P	pumping exchange expressed as equivalent penetration depth
M_T	total turnover exchange expressed as equivalent penetration depth
M_{T_a}	additional turnover due to larger-than-average bedforms
M_{T_i}	turnover due to each larger size class
$M\theta C^*$	accumulated mass transfer into the bed
M'_{at}	rate of particle mass attachment per unit volume of bed

N'_c	number of collectors per unit volume of bed
N_{LO}	London-van der Walls number
p	radius of the fluid envelope in the Happel model, $p = (1- \theta)^{1/3}$
q	flux of tracer through the bed surface
q	accumulated particle concentration with units of moles of particles per unit collector mass
$\overline{q}$	average flux of tracer through the bed surface
q*	dimensionless flux of tracer through the bed surface, $q^* = q/kKh_m$
q_p^*	dimensionless downward flux from the currently mixed portion of the bed
Q	flow rate
R	residence time function
R	hydraulic radius of the stream, $R = dw/(w + 2d)$
R	retardation coefficient
$\overline{R}$	flux-weighted average residence time function
s	coordinate along streamline
S	slope of the energy grade line
S	rate of particle lost from the suspension due to filtration
t	time
t*	dimensionless time, $t^* = k^2Kh_mt$
t_0	initial time
t_1	time since the start of the main experiment
t_2	time since the start of the secondary experiment
t_{ms}	time when scour reaches the depth of maximum scour
T	absolute temperature
u	pore-water velocity in x-direction

u^* dimensionless pore-water velocity in x-direction, $u^* = u/u_m$

u_m maximum pore-water velocity, $u_m = kKh_m$

u_u underflow velocity

u_u^* dimensionless underflow velocity, $u_u^* = u_u/u_m$

U approach velocity of particles (D'Arcy)

U^* average shear velocity, $U^* = \sqrt{gRS}$

U_b bedform velocity

U_b^* dimensionless bedform velocity, $U_b^* = \theta u_b/u_m$

v pore-water velocity in y-direction

v^* dimensionless pore-water velocity in y-direction, $v^* = v/u_m$

v_s particle settling velocity

v_s^* dimensionless particle settling velocity, $v_s^* = \theta v_s/u_m$

$\overline{v}^*(y)$ average downward velocity through a horizontal line at the front depth y

V average stream velocity over the cross section of the channel, $V = Q/wd$

V_c volume of collector grains

w channel width

x horizontal coordinate

x^* dimensionless horizontal coordinate, $x^* = kx$

x' adjusted horizontal coordinate, $x' = x - U_b t$

x_0 initial position

y vertical coordinate

y^* dimensionless vertical coordinate, $y^* = ky$

α collision efficiency, the fraction of impacts that result in attachment

α_{exp} collision efficiency determined from experimental results

η	single collector removal efficiency, the fraction of particles approaching a collector which become attached to it
η_{exp}	removal efficiency determined from experimental results
η_0	the fraction of approaching particles that collide with the collector, calculated
η_D	collision due to diffusion
η_G	collision due to settling (gravity)
η_I	collision due to interception
κ	Debye-Hückel parameter
λ	bedform wavelength
λ^*	dimensionless bedform wavelength
λ_f	filtration coefficient
λ_f^*	dimensionless filtration coefficient, $\lambda_f^* = \lambda_f/k$
μ	dynamic viscosity
θ	porosity
ρ	fluid density
ρ_b	bulk density of collector grains (mass/total volume)
ρ_c	density of the collector grains
ρ_p	particle density
τ	relative time, $\tau = t - t_0$
τ^*	dimensionless relative time, $\tau^* = \tau/kKh_m$

1. INTRODUCTION

1.1 General problem of colloid exchange with stream beds

It is important to consider the stream bed when determining the transport and fate of pollutants in stream systems. Bed sediment and pore water represent a significant reservoir for storage of aqueous pollutants in a stream system Exchange of a pollutant between the stream and stream bed results in some fraction of the pollutant being mixed into the bed. This pollutant will later be carried out of the bed back into the stream. Mixing with the bed is thus responsible for the "tailing" of pollutant clouds--the continued transport of small amounts of pollutant for a long time following the passage of the main pollutant cloud. In addition, chemical interactions can result in pollutants being sorbed or otherwise attached to the bed sediment. In this case, the amount of pollutant accumulated in the bed can be far in excess of that expected by simple mixing. When the bed sediment is loaded by pollutant input over a long period of time, the bed may provide a significant source of pollution to the stream even after the exterior pollutant input ceases. Remediation strategies that do not consider the reservoir of pollutant in the bed can significantly underestimate the volume of pollutant in the system and the time required for cleanup.

Previous studies at Caltech have investigated the hydraulics of exchange with sand beds, and the exchange of sorbing solutes (metal ions). This work adds an understanding of the exchange of colloids between the stream and bed. In this context, colloids are simply fine particles: particles with a diameter less than 10 μm are usually considered to be colloids. Colloid transport can have a major effect on pollutant transport

in streams. Colloidal particles have a large reactive surface area which allows them to carry pollutants which would otherwise be transported primarily as dissolved species. Reactive colloids such as clays, iron oxides, and humic substances are ubiquitous in streams. In many systems, colloidal particles will dominate the total surface area available for sorption. In addition, some important pollutants (including arsenic, metals, and radionuclides) have a high affinity for natural particles under conditions commonly encountered in streams. And finally, in some cases the pollutant of interest will actually be present as a colloid (e.g., mine tailings).

Mixing of water between the stream and bed depends on the shape of the bed surface. Sediment transport at the bed surface causes the bed to develop a roughness determined by the hydraulics of the stream flow. This results in the formation of a periodic series of wavy bed features known as bedforms. Bedforms are classified according to their size and shape, with ripples and dunes being most common in sand bed streams. Ripples and dunes have the same shape, featuring a large aspect ratio (length:height on order of 10:1), a sharp crest, and a steep downstream face, but dunes are larger than ripples. In major rivers, dunes can have heights of several meters, and lengths of tens of meters. Other types of bed forms (flat bed, antidunes, etc.) also occur, but they will not be considered in this work. Readers wishing a more in-depth introduction to stream hydraulics, sediment transport, and bed forms are encouraged to consult Raudkivi (1990) and Vanoni (1975).

Bedforms are responsible for two exchange mechanisms which dominate mixing between the stream and bed: pumping and turnover. Pumping is an advective flow of

pore water in the bed driven by the periodic pressure disturbance at the bed surface induced by stream flow over bedforms. Turnover is the trapping of stream water and release of pore water due to bedform propagation downstream. Pumping can occur without turnover in the case where bedforms are developed at a higher flow rate and then the stream velocity drops to the point where sediment transport no longer occurs.

Colloid exchange between the stream and bed is controlled by these hydraulic processes, but is also significantly influenced by other transport processes unique to particles: filtration and settling. Filtration is the attachment of colloids to the considerably-larger stationary sediment grains in flow through porous media. The magnitude of filtration is affected by both hydraulics and chemistry. Particle settling must be accounted for because pore water velocities in the bed are very low. Particles smaller than ~2 μm will not settle, but instead are kept suspended by Brownian motion. These Brownian colloids have a velocity equal to the pore water velocity. Larger, non-Brownian colloids have a velocity in the bed equal to the vector sum of the flow velocity and their settling velocity. All colloids are sufficiently small that they do not settle appreciably in the stream flow.

1.2 The present study

In this study, a 12-meter-long recirculating flume was used to simulate a stream. By recirculating water over a sand bed, bedforms can be developed which are similar to those found in natural streams. The flume was then used to investigate the exchange due to those bedforms. However, the flume is otherwise a quite simplified version of a

natural stream. The flume has a straight, rectangular channel with impermeable walls and bottom. This prevents the investigation of other types of exchange, such as that with the banks, or due to meanders. The flume is tiltable so uniform stream flow can be established. The flume can thus be considered a good surrogate for a straight reach of stream, and conclusions drawn about exchange due to bedforms should be applicable to natural streams when properly scaled.

Both solute and colloid exchange were studied in the flume. Lithium chloride was used as a conservative tracer to determine the hydraulics of bed exchange. Kaolinite clay was used as the colloidal tracer. Kaolinite was selected because it is a very common naturally-occurring colloid, and because it is the simplest type of clay.

Additional experiments were performed outside the flume to investigate colloid behavior that was not directly observable in the flume. Column experiments were used to measure filtration of colloids by the bed sediment used in the flume. The size distribution of the kaolinite particles was also measured.

Because chemical effects influence filtration behavior, the water, sand, and tracers used for flume experiments had to have a defined chemical state. Most experiments were conducted in deionized water with chemicals added to control the composition. The bed sand was cleaned before each experiment to restore it to a defined surface state. And the kaolinite used as a tracer was prepared to be homoionic with a known size distribution.

Models were developed to predict the exchange of colloids due to bedforms. These models are based on earlier models for solute exchange, but include filtration and settling to account for the behavior of particles. These models are presented in

dimensionless form so that they may be appropriately applied to a variety of systems. Nondimensionalization of major variables also provides an easy method of comparison of competing effects.

The exchange models use only measured parameters as inputs, and can be applied to flume results without fitting or calibration. Parameters measured in the flume are used to characterize the exchange hydraulics. The colloid settling velocity is used to account for the difference between particle paths and pore water streamlines. Chemical processes are summarized by the filtration coefficient, measured in column experiments with the same stream water and bed sediment. This parameterization of chemical processes allows the model to be applied to complex natural systems relatively easily.

The literature on bed exchange, sediment transport, colloid filtration, and pollutant transport in streams is reviewed in Chapter 2. As each of these fields are very broad, general references will be given to summarize each field, and only work of special relevance will be discussed in detail.

The theory of the hydraulics and chemistry of the bed exchange of colloids is presented in Chapter 3. Previous models for the exchange of a conservative solute between a stream and stream bed will be reviewed, and new models will be presented for both solute and colloid exchange.

The flume and column experiments performed for this work are described in Chapter 4. All equipment, methods, and materials used in conducting experiments will be discussed.

The results of the experiments are presented in Chapter 5. Flume experiment results for net exchange are presented in dimensionless form along with model predictions. The stream, bedform, and chemical conditions of all experiments are also given. Column experiment results are discussed in the context of the variation of filtration coefficient with various solution properties.

A number of additional model simulations are presented in Chapter 6. These simulations cover a wider range of variables than was investigated in flume experiments. These simulations can be used to predict the behavior of colloids under different conditions, and demonstrate the sensitivity of the modeling results to various input parameters. Another set of simulations is presented for the exchange of iron oxide particles with a sand bed under different chemical conditions. Some additional discussion is also included in Chapter 6: experimental and modeling errors are analyzed, the implications of this work for colloid transport in natural streams are considered, and worthwhile avenues of future research on this topic are discussed.

In Chapter 7, the techniques, experiments, and models of this work are summarized and major conclusions are presented.

There are two appendices presented in Chapter 8. The first shows the variation in the residence time function due to particle filtration and settling. The second is a comparison of the estimation of bedforms parameters by different methods.

1.3 Definition of terms

It is useful to define some terms within the context of the work presented in this thesis. Many of the words defined here are used in different ways by different members of the scientific community (e.g., colloid, dune).

Bed Exchange: exchange of a tracer between the stream and stream bed. Includes both the exchange of *stream water* with *pore water* and interactions involving the *bed sediment*. Exchange is characterized by an *equivalent penetration depth*, M.

Bed Sediment, Bed Material: the particles that make up the bed. In the experiments discussed here, the bed sediment was always Ottawa-30 sand.

Bedform: periodic variation in the elevation of the stream bed surface caused by the interaction between the free-surface flow, sediment transport, and the bed friction. Different shapes of bedform are stable under different flow conditions. See also *dune*, *ripple*.

Colloid, Colloidal Particle: particle with a diameter between 1 nm and 10 μm. Particles with a diameter less than 2 μm are considered Brownian colloids (non-settleable), while those with a diameter greater than 2 μm are non-Brownian, settleable colloids. Overlaps the traditional sedimentology size cut-off distinguishing clay (particles < 4 μm) and silt (> 4 μm).

Depth of maximum scour: the depth which marks the ultimate extent of scour due to sand transport over the course of the experiment. Defines a boundary between regions where sand transport did and did not occur. Approximately equal to half the height of the largest bedform in the system. Defined in relation to the average position of the bed surface. The depth of maximum scour is used to classify the bed into *upper* and *lower* regions.

Dune: the type of bedform normally found in subcritical flow, characterized by a long upstream slope, sharp crest, and a steep downstream face. Dunes are roughly wedge-shaped, or triangular when viewed from the side. When two distinct size classes of these bedforms are present simultaneously, the larger is termed a dune and the smaller is termed a *ripple*.

Equivalent penetration depth (M): measure of the net accumulated exchange of tracer from the stream to the bed. In general, exchange will produce a non-uniform pore water concentration profile in the bed. M is the depth in the bed such that if the stream were well-mixed with the pore water down to M and unmixed below M the calculated accumulated exchange would be equal to the actual exchange. From mass conservation, $C(0)d' = C(t)[d'+\theta M(t)]$ where C(t) is the concentration of tracer in the stream, d' is the total effective stream depth, and θ is the porosity of the bed. In some cases (e.g., exchange of a conservative solute, turnover of colloids) M represents the average

penetration of a front into the bed. In other cases (e.g., exchange of sorbing solutes, pumping of colloids) M is given by the accumulated mass transfer including mass attached to bed sediment grains.

Hyporheic Zone: region of subsurface pore water near a stream that has significant exchange or interaction with stream water. Typically, this includes near-bed pore water, water in the subsurface stream channel, and groundwater in the surrounding aquifer.

Lower Bed: the stable portion of the bed below the region where sediment transport occurs. In this region, *pumping* is the only mechanism of exchange. The boundary between the lower bed and *upper bed* is the *depth of maximum scour*.

Pore water: in the context of a flume experiment, the water that resides in the pore spaces of the sediment bed. At any instant, the pore water is taken to be distinct from the *stream water*.

Pumping: advective flow of *pore water* induced by the pressure variation at the surface of the bed resulting from stream flow over bedforms. A mechanism of exchange between the *stream* and *pore water*.

Ripple: the smaller of two distinct size classes of bedforms of the type normally found in subcritical flow. Also see *dune*.

Stream Water: in the context of a flume experiment, the free-surface flow over the bed (including the water that recirculates through the return pipe). Also called recirculating water. At any instant, the stream water is considered to be distinct from the *pore water*.

Tracer: substance added to the stream water in small concentrations in order to observe exchange with the bed. Each tracer represents a class of substances which have the same exchange behavior. In these experiments, lithium ion was used to examine the exchange of conservative solutes, and kaolinite was used to examine the exchange of colloids.

Turnover: exchange between the *stream* and *pore water* caused by the propagation of *bedforms* due to sediment transport.

Underflow: small flow induced in the stream bed due to the slope of the stream surface.

Upper Bed: the portion of the bed where sediment transport occurs. The zone where exchange occurs due to *turnover* (in addition to pumping). The boundary between the upper bed and *lower bed* is the *depth of maximum scour*.

2. LITERATURE

Bed-exchange of clay colloids in sand-bed streams is an interdisciplinary problem which falls at the intersection of several traditional areas of study. In essence, this problem is an application of ongoing research in the fields of stream hydraulics, sediment transport, colloid filtration, and surface chemistry. As the literature of each of these areas is quite large, only the most directly applicable references will be discussed here, along with some general reviews.

The main body of references deal specifically with laboratory-based studies of bed exchange and colloid transport. Field studies of bed exchange are discussed separately in Section 2.4.

2.1 Bed exchange processes

The hydraulics of bedform-driven exchange has been studied for some time. Essentially, this area of research grew out of the study of the hydraulics of flow over bedforms. However, the implications of these processes for pollutant transport have only been considered for the last 10 to 15 years. As a result, little work has been done on the exchange of reactive tracers.

2.1.1 Hydraulic exchange

In previous work at Caltech, Elliott conducted a comprehensive study of the bed exchange of a conservative tracer (Elliott 1990, Elliott and Brooks 1997ab). His work included experiments on the exchange of dye between a stream and a sand bed in a

recirculating flume, and resulted in the development of models to predict this exchange based on measured hydraulic parameters. Elliott identified the two main mechanisms of bed exchange: advective "pumping," and bedform "turnover." He developed analytical models for these processes, and used numerical integration to calculate the exchange of a conservative tracer. A summary of Elliott's models is presented in Section 3.1.

A number of researchers at Louisiana State University have studied a variety of types of exchange between a sediment bed and overlying water column. Thibodeaux and Boyle (1987) used dye injections to determine the streamlines underneath a gravel bedform. Similar experiments were also performed with sand bedforms. Experimental results were qualitatively compared with streamlines calculated numerically from an assumed pressure distribution (Savant, Reible, and Thibodeaux, 1987). Reible and Savant-Malhiet (1993) compared the magnitude of the exchange across the sediment-water interface due to the mechanisms of diffusion, advection, and sediment transport. This group was also involved in some studies of the diffusive transport of colloids from sediment beds, described below in Section 2.2.2.

The problem of flow over flat gravel beds was considered by Zhou and Mendoza. While they did not specifically examine exchange between the stream and bed, they did show that there is an induced flow in the bed. This work resulted in a D.Sc. thesis (Zhou, 1992) and several papers (Zhou and Mendoza, 1995, 1993; Mendoza and Zhou, 1993). Shimizu, Tsujimoto, and Nakagawa (1990) conducted experiments on the flow induced in a bed of gravel-sized glass beads by a stream. They used salt as a tracer to determine the

flow pattern in the bed and the exchange between the stream and pore water, and analyzed the exchange as a dispersive process.

The models developed in the previous studies are dependent on measurements of the pressure distribution at the bed surface. Vittal, Raju, and Garde (1977) measured the shear and pressure distribution over both smooth and sand-coated triangular bedforms. This data set provided the surface boundary condition for Savant's numerical model. Later, in a Master's thesis, Fehlman (1985) reexamined the problem and contributed a large amount of new data for shear, pressure, and velocity distributions over smooth and rough triangular bedforms. Some of this data also appears in Shen, Fehlman, and Mendoza (1990), along with additional analysis of the drag due to bedforms. Elliott suggests that the pressure disturbance at the bed surface is well-approximated by a sinusoid with an amplitude given by Fehlman's empirical prediction (Elliott 1990, Elliott and Brooks 1997ab). This is the approach taken here, as discussed in Section 3.1.

2.1.2 Exchange of reactive solutes

In a Ph.D. thesis at Caltech, Eylers studied the bedform-induced exchange of metal ions between a stream and sand stream bed in a recirculating flume (Eylers 1994; Eylers, Brooks, and Morgan 1995). By using ICP-MS for analysis, Eylers was able to measure the simultaneous transport of a conservative lithium ion tracer and several different reactive metal ions (zinc, magnesium, calcium, and copper). To ensure reproducibility, the water chemistry was controlled and the sand was acid-washed between experiments.

Eylers successfully modeled the transport of all species by using Elliott's models of hydraulic exchange along with some additional terms to account for sorption of the metal ions to the sand. The slow rate of transport in the bed meant that only equilibrium sorption had to be considered. The exchange of the different metals could then be predicted by Elliott's models with a time scale reduced by the retardation coefficient. Batch sorption experiments were used to provide input values for the model of metal ion bed-exchange. Eylers' work demonstrated that it is possible to model the exchange of reactive solutes based on a combination of hydraulic parameters measured in the flume and chemical parameters obtained from standard chemistry experiments conducted at a smaller scale.

2.2 Transport of colloidal particles in stream systems

2.2.1 Transport downstream

The transport of fine particles in streams has been studied in the context of downstream sediment transport. Colloids are considered to be part of the "wash load"--particles that do not settle appreciably in the stream flow and are thus transported entirely as suspended load. For a discussion of wash load, see Raudkivi (1990).

2.2.2 Exchange with sediment beds

Einstein (1968) studied the exchange of crushed silica (3.5-30 μm diameter) with a gravel bed in a recirculating flume. The purpose of this paper was to predict the deposition regions for fine particles in the bed, in order to design salmon spawning

grounds. Bedforms were not mentioned, so presumably all experiments were done with a flat bed. Einstein determined that settling was responsible for transport into and through the bed. Advective flows through the bed were not considered; in fact, Einstein qualitatively reports that the fine particles were not observed to move either horizontally or upwards in the bed. However, little deposition was observed for small bed depths (1 and 2 inches), indicating that there probably was an advective flow which dominated the particle motion in the upper portion of the bed, but which was insignificant in the deeper portions of the bed. Chemistry was not considered, but was probably unimportant due to the relatively large size of both the fine particles and bed grains.

Some studies of the release of organic colloids from sediment beds were conducted at Louisiana State University (Valsaraj et al., 1993, 1996). These experiments involved slowly pumping water over a flat bed of lake sediment. Adjusting the ionic strength of the pore water resulted in different rates of flux out of the bed. This work was done in conjunction with studies of colloid-mediated pollutant transport (for example, Sojitra et al., 1994).

A recent study by Huettel, Ziebis, and Forster (1996) examined the transport of pigment colloids into sand bedforms in a recirculating flume. The application of this work is the exchange of particulate organic matter with sea beds. By using colored pigment particles as colloid tracers and dyes as solute tracers, excellent photographs showing the exchange were obtained. In addition, slicing of the bed was used to produce detailed three-dimensional maps of tracer intrusion. Solute streamlines were modeled using potential-flow theory with appropriate sources and sinks. This model is in essence

similar to that of Elliott, but is not developed as fully. This work was apparently done in without knowledge of the work of Elliott and the pressure distributions of Fehlman and Vittal et al. Particle intrusion zones were noted, and the increase in exchange due to the bedforms was discussed but not modeled. The chemistry of the system was not controlled, making particle filtration difficult to interpret.

2.3 Colloid filtration (deep-bed filtration of colloids by porous media)

Filtration of colloids by porous media has a large body of literature. A good review of filtration concepts and the range of filtration problems is given by McDowell-Boyer, Hunt, and Sitar (1986). A more recent review by Ryan and Elimelech (1996) discusses colloid mobilization and transport, the success and failure of filtration models, and the potential for colloid-facilitated contaminant transport in groundwater.

Filtration theory and modeling are the subject of several books. Elimelech et al. (1995) was used as the primary reference for colloid transport in porous media, particle-particle interactions, modeling of filtration, and filtration experiment techniques. Tien (1989) also presents models for filtration behavior as well as additional information on micro-scale transport models.

Solution and surface chemistry greatly influence the filtration behavior of colloids. Stumm and Morgan (1996) is a good reference for these chemical phenomena. Especially relevant are Chapter 9 on the solid-solution interface and Chapter 14 on particle-particle interactions. The additional discussion and examples in Stumm (1992)

are also valuable. Additional reviews of the chemistry and environmental applications of particle-particle interactions were done by O'Melia (1987, 1989).

Most filtration studies are done with colloids small enough so that Brownian motion is sufficient to suspend the particles. Tobiason and O'Melia (1988) discuss the motion of non-Brownian colloids through porous media, derive filtration theory for non-Brownian particles, and present experimental results on the filtration of 4 and 12 μm polystyrene latex particles. Tobiason (1989) also conducted additional experiments to determine the effect of calcium concentration on filtration of these particles.

Litton and Olson (1993) conducted a study of the impact of filter media preparation procedures on filtration. They found that cleaning with strong acid (HCl) did not remove all surface contaminants. A combination of washing in strong acid and aggressive oxidation by combustion or chromic acid removed more contaminants and resulted in decreased filtration.

2.4 Kaolinite properties and filtration behavior

Filtration behavior of kaolinite is interpreted in terms of its structure, composition, and surface chemistry. The classic book of van Olphen (1977) provides an excellent introduction into the properties and behavior of kaolinite and other clays. The compilation Chemistry of Clays and Clay Minerals (Newman, 1987) presents a large amount of data on and analysis of clay properties.

The surface charge of clay is relatively complicated because of its structure and composition. Many studies have addressed the relationship between changes in solution

properties and changes in the properties of the kaolinite surface and the behavior of kaolinite suspensions. Hunter and Alexander (1963abc) examined the effects of ionic strength, pH, and anion adsorption on the electrophoretic mobility of kaolinite. Rand and Melton (1977) studied the change in particle-particle interaction behavior of kaolinite due to changes in pH and ionic strength. They also examined the differences in surface properties of several different kaolinites and the impact of interaction behavior on packing (Melton and Rand, 1977ab). Stumm (1992) presents an example of kaolinite surface charge based on the charge of edge and face sites. Herrington, Clarke, and Watts (1992) measured the change of surface charge vs pH for several kaolinites, and interpret their results in terms of the charge of edge and face sites. Hunter and James (1992) observed the change in kaolinite surface charge due to sorption of various metal ions. Brady, Cygan, and Nagy (1996) modeled kaolinite surface charge based on the properties of edge and face sites.

Filtration of kaolinite has not been studied extensively because its surface charge is relatively complicated. Ives (1987) gave a theoretical discussion of the filtration of clay by sand. Yoshimura (1980) conducted a number of experiments on the filtration of kaolinite by both glass beads and sand, but most of his results are only available in Japanese. Some of Yoshimura's data on kaolinite are reprinted in Tien (1989, Figures 7-17 through 7-19). These data show filtration coefficients varying from around 0.02 to 1 cm^{-1}. The filtration coefficient was found to vary positively with the diameter of the clay particles, and inversely with the diameter of the sand grains and the flow velocity.

2.5 Field applications

Much more work has been done on bed exchange in the field than in the laboratory. In particular, the USGS has an ongoing program of research on the transport of reactive solutes in streams and the connections between hyporheic flow and in-stream processes. These studies represent the direct application of the work of this thesis.

Avanzino et al. (1984) is a USGS report which describes the results of a solute transport experiment at Uvas Creek. Several additional papers present analysis of this data set. Transport of conservative solutes was modeled using a transient storage model which includes the effect of low-flow dead zones (Bencala and Walters, 1983). Additional modeling was presented in Jackman et al., 1984, and Kennedy et al., 1984. The transport of reactive solutes (strontium, potassium) was modeled using the transient storage model with kinetic sorption effects included (Bencala, 1983, Bencala et al., 1983). This model was applied to another experiment on the transport of chloride and several cations (Bencala et al., 1984, Bencala, 1984). Data for solute exchange with the subsurface of this experiment are available in Zellwegger et al. (1986).

These models have been further refined to include more fundamental descriptions of the hydraulic and chemical processes that control solute transport. Additional experiments have also been performed in a variety of small streams and rivers in order to provide data sets for model verification. Bencala, McKnight, and Zellweger (1990) describe experiments on solute transport in a stream, use of a lithium tracer to characterize transport processes, and the application of the knowledge of these processes to model transport of other solutes. McKnight and Bencala (1990) analyzed watershed

and in-stream processes (including bed exchange) that control the chemistry of iron, aluminum, and DOC. Harvey and Bencala (1993) present experimental results on exchange between the stream and hyporheic zone, and compare them with numerical simulations that include exchange due to bed topography.

More recent work has been directed at developing better models which can be used to simulate the exchange of tracers with complicated chemical behavior. Harvey, Wagner, and Bencala (1996) provide a comparison of sub-reach-scale estimates and reach-scale tracer experiments in predicting hyporheic exchange. Runkel, Bencala, Broshears, and Chapra (1996) present a model for transport of reactive solutes that includes stream hydrodynamics and equilibrium chemistry (complexation, precipitation, sorption). Runkel, McKnight, Bencala, and Chapra (1996) apply this equilibrium-chemistry model to the results of an experiment which investigated the change in iron concentration due to modification of the stream pH. Broshears, et al. (1996) examined the importance of kinetic processes for pH, aluminum, and iron.

Other researchers have also examined exchange processes. Castro and Hornberger (1991) studied exchange between a stream, gravel bed, and larger alluvial aquifer. They conducted experiments with conservative solutes and used a fitted model with a residence time function for bed exchange.

Relatively little field work has been done on the exchange of fine particles with stream beds. Jobson and Carey (1989) discussed the need for more knowledge of fine sediment transport in streams. Cushing, Minshall, and Newbold (1993) conducted experiments on the transport of radiolabeled natural particulate organic matter (50 - 100

μm) in streams. The observed continual exchange with surficial bed sediments in the process of downstream transport. Experimental results were modeled by adding settling to the behavior of a conservative tracer.

An overview of the models described above can be found in the review "Modeling within the stream-catchment continuum" (Bencala, et al., 1993). An upcoming book edited by J.B. Jones and P.J. Mulholland will review the consequences of exchange with the subsurface for stream biogeochemistry and ecology.

3. THEORY

Three aspects of this work will be considered theoretically. First, the exchange of conservative tracers between the stream and stream bed is the starting place for all related transport studies. Theory for the fundamental hydraulic exchange will be presented in Section 3.1. Second, in Section 3.2, the theory that describes colloidal transport processes in porous media is applied to transport through the stream bed. And, finally, these two independently-derived theoretical frameworks will be synthesized in Section 3.3 into a model for colloid exchange with the bed.

The bed-exchange models presented in this work and those developed by Elliott and Eylers are listed in Table 3.1. Each new model will be described in detail in this chapter. Model predictions will be compared with the results of flume experiments in Chapter 5, and additional model simulations are presented in Chapter 6.

Table 3.1: Models for bed exchange

Model Name	Source	Hydraulic Conditions	Tracer(s)
Infinite bed pumping	Elliott (1990)	deep bed, stationary bedforms	conservative solutes
Turnover	Elliott (1990)	fast-moving bedforms	conservative solutes
Combined	Elliott (1990)	slowly-moving bedforms	conservative solutes
Pumping with sorption	Eylers (1994)	deep bed, stationary bedforms	reactive solutes with fast sorption
Finite bed pumping	this work	stationary bedforms	conservative solutes
Colloid pumping	this work	stationary bedforms	colloids
Maxpump	this work	stationary bedforms	tracers that are completely trapped
Turnpump	this work	fast-moving bedforms	conservative solutes
Turnpump for colloids	this work	fast-moving bedforms	colloids that are completely trapped

3.1 Bed exchange hydraulics

In sand-bed streams, bedforms such as dunes and ripples at the sediment-water interface result in interfacial mass transfer far in excess of diffusion. As noted previously in the literature review of Section 2, this problem was first modeled successfully by Elliott (1990). The essential parts of Elliott's model for exchange of conservative solutes will be presented here; readers wishing more detail should consult his work. Additional theory for solute transport added in this thesis will be explicitly discussed. The extension of this theory for colloid exchange will be presented in Section 3.3.

Typically, streams will have a bed geometry with roughness elements much larger than the bed sediment size. These features are known as bedforms. Stream flow over an unconsolidated sediment bed results in sediment transport which produces bedforms with an appropriate roughness. Steady, uniform stream flow leads to a periodic series of bedforms whose average geometric parameters do not change in time. In addition, for a straight section of stream, bedforms are generally two-dimensional as well. These conditions always holds in our flume experiments, and thus the theory presented here is initially developed for transport to a single, two-dimensional bedform. The extension of this bedform-scale model to a reach which contains multiple bedforms is very straightforward. The application of the theory presented here to experimental results is contained in Section 5.

There are two mechanisms responsible for hydraulic exchange between a stream and its bed. 'Pumping' is an advective flow through the bed induced by the stream flow over the porous bedforms. Pumping is the main mechanism that drives exchange with

deeper portions of the bed. 'Turnover' is the trapping and release of pore water due to bedform movement. Turnover can be very rapid, but is limited to the upper layer of the bed, down to the maximum scour depth.

In the following analysis, these two exchange mechanisms will first be considered independently, and then the general case of combined pumping and turnover will be considered.

3.1.1 Pumping exchange

The flow of a fluid around an object results in a pressure disturbance at the surface of the object. Where that object is porous, the pressure disturbance causes flow through the object. In this manner, flow over bedforms can induce flow through the bedforms and the bed that lies beneath them. This is the exchange mechanism that we have termed 'pumping.' Pumping will occur whenever there are bedforms of a significant size, without regard to the rate of sediment transport. For the following analysis, it is assumed that no sediment transport occurs, and the bedforms are stationary. As in natural streams, a dune can be a residual feature formed at a higher flow rate. The effect of moving bedforms on pumping will be discussed in Sections 3.1.3 and 3.1.4.

3.1.1.1 Elliott's infinite bed pumping model

Elliott noted that, fortuitously, the pressure distribution over the most common bedform (the dune) can be closely approximated by a sine function, making the flow

through the bed easy to solve analytically. Figures 3.1 and 3.2 show a typical dune, and Fehlman's measurements of the pressure distribution over an artificial dune.

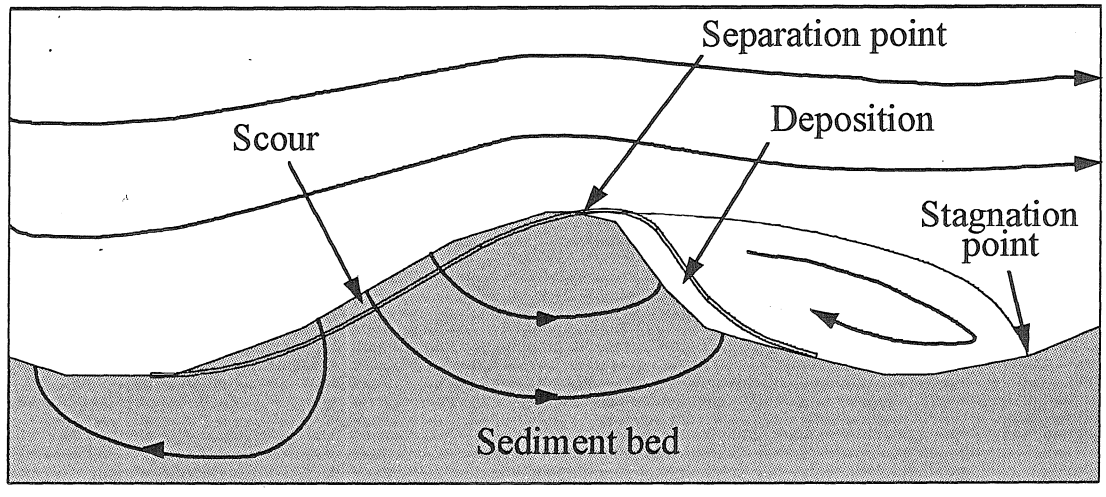

Figure 3.1: Side view of a dune, with flow pattern over and through the bedform. This drawing is exaggerated in the vertical direction for clarity; dunes typically have a wavelength-to-height aspect ratio of greater than 10:1.

Expressing the pressure distribution as head and approximating it with a sinusoid yields:

$$h = h_m \sin(kx) \tag{3.1}$$

Fehlman also developed the following empirical estimate of the maximum head (h_m):

$$h_m = 0.28\frac{u^2}{2g}\begin{cases}\left(\dfrac{H/d}{0.34}\right)^{3/8} & H/d \le 0.34 \\ \left(\dfrac{H/d}{0.34}\right)^{3/2} & H/d \ge 0.34\end{cases} \tag{3.2}$$

Note that Equation 3.1 is the pressure distribution at the surface of the bed. What we really wish to know is the flux into and out of the bed that results from this pressure distribution at the surface. Elliott further simplified the analysis by applying this pressure distribution over a flat surface, as opposed to one with bedforms. This is a good

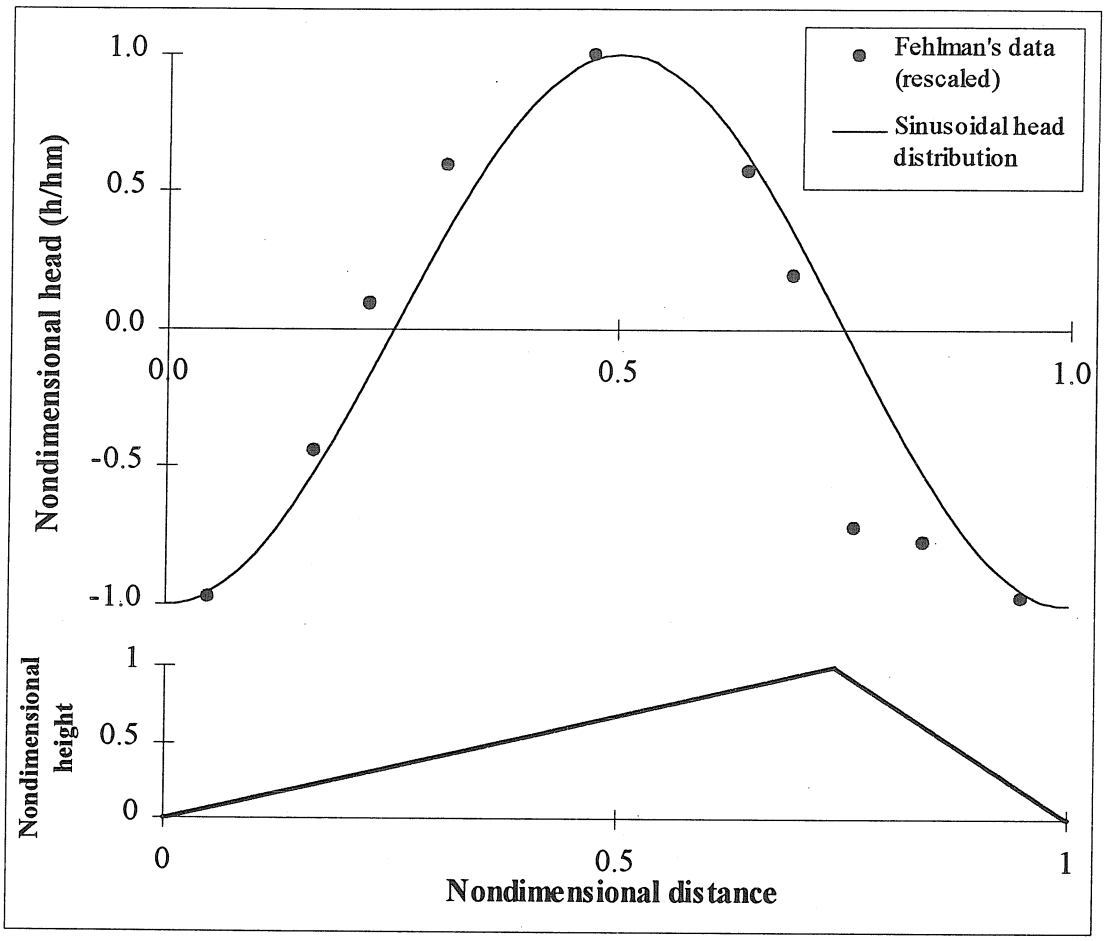

Figure 3.2: Comparison of the measured pressure distribution over an artificial dune-shaped bedform and a sinusoidal profile.

assumption because the bedform height is much smaller than the bed depth, so that the solution will still be the same over most of the domain. In this case, by solving Laplace's equation with this pressure distribution at the bed surface and an infinitely deep bed, and then applying D'arcy's law, the following velocity profile can be obtained for flow in the bed:

$$u = -kKh_m \cos(kx)\, e^{ky} \tag{3.3}$$

$$v = -kKh_m \sin(kx)\, e^{ky} \tag{3.4}$$

The streamlines resulting from this velocity distribution are shown in Figure 3.3, at the end of this section.

The velocity profile can be nondimensionalized by using scales related to the bedform geometry:

$$x^* = kx \tag{3.5}$$

$$y^* = ky \tag{3.6}$$

$$u^* = u/kKh_m = u/u_m \tag{3.7}$$

$$v^* = u/kKh_m = v/u_m \tag{3.8}$$

$$t^*/\theta = k^2Kh_mt/\theta = ku_mt/\theta \tag{3.9}$$

Note that t^* is based on time to travel a distance $1/k$. Also, t^* appears with θ because velocities are calculated as D'arcy velocities, which requires a factor of $1/\theta$ to yield the actual pore water velocities.

The normalized velocity profiles are

$$u^* = -\cos x^* \, e^{y^*} \tag{3.10}$$

$$v^* = -\sin x^* \, e^{y^*} \tag{3.11}$$

Underflow due to the stream slope may simply be superimposed on the above velocity distribution. The underflow velocity occurs in the x-direction and is given by

$$u_u = KS \tag{3.12}$$

The velocity distribution in the bed will then be given by

$$u = u_{pumping} + u_u \tag{3.13}$$

$$v = v_{pumping} \tag{3.14}$$

Underflow tends to reduce exchange by carrying downward-moving parcels of fluid horizontally to regions where the pumping velocity is upward. The net effect of this is a deflection of the pumping streamlines horizontally and upwards. Underflow is also nondimensionalized by the maximum pumping velocity

$$u_u^* = u_u/u_m \tag{3.15}$$

u_u^* typically has a value between 0.03 and 0.10. Elliott showed that, with an infinite bed, underflow tends to be insignificant at short times, but bounds the pumping exchange at long times by limiting the ultimate penetration into the bed.

3.1.1.2 Finite bed pumping model

While the infinite-bed assumption was adequate for modeling of Elliott's experimental setup, it does not apply to the current experiments. Elliott's flume had a depth of 50 cm, so that the ratio of bed depth to bedform wavelength was generally greater than one. However, the flume used for the colloid transport experiments only had a depth of 24.5 cm, so that all experiments had a bed depth less than one-half the bedform wavelength. Thus, it was necessary to rederive the velocity profile with an impenetrable bottom boundary condition. In this case, the simple exponential decay term becomes expanded into hyperbolic functions dependent on the bed depth:

$$u = - kKh_m \cos(kx) \{\tanh(kd_b)\sinh(ky) + \cosh(ky)\} \tag{3.16}$$

$$v = - kKh_m \sin(kx) \{\tanh(kd_b)\cosh(ky) + \sinh(ky)\} \tag{3.17}$$

Note that d_b is the depth of the bed, a positive number, whereas y is always negative in the bed. The streamlines for this velocity distribution are shown in Figure 3.4.

Underflow can be included in this velocity distribution exactly as it was for the infinite bed case, by adding u_u to the right side of Equation 3.16. However, underflow will generally not have a significant effect in the finite bed case because the impenetrable bed bottom tends to control the exchange. (For proof of this, see Figure 6.3 and the accompanying discussion in Chapter 6.)

The finite bed velocity profile is nondimensionalized exactly as for the infinite bed case, with

$$d_b^* = kd_b \tag{3.18}$$

resulting in

$$u^* = -\cos x^* (\tanh d_b^* \sinh y^* + \cosh y^*) \tag{3.19}$$

$$v^* = -\sin x^* (\tanh d_b^* \cosh y^* + \sinh y^*) \tag{3.20}$$

3.1.1.3 Pumping mass transfer

The velocity profile, and some geometric information about the larger stream system, is all that is needed to predict the pumping exchange of a conservative tracer with the stream bed. However, this calculation is not straightforward. To predict the disappearance of a tracer into the stream bed, it is necessary to integrate the flux over time while taking into account the previous penetration into the bed. To address this, Elliott used the residence time function.

The residence time function, $R(t,t_0,x_0)$, is the fraction of tracer that entered the bed at time t_0 and position x_0 which remains in the bed at a later time t. Often the residence time function will be constant with time, and thus independent of the time the tracer

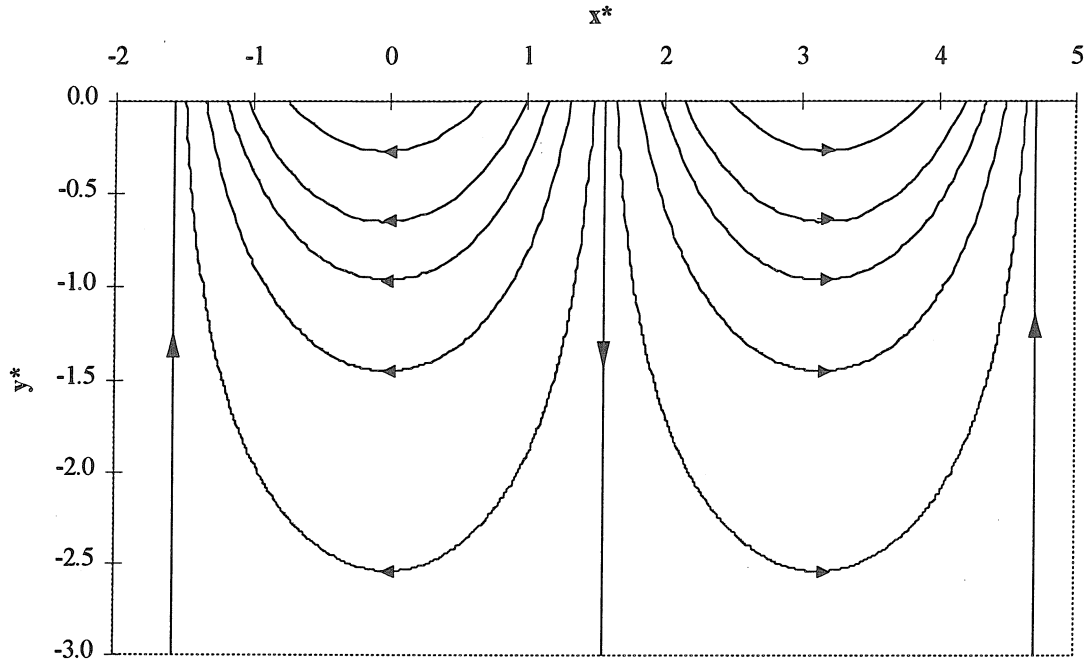

Figure 3.3: Streamlines for pumping into an infinite bed. Note that the scale is exaggerated in the y-direction. After Elliott, 1990.

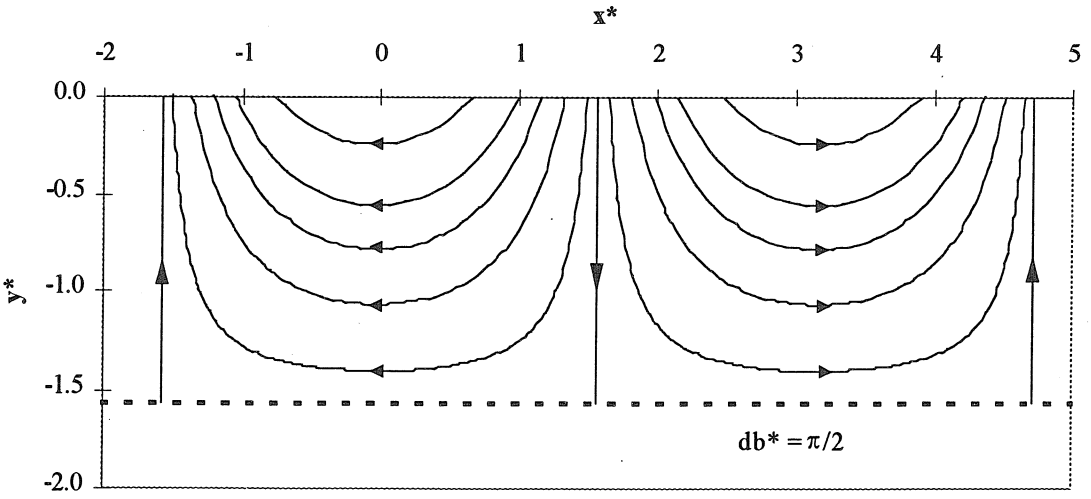

Figure 3.4: Streamlines for pumping into a finite bed of depth $d_b = \lambda/4$, $d_b^* = \pi/2$. Distortion in the y-direction is the same as Figure 3.3.

entered the bed, t_0. This is always the case in the flume experiments due to the steady, uniform stream flow and fully-developed bedforms. In this case, R is only a function of x_0 and $\tau = t - t_0$, the time that has elapsed since the particles entered the bed. R must be modified to account for the nonuniform flux of tracer through the bed surface, q(x), and then normalized by the average flux, $\bar{q}$. The flux-weighted average residence time function, $\bar{R}$, is given by:

$$\bar{R}(\tau)=\frac{\overline{qR_f}}{\bar{q}}=\frac{\frac{1}{\lambda}\int_{x=0}^{x=\lambda} q(x)R(\tau,x)\,dx}{\bar{q}} \tag{3.21}$$

Both R and q are easily determined from the pore-water velocity distribution.

$\bar{R}$ is integrated in time to give the accumulated mass transfer. Mass transfer will be expressed by M, the equivalent penetration depth into the bed. The definitions of M and other modeling parameters are presented in Figure 3.5. Use of the penetration depth makes it easier to compare mass transfer for pumping and turnover. The actual accumulated mass per unit bed area is given by $M\theta C_0$. Use of the penetration depth for mass transfer also leads to use of the normalized concentration

$$C^* = C/C_0 \tag{3.22}$$

For transport to the bed (the tracer is initially well-mixed in the stream, but not present in the bed, so $C^* = 1$, $C_{bed} = 0$ initially), the penetration depth is given by

$$M(t)=\frac{\bar{q}}{\theta}\int_{\tau=0}^{t}\bar{R}(\tau)C^*(t-\tau)d\tau \tag{3.23}$$

Mass transfer is normalized according to

$$M^* = 2\pi k M \tag{3.24}$$

The 2π is not required, but is included to follow Elliott's nondimensionalization. Note however, that M is different from Elliott's by a factor of θ. This was done to make M, rather than M/θ, equal to the equivalent penetration depth.

The mass transfer is then represented by the dimensionless penetration:

$$M^* = 2\pi \bar{q}^* \int_0^{t^*/\theta} \bar{R}^*\left(\frac{\tau^*}{\theta}\right) C^*\left(\frac{t^*}{\theta} - \frac{\tau^*}{\theta}\right) d\left(\frac{\tau^*}{\theta}\right) \tag{3.25}$$

where $q^* = q/kKh_m$ and $t^* = k^2Kh_m t$.

The change in concentration is also related to the mass transfer by the geometry of the system. In the flume, there is a reservoir of tracer in the recirculating stream which is depleted due to exchange with the bed. For the case of transport to the bed, the total mass of tracer in the flume is given by $C_0 d'$, where d' is the effective depth, the total stream volume (including return pipe, etc.) per unit bed area. Exchange with the bed is then related to the stream concentration by

$$C^* = \frac{d'}{d' + M\theta} \tag{3.26}$$

Using dimensionless variables, this is

$$C^* = \frac{d'^*}{d'^* + M^*} \tag{3.27}$$

with d' nondimensionalized as

$$d'^* = \frac{2\pi k d'}{\theta} \tag{3.28}$$

and M^* as

$$M^* = 2\pi kM \tag{3.29}$$

Alternatively, the θ from the nondimensionalization of d'* could be dropped, in which case M*θ would appear in Equation 3.27 (just as Mθ appears in Equation 3.26). Note that Elliott chose to nondimensionalize both M and d' in the same way, using 2πk/θ, so that θ never appears in his equations for C*. In Elliott's formulation, the accumulated exchange is given by M(t)C(t) and the equivalent penetration depth is given by M/θ. In this thesis, θ has been included in Equation 3.24 making M the penetration depth and M(t)θC(t) the total exchange.

The actual calculation of M(t) and C*(t) is done by numerical integration. Again, the pore water velocity distribution is used to determine the surface flux and residence time function.

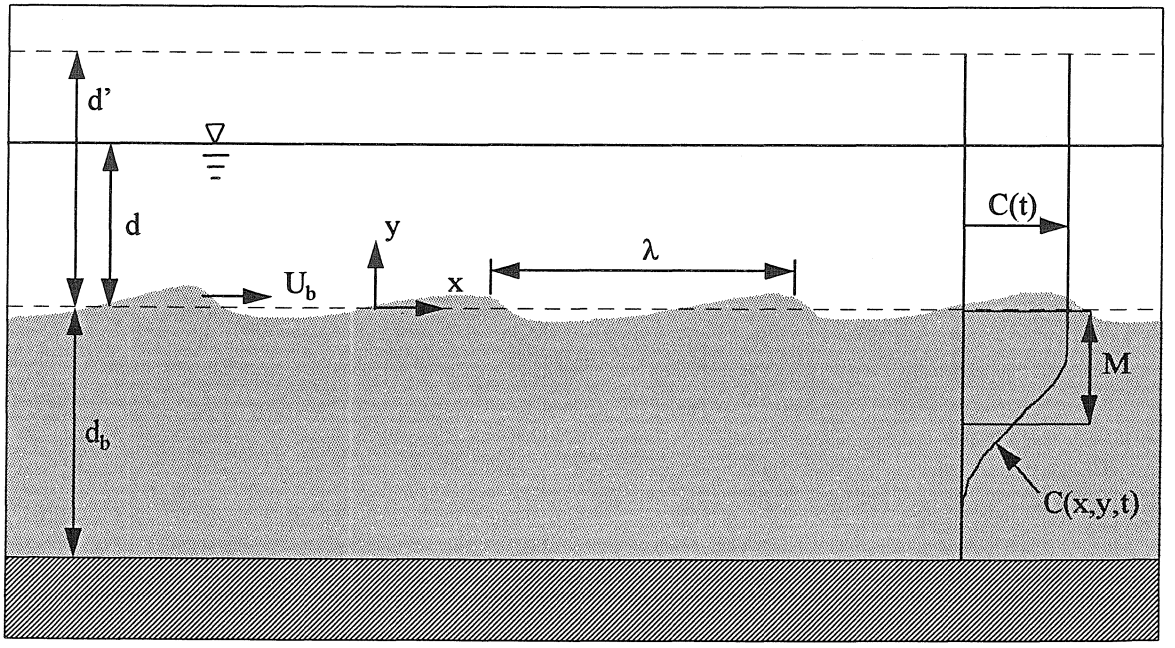

Figure 3.5: Definition of variables for exchange models.

3.1.2 Turnover exchange

Transport of the bed sediment causes the development of bedforms. In the case of dunes, the bedform shape is maintained by bed-load sediment motion along the upstream side of the dune, and deposition at the downstream face. Consequently, there is a net motion of the bedform downstream and a corresponding exchange of pore water, as shown in Figure 3.6.

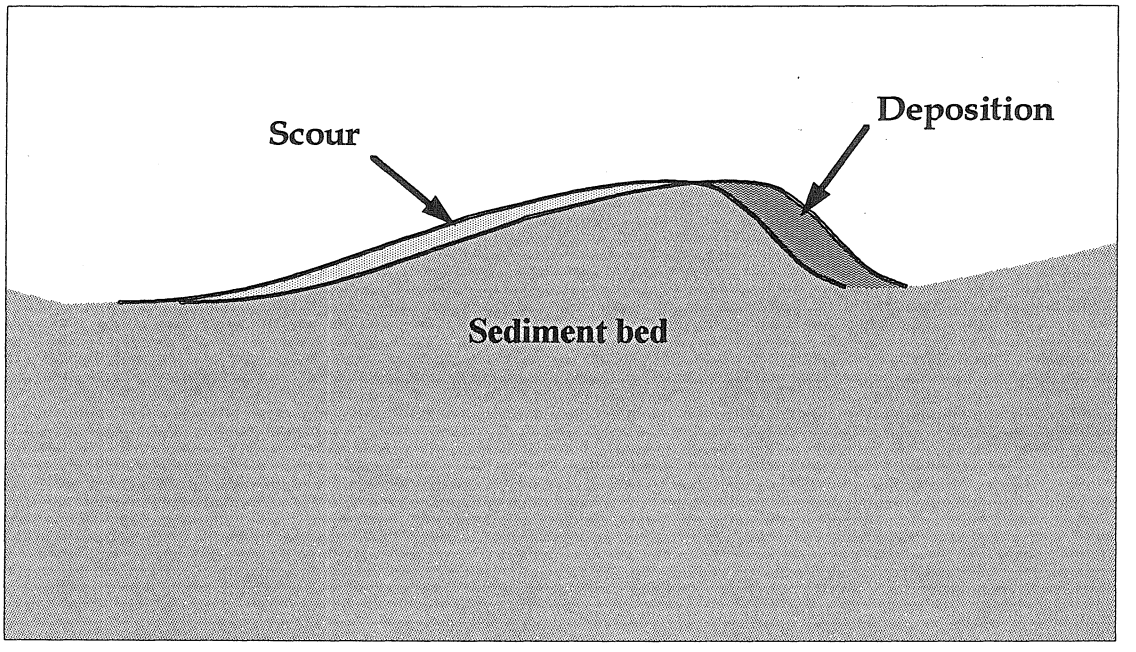

Figure 3.6: Bedform turnover.

Calculating the exchange due to turnover is very straightforward. Since the extent of exchange is directly proportional to the cross-sectional area of the bed that is scoured or newly-deposited, the rate of volumetric exchange can be determined geometrically. The transport of a conservative tracer from the stream to an uncontaminated bed is

conveniently expressed as an equivalent penetration depth (M). The motion of a regular, triangular bedform with velocity U_b (as shown in Figure 3.6) results in a mean penetration of:

$$M=\begin{cases}\frac{H}{2}\left(1-\left(1-\frac{U_b t}{\lambda}\right)^2\right) & \text{for } t<\frac{\lambda}{U_b} \\ \frac{H}{2} & \text{for } t\geq\frac{\lambda}{U_b}\end{cases} \tag{3.30}$$

Note that turnover can only cause exchange down to the maximum scour depth, H/2.

For a perfectly regular series of bedforms, the maximum scour depth is the same for all bedforms. However, in reality there will be some distribution of bedform shapes under any given flow conditions. Elliott developed solutions for the mass exchange for a given distribution of bedform heights (e.g., gaussian). However, in general it is not necessary to use this level of modeling detail because turnover will almost always be only a small fraction of the overall transport (for proof of this, see Section 3.1.3 on Combined Pumping and Turnover).

In the present study, the simple relation given in Equation 3.30 was typically used with only the average bedform parameters. However, a correction had to be introduced when there was a considerable difference between the height of the average and largest bedform. In other words, the bedform size distribution had to be accounted for when the distribution was wide. This correction involves including the additional turnover responsible for mixing between the average scour depth and the maximum scour depth. It is quite important to include turnover down to the maximum scour depth, since this

defines the limit of turnover at long times. However, it is not as important to know the exact rate of turnover between the average and maximum values. Indeed, it is impossible to develop a deterministic expression for this additional turnover since bedform production has a probabilistic character and bedforms are randomly distributed to begin with.

To analyze this case, a simple model was developed which includes the basic elements of exchange due to larger bedforms. This model will correctly compute the ultimate turnover due to the larger bedforms, but only approximates the actual time-dependent exchange. Two to four size classes were arbitrarily determined from the experimental data set, with each size class given a corresponding height, H_i ,and relative frequency of occurrence, f_i. All bedforms are assumed to have the same wavelength and velocity. The exchange due to average-sized bedforms is still calculated with Equation 3.30. Exchange due to bedforms in larger size classes is assumed to occur over a time scale inversely proportional to the frequency of occurrence of each size. This is a simple attempt to account for the fact that the larger bedforms will tend to appear at later times. The turnover exchange due to the larger bedforms is given geometrically by rectangular strips of height $\Delta H/2$, where ΔH is the difference in height between successive size classes. The total turnover is given by the average parameters for $t < \lambda/U_b$ (by Equation 3.30), and then by

$$M_T(t) = \frac{H}{2} + \sum M_{T_i}(t) \quad \text{for } t > \frac{\lambda}{U_b} \tag{3.31}$$

where M_{T_i} is the turnover due to each larger size class, given by:

$$M_{T_i}(t)=\begin{cases}\dfrac{(H_i-H_{i-1})}{2}f_i\left(\dfrac{U_b t}{\lambda}-1\right) & \text{for } t<\dfrac{\lambda}{f_i U_b}+\dfrac{\lambda}{U_b}\\[2ex] \dfrac{(H_i-H_{i-1})}{2} & \text{for } t\geq\dfrac{\lambda}{f_i U_b}+\dfrac{\lambda}{U_b}\end{cases} \tag{3.32}$$

$H_{i=0}$ represents the average height, H. The total additional turnover exchange is just the sum of the exchange from all the size classes. A sample calculation is shown in Figure 3.7.

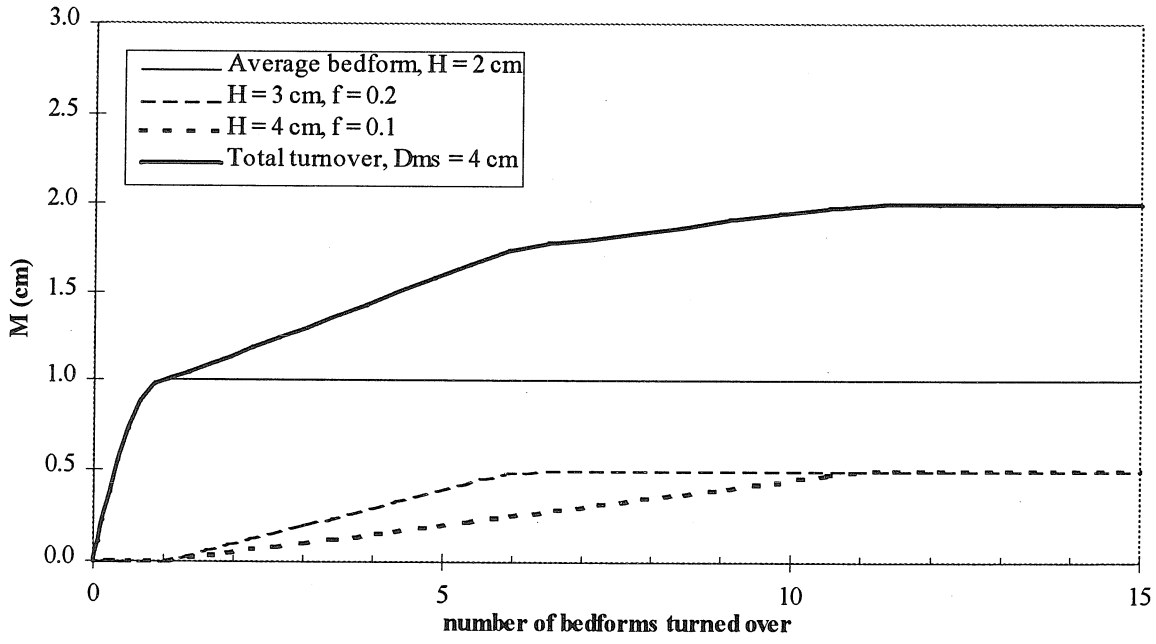

Figure 3.7: Exchange due to turnover of bedforms of size classes H_{avg} = 2 cm, H_2 = 3 cm, H_3 = 4 cm, with frequencies f_1 = 0.7, f_2 = 0.2, f_3 = 0.1. The total turnover is the sum of the turnover due to each size class.

3.1.3 Elliott's model for combined pumping and turnover

In the general case, both pumping and turnover will occur at the same time. The previously described models for pure pumping and pure turnover are used as a base for models of the combined case. Elliott used the nondimensional turnover velocity (U_b^*) to predict ranges where turnover and pumping are dominant.

$$U_b^* = \theta U_b / u_m \tag{3.33}$$

The θ appears because u_m is calculated as a D'Arcy velocity. Elliott considered cases with $U_b^* << 1$ to be pumping dominated, $U_b^* >> 1$ to be turnover dominated, and $U_b^* \sim 1$ to be combined. For the dominated cases, Elliott then used only the applicable 'pure' model to predict the exchange.

For the combined case, Elliott used a modified pumping model, in which the bed motion is included by taking a Lagrangian framework that follows the moving bedforms. Effectively, this superimposes the bed and pumping velocities so that

$$u^* = u_{pumping}^* + u_u^* - U_b^* \tag{3.34}$$

$$v^* = v_{pumping}^* \tag{3.35}$$

The net exchange is then calculated as for the pure pumping model.

This modeling framework (including the pumping model, turnover model, and combined model) yields good predictions for pure pumping cases, but greatly underestimates the exchange for pure turnover cases. Combined exchange is predicted well at short times, but is underpredicted at later times.

Elliott's pure turnover model greatly underpredicts exchange because it does not account for the fact that turnover only occurs in a thin layer at the top of the bed, and that

pumping to the deeper bed will always be an important exchange mechanism. Turnover can only be the dominant exchange mechanism at relatively short times, until the entire turnover zone has been mixed. At later times, even a small amount of pumping to the deeper bed will be a significant exchange mechanism. Thus, there is really no 'pure turnover' case. (Exception: there can obviously be pure turnover if the bed is very shallow such that practically the entire bed is scoured.)

Elliott's combined model underestimates the long-term exchange because it does not account for pathlines that do not come in through the bed surface. Careful attention must be paid to the difference between the Eulerian streamlines and pathlines in the combined case. At any time, the streamlines in the bed are given by the velocity field due to the pressure distribution at the surface. These streamlines will always have the pattern shown in Figure 3.3 or 3.4, but they will be displaced in the x-direction as bedforms move downstream. So, the streamline pattern is exactly the same for both nonmoving and moving bedforms. However, in the steady case (nonmoving bedforms) the streamlines and pathlines correspond exactly, while they will be different in the unsteady case (moving bedforms). The deviation of the pathlines from the streamlines will depend on the bedform velocity, U_b.

Bedform motion causes the pathlines which enter through the surface to penetrate the bed less and exit more quickly. This can be seen in Figure 3.8, which compares the surface pathlines for moving vs. nonmoving bedforms. As U_b^* increases, the depth of penetration is limited even more. Based on these kinds of results, Elliott concluded that

the effect of turnover was to reduce the net exchange, and that pumping would be unimportant at high values of U_b^*.

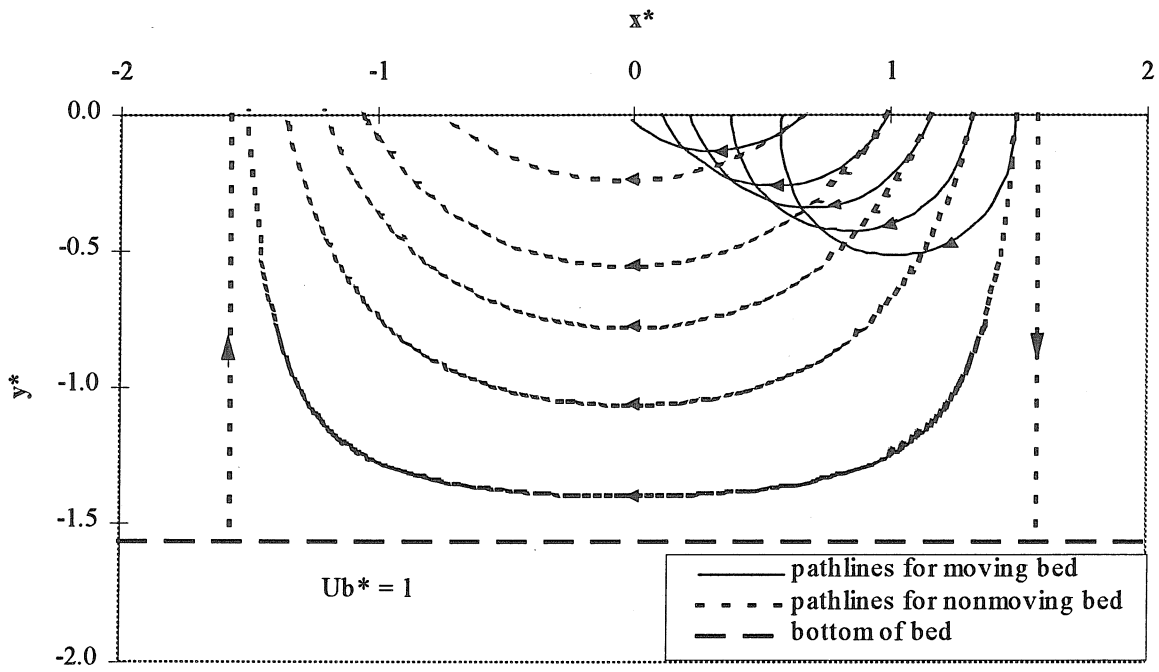

Figure 3.8: Pathlines responsible for flux through the surface of the bed, with and without turnover. These pathlines were calculated using Equations 3.19 and 3.20 for the velocity field. Pathlines for the nonmoving bed case are identical to streamlines. In the moving bed case, $x' = x - U_b t$ was used in the velocity distributions (Equations 3.16 and 3.17) to determine the velocity vector at position x and time t.

It is also important to consider the effect of the velocity field deeper in the bed. For the nonmoving bedform case, streamlines and pathlines coincide, and any arbitrary point in the bed will fall on one of the pathlines that enters through the bed surface. But this is not true for the moving bedform case. The streamlines still have the same pattern, but the surface pathlines have a limited penetration, and there is a region deeper in the bed where other pathlines occur. Elliott's model only considers flow in the upper region of the bed, i.e., that accessible to the surface-penetrating pathlines. In reality, there is

flow in the entire bed, just as for the nonmoving bedform case. One set of deep-bed pathlines are shown in Figure 3.9. These pathlines are roughly circular due to the periodic nature of the pressure disturbance which drives them. Also, the size of the circles is inversely related to the turnover velocity.

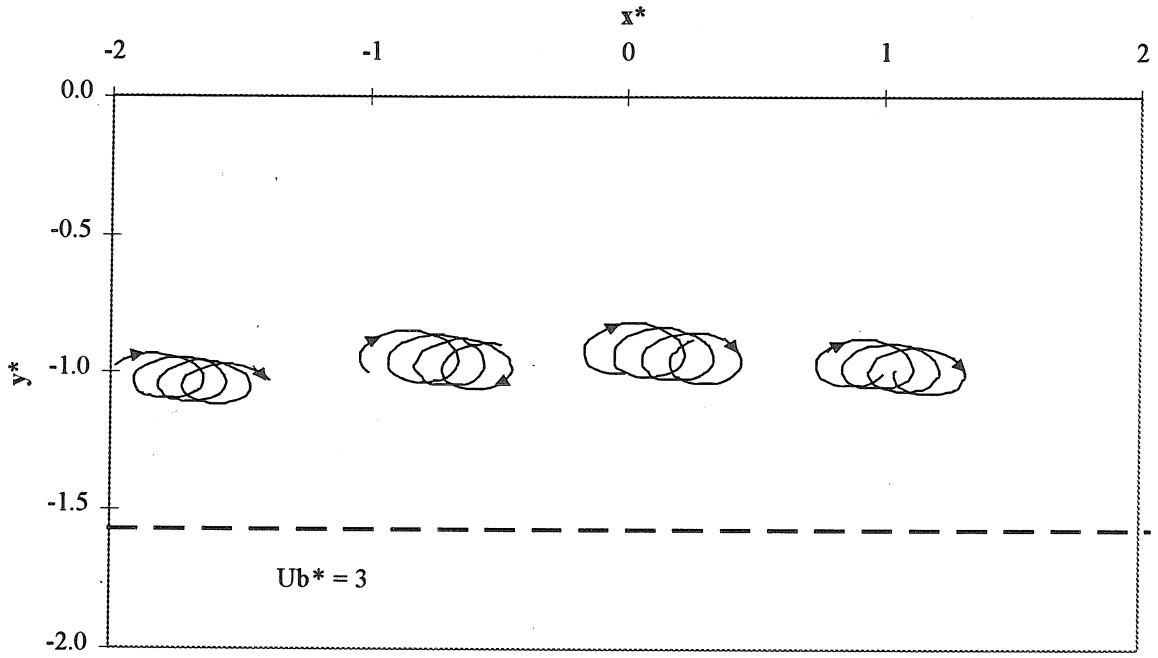

Figure 3.9: Examples of pathlines present in the deep bed in the case of moving bedforms with $U_b^* = 3$. Pathlines were calculated starting at $y^* = -1$ and $x^* = -2, -1, 0,$ and 1.

Elliott's model worked relatively well at early times because the surface-penetrating streamlines control the early exchange. However, his model underpredicted exchange at later times because it did not account for pathlines deeper in the bed. In addition, since Elliott only applied this combined model at relatively low values of U_b^*, he achieved some agreement with experimental results. However, the increasing importance of the deep-bed pathlines resulted in poorer model agreement at higher U_b^*.

Elliott's pure pumping model also does not consider the flow present in the deeper bed. In the pure pumping case with an infinite bed, underflow bounds the penetration of the surface-penetrating streamlines. Underflow also is responsible for flow below this region. The underflow streamlines will primarily be directed downstream, but will have some vertical sinusoidal variation due to the effect of the surface pressure distribution. In some cases, these underflow streamlines could also have an impact on the long-term exchange. However, underflow is always very small, so it does not limit the surface-penetrating streamlines very much, and it can only result in a slow rate of exchange in any case. As a result, Elliott's pure pumping model will be correct for very long times. In fact, this model was very successful in predicting the results of flume experiments.

It should also be noted that Elliott's combined model would be correct if there were no mixing between the surface-penetrating and deep-bed pathlines. However, in reality there may be significant mixing across the interface which separates the surface-penetrating flow from the deeper bed. The mechanisms responsible for this mixing will be discussed in Section 3.1.4.3.4.

3.1.4 New combined model (turnpump model)

This section presents a new model for the combined exchange of both pumping and turnover. The new model, which will be called the turnpump model, takes advantage of the fact that turnover is distinct from pumping exchange both temporally and spatially. Essentially, these two processes are separated in this model, so that the applicable pure models can be used to calculate the penetration due to each process independently. Then, the turnover and pumping penetrations are combined to yield the net exchange.

3.1.4.1 Modeling framework

The key to the turnpump model is the development of the correct conceptual framework with which to consider the exchange in the combined case. First, it is important to realize that turnover is limited to the upper layer of the bed, while pumping can reach the whole bed. Second, turnover is often very fast compared to pumping, and dominates exchange at early times. Taken together, these two observations lead to the conclusion that turnover continuously mixes the upper layer of the bed with a fast time scale, and that pumping results in exchange between the upper and deeper layers of the bed at slower time scale. As a result, turnover dominates the early exchange, while pumping dominates the later exchange. The concept of the turnpump model is depicted in cartoon form in Figure 3.10.

Obviously, the main difference between the turnpump model and Elliott's combined model is the treatment of pumping in the combined case. In the new modeling

framework, pumping is responsible for advective motion throughout the entire bed even in cases of high turnover. Turnover can never be the dominant transport mechanism

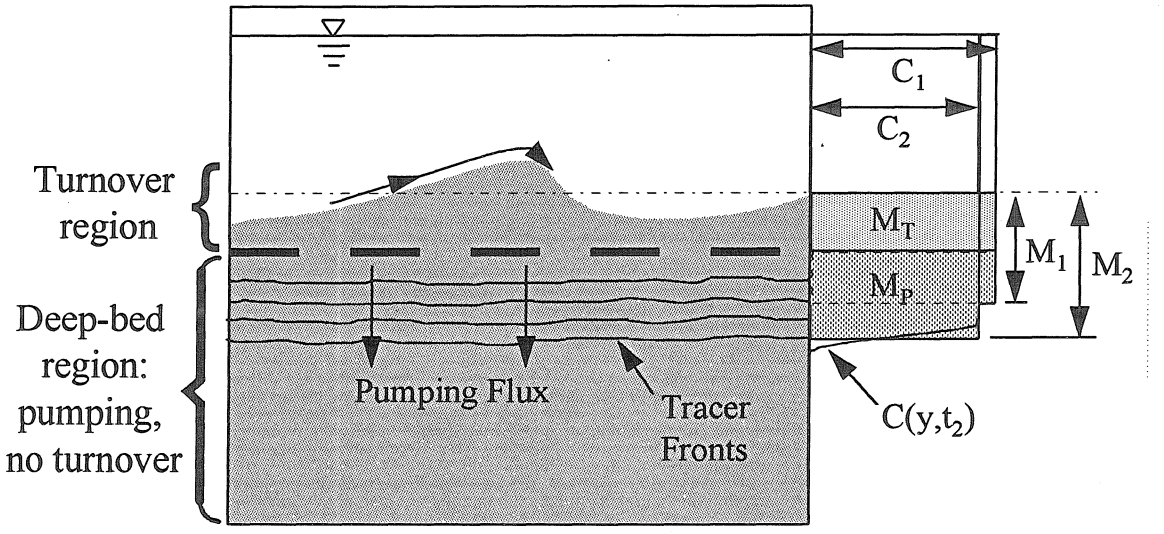

Figure 3.10: Zones of turnover and pumping for combined exchange, and the relationship between turnover exchange (M_T), pumping exchange (M_P), total exchange (M), and stream- and pore-water concentration (C) at two times (denoted by subscripts 1 and 2).

since it only results in exchange with a thin layer at the top of the bed. Ultimately, the transport to the bed will be controlled by advective mixing, since this is the only mechanism that can reach the large volume of the deep bed.

Elliott used the nondimensional turnover velocity U_b^* to determine whether pumping or turnover was the dominant exchange process. The results of the previous section indicate that it is incorrect to characterize the long-term exchange with this parameter. However, U_b^* does indicate which type of exchange dominates in the upper part of the bed. Large values of U_b^* indicate that the bedform celerity is much higher than the maximum pumping velocity. In this case, turnover alone will clearly be

sufficient to calculate the exchange into the turnover region. That is, for fast-moving bedforms, turnover will be the dominant exchange mechanism *wherever it occurs*.

It is also useful to note that turnover exchange is limited in time as well as depth. For regular bedforms, turnover only results in net exchange until the time that the bedforms have traveled through one wavelength. After that time, turnover causes no further dilution of stream water, but continues to keep the upper bed well-mixed with the stream. Pumping is, of course, the dominant mechanism deeper in the bed, and at later times. At these later times when pumping controls the net exchange, turnover transfers solute from the stream to the deep bed region.

This naturally leads to a separation of these two exchange mechanisms. By taking advantage of the spatially and temporally limited nature of turnover, it is possible to develop a model which includes turnover exchange in the upper layer of the bed at early times, and pumping exchange to the deep bed at later times. Fortuitously, it is easy to identify the turnover region of the bed, both theoretically and experimentally. The largest bedform present in the system causes scour down to the maximum scour depth, D_{ms}. This depth is easily included in an analytical model, and the line corresponding to that depth is easily observable in the flume.

3.1.4.2 The turnpump model for combined turnover and pumping

Based on the framework presented in the previous section, a new model was developed for the exchange of a conservative tracer in the general case of combined turnover and pumping. This model will be referred to as the 'turnpump' model, to

differentiate it from Elliott's combined model. 'Turnpump' indicates that the model is based on calculating turnover first, at early times, and then adding pumping at later times. In the following analysis, it is always assumed that $U_b^* >> 1$, i.e., that turnover exchange dominates pumping exchange in the turnover region. The turnover and pumping portions of the turnpump model will be taken from the pure models described in sections 3.1.1. and 3.1.2. The key to the turnpump model is the correct combination of these two separate mechanisms.

Turnover exchange is calculated exactly as given by Equation 3.30 for uniform bedforms. It is assumed that pumping is not an important process until the initial turnover exchange ends, i.e., until the bedforms have moved one wavelength, corresponding to $t = \lambda/U_b$. Thus at early times the net exchange is just equal to the equivalent penetration due to turnover, given by

$$M(t) = M_T(t) = \frac{H}{2}\left(1 - \left(1 - \frac{U_b t}{\lambda}\right)^2\right) \quad \text{for } t < \frac{\lambda}{U_b} \tag{3.36}$$

After $t = \lambda/U_b$ it is assumed that the bed stays well-mixed with the stream down to the maximum scour depth, which is just H/2 for regular bedforms. Further exchange is all due to pumping from the turnover region to the deeper bed. Thus the net exchange is given by

$$M(t) = M_T(t=\lambda/U_b) + M_P(t) = H/2 + M_P(t) \quad \text{for } t > \lambda/U_b \tag{3.37}$$

The exchange due to pumping, $M_P(t)$, is calculated from the flux out of the turnover region into the lower, unmixed portion of the bed. When turnover is very high, the pumping pathlines in the bed are very small circles, as discussed in Section 3.1.1. As a

result, pumping results in an incremental exchange to successively deeper layers of the bed. This is shown quite clearly by the results of Elliott, who observed the passage of dye fronts into the bed under different bedform velocities. Figures 3.11 and 3.12 compare the fronts for nonmoving and fast-moving bedforms.

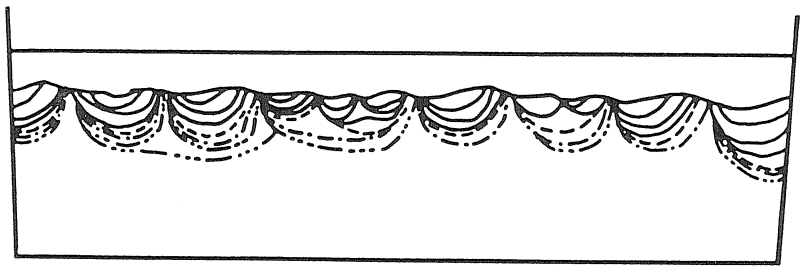

Figure 3.11: Dye fronts for stationary natural bedforms. Fronts were recorded at 5 hr, 23 hr, 49 hr, 101 hr, 167 hr, 240 hr and 336 hr. After Elliott (1990).

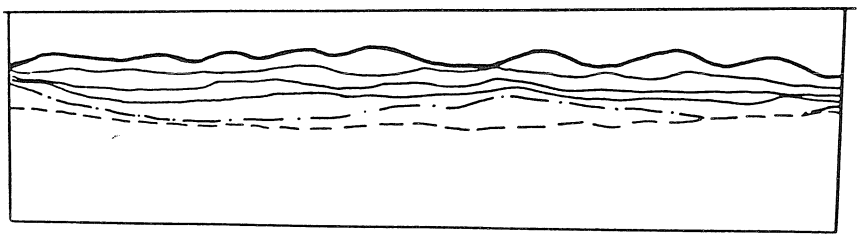

Figure 3.12: Dye fronts for rapidly-moving bedforms ($U_b^* = 16$). Fronts were recorded at 0.75 hr, 2 hr, 9 hr, 20 hr, 45 hr, and 114 hr. After Elliott (1990).

The net pumping exchange under fast-moving bedforms can be modeled by assuming that a front of well-mixed fluid is driven down into the bed by pumping. Essentially, this assumes that the pumping pathlines are differentially small circles, so that the transport

may be represented simply by an effective downward velocity. Then, the net pumping exchange at any time is given by the downward flux from the currently mixed portion of the bed

$$q_p^*(t) = C^*(t)\ \bar{v}^*(y) \tag{3.38}$$

where $C^*(t)$ is just the stream concentration since the upper part of the bed is assumed to be well-mixed with the stream, and $\bar{v}^*$ is the average downward velocity through a horizontal line at the front depth y. $\bar{v}^*$ is calculated by averaging the downward component of the pore-water velocity distribution over one wavelength. This calculation is more easily performed nondimensionally:

$$\bar{v}^*(y^*) = \frac{1}{\lambda^*}\int_0^{\lambda^*} v^*(x^*,y^*)\,dx^* = \frac{1}{2\pi}\int_0^{\pi} v^*(x^*,y^*)\,dx^* \tag{3.39}$$

Distances are nondimensionalized using the wavenumber, so $\lambda^* = 2\pi$. However, the integration is performed over 0 to π for the sinusoidal pressure distribution because the flux only goes into the bed over one-half the wavelength (this can be seen be examining the streamlines given in Figures 3.3 and 3.4). Evaluating for the finite bed velocity profile given in Equation 3.20,

$$\bar{v}^*(y^*) = \frac{\tanh(d_b^*)\cosh(-y^*) + \sinh(-y^*)}{\pi} \tag{3.40}$$

The pumping flux results in an accumulated exchange given by

$$M_P^*\left(\frac{t^*}{\theta}\right) = 2\pi \int_{\tau^*/\theta = \lambda^*/\theta U_b^*}^{t^*/\theta} q_p^*\left(\frac{\tau^*}{\theta}\right)\frac{d\tau^*}{\theta} = 2\pi \int_{\tau^*/\theta = \lambda^*/\theta U_b^*}^{t^*/\theta} C^*\left(\frac{\tau^*}{\theta}\right)\bar{v}^*\left(y^*\left(\frac{\tau^*}{\theta}\right)\right)\frac{d\tau^*}{\theta} \tag{3.41}$$

Note that this is an implicit equation since the current front position must be used for the depth y* used to evaluate $\bar{v}^*$. The front position is exactly given by the equivalent penetration depth, M, as discussed in Section 3.1.1.3. Thus, the depth

$$y = M(t) = H/2 + M_P(t) \tag{3.42}$$

is used to calculate the average velocity term $\bar{v}^*$.

In practice, this problem was solved numerically through a finite difference scheme, depicted in flowchart for in Figure 3.13.

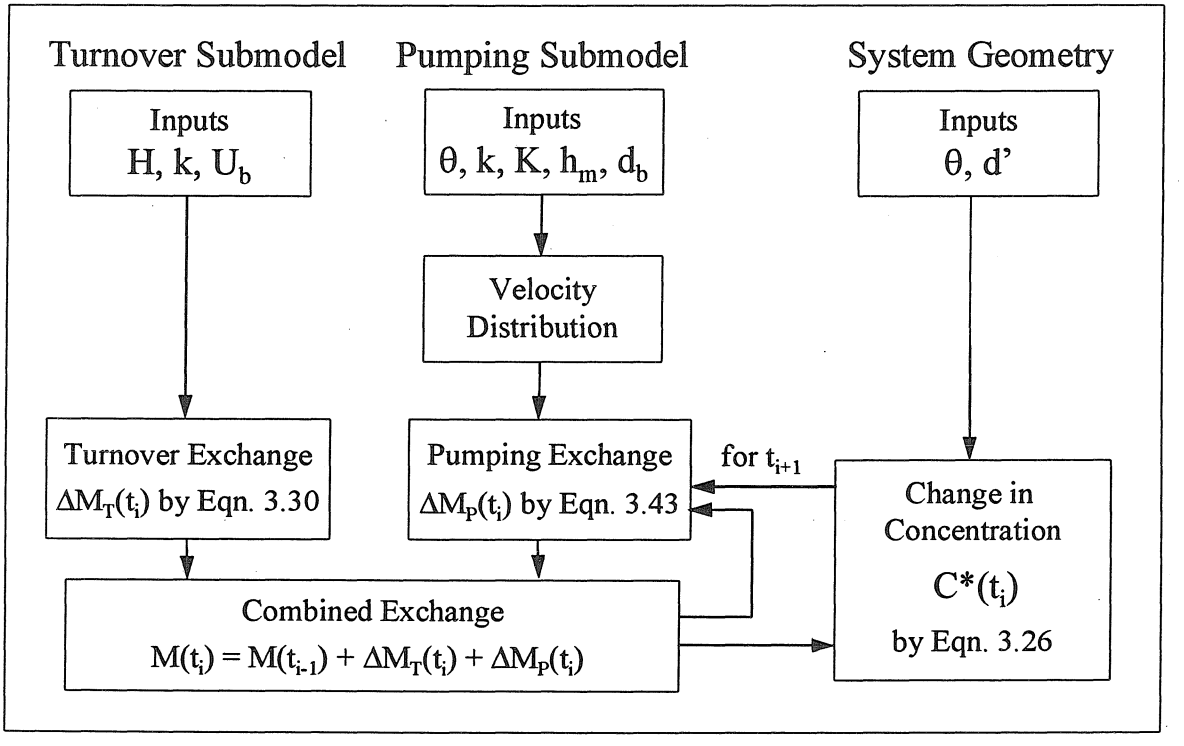

Figure 3.13: Flowchart showing inputs, calculation steps, and outputs for the turnpump model for conservative solutes. M and C* from the previous time step are used in the calculation of M_P in the current time step. See also the definition sketch in Figure 3.10.

The calculation steps are performed in an EXCEL spreadsheet as follows:

Step 1: Calculate the incremental mixing due to turnover, $\Delta M_T(t_i)$, using Equation 3.30 for uniform bedforms or Equations 3.31 and 3.32 for bedforms with multiple size classes, starting from $M_T(0) = 0$.

This calculation requires only H, λ, and U_b as inputs. Since turnover exchange is calculated geometrically, the stream concentration and geometry (i.e., C* and d') are not used in the calculation of M_T. With regular bedforms, $\Delta M_T(t)$ always equals 0 after $t = \lambda/U_b$ (by Equation 3.30).

Step 2: Calculate the incremental mixing due to pumping, $\Delta M_P(t)$, starting at $t = \lambda/U_b$:

$$\Delta M_P^*(t_i) = 2\pi\, C^*(t_{i-1})\, \bar{v}^*\left(M^*(t_{i-1}^*)\right)\Delta t^*/\theta \qquad \textbf{between } t_{i-1} \textbf{ and } t_i \tag{3.43}$$

The normalized equivalent penetration depth from the last time step, $M^*(t^*_{i-1})$, is used as y_i^* to evaluate $\bar{v}^*$. $C^*(t^*_{i-1})$ is also taken from the last time step.

It was assumed that $M_P = 0$ for $t < \lambda/U_b$ for the turnpump model. At the assumed onset of pumping ($t = \lambda/U_b$), the bed has been mixed throughout the turnover region, so the bed has a concentration C*(t) down to a depth H/2 and a

concentration of 0 below H/2. That is, the initial condition for the calculation of pumping exchange is that $M = M_T = H/2$ and $M_p = 0$ at $t = \lambda/U_b$.

Step 3: Calculate the total incremental exchange in the current time step, $\Delta M(t_i)$, from the turnover and pumping exchanges:

$$\Delta M(t_i) = \Delta M_T(t_i) + \Delta M_P(t_i) = \Delta M_T(t_i) + \Delta M_P{}^*(t_i^*)/2\pi k \qquad (3.44)$$

While the calculation for ΔM and ΔM_T is done dimensionally in real time, the calculation for ΔM_P is done nondimensionally in nondimensional time and then converted by $1/2\pi k$. This is somewhat confusing, but it is desirable in order to simplify the calculation for ΔM_P while keeping the other exchanges as actual penetration increments. Penetration depth is the most easily interpretable exchange parameter, since it allows direct comparison with observed scour and front depths. It is quite simple to switch between dimensional and nondimensional values in the EXCEL spreadsheet.

Step 4: Calculate the total penetration, M(t). This is just the sum of the incremental exchanges.

$$M(t_i) = M(t_{i-1}) + \Delta M(t_i) \qquad (3.45)$$

Remember that M(t) is the equivalent penetration depth at the current time, and is also equal to the current front position.

Step 5: Calculate the concentration in the current time step. This is just given by dilution due to mixing down to the equivalent penetration depth, M.

$$C^*(t_i)=\frac{d'}{d'+\theta\, M(t_i)} \tag{3.46}$$

Step 6. Proceed to next time step. Iterate to Step 2. Calculate $\Delta M_P(t_{i+1})$ in the new time step using the values just calculated for $M(t_i)$ and $C^*(t_i)$.

It should be noted that pumping exchange does not directly deplete the tracer from the turnover region because turnover continuously brings in additional tracer from the stream. Remember that it is assumed that the rate of turnover exchange is much faster than the rate of pumping exchange, so the turnover region always stays well-mixed with the stream. Pumping causes a gradual decrease in the concentration of both the stream water and the pore water in the previously-mixed portion of the bed. The net exchange out of the stream for the time increment Δt, given by $d'\Delta C$, is different from the exchange based on the penetration depth, $\Delta M\theta C$. The difference is due to the additional exchange from the previously-mixed part of the bed to the newly-mixed layer, $M\theta\Delta C$. These exchanges are illustrated by the corresponding areas under the concentration profiles in Figure 3.10.

Also note that the model automatically bounds the overall exchange. At long times, the penetration depth, M, asymptotically approaches the bed depth, d_b, and the net flux drops to 0. This occurs because the velocity distribution includes the effect of the

bed depth, and the downward velocity $\bar{v}^* \rightarrow 0$ as $M \rightarrow d_b$. Thus, the model includes the physical reality that mixing cannot occur beyond the depth of the bed.

3.1.4.3 Model application

3.1.4.3.1 Range of applicability: criteria for U_b^*

The nondimensional turnover velocity (U_b^*) can be used to predict which model should be used. Pure pumping occurs only for $U_b^* \sim 0$, while the combined (turnpump) model applies whenever there is appreciable turnover. Again, there is no pure turnover case. U_b^* is also useful in characterizing the extent of turnover, exactly as described by Elliott. Cases with $U_b^* << 1$ can be considered slow turnover, cases with $U_b^* >> 1$ are fast turnover, and cases with $U_b^* \sim 1$ are intermediate. The deviation from the pure pumping model is predicted by U_b^*, with decreasing net exchange for increasing U_b^*. Experimental results show that the pumping model still works well for cases with very low turnover, while the turnpump model begins to work well for cases with U_b^* near 1. The validity of the pure pumping and turnpump models at different U_b^* will be discussed further in Chapters 5 and 6.

3.1.4.3.2 Correction for pumping at early times

The turnpump model assumes complete separation between the turnover and pumping time scales when bedforms are fast-moving. As a result, pumping exchange is only considered to start after the bed has been mixed down to the average bedform height. In reality, however, both pumping and turnover would start simultaneously at t = 0 (i.e.,

immediately after tracer addition). The actual distribution of the tracer in the turnover region is very complicated, since tracer brought into the bed by turnover would be subject to pumping, and vice versa. Exact calculation of simultaneous pumping and turnover in the same part of the bed would be very difficult. This calculation would necessitate the use of a finite-element or similar numerical model to track the exchange at every location in the bed at all times. However, for high U_b^*, turnover will tend to dominate the exchange wherever it occurs, allowing for a useful simplification. Turnover can be assumed to control exchange from the stream into the upper layer of the bed. But pumping will cause some transport from the turnover zone to the deep bed even before the bed becomes well-mixed in the turnover region. This effect can simply be included in the model by allowing pumping to the deep bed to start at $t = 0$ instead of at $t = \lambda/U_b$. When this assumption is used, Equation 3.41 becomes

$$M_P^*(t) = \int_{\tau=0}^{t^*} C^*(\tau^*)\bar{v}^*(\tau^*)d\tau^*. \tag{3.47}$$

Turnover is still calculated using Equation 3.30.

The assumption that pumping to the deep bed begins at $t = \lambda/U_b$ results in some underestimation of the early exchange, while the assumption that pumping begins at $t = 0$ results in some overestimation of the early exchange. In reality, the early pumping exchange will lie between the values given by these two predictions. However, the difference is minor since turnover tends to dominate the net exchange at early times, as shown in Figure 3.14.

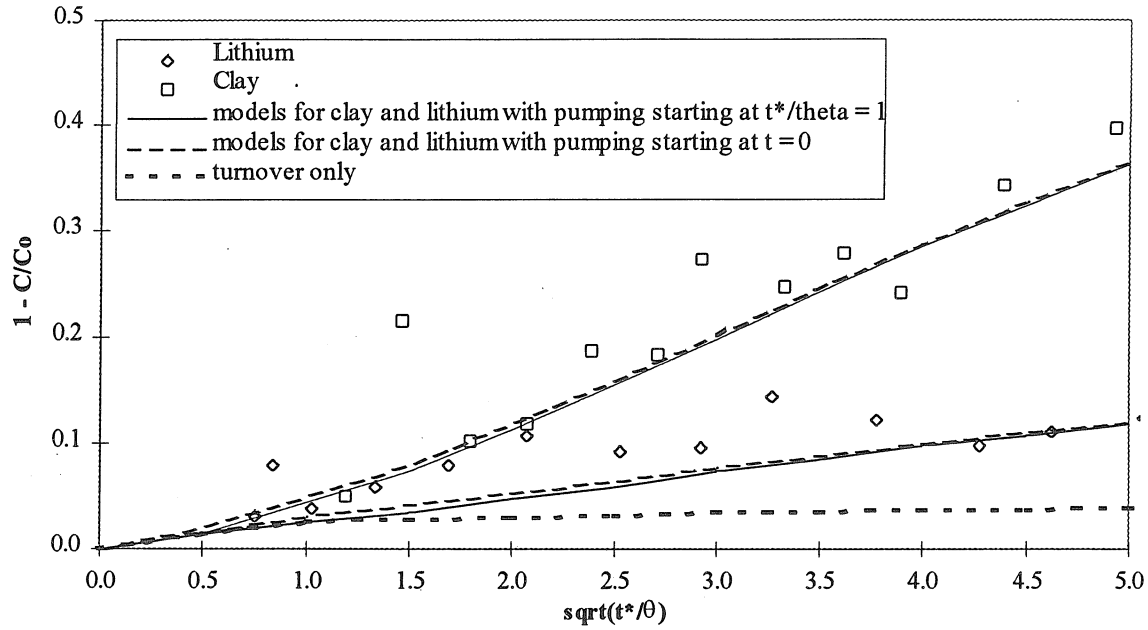

Figure 3.14: Comparison of modeling results for different pumping assumptions, plotted as fraction of tracer in bed versus the square root of dimensionless time. Model inputs were taken from Experiment #11, with fast-moving bedforms ($U_b^* = 8.43$). Experimental results are provided for comparison. ($t^*/\theta = k^2 K h_m t/\theta$ where k = bedform wavenumber ($2\pi/\lambda$), K = coefficient of permeability, h_m = amplitude of piezometric-head variation due to flow over bedforms, t = time since the addition of tracer, and θ = porosity.)

3.1.4.3.3 Correction for irregular bedforms

Irregular bedforms can easily be included in this model. It is important to note that the large majority of bedforms will still have approximately average geometry and celerity. With this in mind, the pumping exchange is still calculated using Equation 3.41 with the average bedform parameters. Larger-than-average bedforms have more impact on the turnover exchange, since they will cause turnover below depth H/2 and at times after $t = \lambda/U_b$. As mentioned earlier, the maximum scour depth is an important variable, and it is useful to calculate the turnover between the average scour (H/2) and the maximum scour (D_{ms}). Equation 3.30 still applies for the average bedform parameters up

to $t = \lambda/U_b$, but the exchange due to additional turnover must be included for $t > \lambda/U_b$. When calculating the total exchange, M(t), for $t > \lambda/U_b$, the additional turnover exchange, $M_{Ta}(t)$, is simply added along with the pumping exchange, $M_P(t)$:

$$M(t) = H/2 + M_{Ta}(t) + M_P(t) \quad \text{for } t > \lambda/U_b \tag{3.48}$$

The additional turnover is calculated from Equations 3.31 and 3.32 just as described in Section 3.1.2. Eventually, at some time (t_{ms}) the bed will be turned over down to the maximum scour depth (D_{ms}) and turnover will again result in no net exchange. After this time, Equation 3.48 reduces to

$$M(t) = D_{ms} + M_P(t) \quad \text{for } t > t_{ms} \tag{3.49}$$

D_{ms} is of course equal to the turnover due to the bedforms of the largest size class.

Note that this method is only an approximation for the actual effect of additional turnover. Small errors may be introduced because the total incremental exchange (ΔM) is simply obtained by adding the incremental pumping and turnover (ΔM_{Ta} and ΔM_P). An exact calculation would be very difficult, as described in Section 3.1.4.3.2. However, the approximate method presented works well because slight over- or underestimation of the combined M in the additional turnover region is corrected in the next time step through the impact of M(t) on ΔM_P. It is also helpful that the incremental additional turnover exchange (ΔM_{Ta}) is generally quite small. Finally, these errors are also limited in time due to the temporally and spatially limited nature of turnover, and the long-term exchange predictions will be correct after $t = t_{ms}$.

3.1.4.3.4 Mechanisms of exchange between upper and lower bed

It is useful to consider mechanisms that can result in mixing between the surface pathlines and deep-bed pathlines. In theory, these pathlines would always be stable and would never cross, indicating that no mixing will occur with the deep bed by purely advective processes. However, in reality there are several mechanisms which could cause mixing between these upper and lower sections of the bed. Turnover itself can be one mechanism of bringing surface water to the deep bed. This would occur whenever turnover resulted in scour below the region of the surface pumping pathlines. In addition, there would always be some diffusive mixing across the pathlines. Finally, and probably most importantly, any real system has enough variation of the bedform geometry and velocity to provide for substantial variation in pathlines. This means that the position of the separation between the upper and lower pathlines would continuously fluctuate in the bed, causing some overlap between the surface and deep-bed pathlines. Even a small overlap of this type would result in considerable exchange to the deep bed over long times.

3.2 Colloid filtration

Filtration is the process whereby fine particles suspended in a flow through a porous medium become attached to the stationary grains of that medium. The overall process of filtration includes hydrodynamic, chemical, and electrostatic components: fluid flow carries the suspended particles around stationary bed grains, while the solution and particle surface chemistry results in both chemical and electrostatic interactions which can cause attachment.

Filtration theory can be developed using several different approaches. Theory for macroscopic and microscopic approaches will be discussed here. The influence of solution and surface chemistry will also be considered.

3.2.1 Macroscopic approach (advection-diffusion equation with filtration)

In the macroscopic approach, theory is developed to describe the mass balance of the bulk concentration of suspended particles as they flow through the porous medium. This is represented by the advection-dispersion equation for particles with a term for filtration

$$\frac{\partial C}{\partial t} + u\frac{\partial C}{\partial x} + v\frac{\partial C}{\partial y} = D\left(\frac{\partial^2 C}{\partial^2 x} + \frac{\partial^2 C}{\partial^2 y}\right) - S \qquad (3.50)$$

where S represents the rate of particle removal from the suspension due to filtration (per unit volume of pore fluid). It can be shown that the dispersion term will generally be negligible (Mau, 1992), resulting in

$$\frac{DC}{Dt}=\frac{\partial C}{\partial t}+u\frac{\partial C}{\partial x}+v\frac{\partial C}{\partial y}=-S \tag{3.51}$$

Thus, the total derivative of concentration, DC/Dt, is given by the loss due to filtration. The particles lost from suspension obviously accumulate on the collector surface, yielding

$$S = \rho_b \frac{\partial q}{\partial t} \tag{3.52}$$

where ρ_b is the bulk density of collector grains (mass/total volume), and q is the accumulated particle concentration in units of moles of particles per unit collector mass. This is related to the surface collection of particles by

$$C_s A_c = q \rho_c V_c \tag{3.53}$$

where C_s is the surface concentration of particles, A_c and V_c are the surface area and volume of collector grains, and ρ_c is the density of the collector grains. Noting that

$$\rho_b = (1 - \theta) \rho_c \tag{3.54}$$

and substituting for ρ_b and q into Equation 3.52 yields

$$S=(1-\theta)\rho_c\frac{\partial}{\partial t}\left(\frac{C_s A_c}{\rho_c V_c}\right)=(1-\theta)\frac{A_c}{V_c}\frac{\partial C_s}{\partial t} \tag{3.55}$$

for spherical collector grains

$$\frac{A_c}{V_c} = \frac{4\pi a_c^2}{\frac{4}{3}\pi a_c^3} = \frac{3}{a_c} \tag{3.56}$$

where a_c is the collector radius. Substituting in Equation 3.55 yields

$$S = (1 - \theta)\frac{3}{a_c}\frac{\partial C_s}{\partial t} \tag{3.57}$$

At this point, it is necessary to relate the surface accumulation of particles to the concentration of particles in the surrounding fluid. The simplest approach is to use the filtration coefficient (λ_f), defined so that

$$S = \lambda_f U C_f \tag{3.58}$$

where U is the seepage velocity. The rate of removal, S, is proportional to the flux of particles through the medium with a empirical constant: the filtration coefficient, λ_f. Note that λ_f, which has units of inverse length, includes all the microscopic information about particle filtration--pore geometry, microscopic flow processes which bring particles to the collector surfaces, and the physicochemical interactions responsible for attachment. λ_f is an experimentally determined parameter for any given filtration system.

Substituting for S in Equation 3.51 yields

$$\frac{DC}{Dt} = -\lambda_f U C \tag{3.59}$$

By using a Lagrangian framework and considering a streamline along which

$$U = \frac{\partial s}{\partial t} \tag{3.60}$$

a relationship for the concentration gradient along the streamline is given by

$$\frac{\partial C}{\partial s} = -\lambda_f C \tag{3.61}$$

Solving this equation for typical initial condition of a constant input of concentration C_0 at position s = 0 yields the familiar filtration equation

$$\frac{C}{C_0} = e^{-\lambda_f L} \tag{3.62}$$

where L is simply the distance traveled along the streamline. This equation is normally thought of as applying to the one-dimensional case, but this derivation shows that it is also applicable along any streamline. The filtration equation was originally obtained from empirical observations of colloid transport through porous media.

3.2.2 Microscopic approach (single collector removal efficiency)

In the microscopic approach, theory is developed for the removal of suspended particles flowing around an individual collector grain. The discussion here will primarily follow the presentation in Elimelech et al. (1995).

The microscopic approach is based on the single collector removal efficiency, η, the fraction of particles approaching a collector which become attached to it. This overall collection efficiency is then broken up into physical and chemical collection efficiencies

$$\eta = \alpha\eta_0 \tag{3.63}$$

where α is the collision efficiency, the fraction of impacts that result in attachment. η_0 then represents the fraction of approaching particles that collide with the collector. The rate of particle approach is given by the mass flux through the projected collector area

$$m'_{ap} = UC\pi a_c^2 \tag{3.64}$$

U is now the superficial approach velocity (D'Arcy). (Note: it is also possible to define other projected areas for the rate of particle approach. It is important to consistently use the same definition through the entire derivation. See Elimelech et al. for more details.)

In this formulation, it is assumed that electrical double layer interactions will only influence α, and will not have any effect on η_0. For favorable attachment conditions, all

particles that collide with the collector become attached, and $\alpha = 1$. In unfavorable cases ($\alpha < 1$), α is difficult to estimate and is generally reported as an experimental value.

η_0 is calculated based on the collision mechanisms of diffusion, interception, and settling (or gravity), given by

$$\eta_0 = \eta_D + \eta_I + \eta_G \tag{3.65}$$

Fundamentally, these terms are given by (Yao et al., 1971)

$$\eta_D = 4.0\, A_s^{1/3} \left(\frac{D_\infty}{U d_c} \right)^{2/3} \tag{3.66}$$

$$\eta_I = \frac{3}{2} A_s \left(\frac{d_p}{d_c} \right)^2 \tag{3.67}$$

$$\eta_G = \frac{v_s}{U} \tag{3.68}$$

A_s is a parameter which accounts for the flow through a packed bed. It is derived from models of the flow in this system. Typically, Happel's sphere-in-cell model is used (Happel, 1958), which yields

$$A_s = \frac{2\left(1-p^5\right)}{\left(2-3p+3p^5-2p^6\right)} \tag{3.69}$$

where $p = (1- \theta)^{1/3}$.

D_∞ is the particle diffusion coefficient given by the Stokes-Einstein equation

$$D_\infty = \frac{kT}{6\pi a_p \mu} \tag{3.70}$$

where k is Boltzmann's constant, T is the absolute temperature, a_p is the particle radius, and μ is the viscosity.

d_p and d_c are the particle and collector diameters. v_s is the particle settling velocity, given by

$$v_s = \frac{g(\rho_p - \rho)d_p^2}{18\mu} \tag{3.71}$$

A better estimate of η_0 was developed by Rajagopalan and Tien (1976). It is derived from the same model presented in Equation 3.65, but incorporates a term for hydrodynamic retardation as well as fitting terms to match numerical simulations. This model uses the same diffusion term given in Equation 3.66, and interception and settling terms given by

$$\eta_I = A_S N_{LO}^{1/8} \left(\frac{d_p}{d_c}\right)^{15/8} \tag{3.72}$$

$$\eta_G = 3.38 \cdot 10^{-3} A_S \left(\frac{v_s}{U}\right)^{1.2} \left(\frac{d_p}{d_c}\right)^{-0.4} \tag{3.73}$$

N_{LO} is a London-van der Waals number

$$N_{LO} = \frac{4A}{9\pi\mu U d_p^2} \tag{3.74}$$

where A is the Hamaker constant.

The single collector efficiency can be applied to a packed bed by relating the overall removal of particles by the bed to the removal at all the individual collectors. Considering an overall removal of $1 - C/C_0$ over a bed of length L gives

$$C/C_0 = e^{-3/4\,(1-\theta)\eta L/a_c} \tag{3.75}$$

As noted earlier, the rate of particle approach to a single collector is given by

$$m'_{ap} = UC\pi a_c^2 \tag{3.76}$$

The rate of attachment to that collector is then

$$m'_{at} = \eta UC\pi a_c^2 \tag{3.77}$$

For a homogenous packed bed of collectors with porosity θ, the number of collectors per unit volume of bed is

$$N_c' = \frac{1-\theta}{\frac{4}{3}\,\pi\, a_c^3} \tag{3.78}$$

The rate of particle mass attachment per unit volume of bed is then

$$M'_{at} = N_c' \, m'_{at} = 3/4\,\eta UC(1-\theta)/a_c \tag{3.79}$$

Relating this to the loss of particles from the bulk fluid per unit volume

$$M'_{at} = -\,U\,dC/dx \tag{3.80}$$

gives the change in concentration per unit length of bed

$$dC/dx = -\,3/4\,\eta C(1-\theta)/a_c \tag{3.81}$$

For the typical filtration boundary conditions described earlier, this yields

$$C/C_0 = e^{-3/4\,\eta(1-\theta)L/a_c} \tag{3.82}$$

Note that this is exactly the same as the filtration equation given earlier in Equation 3.62, with the substitution

$$\lambda_f = 3/4\,\eta(1-\theta)/a_c = 3/4\,\alpha\,\eta_0\,(1-\theta)/a_c \tag{3.83}$$

This framework provides a way to compare theoretical collector efficiencies with experimentally determined filtration coefficients. The way this is typically done is to

determine the difference between the actual filtration and that predicted by η_0. That is, an experimental value of α is calculated in order to evaluate the favorableness of filtration. α values for the experiments of this work can be found in Section 5.2, Column Experiment Results.

3.2.3 Influence of solution and surface chemistry

Solution and particle surface chemistry are not explicitly described in the filtration equations given above. Instead, all chemical effects are lumped together into either λ_f or α. The approach of using λ_f to summarize the physicochemical processes of filtration will be employed in developing models of colloid transport in the stream bed. However, it is useful to understand how various chemical parameters affect λ_f in order to determine the importance of stream chemistry. The following discussion will be qualitative rather than quantitative, since the goal is to interpret the chemical portion of λ_f (i.e, the collision efficiency, α) and not to calculate the interaction force.

Filtration behavior can be affected by changes in the chemical or electrostatic properties of the colloidal particles, collector particles, or intervening fluid. The composition of the particles involved has a large impact on filtration. Surface coatings, which may represent only a small fraction of the overall particle mass, are also important in determining filtration behavior. Common coatings in natural environments include metallic oxides, notably those of iron and manganese, and organic material such as humic acids. Particle surface chemistry is also strongly influenced by solution chemistry. Most particles have a surface charge that is strongly dependent on the solution pH. In addition,

molecules in solution which form strong complexes with surface functional groups can greatly influence the particle surface charge. Dissolved species that are typically important include naturally occurring organic matter such as humic acids, strong ligands such as EDTA, natural or man-made polymers, and inorganic species such as phosphate. Inert dissolved ions (i.e., those that have no specific interaction with the particle surface) can also influence filtration by changing the electrostatic properties of the intervening water solution. Higher ionic strength causes the effect of particle surface charge to decrease more rapidly in the surrounding aqueous solution. This is measured by the inverse Debye-Hückel parameter, κ^{-1}, the distance between a particle surface and its associated diffuse layer of ions. The Debye-Hückel parameter, κ, is proportional to the square-root of ionic strength, so κ^{-1} is inversely proportional to the square-root of ionic strength. In the typical case of interest where electrostatic interactions between particles tend to be repulsive, higher ionic strength favors additional filtration.

To summarize, filtration will generally be influenced by

1. the composition of the particle surfaces, including any complete or partial coatings,
2. interactions between the particle surfaces and dissolved species, and
3. the ionic strength of the water surrounding the particles.

3.2.3a Surface chemistry of kaolinite

Kaolinite is a 1:1 layer clay with the ideal chemical formula $Al_4Si_4O_{10}(OH)_8$. In kaolinite, a tetrahedrally-coordinated silica-oxygen sheet shares oxygen atoms with an octahedrally-coordinated aluminum-oxygen-hydroxide sheet. There is generally a small amount of isomorphous substitution for aluminum and silica. Kaolinite occurs as particles composed of a stacked arrangement of small hexagonal sheets. These sheets form because it is much easier to fracture the mineral along the plane of the sheets than across this plane. The faces of kaolinite particles have a permanent negative charge due to substitution of trivalent metal ions for silica. The sheet edges resemble an aluminum hydroxide surface, with a corresponding pH-dependent surface charge. Thus, while the faces are always negative, the edges can be either positive or negative. Measured values of the overall pH of zero charge of various kaolinites are typically in the range 4 - 5, while the pH of zero charge of the edges is in the range 7 - 8.

Due to the nature of its edges and faces, kaolinite particles can experience several modes of particle-particle interaction. Depending on the situation, either the edges or faces may be attracted to another surface. For example, kaolinite particles may aggregate in a face-to-face, edge-to-edge, or edge-to-face geometry. Considering the interaction of kaolinite and silica particles, an attraction between negative silica surface and positive kaolinite edges would be expected over neutral to moderately-acidic pH's. (Silica is known to have a negative surface charge above pH ~ 2.5.)

Some anions, notably phosphate and oxalate, are known to sorb strongly to clay edge sites. These ions form strong surface complexes with exposed aluminum groups,

resulting in the edge charge becoming negative. Solutions of these ions can be used as a dispersing agent for kaolinite particles.

On the other hand, negatively-charged kaolinite can be coagulated by inert cations, which nonspecifically sorb to the particle surface and reduce the electrostatic repulsion between particles. The concentration of a cation required to coagulate a clay suspension (the critical coagulation concentration) is controlled by the valence of the cation. (This is an example of the Schulze-Hardy rule.) Monovalent cations require a concentration of at least 10 mM to coagulate kaolinite, while bivalent cations require only on the order of 1 mM.

As mentioned previously, all of the properties discussed here vary according to the impurities present in any particular kaolinite sample. Various preparation methods also influence the surface properties. The specific kaolinite used in this study and all preparation procedures are described in Section 4.4.3.

3.3 Bed exchange and trapping of colloids

The models presented in the previous two sections must be combined in order to model colloid exchange with the stream bed. The approach taken here is to modify the hydrodynamic models of Section 3.1 to include the colloid transport mechanisms discussed in Section 3.2. The combined model is developed for the finite bed case; application to an infinite bed is straightforward.

3.3.1 Exchange of colloids with nonmoving bedforms (clay pumping model)

The model developed in Section 3.1.1 for pumping exchange was based on the velocity profile in the bed due to the pressure disturbance caused by bedforms. The same model can be used for colloid transport provided that particle paths are used instead of streamlines. This can be accomplished by adding particle settling to the velocity profile given in Equations 3.16 and 3.17. By superposition, the resulting equation for the velocity of a particle in the bed is

$$u = - kKh_m \cos(kx) \{\tanh(kd_b)\sinh(ky) + \cosh(ky)\} \tag{3.84}$$

$$v = -kKh_m \sin(kx) \{\tanh(kd_b)\cosh(ky) + \sinh(ky)\} - v_s \tag{3.85}$$

The settling velocity is normalized in the same way as other velocities, so that

$$v_s^* = \theta v_s / u_m \tag{3.86}$$

The θ appears because u_m is calculated as a D'Arcy velocity.

The nondimensional particle paths are given by

$$u = -\cos x^* (\tanh d_b^* \sinh y^* + \cosh y^*) \tag{3.87}$$

$$v = -\sin x^* (\tanh d_b^* \cosh y^* + \sinh y^*) - v_s^* \qquad (3.88)$$

Settling is purely a trapping mechanism: it can only be responsible for enhanced transport to the deeper portions of the bed. This is shown in Figure 3.15, which compares particle paths for a low value of v_s^* with water streamlines under the same hydrodynamic conditions. Settling can be an important trapping mechanism for larger colloidal particles. In the extreme case where $v_s^* > 1$, pumping will be unable to carry particles upwards in the bed, and all particles that enter the bed will be trapped there.

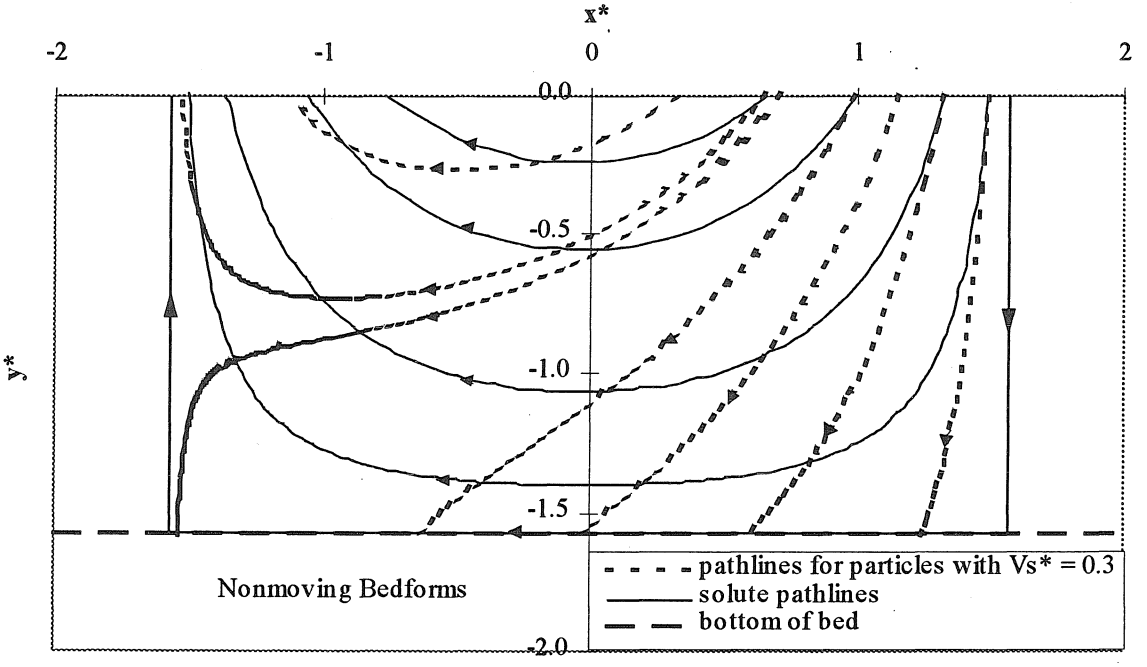

Figure 3.15: Comparison of particle paths for $v_s^* = 0.3$ with solute pathlines. Solute pathlines are identical to streamlines.

Filtration of colloids must also be included in the pumping model. The approach taken here is to apply the filtration as described by Equation 3.62 along the particle paths

given by Equations 3.87 and 3.88. Again, the filtration coefficient is used to summarize all the physicochemical processes responsible for filtration.

The filtration coefficient is nondimensionalized by the bedform wavenumber

$$\lambda_f^* = \lambda_f / k \tag{3.89}$$

which simply indicates that the dimensionless filtration is dependent on the length scale over which filtration occurs. As $\lambda_f^* \rightarrow \infty$, all colloids will be filtered by the stream bed.

Filtration is included incrementally in the numerical integration for the residence time function. For each time step dt, the particle paths given by Equations 3.87 and 3.88 result in an incremental change of position

$$ds = \sqrt{dx^2 + dy^2} = \sqrt{(udt)^2 + (vdt)^2} \tag{3.90}$$

Filtration over this incremental distance results in a reduction of concentration given by

$$\frac{C(s+ds)}{C(s)} = e^{-\lambda_f ds} \tag{3.91}$$

This calculation is performed at every time step, along all the particle paths, yielding the overall reduction of transported particles due to filtration. The amount filtered can also be determined simply by summing the incremental concentration reductions.

The net effect of filtration applied in this fashion is to increase the residence time function compared to the case where there is no filtration. That is, filtration causes some fraction of particles that enter the bed to become permanently trapped, resulting in a lower fraction of particles escaping the bed. When filtration is very high, essentially all the particles that enter the bed are trapped there. This is equivalent to having a residence time function of one at all times. (When R(t) = 1, 100% of the tracer is still in the bed at

time t, and 0% has returned to the surface.) Variation of the residence time function due to filtration and settling is shown in Appendix 8.1.

3.3.1a Simplification for complete trapping (maxpump model)

When either the settling velocity or the filtration coefficient is very high, essentially all particles that enter the bed are trapped there. In this case, it is not necessary to use the complete residence time formulation. Instead, it can be assumed that no particles leave the bed, and the problem may be simplified to one of simply calculating the flux to the bed. The model based on this approach will be called the maxpump model.

Elliott showed that for the sinusoidal pressure distribution and an infinite bed, the mass transfer for R = 1 is given by

$$M^* = 2\, t^*/\theta \tag{3.92}$$

This is just the maximum exchange rate with the bed. In the normal case, the residence time function has a value between 0 and 1, and the actual exchange is less than the maximum exchange.

Elliott used Equation 3.92 as an approximation for the exchange of a conservative tracer at small times, when no tracer will have penetrated to the point where it can exit the bed (so that R = 1). However, this equation is equally valid in the case where no tracer will leave the bed because it has all been irreversibly trapped (R = 1 always).

Equation 3.92 must be modified to account for the finite bed and particle settling. The maximum flux to the bed is given by evaluating Equation 3.38 for q_p^* using $\bar{v}^*(0)$.

$\bar{v}^*(y^*)$ for solute transport to a finite bed was given in Equation 3.40. Evaluating at $y^* = 0$ gives

$$\bar{v}^*(0)=\frac{\tanh(d_b^*)}{\pi} \tag{3.93}$$

For very small changes in concentration, $q_p^* = \bar{v}^*$. Applying this to Equation 3.41 gives

$$M^* = 2 \tanh(d_b^*)\, t^*/\theta \tag{3.94}$$

For reasonable bed depths, $\tanh(d_b^*)$ will be close to one. Thus, Equation 3.94 is the same as Elliott's equation for solute transport at small times with a correction for the finite bed.

Particle settling results in an increased flux of particles though the bed surface. Particles settle with a velocity v_s^*, and are brought into the bed over one-half of the bedform wavelength. (Particles cannot settle through the bed over the entire wavelength because the settling velocity is negligible compared to the stream flow, and there is only flow into the bed over half the wavelength.) Including particle settling in the velocity distribution for finite beds yields

$$\bar{v}^*(0)=\frac{\tanh(d_b^*)}{\pi} + \frac{v_s^*}{2} \tag{3.95}$$

$$M^* = [2 \tanh(d_b^*) + \pi\, v_s^*]\, t^*/\theta \tag{3.96}$$

As written, Equation 3.96 only applies for small times when $C^* \sim 1$. However, it can easily be applied to larger changes in concentration by including the effect of $C^*(t)$. This

is done by considering a differential form of Equation 3.41, and noting that in general $q_p^* = C^* \bar{v}^*$.

$$\Delta M^* = C^*(t) \, [2 \tanh(d_b^*) + \pi \, v_s^*] \, \Delta t^*/\theta \qquad (3.97)$$

$M^*(t)$ and $C^*(t)$ can then be calculated by a simple finite difference scheme where the current value of ΔM^* is found by using C^* from the previous time step. This is the maxpump model for particle exchange. Recall also that M^* and C^* are related by the system geometry through Equation 3.27.

3.3.2 Exchange of colloids with moving bedforms (clay turnpump model)

The turnpump model for exchange with moving bedforms can be applied to colloids without substantial modification. Obviously, the colloid pumping model described in the previous section must be used instead of the conservative tracer pure pumping model of Section 3.1. In addition, the effects of turnover on colloid transport must be included correctly.

At first glance, it would appear difficult to determine how colloids would behave in the turnover region. Presumably, turnover exchange and filtration are independent, but pumping through the moving bedforms would lead to some difficult-to-quantify amount of filtration. However, this entire question is moot because colloidal particles cannot be *permanently* trapped in the turnover region. Filtration as presented in Section 3.2 only applies to stable deep beds, and attachment of colloids to collector particles is only irreversible as long as the system stays unperturbed. In the turnover region, sediment transport results in all the bed sand grains being periodically scoured and moved by the

stream flow. As a result, colloids attached to those sand grains are subjected to the high-shear conditions of the stream flow, which causes them to become detached and released back to the stream. Thus, colloids cannot accumulate in the turnover region. Again, this leads to the situation where pumping transport to the deep bed controls the ultimate exchange.

It is useful to note that pumping transport of colloids to the deep bed will often result in 100% trapping. Since pumping only occurs at some depth within the bed (below the turnover region), the actual maximum pumping velocity in the combined case will be less than u_m calculated for the pure pumping case. This means that it is more likely that settling will dominate the particle velocity. In this case, or when filtration is very high, anything pumped out of the turnover region will be irreversibly trapped by the deep bed. While conservative tracers continuously mix into deeper layers of the bed, colloids tend to get pumped into a region where they are permanently trapped. The net exchange from the stream is then always controlled by the flux to the trapping region, i.e., below D_{ms}. Thus, the

$$q_p^*(t) = C^*(t)\ \bar{v}^*(D_{ms}) \tag{3.98}$$

In this case, $\bar{v}^*(y)$ is not a function of time since the exchange always occurs at the depth D_{ms}. $\bar{v}^*(D_{ms})$ must also be based on the velocity distribution for particles, given in Equations 3.87 and 3.88. This yields

$$\bar{v}^*(D_{ms}^*) = \frac{\tanh(d_b^*)\cosh(-D_{ms}^*) + \sinh(-D_{ms}^*)}{\pi} + \frac{v_s^*}{2} \tag{3.99}$$

The particle settling velocity can obviously result in a dramatically increased flux to the deep bed. The pumping exchange is then given by

$$M_P^*\left(\frac{t^*}{\theta}\right) = 2\pi \int_{\tau^*/\theta=\lambda^*/\theta U_b^*}^{t^*/\theta} C^*\left(\frac{\tau^*}{\theta}\right) \bar{v}^*\left(D_{ms}^*\right) \frac{d\tau^*}{\theta} \qquad (3.100)$$

This is exactly the same as Equation 3.41 for conservative tracers, except that the effective depth of pumping is always D_{ms} instead of M(t), and settling is included. Filtration is not explicitly included because it is assumed that filtration is sufficiently high to result in complete trapping of colloids pumped to the deep bed. Note that the equivalent penetration depth, M, is now a virtual penetration that includes the actual penetration downwards in the bed and the filtration of colloids by the bed sediment. M will always be a virtual penetration when a tracer behaves nonconservatively because the tracer interaction with the bed sediment must be included when determining the net mass exchange from the stream.

The turnpump model for particles is implemented in a finite-difference scheme exactly as it was for solutes. The only difference is in the pumping mass transfer term, which uses $\bar{v}^*(D_{ms})$ for particles as given by Equation 3.99 above.

Settling causes particles to have a higher rate of exchange compared to conservative tracers. In addition, irreversible trapping due to both filtration and settling allows a much greater reduction of the surface water concentration of colloids compared to conservative tracers. Conservative tracers are limited to a finite dilution due to the geometry of the system. On the other hand, colloids have no such limitation, and tend to

end up either irreversibly filtered to grains of the deep bed or settled onto the bottom of the bed. The experimental results of Chapter 5 clearly show these differences.

4. Experimental Equipment, Materials, and Methods

The experimental part of this work involved simulating a small sand-bed stream in the laboratory, observing the transport of clay in this system, and performing additional preparations and analyses to define all the variables required for modeling. Key features of this work were:

1. the use of a recirculating flume for bed-exchange experiments,
2. use of natural materials and naturally-formed bedforms,
3. control of the chemical conditions in the flume and the surface conditions of all particles,
4. use of a conservative lithium chloride tracer to verify the hydraulics of exchange between the stream and bed, and
5. use of column experiments to quantify the effects of filtration in the bed.

4.1 Flume experiments

4.1.1 Flume description

The flume used for all experiments has a channel 12 m long, 26.5 cm wide, and 25.4 cm deep. A photograph of the flume is given in Figure 4.1. The flume is constructed of steel, and the channel was painted with a chemically-resistant, high-solids epoxy paint. To simulate a stream, sand or other bed sediment is placed in the channel and water is continuously recirculated over the bed. A variable speed pump recirculates water and suspended sediment through a return pipe 10.2 cm in diameter. The entire flume and supporting truss is tiltable to control the slope. Steady, uniform flow can be

obtained in the channel by matching the channel slope with the slope of the energy grade line.

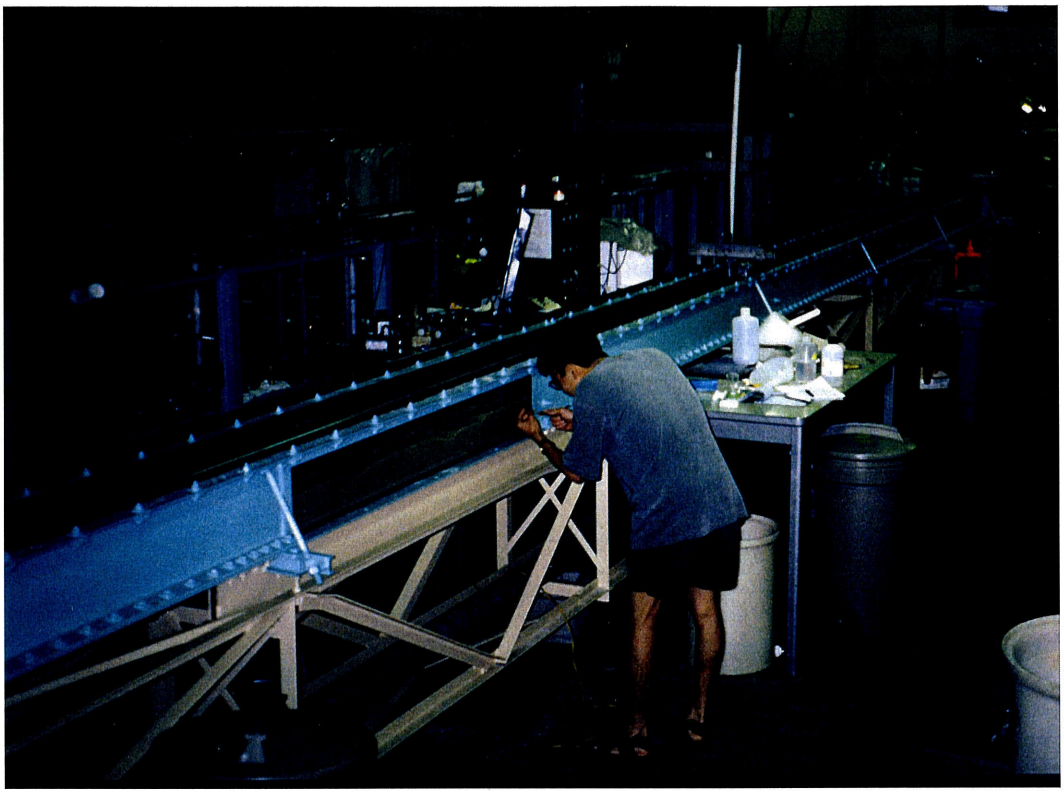

Figure 4.1: Photograph of the recirculating flume used for all experiments.

The flume contains many features which aid in conducting experiments. The recirculated flow with suspended sediment was introduced over a gradual ramp-up to the bed surface to avoid excessive scour in the inlet region. The sand bed was retained in the channel at the downstream end by means of an adjustable-height nylon mesh screen. The objective was to obtain a relatively constant average sand depth everywhere along the flume. Instrument carriages run along rails mounted along the entire channel. The rails

are thus parallel to the horizontal when the flume slope is zero. Typical carriage-mounted instruments are point gauges and laser sensors for distance measurement. The main channel has a glass section (shown in Figure 4.1) to allow visual observation of the conditions in the flume. The return pipe has a lucite section to allow observation of the return flow. The main-channel window has a vertical series of sampling ports with 1 cm spacing to allow water collection by means of a hypodermic needle and syringe. Figure 4.2 is a photograph through the window showing these sampling ports as well as the bedforms present during experiment #10.

Figure 4.2: Photograph through the flume window.

For these transport experiments, the flume was filled with sand and water to simulate a stream. A high-purity silica sand with a geometric mean diameter of 480 microns was used for the bed material. Deionized water was used for the bulk of the experiments, with salts, acids, and bases added to control the pH and ionic strength. Lithium chloride was used a conservative tracer to determine the hydraulic exchange, and a natural kaolinite clay was used as the colloidal tracer for most experiments. The experiment procedure is described in the next section, and all material properties and preparation procedures are provided in Section 4.4.

4.1.2 Description of flume experiment

Each flume experiment involved several distinct parts. First, there was a setup phase which involved bringing the stream, bed, and tracers to the desired physical and chemical conditions for the experiment. Second, the exchange of the conservative lithium ion tracer was observed. Third, the exchange of the colloidal tracer was observed. And finally, some additional "secondary" experiments were often performed, which typically involved monitoring the transport of colloids due to some perturbation of the system.

4.1.2.1 Flume experiment setup

Prior to each bed-exchange experiment, the desired hydraulic and chemical conditions were established. The following physical parameters were controlled: the depth of the stream and stream bed, the stream velocity, the channel slope, and the

bedform geometry and velocity. Chemical parameters controlled were: the pH and ionic strength of both the stream water and colloid suspension. All materials were prepared and/or cleaned according to the procedures described in Section 4.4 prior to their use in flume experiments.

The pH and ionic strength of the stream was controlled for most flume experiments. The first five experiments used tap water, without any modification. Later experiments used deionized water from the Caltech supply. A large tank was used to prepare the deionized water prior to its introduction to the flume. NaCl was added to the water in the tank to raise the ionic strength to the desired level, while HCl or NaOH was used to alter the pH. The bed sand and colloidal tracer were brought into equilibrium with water of the same composition prior to the experiments. pH adjustment of the particle surfaces required a long preparation time due to slow buffering. Clay suspensions were stirred in a one- or two-liter flask with acid or base added over several days. Sand was soaked in water of the appropriate pH in large storage buckets; in some cases additional pH adjustment was also done in the flume. Once the stream pH and ionic strength were established, they remained unchanged throughout the entire experiment.

Prior to each experiment, the channel slope was set to yield approximately uniform flow for the desired stream depth and velocity. Water and sand were then loaded into the flume in a defined fashion in order to develop a packed bed without any air pockets. Stream water was pumped in first, to approximately the desired bed depth. Then the presoaked sand was scooped into the flume by hand, to yield a relatively even

(but not smooth) bed of the desired depth. That is, sand was added in equal volume over the entire channel length, but no effort was made to smooth out the sand. Then additional water was added until the desired stream depth was achieved. Typically, the bed depth was 8-11 cm, and the stream depth was approximately 10 cm. These values were limited by the overall channel depth of 25.4 cm.

At this point the flume pump was turned on, and the stream was recirculated at the desired rate until a regular series of bedforms developed under uniform flow. For the bed exchange experiments, it was necessary to have an equilibrium state where the stream surface is parallel to both the average bed surface and the channel bottom. From an energy standpoint, this is obtained when the gravitational potential given by the channel slope exactly matches the frictional loss, which is dominated by the bedform shape roughness. The interaction between the stream velocity and sediment transport causes the bed to adjust its slope and roughness in response to changes in the stream flow. Sediment transport tends to produce uniform flow over time since there is more transport in regions of higher velocity and lower depth, resulting in net scour from regions of higher velocity and net deposition to regions of lower velocity. In the flume, this means that the sand bed will tend to develop a slope equal to the energy grade line, even if this is different from the channel slope. What is then required is to match the energy grade line and the channel slope.

In this flume setup, either the channel slope or recirculation flow rate was adjusted to obtain the uniform flow condition. One to three adjustments were typically necessary. After each adjustment, the flume had to be run for a sufficiently long time for the

bedforms to reach a new equilibrium. Then it was determined if the stream was in the desired uniform flow condition, or if further adjustment was necessary. The overall process of obtaining steady, uniform flow required at least 12 hours, and sometimes took several days. Slower stream velocities required longer setup time, because it took longer to establish a stable bedform pattern after each adjustment.

Experiments were performed with both moving and nonmoving bedforms. For moving bedforms, uniform flow with sediment transport was established as described above and then maintained throughout the course of the experiment. This resulted in the continuous production, motion, and disappearance of bedforms during the course of the experiment. While the individual bedforms changed, their average height, wavelength, and velocity remained the same throughout the experiment. For nonmoving bedform experiments, a series of bedforms was developed in uniform flow, and then the recirculation rate was reduced so that sediment transport no longer occurs (stream velocity less than 20 cm/s for the sand used). Thus, one series of bedforms was kept in place along the flume for the entire experiment.

4.1.2.2 Exchange experiment

The transport experiment was composed of two separate phases: exchange of a conservative tracer, and exchange of a colloidal tracer. The procedure for the two exchange portions of the experiment was exactly the same, except for the preparation required for the different tracers and the analysis method for the different tracer samples.

The experimental procedure is presented in this section, while sampling methods are described in the next section.

Lithium was used as a conservative tracer in order to quantify water exchange with the bed. Lithium was used as a tracer because it does not react with the particle surfaces, is not present in the water supply, and could be used in extremely low concentrations. After the hydraulic conditions were established in the flume, around 4 L of flume water was removed for use in sample preparations. The tracer solution was prepared by dissolving LiCl into 1-2 L of this reserved flume water in a flask. About 1 g of LiCl was used to provide an initial Li^+ concentration of 30-50 μM in the recirculating water of the flume.

To start the experiment, the tracer solution was poured into the flume over one recirculation period. This resulted in the entire volume of recirculating water (500-600 L) being rapidly brought to approximately the same lithium concentration. Ideally, if the tracer were added uniformly to the stream water over exactly one recirculation, the stream would all have an initial Li^+ concentration C_0, and the bed would all have an initial concentration of zero. However, the practical details of adding the tracer solution to the flume result in a spatial variation of concentration from the initial average C_0. In particular, it was difficult to add the tracer over exactly one recirculation, and practically impossible to achieve complete mixing during tracer addition. These factors were controlled somewhat by estimating the recirculation time and adding the tracer over exactly that time, and by adding the tracer to the downstream end-well to take advantage of mixing due to the pump impeller. Another deviation from ideality is that bed

exchange begins even before the entire stream attains the initial concentration. As a practical matter, these difficulties caused scatter of the data at early times, and some difficulty in estimating the actual C_0 from experimental data. The initial tracer concentration was typically uniform within ±20% (some experiments showed <5% variation, and the worst was ±50%). The initial nonuniformity decreases relatively rapidly over time, and the experimental data indicate that the stream water generally became reasonably uniform (±10%) within 15 minutes of the tracer addition, and was always well mixed within 40 minutes. Experiments with a greater degree of initial uniformity or a higher recirculation rate took less time to achieve a uniform tracer concentration in the stream water.

After the initial addition phase, the flume water continually flows over the bed resulting in the exchange of lithium-bearing stream water with pore water. The lithium concentration of the stream water then decreases due to dilution with pore water. The change in concentration of the stream water was observed over time, in order to provide a basis of verification of the exchange model. The pore-water profile of lithium at a specific location in the bed was also obtained at several different times during the experiment. Lithium exchange was monitored for 24 hours, though the bulk of the exchange generally took place in the first 6-12 hours. Typically, stream water samples were taken every few minutes initially, then every 10-15 minutes for the first hour, then every half-hour for around two hours, then every hour or two for around eight hours. Later samples were taken at intervals ranging from 4-12 hours. Eventually, net exchange ends because the pore water and the recirculating water reach the same lithium concentration. The ultimate

dilution can be calculated by a simple mass balance based on the volumetric reservoirs of water in each part of the system.

$$\frac{C_f}{C_0} = \frac{\textbf{volume of recirculating water}}{\textbf{total volume of water in flume}} = \frac{d'}{d'+\theta d_b} \qquad (4.1)$$

The flow depth (d) and the bed depth (d_b) were each usually in the range 8-10 cm. d' is the total volume of recirculating water (including end-wells and return pipe) per unit bed area. d' was typically 15-17 cm. Thus lithium was typically diluted to around 85% of its initial concentration. Dilution to the ultimate value was almost always observed in the 24 hours of sampling. In the experiments with the highest exchange rates, complete mixing required just 6-8 hours.

After the lithium-tracer portion of the experiment, kaolinite was added to the flume in slurry form, again over one recirculation, and the kaolinite transport to the bed was observed. The kaolinite tracer suspension was prepared by diluting a "stock" kaolinite suspension with approximately 2 L of reserved stream water, and then stirring overnight. This stock suspension was developed through the preparation procedure described in Section 4.4.3, and subjected to pH and ionic strength adjustment as described in Section 4.1.2.1. The dilution with flume water corrects for minor deviations between the composition of the flume and stock waters by allowing the clay to come into equilibrium with stream water prior to introduction into the flume. Stirring provides for the break-up of clay flocs which may have formed in the high-concentration stock suspension. For most experiments, 90-100 g of clay was added to the flume, resulting in

an initial clay concentration of around 200 mg/l. Lower initial concentrations were also used.

The kaolinite suspension was poured into the downstream end-well over one recirculation period, exactly as the lithium solution was. Initial mixing of kaolinite was clearly visible: at 200 mg/L the flow was milky-white, but eddies of clear water could be observed for a few minutes after clay addition. The clay concentration of the stream water was monitored for 24 to 48 hours. Pore water profiles were also measured at several different times during the experiment. Unlike lithium, clay does not mix conservatively. The clay concentration is reduced in excess of dilution, indicating that there are some trapping processes (filtration and settling) for colloids in the bed. Nonmoving bedform experiments were typically run until essentially all clay had been trapped by the bed. In this case, the stream water was observed to go from a milky-white opaqueness at the start of the experiment back to a colloid-free clear state.

Following the primary colloid transport part of the experiment, some secondary experiments were performed in order to observe the effect of some perturbation on clay transport. It was convenient to use the already-set-up flume to investigate some additional effects besides the main bed-exchange experiment. These secondary experiments included: increasing or decreasing the recirculation rate, adding more clay to the recirculating water, and replacing the clay-bearing surface water with clay-free water. Following the perturbation, the stream water clay concentration was observed for 12-24 hours.

The entire flume experiment can be summarized as follows:

Prior to Experiment:

- prepare flume water supply with correct pH and ionic strength
- bring sand into equilibrium with water of correct pH
- prepare clay suspension with correct pH and ionic strength

Day 1:
- fill flume with water and sand
- establish uniform flow with stable bedforms (sometimes requires additional day or two)

Day 2:
- prepare lithium chloride tracer solution and add to flume (early)
- observe lithium transport to bed (i.e., measure time-series of lithium concentration in stream water; at several times, obtain profiles of lithium concentration in the pore water with depth in the bed)
- measure stream and bedform parameters (noninvasive)
- prepare clay suspension, stir overnight

Day 3:
- take final lithium sample (early)
- add clay to flume
- observe colloid transport to bed (same procedure as for lithium)

Day 4:
- continue to observe colloid transport to bed
- initiate secondary experiment, if desired

Day 5:
- continue to observe colloid transport for primary or secondary experiment, if necessary

After Experiment:
- measure bedform parameters, bed elevation profile (invasive)
- analyze samples

4.1.3 Data collection

4.1.3.1 Stream and bed parameters

The recirculation flow rate was measured by means of a Venturi meter in the return pipe. A water-air manometer was used to measure the head difference across the Venturi meter. The average stream velocity was simply calculated by dividing the recirculation flow rate by the average stream cross-sectional area.

Stream and channel slopes were measured using a point gauge attached to the carriage which runs along the flume rails. Profiles of y-position of the water surface vs. x-position measured with the point gauge along the flume give a slope relative to the slope of the flume. A point-gauge profile for perfectly still water was used as a reference for the horizontal. By expressing elevation measurements in terms of the deviation from the still water level, the true channel slope, the water surface slope, the energy grade-line

slope, and the average bed slope can all be found. The average bed slope was obtained after the experiment by leveling the bed in 1 m sections, and then measuring the y-position of each section. The stream depth was also calculated from point gauge readings.

The stream temperature was determined by a thermometer mounted in the downstream end-well. Stream pH was measured by a portable pH meter (Radiometer PHM80 with Beckman Futura Plus combination electrode) mounted on an instrument carriage. pH was measured just upstream of the downstream end-well, in order to provide sufficient flow past the probe while avoiding any disturbance of the bed.

Bedform parameters (height, wavelength, velocity) were usually obtained by visual and point gauge measurement. Bedforms can be viewed in two ways: from above the channel, and through the viewing window. It was much easier to view the bedforms through the window, but typically only 3-4 bedforms could be seen through the window at any time. Thus bedform height and wavelength were estimated by measurements made both through the window and from above the channel. Bedform height and wavelength could be measured visually through the window simply by use of a ruler. Bedform velocity was determined by recording front positions visible in the window vs. time. Bedform wavelength could be determined from above simply by noting the crest positions along the flume. Bedform heights were measured by point gauge. Point gauge measurements were somewhat limited because they could only be obtained when the flume was not running, and because they resulted in some disturbance of the bed.

For nonmoving bedform experiments, the height and wavelength of all bedforms were measured at the end of the experiment. In this case, window observations were not used. For moving bedform experiments, many different bedforms progressed through the window region, so visual observations through the window were the primary data set for all bedform parameters. Additional data were collected along the flume at the end of the experiment.

In later experiments, a laser profiler (Keyence LB-1101) was used to gather bed surface data automatically and noninvasively. This device emits a laser beam and then measures the light intensity returned when the beam strikes a target. The reflected light produces a voltage signal which is calibrated to position, with an accuracy of ~10 μm. The laser profiler was mounted on an instrument carriage driven by a stepper motor, as shown in Figure 4.3. To avoid reflection from the water surface, the profiler was housed in a waterproof box with a glass bottom, which was then lowered into the stream. The laser was positioned 10 cm from the average bed position, and the underwater housing projected another 4 cm downward. The profiler could not be used with running stream water, because flow around the box would result in local scour of the bed. Both the laser and the stepper motor were interfaced with a computer, so that profiles of y-position vs. x-position could be obtained automatically. By means of this device, a bedform profile was obtained on a line down the flume, with measurements every 6 to 12 mm. Bedform heights and crest-to-crest wavelengths were determined by manual analysis of the data. Visual and point-gauge estimates of bedform height and wavelength agree well with laser profiler results. (See Appendix 8.2 for a comparison of data from one experiment.)

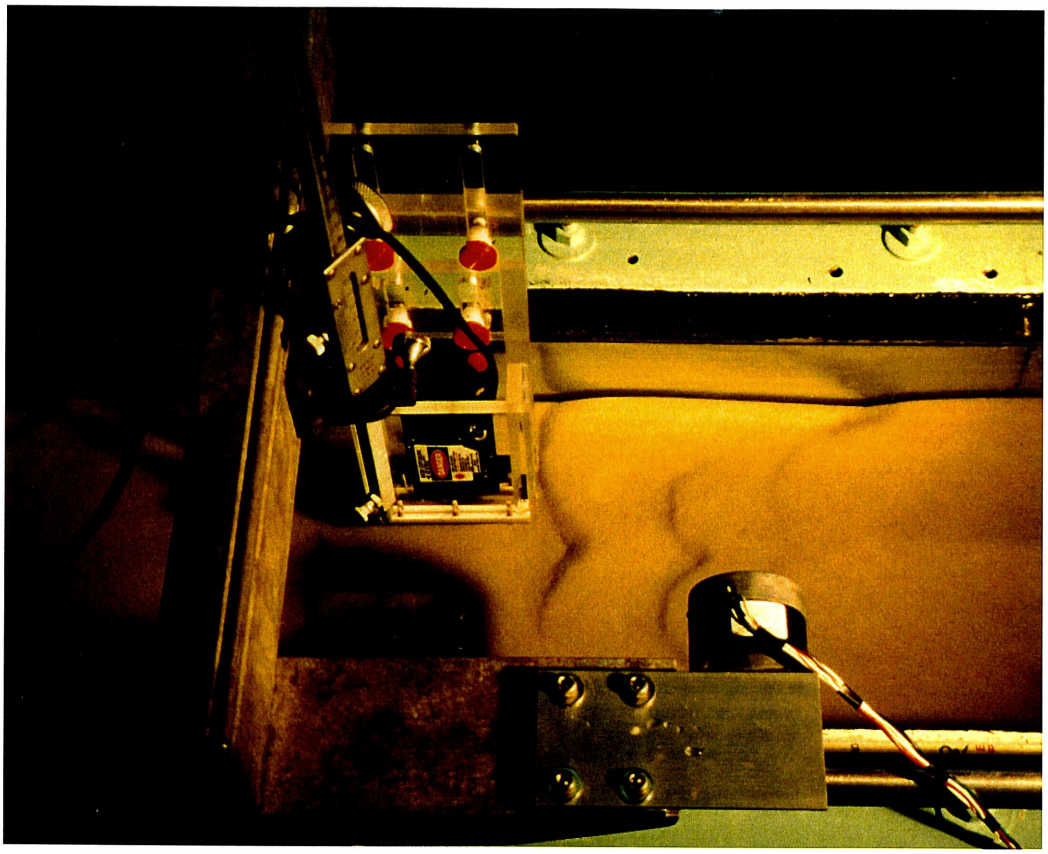

Figure 4.3: Laser bed profiler. The laser and photoreceptors are contained in the small black box. The stepper motor, visible to the right, uses a rubber wheel (hidden under the metal mounting plate) to drive the carriage.

4.1.3.2 Tracer samples

The main data set for the flume experiments is a time series of the stream-water concentrations, which decrease over time showing the net exchange of tracer between the stream and the bed. The stream-water concentration of any tracer can be determined from a simple test-tube grab sample of the recirculating water. One sample from anywhere along the flume is sufficient to characterize the entire volume of recirculating water at any particular time. Because the flume recirculation time (1-2 min.) is orders of

magnitude faster than the characteristic bed-exchange time (hours), the stream is essentially well-mixed in the entire recirculating portion of the flume. (Exception: if a tracer is added to the stream nonuniformly, it will require several minutes to become well-mixed.) While the stream-water concentration decreases over time, it does so slowly and uniformly.

As mentioned previously, some downstream variation in concentration was observed early in the experiment due to nonuniform tracer addition. For later experiments, this problem was addressed through use of volume-averaged stream-water samples. For the first 5-10 minutes after tracer addition, the stream water was continuously collected by repeated grab-sampling into test tubes. Each test tube was slowly allowed to fill, so that each tube then contained water which had flowed past the sampling location over a period of around 1 minute. The data collected by this method showed much less scatter than that obtained by simple grab-sampling.

A secondary data set is pore-water concentration profiles, derived from samples collected at 1 cm intervals in the bed through the sampling ports shown in Figure 4.2. A hypodermic syringe was used to collect 1 mL of pore water through each port. The needle tip was placed at different horizontal penetration lengths into the bed to avoid interference of successive samples. The penetration length was alternated between ~3 cm and ~6 cm. Pore water samples were diluted with tracer-free stream water to 5 mL for analysis.

These profiles show the penetration of tracer at a specific location in the bed, as opposed to the overall transport to the whole bed. Thus they can be used qualitatively to

show zones of transport or trapping, or to support general arguments about the mechanisms of penetration in the bed. It is difficult to draw general conclusions from the pore-water profiles because they are dependent on the stream geometry near the location of the sampling ports and may be influenced by their proximity to the sidewall. Profiles are more useful for analysis of moving-bedform experiments, because the sampling ports are exposed to the entire range of bedforms in this case.

4.2 Column experiments

Column experiments were used to measure the filtration of the tracer colloids by the bed sand in the absence of the complex hydrodynamics present in the flume. Also, because column experiments took much less time than flume experiments, the column provided a convenient way to investigate the influence of different chemical conditions. Thus, besides providing the filtration coefficient for input in the bed-exchange model, column experiments were also used to select the conditions for future flume experiments.

4.2.1 Column apparatus

The column used for these experiments was simply an open glass tube with a bottom end-cap and mesh for retaining the sand. Two different glass columns were used--initially a column with a one inch (2.54 cm) internal diameter was used; later experiments were done with a two inch (5.08 cm) column. Rinse water and colloid suspensions were pumped out of storage flasks into the column by means of a peristaltic pump. Input suspensions were continuously stirred to ensure that they had a constant

concentration. Column effluent was simply collected into a beaker. Flow through the column was driven by gravity, and the rate of flow was controlled by means of a stopcock in the effluent line. A water column was always maintained above the sand filter. Figure 4.4 is a photograph of the column setup.

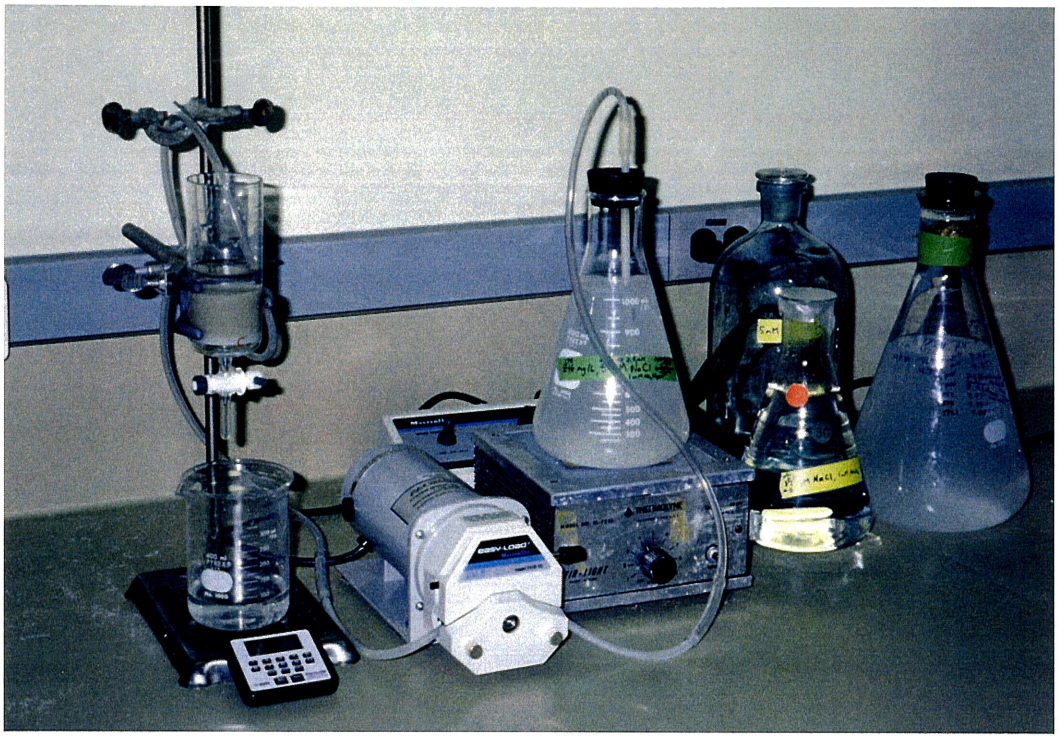

Figure 4.4: Column experiment apparatus.

4.2.2 Column experiment description

All the column experiments were for clean-bed filtration. That is, they involved pumping a colloidal suspension through a previously-clean sand bed and obtaining a breakthrough curve where the steady effluent concentration was less than the input concentration. The materials, preparations, and chemical conditions for column experiments were the same as for flume experiments. In addition, the velocity for column

experiments was selected to be similar to the advective velocity of the pore water in the flume. The bed depth, typically around 3 cm, was selected to give a reasonable reduction in concentration due to filtration over the length of the column.

4.2.2.1 Column experiment setup

Prior to the column experiment, the colloid and sand were brought into equilibrium with water of the desired pH and ionic strength. The procedure was essentially the same as that used for flume experiments. pH adjustment of sand for column experiments was done in plastic bottles. The clay suspension was prepared by diluting stock clay suspension in approximately one liter of water with the correct ionic strength, and then adding HCl or NaOH for pH adjustment. pH adjustment again took several days.

The column was loaded with sand in a manner similar to that used in the flume. First, the column was filled with water at the correct pH and ionic strength, with the outlet stopcock shut off to retain water in the column. Then sand was slowly poured into the column so that a packed bed developed without air pockets. The column was filled to the desired bed depth, and then tapped lightly to develop a flat upper bed surface. At this point the stopcock was opened so that the rinse solution flowed through the column. Additional fresh rinse water was pumped into the column to make up for the outflow. Several pore volumes of rinse water were then flushed through the column. During this period, the flow rate through the column was set to give the desired pore water velocity.

The flow rate was determined simply by measuring the volume of effluent collected during a defined period of time.

Just prior to the start of the actual filtration experiment, a spectrophotometer (HP model 8450 or 8451) was referenced to the rinse water effluent, and the absorption of the colloid suspension was measured (to determine the input colloid concentration).

4.2.2.2. Filtration experiment procedure

To begin a filtration experiment, the remaining rinse water was allowed to drain down until there was a minimal amount of water column left (~1 cm), and then the colloid suspension was pumped into the column. The clay suspension was initially added at a slightly higher rate than the flow rate through the column in order to build up a larger head reservoir (~5 cm), and then reduced to again match the column flow rate. The presence of the water column meant that there was some difficulty in defining a start time for the filtration experiment, since some time was required for the colloid suspension to mix with the rinse water left in the column. This was deemed acceptable, however, because the only experimental parameter of interest was the ratio of the final, steady-state effluent concentration to the input concentration.

Sampling began after the suspension was pumped into the column. Column effluent was collected directly into a spectrophotometer cuvette and immediately analyzed. For the 1-inch diameter column, it typically took 20-60 seconds to accumulate the 2-3 ml required for analysis. This sample volume was about 1/2 of a pore volume, which resulted in a lack of precision in the concentration vs. time data. This motivated

the switch to the 2-inch column, which had four times as much pore volume for the same bed depth, and used a proportionately faster flow rate. Samples were initially collected once every minute, and the sampling rate was gradually decreased over time. The filtration experiment was typically run for 20-25 minutes.

The effluent flow rate was monitored during the experiment, again by measuring the accumulated effluent volume. Accumulation of filtered colloids during the course of the experiment sometimes resulted in plugging of the filter and an associated decrease in both the flow rate through the column and the effluent colloid concentration. In this case, the initial plateau of effluent concentration was used to calculate the filtration coefficient. In early experiments, this flow rate decrease was simply measured, but no steps were taken to correct for it. In later experiments, the stopcock was opened to maintain the original flow rate. The effluent pH and the concentration of the input suspension were also measured at least one more time during the experiment (typically at the end).

4.3 Data analysis

4.3.1 Lithium

Lithium concentrations were determined by ICP-MS (Perkin-Elmer Elan 5000) which allowed the use of extremely small initial concentrations (30-50 μM). It was important to have a low tracer concentration in order to avoid significant changes in the stream water chemistry and the associated clay surface properties. Lithium samples taken from the flume were immediately acidified with a few drops of 2% HCl. They were

typically stored for a day or two, then analyzed on the ICP-MS. The instrument was calibrated by preparing reference solutions of known lithium concentration with the same background water composition. Drift was sometimes a problem during analysis, requiring frequent remeasurement of one of the known concentrations. Beginning with experiment #11, all data have been drift-corrected by comparison with the slope of the reference concentration data vs. time.

4.3.2 Colloids

Colloid concentrations were measured with a spectrophotometer (HP model 8450 or 8451). Particle concentration was calibrated to the absorbance at a wavelength of 500 nm. This method was found to be very quick and reliable, with a linear calibration up to a concentration of 250 mg/l. Samples were typically stored for 1-2 days before analysis. Simple shaking was sufficient to disperse stored samples. It was verified that this handling procedure did not change the sample absorbance. (But samples left for many weeks would form a compact layer of particles on the bottom which would impair analysis.) A Coulter Counter was also used to determine concentration, but the results were found to be very sensitive to the presence of a few colloid grains of the largest size class in the sample. This was especially a problem because flume samples had to be diluted by a factor of 30-100 in order to be analyzed with the Coulter Counter.

The Coulter Counter was used to measure the size distribution of the colloids used in the experiments. Coulter Counter is a good instrument to measure clay sizes since it actually classifies particles according to volume. Sizes are reported as spherical-

equivalent diameter, and they actually correspond to clay particles with a volume equal to a sphere of that size. Thus the instrument does not introduce any errors due to the non-spherical nature of clay particles. Particle size distributions are presented in Section 4.4.3, colloid properties.

4.4 Materials: properties and preparations

4.4.1 Water supply

Pasadena tap water was used for the first five flume experiments. Initially, this was the only water available in sufficient quantity to fill the flume. Pasadena tap water has a highly variable composition due to seasonally-dependent blending of different water supplies. Water used for flume experiments had pH in the range 8.0-8.3, and an ionic strength on the order of 15 mM. Major cations in Pasadena water are calcium (average concentration ~1.5 mM), magnesium (~1 mM), and sodium (~3 mM). Tap water was found unacceptable because it severely limited the range of particle-particle interactions that could be investigated. In particular, the presence of multivalent ions at millimolar concentrations reduces clay particle repulsive forces the extent that they will readily coagulate or become attached to other kinds of particles. (Van Olphen, 1977)

Deionized (DI) water was used for later experiments. To provide a sufficient supply of DI water, a direct connection to the Caltech DI supply was brought into the hydraulics lab, and plumbed to a 1000 L tank near the flume. This tank was then used to prepare water of any desired composition. NaCl was added to the tank for ionic strength adjustment, and HCl and NaOH were used for pH adjustment. The baseline chemical

condition for flume experiments was pH 7 and ionic strength 5 mM. Additional experiments were run with ionic strength down to 0.5 mM, and pH as high as 8. (Column experiment results indicated that it was not useful to do flume experiments at high ionic strength or low pH, because the colloid behavior at these conditions was similar to that at the baseline conditions. See Section 5.2 for column experiment data.)

4.4.2 Sand

4.4.2.1 Description

The sand used in all experiments was supplied by U.S. Silica from the well-known deposits in Ottawa, Illinois. This sand is commonly used in laboratory experiments because of its high purity, as shown in Table 4.1.

mineral	% mass
SiO_2	99.810
Al_2O_3	0.042
Fe_2O_3	0.015
TiO_2	0.013
MgO	< 0.01
CaO	< 0.01
other	0.10

Table 4.1: Manufacturer's chemical analysis of Ottawa sand.

The sand was graded by the manufacturer into different size classes. The "F30 Flintshot" size (also known as "3.0 Flintshot," "Ottawa 3.0," or "Ottawa 30") was selected for these experiments. The results of a sieve analysis are given in Figure 4.5. This sieve analysis indicates that the sand has a d_{50} of 500 μm, a geometric mean diameter of 480 μm, and a

geometric standard deviation of 1.2. Eylers (1994) measured the porosity and permeability of this sand and found $\theta = 0.325$ and $K = 9.0$ cm/min.

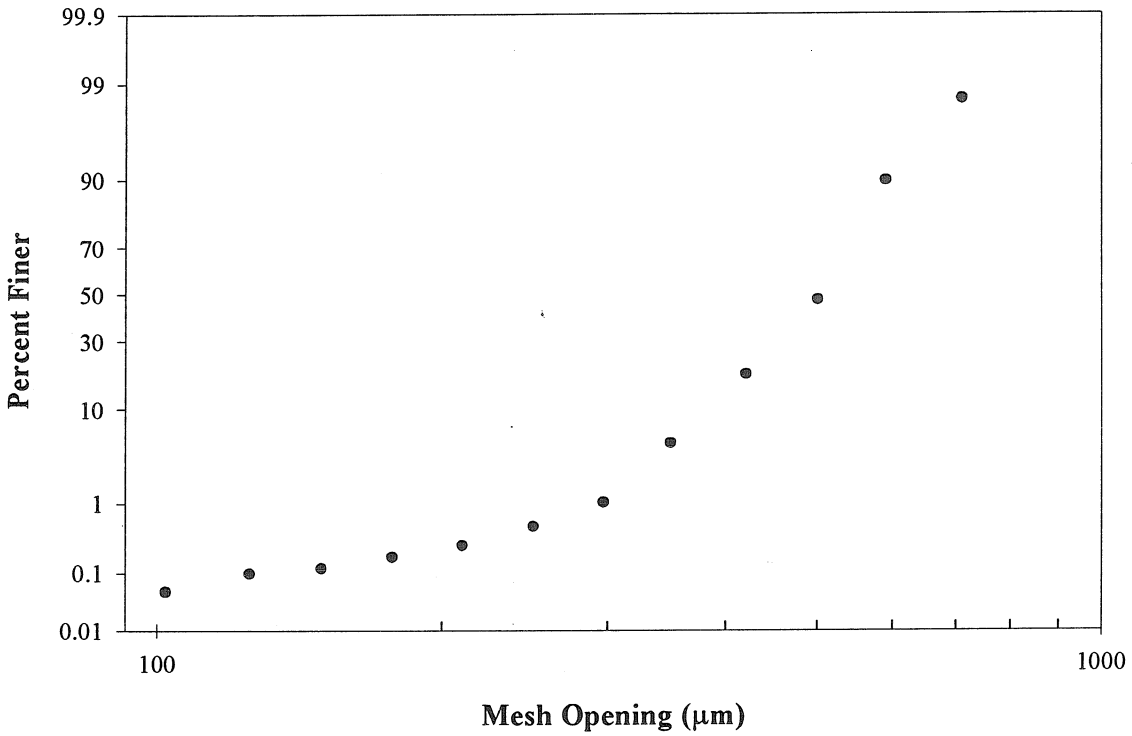

Figure 4.5: Sieve analysis of Ottawa F30 Flintshot sand, plotted as a cumulative size distribution on a log-probability plot. This sand has a log-normal size distribution with a mean diameter of 480 μm and a geometric standard deviation of 1.20.

4.4.2.2 Cleaning procedure

The sand was cleaned before each experiment in order to desorb contaminants and remove attached colloids. Cleaning was accomplished by fluidizing the sand in an upflow washing apparatus, shown in Figure 4.6. The sand washer was composed of a storage reservoir, pump, in-line filter, inlet manifold, washing tubes, and return tubing. The sand was actually washed in six lucite tubes, each 6 inches in diameter and 3 feet

high, with mesh at the bottom to hold the sand in place. The cleaning solution flowed in through the bottom of the tubes, around a flow-straightening cone, and up through the sand causing relatively uniform fluidization. The washing tubes were removable for easier loading and unloading, with a waterproof o-ring connection locking each tube into a permanent base. A large tank (~200 L) was used as a reservoir; the cleaning solution was prepared directly in this tank. A 5 μm cartridge filter was placed in the recirculation line in order to remove colloids and other fines. Even though this filter was nominally not small enough to remove all clay, multiple passes provided complete filtration.

Deionized water of the appropriate pH was used for sand washing (Litton and Olson, 1993; Eylers, 1994). Basically, the pH of the cleaning solution was controlled in order to cause desorption or detachment of contaminants from the sand surface. Low pH was used to desorb metal ions that may have accumulated on the sand. High pH was used to induce electrostatic repulsion to detach clay colloids from the sand surface. The high shear induced by the upflow washing also contributed to detachment of colloids.

The exact procedure used before each experiment was:

Step 1: an initial rinse with deionized water (to remove free fines and scum)

Step 2: acid wash for several hours with HCl solution at pH ~ 3.5

Step 3: an intermediate rinse with deionized water

Step 4: base wash overnight with NaOH solution at pH ~10.5

Step 5: a final rinse with deionized water

Step 6: removal of washed sand to storage bins.

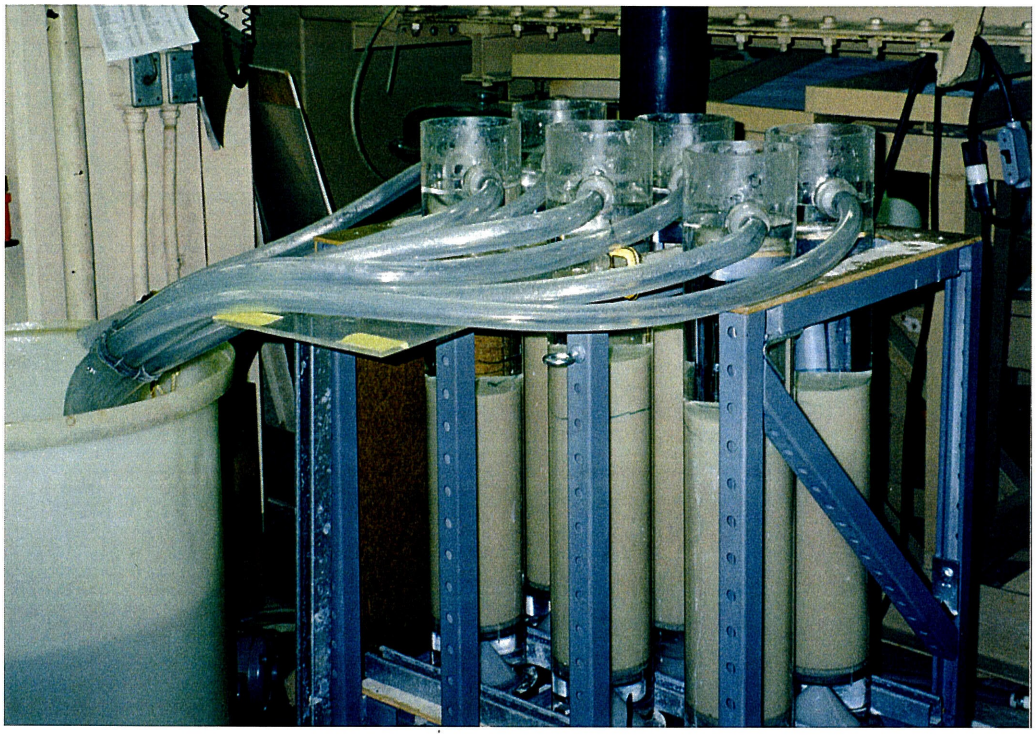

Figure 4.6: Sand washing apparatus.

The storage tank and all tubing were completely drained after each step. In addition, the cartridge filter was checked once every washing cycle to determine if it had become plugged.

New sand (i.e., direct from the manufacturer) was subjected to this same procedure, except that each cleaning step was done for a considerably longer period of time (typically 2-3 days). Previously unwashed sand contained a large amount of fine material, presumably silica flour, which had to be removed.

Large volumes of sand were cleaned using this setup. Typically, around 40 kg of sand were washed each day in order to provide the 400 kg required for every flume

experiment. Obviously, this limited the type of cleaning that could be performed. Litton and Olson noted that simple acid washing was insufficient to remove all contaminants from particle surfaces. However, their recommended procedures could not be used due to the volumes of sand and water required for flume experiments. The acid/base washing procedure described above was selected because it is sufficient to restore the sand surface to a similar condition before every experiment. While this level of cleaning may not remove all contaminants, perhaps precluding direct comparison of filtration data with other researchers' results, it is sufficiently reproducible to allow comparison of results from different flume and column experiments.

4.4.3 Clay

4.4.3.1 Clay composition

The kaolinite used for these experiments was purchased from Ward's Natural Scientific; the source of this material was the well-known deposits in Georgia. The kaolinite composition was verified by a combination of SEM, electron microprobe, and XRD. SEM/microprobe showed that this clay was composed primarily of kaolinite particles with a few larger grains of other minerals (feldspar, silica, etc.). The raw kaolinite particles were aggregated in some fashion, typically with a 'stacked sheet' geometry. Most conglomerate clay particles had a largest dimension less than 30 μm, but stacks up to 100 μm long were observed. All non-clay particles were on the order of 100 μm. A photomicrograph of the kaolinite is shown in Figure 4.7. XRD indicated that some titanium was present in the kaolinite, which is consistent with the literature (Jepson

and Rowse, 1975; Newman and Brown, 1987). The measured composition of one Georgia kaolinite is given in Table 4.2.

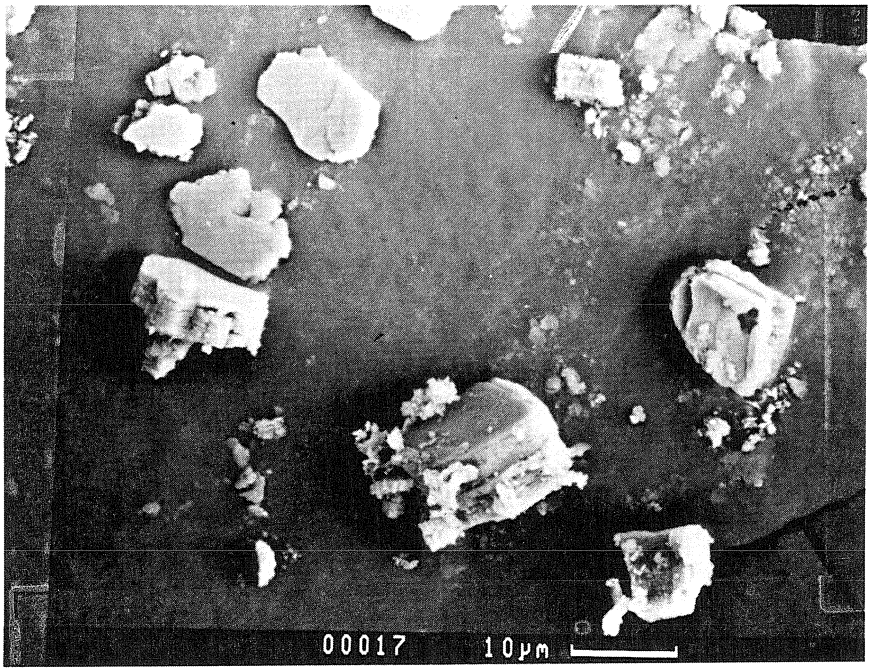

Figure 4.7: Photomicrograph of kaolinite used for these experiments. The clay shown had been ground by hand, suspended in tap water, and dried onto a SEM sample stage.

mineral	% mass
SiO_2	45.2
Al_2O_3	39.2
TiO_2	1.21
Fe_2O_3	0.17
MgO	0.08
CaO	0.06
Na_2O	0.03
K_2O	0.02
H_2O^+	13.3
other	0.7

Table 4.2: Composition of kaolinite from Washington County, Georgia (after Newman and Brown, 1987). This corresponds to a 2.3% substitution (by number) of aluminum into the tetrahedral silica layer, and a 2.5% substitution of titanium, iron, etc., into the octahedral aluminum layer.

4.4.3.2 Preparation procedure

The "raw" kaolinite obtained from the manufacturer came in chunks on the order of a few centimeters in diameter. This clay had to be prepared in a defined fashion to ensure that the tracer introduced to the flume always had the same size distribution and chemical properties. This was accomplished by grinding the clay and converting it to a sodium-kaolinite.

A mortar and pestle was used to break up the clay chunks into a powder. Further grinding was done in a roll-mill of our own design. Roll-milling involved tumbling the clay in a container with a grinding agent. The container was made of high-density alumina, and the grinding agent was 1 cm diameter balls of the same material (the container and balls were purchased from Paul O. Abbe, Inc.). Roll-milling was used to break up the clay because it is a relatively gentle milling method. Impacts of the alumina

balls in the roll-mill should not have sufficient energy to break individual crystals. Thus, roll-milling should separate aggregated clay particles, but not break up individual clay platelets or non-clay particles.

Following roll-milling, the clay was wet-sieved to remove particles larger than 45 μm. This was done principally to separate non-clay particles, but also to remove clay aggregates that had not been sufficiently broken down. Typically, only a small amount of material was removed in this step.

After sieving, the clay was converted to a homoionic sodium-kaolinite by ion exchange. This was done by stirring the clay in a 2 M NaCl solution for two days. The high concentration of Na^+ in this solution displaces all other cations on the kaolinite surface. Deionized water was used to prepare the ion exchange solution. Typically, several hundred grams of clay were ion exchanged at one time, in about 5 L of solution.

At the end of ion exchange, the clay remained suspended in the extremely high ionic strength NaCl solution. The excess salt then had to be removed from the clay suspension. This was accomplished by repeatedly settling the clay, removing the salt water supernatant, and resuspending the settled clay in DI water. Several rinsings of this type were required, because it was impossible to dewater the settled clay--typically only 80-90% of the water could be removed in each cycle. The large volume of clay processed made it impossible to use a centrifuge, so the clay was simply allowed to settle in the same container that had been used for ion exchange. Clay aggregation is controlled by ionic strength, so that the clay settling time was inversely dependent on the remaining salt concentration (van Olphen, 1977). The clay typically took a few hours to settle in the

2 M solution, and the rinsing cycle was repeated until settling required several days. At this point, the NaCl concentration had dropped to less than 10 mM. The clay was then stored in this solution until used for an experiment, at concentrations of 200-300 g/L.

The kaolinite preparation procedure is summarized as follows:

Step 1: break up "raw" blocks of clay with mortar and pestle

Step 2: grind clay in roll-mill for 2 days, or until all clay is a very fine powder

Step 3: wet sieve clay to remove large particles (sieve #325, 45 μm mesh opening)

Step 4: convert all clay to homoionic form by stirring in 2 M NaCl for 2 days

Step 5: wash clay to remove excess NaCl

5a: settle clay

5b: pour off supernatant, resuspend settled clay in tap DI water

5c: repeat until clay no longer settles quickly (typically required 4-5 rinses); "quick" settling = hours; "slow" settling = days

Step 6: Store clay in tap DI water with some residual NaCl concentration (<10 mM)

4.4.3.3 Clay size distribution

The size distribution of the colloids used in flume experiments is very important, as it indicates the relative importance of settling as a particle transport mechanism. In addition, the size distribution is dependent on chemical parameters such as pH and ionic strength. As a result, the kaolinite size distribution was measured both for flume samples and stirred suspensions under different chemical conditions.

Figures 4.8 and 4.9 show the variation of the size distribution due to pH at an ionic strength of 5 mM. There is a trend to have fewer particles in larger size classes at higher pH. This is probably the result of higher electrostatic repulsion as the particles become more negative. A similar trend is not observed at low pH because of permanent negative charges due to substitution in the clay structure. Figures 4.10 and 4.11 show the size distribution at ionic strengths of 0.5 and 50 mM (due to NaCl), at a pH of 7.2. Ionic strength should not change the size distribution for NaCl concentrations less than 10 mM. Higher ionic strengths should result in coagulation of the kaolinite and a coarsening of the size distribution. This effect was observed to some extent for an ionic strength of 50 mM. Additional coagulation could have been inhibited by the stirring of the suspension.

Flume experiments were conducted with the prepared water supply over a narrower range of chemical conditions than were used to investigate the clay size distribution (pH: 6.8 - 8.2, ionic strength: 0.5 - 5 mM). As a result, one average particle size was used to characterize the clay in all these flume experiments. Based on the distributions shown in Figures 4.8 - 4.13, an average particle diameter of 7 μm was used to calculate the settling velocity (v_s) for input into the exchange models.

It is difficult to estimate the average particle size for the early flume experiments which used tap water and did not include the complete clay preparation procedure. It might be expected that the size distribution in these early experiments would be somewhat coarser than in later experiments due to the use of simple hand grinding instead of milling, the high ionic strength, and the presence of multivalent cations such as calcium. However, these differences are not expected to have a major effect on the mean

size (perhaps varying by ±50%). The experiments with tap water were still modeled assuming that the clay particles had an average diameter of 7 μm, but it was noted that this value has high uncertainty. This issue will be addressed in the discussion of errors in Section 6.3.

Figures 4.12 and 4.13 show the change of the clay size distribution in the flume over the course of an experiment. These data seem to show some change of the size distribution--some breakup of medium-sized particles and combination into larger sizes (~10 μm). However, in an overall sense there was no significant change in the size distribution over time.

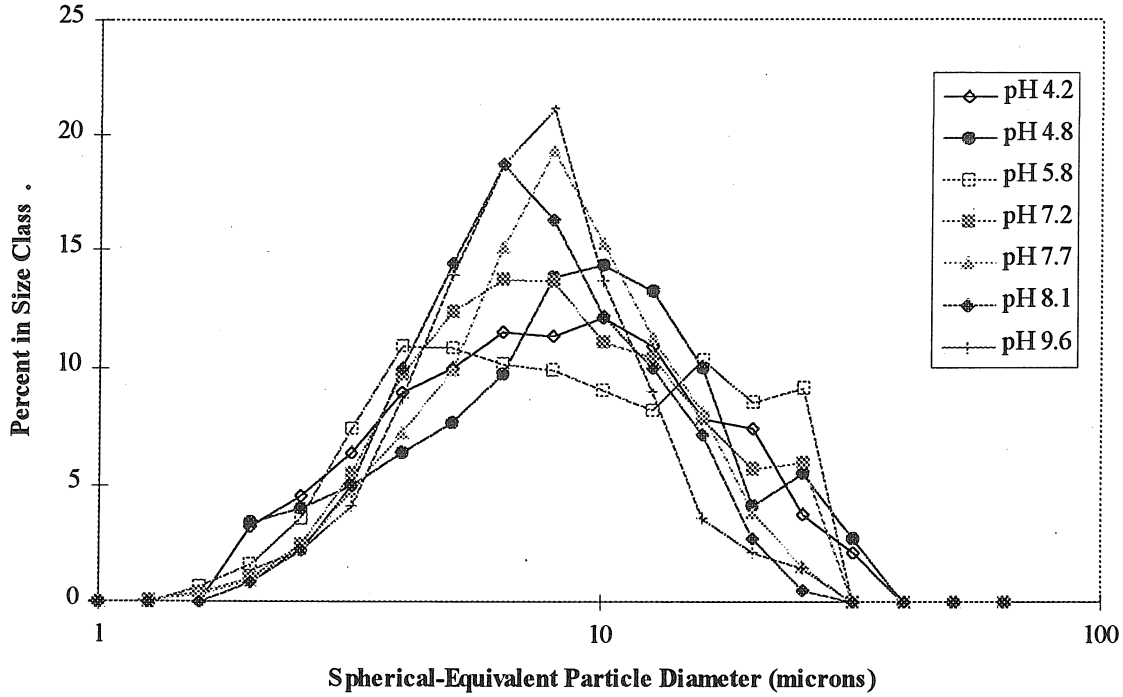

Figure 4.8: Kaolinite particle size distributions at different pH's. Data are the same as in Figure 4.9.

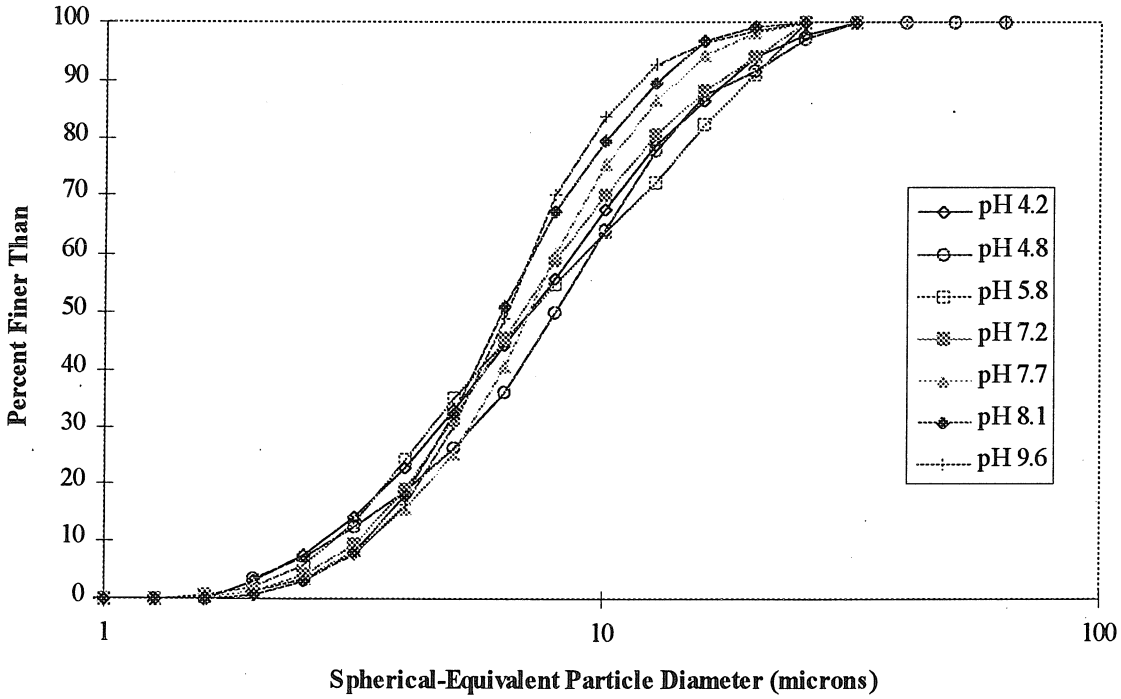

Figure 4.9: Kaolinite cumulative particle size distributions at different pH's. Data are the same as in Figure 4.8.

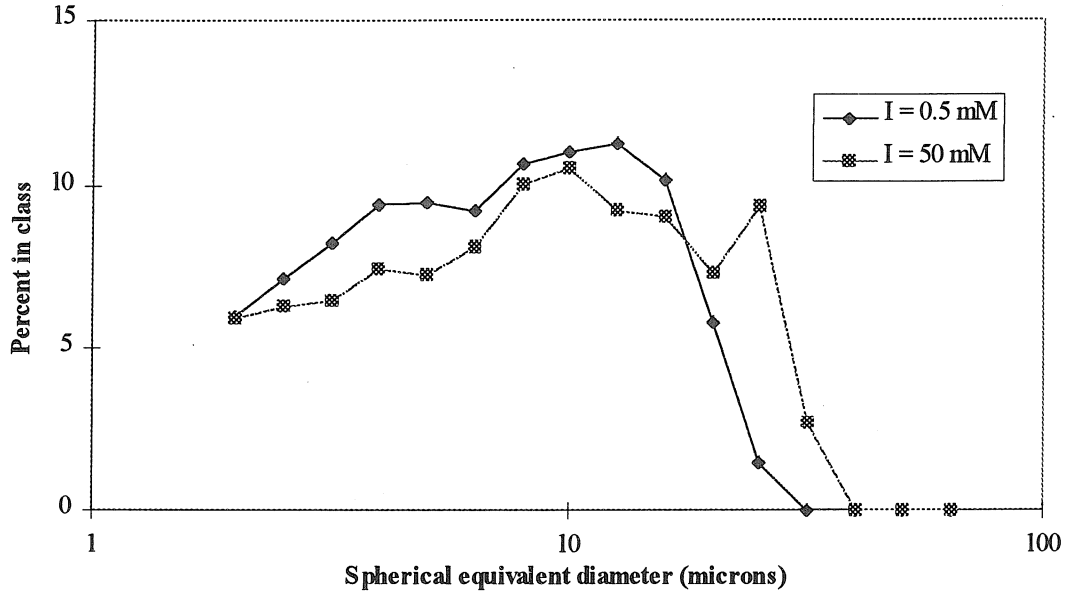

Figure 4.10: Kaolinite particle size distributions at different ionic strengths. Ionic strength was composed entirely of NaCl. Data are the same as in Figure 4.11.

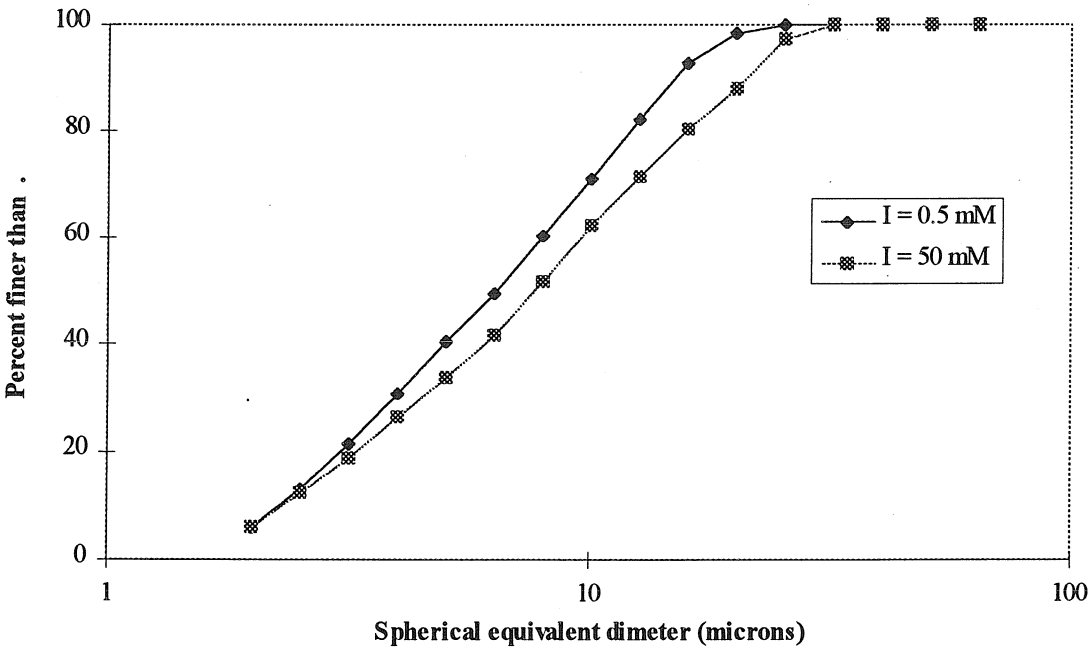

Figure 4.11: Kaolinite cumulative particle size distributions at different ionic strengths. Ionic strength was composed entirely of NaCl. Data are the same as in Figure 4.10.

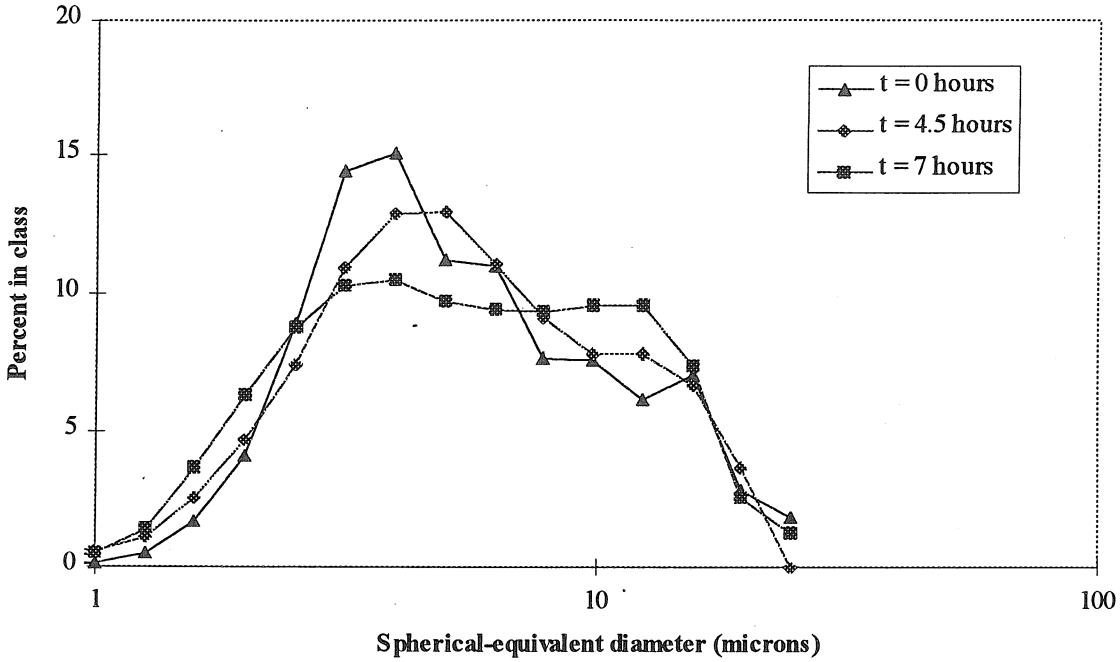

Figure 4.12: Kaolinite particle size distributions for different residence time in flume. Samples were collected during the course of flume experiment #13, conducted at pH 7.9. Data are the same as in Figure 4.13.

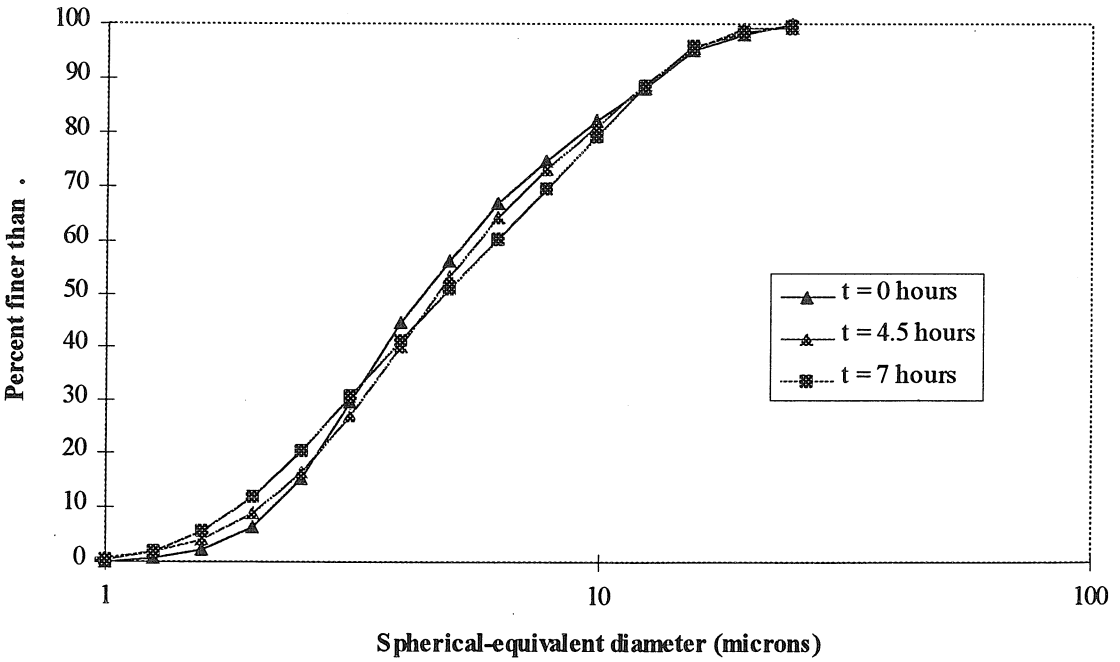

Figure 4.13: Kaolinite cumulative particle size distributions for different residence time in flume. Data are the same as in Figure 4.12.

4.4.4 Glass beads

One flume experiment was performed using glass beads as the colloidal tracer. These beads were obtained from Potters Industries in a mixture of sizes, and were separated in our lab by differential sedimentation. The beads used for this study were nominally in the 2-10 μm size class; the actual size distribution is given in Figures 4.14 and 4.15. No additional preparation was used on these beads. The glass beads were made of soda-lime glass, which is known to have significant compositional impurities (e.g., iron). As a result, they were readily filterable. Column and flume results for these beads are presented in Section 5.

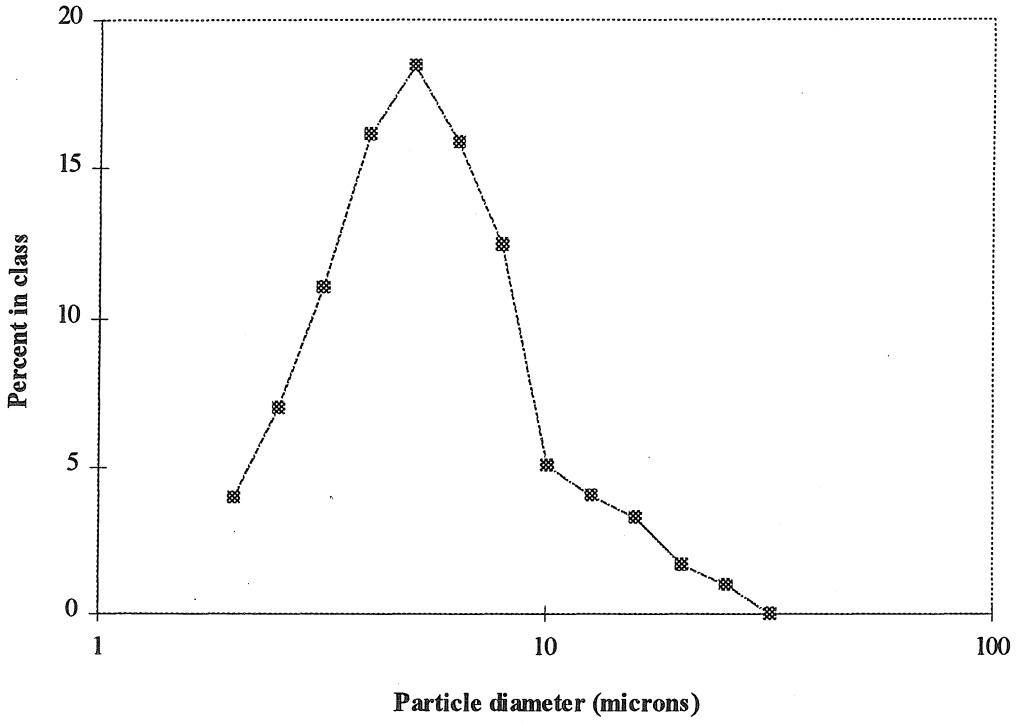

Figure 4.14: Glass beads particle size distribution. Data are the same as in Figure 4.15.

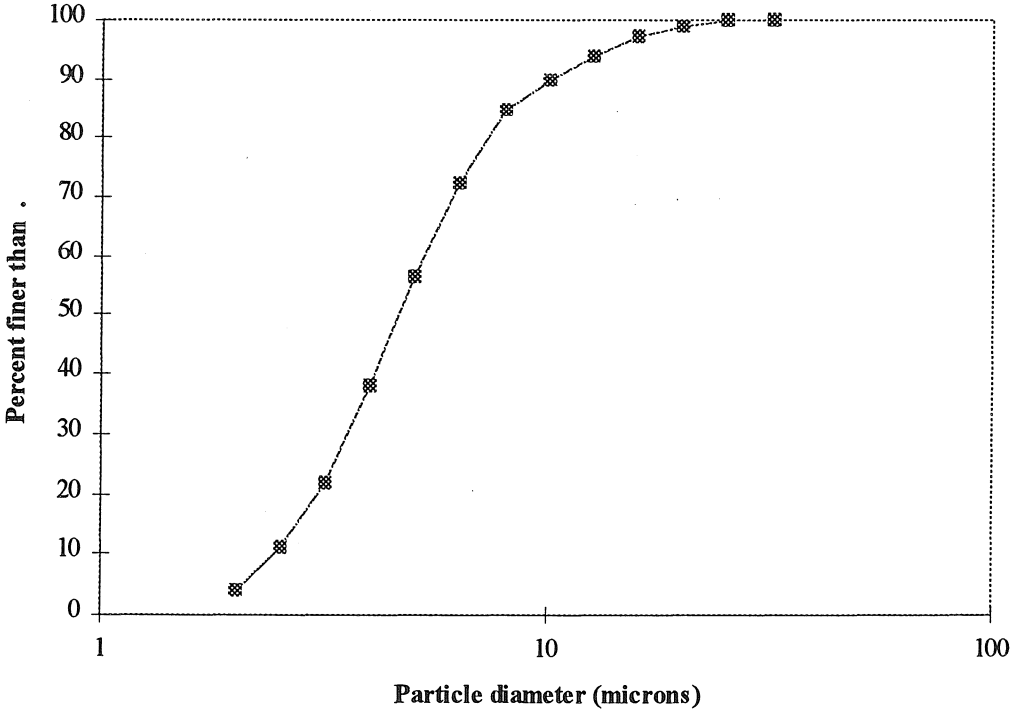

Figure 4.15: Glass beads cumulative size distribution. Data are the same as in Figure 4.14.

5 RESULTS

This chapter presents the experimental results in two parts: Section 5.1 deals with the flume experiments on colloid exchange between a stream and sand bed, and Section 5.2 gives the results of column experiments on filtration using the same materials.

5.1 Flume experiment results

This section provides the results of all flume experiments. The summary parameters that describe the hydraulic and chemical conditions will be presented in Section 5.1.1. One experiment will be analyzed in detail in Section 5.1.2 to demonstrate the calculation of the summary parameters from basic measured data. Results of net solute and colloid exchange will be presented graphically in Sections 5.1.3-5.1.6. Separate sections will be devoted to experiments with moving bedforms, experiments with nonmoving bedforms, experiments with different chemical conditions, and the application of both new and old models to the exchange of lithium. The results of secondary experiments will be presented in Section 5.1.7, and pore-water profiles in Section 5.1.8.

5.1.1 Summary of overall data set

A total of 17 separate flume experiments were performed. Seven of these also involved some secondary experiment, which examined the exchange due to a perturbation from the conditions of the main experiment. The hydraulic variables describing the flow of each of these experiments are given in Table 5.1, the bedform and modeling variables

are given in Table 5.2, and the tracer and chemical parameters are given in Table 5.3. A key describing each variable is provided after the tables.

Table 5.1: Flow parameters of all flume experiments.

Run No.	Experiment Start Date	Flow Rate Q (L/s)	Stream Depth d (cm)	Stream Velocity V (cm/s)	EGL Slope S	Shear Velocity U* (cm/s)	Froude Number F	Friction Factor f
1	12/16/92	1.4	3.5	15.0	0.0030	2.84	0.26	0.288
2	3/17/93	6.0	6.2	36.2	0.0018	2.76	0.46	0.046
3	8/31/93	15.4	9.0	64.9	0.0049	5.05	0.69	0.048
4	11/11/93	8.3	7.3	42.7	0.0020	3.04	0.50	0.041
4a		"	"	"	"	"	"	"
5	4/13/94	6.1	8.0	28.8	0.0014	2.57	0.33	0.064
5a		"	"	"	"	"	"	"
6	8/7/95	3.0	6.9	16.5	0.0003	1.22	0.20	0.044
7	2/6/96	5.1	12.7	15.2	0.0002	0.99	0.14	0.034
8	2/26/96	6.4	11.0	22.1	0.0014	2.84	0.21	0.133
8a		8.6	"	29.4	-	-	0.28	-
9	3/20/96	9.7	9.4	39.0	0.0014	2.77	0.41	0.040
9a		6.9	"	27.5	0.0011	2.77	0.28	0.082
10	4/2/96	4.1	9.8	15.7	0.0005	1.70	0.16	0.093
11	4/29/96	11.2	9.4	45.2	0.0024	3.57	0.47	0.050
11a		3.3	"	13.5	0.0001	0.78	0.14	0.027
12	5/15/96	4.0	9.6	15.7	0.0003	1.25	0.16	0.051
13	6/11/96	3.4	9.0	14.4	-	-	0.15	-
14	6/24/96	3.9	9.4	15.9	0.0002	1.13	0.17	0.041
14a		"	"	15.9	"	"	"	"
15	7/9/96	2.6	7.9	12.6	0.0003	1.28	0.14	0.084
15a		"	"	12.6	"	"	"	"
15b		9.1	"	43.6	-	-	0.50	-
16	7/29/96	8.1	8.9	34.3	0.0012	2.47	0.37	0.041
17	9/9/96	4.3	9.8	16.7	0.0002	1.07	0.17	0.033

" indicates that the variable was not changed from the primary experiment.
- indicates that the variable was not measured.

Run No.: run number. Letters indicate secondary experiments.

Flow Rate (Q): recirculation flow rate as measured by Venturi meter/manometer combination.

Stream Depth (d): mean stream depth along the flume. Calculated as the average difference between elevations of the flowing water surface and average bed surface. Measurements were typically made each meter or half-meter along the flume.

Stream Velocity (V): average stream velocity over the cross section of the channel. $V = Q/wd$, where w is the channel width (26.5 cm).

EGL Slope (S): slope of the energy grade line. Points on the EGL were determined by summing the piezometric head (water level) and velocity head ($V^2/2g$) at each measurement station along the flume.

U*: average shear velocity. $U^* = \sqrt{gRS}$ where $R = dw/(w + 2d)$ is the hydraulic radius. Calculated as an average of values determined at each measurement station using the local R and the overall EGL slope.

Froude Number (F): $F = \frac{V}{\sqrt{gd}}$.

Friction Factor (f): Darcy-Weisbach friction factor. $f = 8(U^*/V)^2$.

The shear velocity, Froude Number, and friction factor were not used in modeling, and are provided for information only.

The flume is housed in a temperature-controlled laboratory. Stream temperature varied between 19 and 21 C.

Table 5.2: Bedform and modeling parameters of all flume experiments.

Run No.	Bedform Height H (cm)	Bedform Wavelength λ (cm)	Bedform Velocity U_b (cm/min)	Bed Depth d_b (cm)	h_m (cm)	u_m (cm/min)	u_u*	U_b*	v_s*	d'/λ	d_b/λ
1	3.3	17	0.2	5.3	0.149	0.50	0.05	0.13	0.17	0.64	0.31
2	1.5	17	3.2	5.6	0.165	0.55	0.03	1.91	0.15	0.82	0.33
3	2.3	73	10.0	7.0	0.529	0.41	0.11	7.89	0.20		0.10
4	1.1	20	3.5	9.3	0.192	0.55	0.05	2.09	0.15	0.80	0.47
4a	"	"	"	"	"	"	"	"	"	"	"
5	2.0	23	0.6	9.2	0.106	0.26	0.05	0.77	0.33	0.70	0.39
5a	"	"	"	"	"	"	"	"	"	"	"
6	1.0	21	0	5.7	0.028	0.08	0.04	0	1.09	0.70	0.27
7	1.9	70	0	11.9	0.024	0.02	0.07	0	4.23	0.24	0.17
8	2.4	24	0.2	9.5	0.059	0.14	0.09	0.35	0.59	0.71	0.40
8a	1.7	31	1.0	"	0.121	0.22	-	1.51	0.38	"	"
9	1.7	32	2.2	8.2	0.171	0.30	0.04	2.40	0.28	0.53	0.26
9a	2.0	22	0.3	"	0.103	0.26	0.05	0.40	0.31	"	"
10	1.5	29	0	8.6	0.026	0.05	0.09	0	1.61	0.58	0.30
11	2.7	64	6.1	10.2	0.272	0.24	0.09	8.43	0.35	0.26	0.16
11a	2.4	64	0	"	0.024	0.02	0.00	0	3.89	"	"
12	1.5	31	0	9.5	0.026	0.05	0.05	0	1.69	0.53	0.31
13	1.4	33	0	10.0	0.022	0.04	0.38	0	2.23	0.49	0.30
14	1.6	29	0	9.1	0.028	0.05	0.04	0	1.53	0.49	0.32
14a	"	"	"	"	"	"	"	"	"	"	"
15	1.5	23	0	9.7	0.018	0.04	0.07	0	1.87	0.68	0.42
15a	"	"	"	"	"	"	"	"	"	"	"
15b	3.0	60	fast	"	"	-	-	fast	"	"	"
16	1.7	33	1.1	10.7	0.136	0.23	0.05	1.56	0.36	0.45	0.33
17	1.4	34	0	10.5	0.029	0.05	0.04	0	1.72	0.47	0.31

Bedform Height (H): average trough-to-crest height of major bedforms (dunes), determined from a relatively large number of bedforms (20-50). Nonmoving bedform experiments include measurement of every bedform present in the flume. Bedforms of smaller size classes (ripples an order of magnitude smaller than dunes) are not included in the average.

Bedform Wavelength (λ): average dune crest-to-crest distance.

Bedform Velocity (U_b): average dune celerity, measured by tracking the position of bedforms crests over time.

Bed Depth (d_b): mean depth of sand bed. Average of measurements every half meter.

h_m: amplitude of the sinusoidal pressure distribution at the bed surface, estimated using Equation 3.2.

u_m: maximum D'arcy velocity in the bed calculated from the pumping model (Equation 3.7). The maximum seepage velocity is given by u_m/θ, where θ is the porosity ($\theta = 0.325$ for all experiments).

u_u^*: nondimensional underflow velocity. $u_u^* = KS/u_m$, where K is the coefficient of permeability (K = 9.0 cm/min for all experiments). Used in modeling to calculate the pore water velocity profile.

U_b^*: nondimensional bedform velocity. $U_b^* = U_b/(u_m/\theta)$. Used to characterize the extent of turnover.

d'/λ: d' is the effective water column depth, given by the total volume of recirculating water divided by the bed area. Thus it is the stream depth plus an additional effective depth corresponding to the volume of water in the return pipe and end sections of the flume. Used in modeling to convert mass exchange to the change of concentration in the surface water.

d_b/λ: ratio of bed depth to bedform wavelength. Used in modeling to determine the pore water velocity profile for finite beds.

Table 5.3: Tracer and chemical parameters of all flume experiments.

Run No.	Colloidal Tracer	Preparation Procedure	C_0 (mg/L)	Sand Cleaning	Water Supply	pH	I (mM)	λ_f (1/cm)	λ_f*
1	kaolinite	grinding/stirring	~200	rinsing only	tap water	~8.2	~15	v. high	v. high
2	kaolinite	grinding/stirring	~200	rinsing only	tap water	~8.2	~15	v. high	v. high
3	kaolinite	grinding/stirring	~200	rinsing only	tap water	~8.2	~15	v. high	v. high
4	kaolinite	grinding/stirring	~200	rinsing only	tap water	~8.2	~15	v. high	v. high
5	kaolinite	grinding/stirring	~200	rinsing only	tap water	~8.2	~15	v. high	v. high
6	kaolinite	grinding/stirring	~200	Sec. 4.4.2.2	prepared water	6.8	5.0	0.6	2.01
7	kaolinite	Sec. 4.4.3.2	~200	Sec. 4.4.2.2	prepared water	7.1	5.0	0.6	6.67
8	kaolinite	Sec. 4.4.3.2	~200	Sec. 4.4.2.2	prepared water	7.0	5.0	0.6	2.26
9	kaolinite	Sec. 4.4.3.2	~200	Sec. 4.4.2.2	prepared water	7.1	5.0	0.6	3.06
10	kaolinite	Sec. 4.4.3.2	~200	Sec. 4.4.2.2	prepared water	7.1	5.0	0.6	2.73
11	kaolinite	Sec. 4.4.3.2	~200	Sec. 4.4.2.2	prepared water	7.1	5.0	0.6	6.11
12	kaolinite	Sec. 4.4.3.2	~200	Sec. 4.4.2.2	prepared water	8.0	5.3	0.2	0.97
13	kaolinite	Sec. 4.4.3.2	~200	Sec. 4.4.2.2	prepared water	7.9	0.5	0.2	1.05
14	kaolinite	Sec. 4.4.3.2	40	Sec. 4.4.2.2	prepared water	7.4	0.6	0.4	2.01
14a	"	"	~200	"	"	"	"	"	"
15	kaolinite	Sec. 4.4.3.2	40	Sec. 4.4.2.2	prepared water	7.3	5.0	0.5	1.76
15a	"	"	~200	"	"	"	"	"	"
16	kaolinite	Sec. 4.4.3.2	120	Sec. 4.4.2.2	prepared water	7.9	5.0	0.2	1.05
17	glass beads	acid wash	30	Sec. 4.4.2.2	prepared water	7.3	5.0	0.5	3.75

Secondary experiments other than 14a and 15a are omitted from this table because the tracer and chemical parameters did not change from the main experiment (exception: λ_f* will change with the bedform wavelength).

Preparation Procedure: method used to prepare the colloidal tracer before use in the experiment. For the first six experiments, the clay was ground with a mortar and pestle and then stirred overnight in tap water. For later experiments, the procedure described in Section 4.4.3.2 was used.

Sand Cleaning: method used to clean sand before use in the experiment. For the first five experiments, the sand was simply rinsed with tap water before use. For later experiments, the cleaning procedure described in Section 4.4.2.2 was used.

C_0: initial concentration of colloid in the recirculating water. Most are given as approximate because the exact mass of clay added to the system was usually not measured. (Prepared clay was stored in suspension, and the clay to be added to the flume

was removed from a suspension known to contain a certain mass of clay. The initial mass of clay added to the flume was not measured directly, but was estimated from the volume and concentration of the suspension. Thus, C_0 in the flume was known within ~10%). Experimental values of C/C_0 were calculated directly from absorbance ratios.

pH: average stream pH as measured by in-stream pH probe. Values for tap water were not measured during the experiment but are typical for the Pasadena water supply. In the prepared water, the pH was controlled by adding HCl or NaOH to deionized water.

I: stream ionic strength, determined by direct preparation of the stream water. Values for tap water were not measured during the experiment but are typical for the Pasadena water supply. Tap water had multivalent cations (e.g., Ca^{2+}, Mg^{2+}) on the order of a few mM. In the prepared water, the ionic strength was controlled by adding NaCl to deionized water.

λ_f: filtration coefficient, determined by selecting a value from the column experiment data (Section 5.2) based on the pH and ionic strength of the flume experiment. Filtration coefficients were not determined for tap water, but are certainly >0.6 cm^{-1}.

λ_f^*: dimensionless filtration coefficient, $\lambda_f^* = \lambda_f/k = \lambda_f^* \lambda/2\pi$. Used to characterize the extent of filtration over the typical pumping length scale. $\lambda_f^* > 1$ indicates that filtration is very high so that colloids will be completely trapped when pumped through the bed.

5.1.2 Typical experimental results and model application

In order to make the experimental results absolutely clear, the complete data set of one experiment (#9) will be presented and discussed in detail. As discussed previously, there are several types of data for every experiment: hydraulic data that describe the flow in the stream, bed data principally used to define the average bedform shape, chemical data which govern the interactions between colloidal particles and bed sediment grains, and data on the distribution of dissolved or colloidal tracer in the flume. The measurement of each of these variables was discussed in Chapter 4. Here, the results of these measurements will be presented and discussed. In addition, the use of measured variables in the exchange models will be discussed. All of the data presented in the following sections come from Experiment #9, which involved rapidly moving bedforms, and included a secondary experiment (reduction of the flow rate).

5.1.2.1 Hydraulic data

The principal tool used to obtain depth and slope data is a point gauge on the movable instrument carriage. By means of this device, the position of a surface can be measured down the flume. This data is used to calculate depths, slopes, and profiles of the water and surfaces. The basic data set of point gauge measurements for Experiment #9 is given in Table 5.4.

Table 5.4: Point gauge readings for Experiment #9. Position is measured starting at the beginning of the sediment bed at the upstream end of the flume. Point gauge readings have no defined zero reference point (i.e., only differences are important). The point gauge reading of the bottom of the flume was 32.3 cm.

Position (m)	Flowing Water Surface (cm)	Still Water Surface (cm)	Avg. Bed Surface (cm)
3	50.05	49.70	40.4
4	50.05	49.85	40.4
5	49.94	49.98	40.4
6	50.06	50.08	41.0
7	49.90	50.21	41.0
8	49.99	50.37	41.0
9	49.90	50.47	40.3
10	49.91	50.61	40.3
11	49.95	50.70	40.3

Other hydraulic basic data are:

Flow rate: $Q = 9.7$ L/s (measured by Venturi meter)

Porosity: $\theta = 0.33$ (for Ottawa-30 sand)

Total water volume: 644 L

The basic hydraulic data are used to compute derived parameters at each measurement station down the flume. Differences between point gauge readings are used to give relative elevations. The point gauge reading of the bottom of the flume is used as a reference for the bed depth. The data from each measurement location are then used to calculate the average parameters used to describe the overall experiment. The derived data vs. downstream position are presented in Table 5.5, average and summary parameters are given in Table 5.6, and the flow conditions are displayed graphically in Figures 5.1 and 5.2.

Table 5.5: Derived hydraulic data vs. downstream position for Experiment #9. The local flow velocity is calculated by dividing the flow rate by the local stream area.

Position (m)	Difference Between Flowing & Still (cm)	Bed Depth d_b (cm)	Stream Depth d (cm)	Effective Stream Depth d' (cm)	Flow Velocity V (cm/s)	E.G.L. (cm)	Shear Velocity U* (cm/s)
3	0.35	8.1	9.65	17.2	37.9	1.083	2.79
4	0.20	8.1	9.65	17.2	37.9	0.933	2.79
5	-0.04	8.1	9.54	17.1	38.4	0.710	2.78
6	-0.02	8.7	9.06	16.6	40.4	0.812	2.74
7	-0.31	8.7	8.90	16.5	41.1	0.552	2.72
8	-0.38	8.7	8.99	16.5	40.7	0.465	2.73
9	-0.57	8.0	9.60	17.2	38.1	0.171	2.78
10	-0.70	8.0	9.61	17.2	38.1	0.039	2.78
11	-0.75	8.0	9.65	17.2	37.9	-0.017	2.79

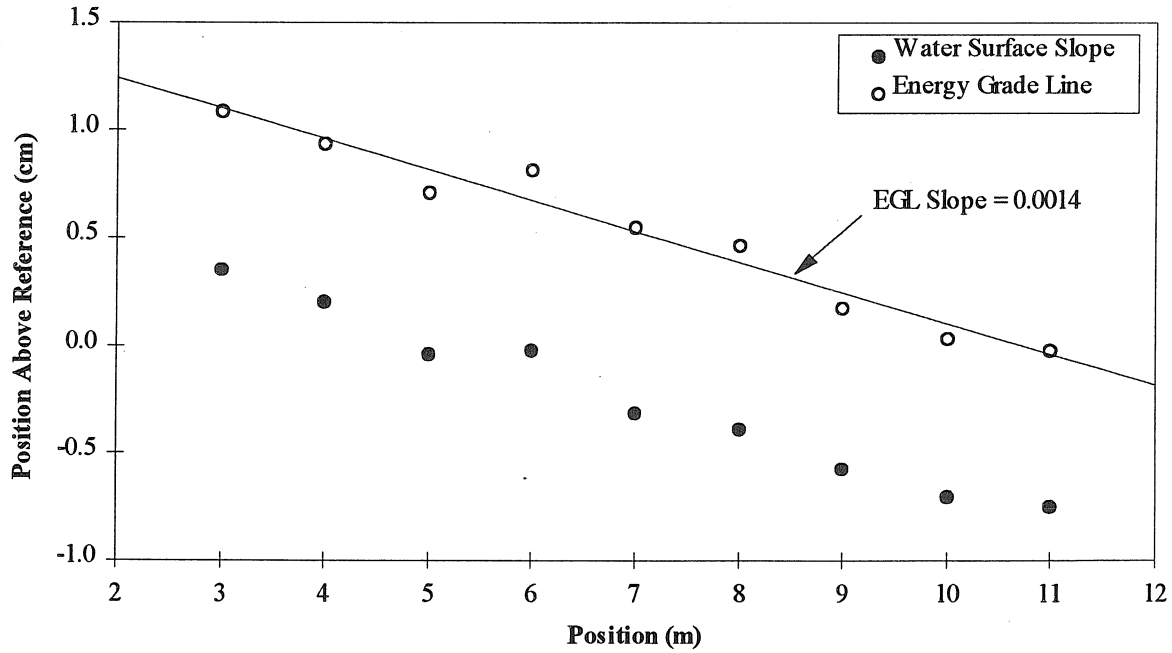

Figure 5.1: Water surface and energy grade line for Experiment #9. Slopes of these lines are calculated relative to horizontal.

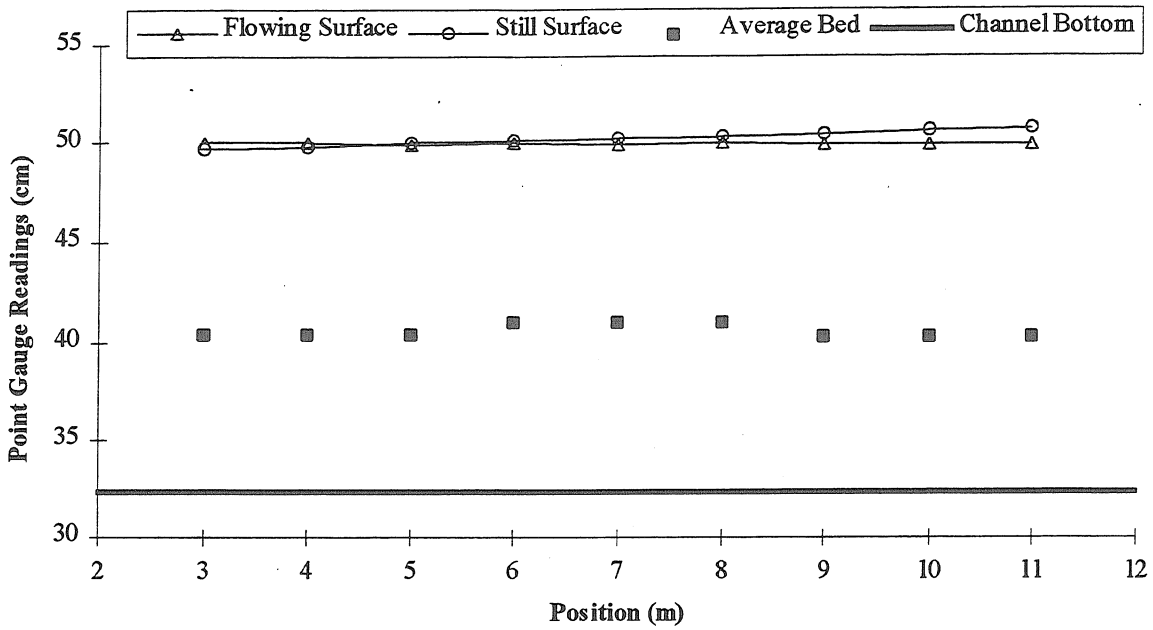

Figure 5.2: Bed and flow geometry for Experiment #9. The channel surface and flume rails are parallel, so the flume bottom has a constant point gauge reading. In uniform flow, the flume is tilted so that the flowing water surface and the bed surface will both be parallel to the flume bottom as well. The still water surface gives the true horizontal.

Table 5.6: Average and summary hydraulic parameters for Experiment #9.

Flow Rate Q (L/s)	Stream Velocity V (cm/s)	Shear Velocity U* (cm/s)	Froude Number F	Stream Depth d (cm)	Effective Stream Depth d' (cm)	Bed Depth d_b (cm)	Surface Slope	E.G.L. Slope S	Friction Factor f
9.7	39.0	2.77	0.41	9.4	17.0	8.2	0.0014	0.0014	0.0403

Finally, the reservoirs of stream and pore waters can be estimated. The volume of pore water is just given by the bed volume times the porosity, and the volume of stream water is just the total volume of water in the flume minus the pore water. The ultimate dilution of a conservative tracer is given by the ratio of the total volume to the stream volume. For Experiment #9:

Pore water volume: 89 L

Stream water volume: 555 L

Total water volume: 644 L

Expected final concentration: $C/C_0 = 555/644 = 0.862$, $1 - C/Co = 0.138$

5.1.2.2 Bedform data

As discussed in Section 4.1.3.1, bedform parameters were measured in two ways--through the viewing window, and from above. Window observations yield measurements of the bedform height, wavelength, and position vs. time. Observations from above during the experiment give only the crest positions, which are used to calculate wavelength. Point gauge measurements along longitudinal transects made after the experiment give bedform heights. Thus, the average wavelength is estimated from window observations and crest positions determined from above, average height is estimated from window observations and point gauge measurements, and average velocity is estimated from window observations only.

The complete set of measurements for Experiment #9 are presented in Tables 5.7 and 5.8. For this particular experiment, point gauge measurements were not taken after the main experiment because the secondary experiment involved observing the exchange due to a reduction in flow rate. Thus, bedform heights were estimated from window observations only.

Table 5.7: Observations from above of dune crest positions from Experiment #9, with calculated wavelengths and visual descriptions. Average $\lambda = 30$ cm.

Crest Position (m)	Wavelength λ (cm)	Visual Description (arbitrary classification)
1.00	-	dune
1.39	39	large dune
1.68	29	ripple/small dune
1.95	27	large dune
2.44	49	large dune
2.70	26	large dune
3.20	50	large dune
3.47	27	dune
3.82	35	dune
4.19	37	dune
4.62	43	large dune
4.81	19	edge dune
5.10	29	dune
5.41	31	dune
5.77	36	dune
6.21	44	ripple/small dune
6.40	19	large dune
6.81	41	dune
7.05	24	edge ripple
7.25	20	ripple/small dune
7.44	19	dune
7.59	15	ripple/small dune
7.80	21	dune
7.99	19	edge dune
8.15	16	large dune
8.51	36	large edge dune
8.80	29	dune
9.20	40	edge ripple
9.49	29	dune
9.85	36	edge ripple
10.16	31	large dune
10.73	57	ripple/small dune
10.84	11	dune
11.22	38	dune
11.41	19	dune
11.65	24	ripple/small dune
11.99	34	ripple/small dune
12.10	11	large dune

Table 5.8: Observations through window of dune heights, wavelengths, and crest positions vs. time from Experiment #9, with calculated bedform velocities. Bedforms were observed at three different time periods, so each group (a, b, c) represents a series of bedforms that passed through the window region consecutively. The a-series bedforms appeared to be atypically long. Δt and Δx are the observation time and the distance the bedform moved in that time.

Bedform #	H (cm)	λ (cm)	Δt (min)	Δx (cm)	Velocity (cm/min)
a1	1.2	13.0	5	7.8	1.6
a2	1.8	57.0	5	19.9	4.0
	2.2	67.0	5	9.7	1.9
			5	10.0	2.0
			5	7.8	1.6
a3	2.0	22.0	5	16.6	3.3
	1.9		5	10.6	2.1
a4	1.9	46.0	5	21.8	4.4
	1.7	60.0	5	18.1	3.6
	2.1		5	10.9	2.2
			5	9.9	2.0
			15	40.5	2.7
			15	14.0	0.9
a5	1.9				
a6	2.1		15	26.7	1.8
b1	1.0				
b2	1.3	32.5	10	28.6	2.9
			10	16.3	1.6
b3	2.0	33.7	10	19.4	1.9
			10	8.8	0.9
b4	2.3		10	22.7	2.3
			10	25.7	2.6
			10	22.4	2.2
			10	8.7	0.9
b5	1.8	26.0	10	14.6	1.5
b6	1.1	27.1			
b7	1.3		10	16.4	1.6
c1	2.4	38.2	5	12.5	2.5
c2	1.9	34.3	5	20.2	4.0
c3	1.6	20.0	5	25.2	5.0
c4	1.6	45.0	5	18.7	3.7

The bedform data for this experiment is summarized in Table 5.9. Two additional factors were considered in choosing the parameters used in modeling. First, the wavelength estimated using crest positions identified from above is probably somewhat low because it includes some ripples. Second, the a-series bedforms observed through the window appeared to be atypically long. Bedform parameters for Experiment #9 were difficult to estimate due to the high stream velocity and correspondingly high rate of sediment transport. This experiment had a greater-than-normal rate of bedform appearance/disappearance and frequency of occurrence of atypical bed features (ripples, edge features, etc.).

Table 5.9: Comparison of estimates for bedform parameters for Experiment #9.

Data type	Height H (cm)		Wavelength λ (cm)		Velocity U_b (cm/min)
	avg.	std. dev.	avg.	std. dev.	avg.
window, a-series	1.8	0.3	37.5	23.7	2.2
window, b- and c-series	1.7	0.5	32.1	7.7	2.2
from above			30	11	
used in model	1.7		32		2.2

5.1.2.3 Chemical data

The pH and ionic strength of flume water are used to characterize the stream water chemistry. Ionic strength was controlled by adding the desired concentrations of the desired ionic species into deionized water. Since ionic strength does not vary over time, it was not measured in the flume. Experiment #9 had the baseline composition of 5

mM NaCl; all other ionic species had concentrations orders of magnitude less than this. Stream pH was measured by a portable pH meter with the electrode placed directly in the flowing stream water. Observed stream pH varied between 7.11 and 7.20 during the course of the experiment.

5.1.2.4 Tracer concentration data

The main data set used to interpret bed exchange is the time-series of normalized tracer concentration in the recirculating water. The complete data sets for lithium and kaolinite exchange during Experiment #9 are graphed in Figures 5.3 and 5.4 respectively. Exchange can be considered in three phases, an input phase, a period of rapid exchange, and a period of slow exchange.

The input phase for this experiment occupies approximately the first 15 minutes after tracer addition. In this period, the tracer has not yet established a completely uniform concentration in the recirculating water. The initial concentration used to nondimensionalize the concentration data, C_0, is determined by averaging several samples taken during the first 5-10 minutes of the experiment. These initial samples are collected by filling a test tube over a period of around one minute. Another estimate of C_0 comes from knowledge of the mass of tracer added to the system. Generally the volume-averaged sample estimate works better because it includes the same instrument calibration used for the rest of the samples.

Coinciding with and following the input phase, there is a period of rapid disappearance of tracer from the recirculating water. In this phase, net exchange is high

because turnover and pumping carry tracer-laden stream water into the bed, but the water coming out of the bed is tracer-free. Net exchange will slow when the water coming out of the bed begins to bring tracer back with it. For conservative solutes, exchange will occur at a progressively slower rate until all the water in the flume has the same concentration, at which point net exchange ends even though water is still being exchanged between the stream and bed. Net exchange will also decrease when the stream water becomes depleted of tracer, especially for colloid exchange where progressively more colloids are filtered by the bed.

Figures 5.3 and 5.4 both show the variation around C_0 due to initial mixing. The kaolinite data (Figure 5.4) show the expected rapid early decrease and later tailing off of the concentration. However, the lithium concentration decreases slowly, and has not yet reached the asymptotic value for complete mixing (0.862) after 24 hours. This could possibly be attributed to some uncorrected drift error during ICP-MS analysis.

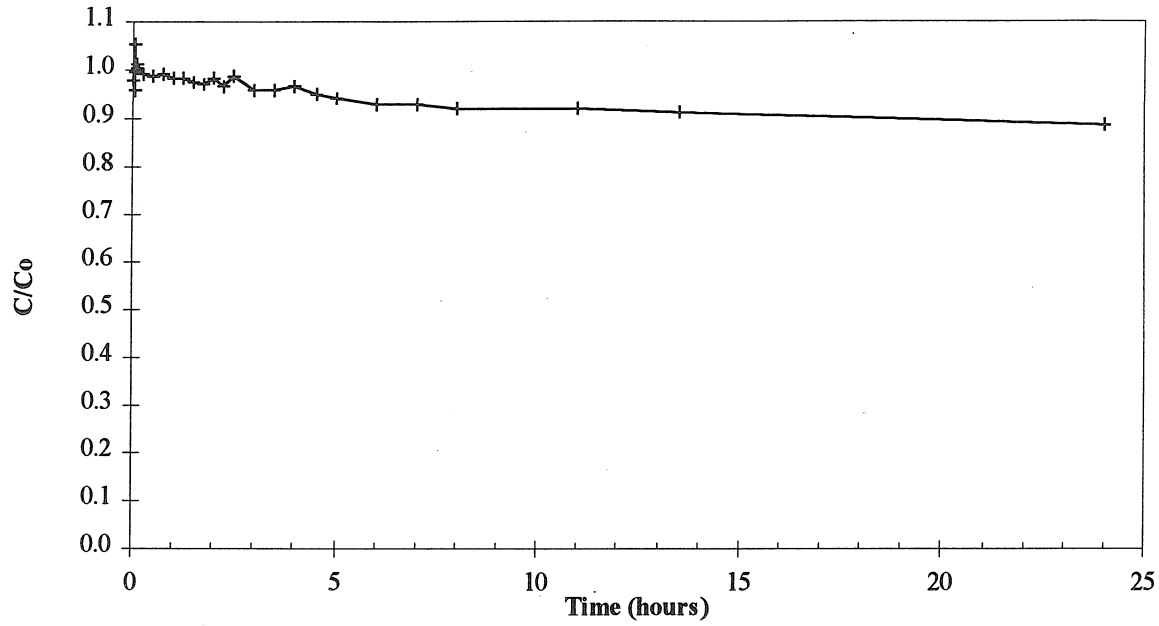

Figure 5.3: Normalized lithium concentration in stream water versus time for Experiment #9. Some values of C/C_0 are greater than one at early times due to incomplete initial mixing. The line connecting data points is for clarity only.

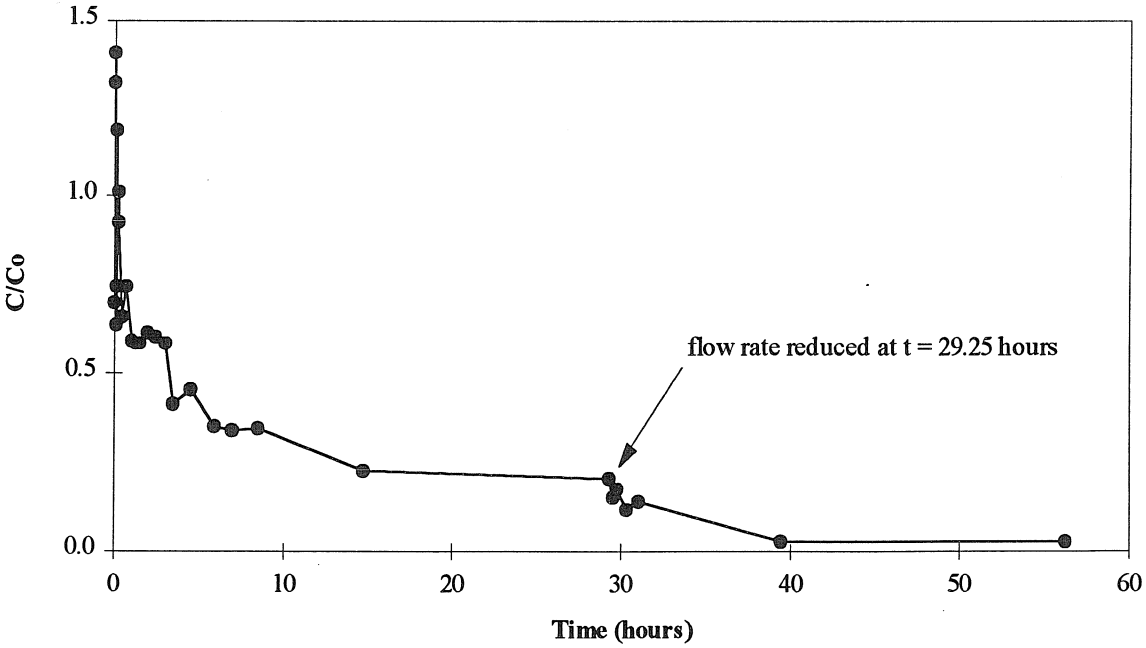

Figure 5.4: Normalized kaolinite concentration in stream water versus time for Experiment #9, including secondary experiment #9a. Some values of C/C_0 are greater than one at early times due to incomplete initial mixing. The line connecting data points is for clarity only.

Pore-water concentration measurements of kaolinite were also made for Experiment #9. These data are presented in Figure 5.5. These samples were collected through a vertical series of sampling ports at a particular location in the flume. Note the difference between the profiles from the primary and secondary portions of the experiment. In the main experiment, with high stream velocity and turnover, no kaolinite was suspended in the pore water at deeper portions of the bed. For the secondary experiment with lower stream velocity, suspended kaolinite had a maximum deeper in the bed. These paired observations are consistent with the idea that higher turnover hinders pumping to the deep bed. This will be discussed in more detail in Section 5.1.4.

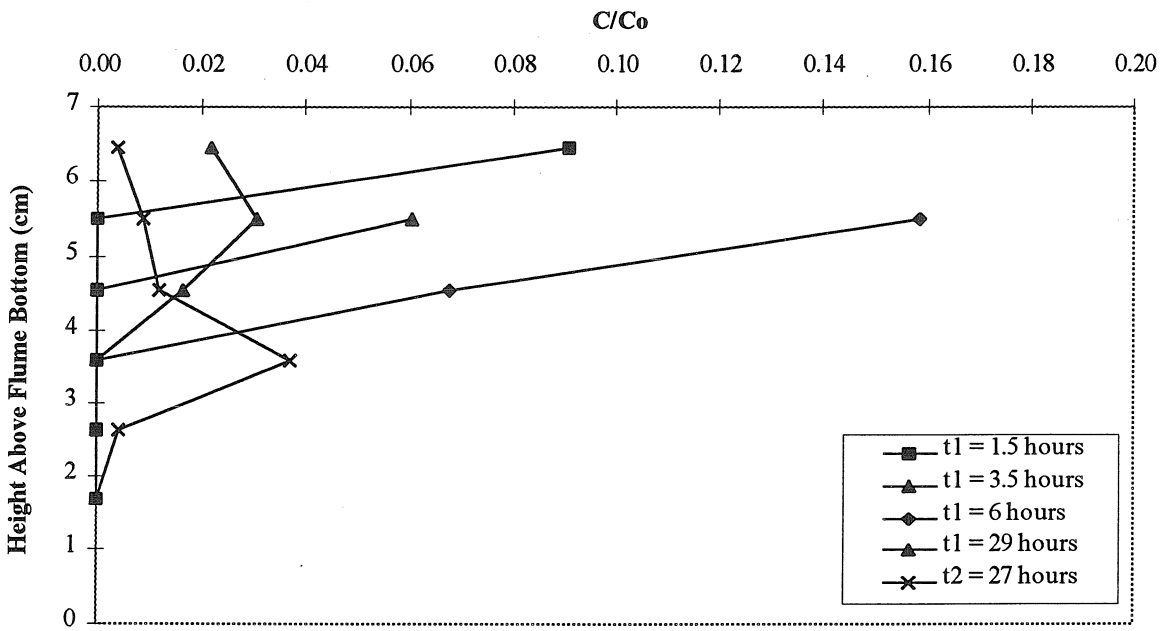

Figure 5.5: Pore water profiles of kaolinite concentration for Experiment #9. The highest point in each profile varies because bedforms continually passed the sampling location, and the upper ports were not always covered by the bed. In addition, it was generally not possible to take samples in the uppermost 1 cm of the bed. t1 and t2 indicate time elapsed since the start of the main experiment and secondary experiment, respectively.

5.1.2.5 Secondary experiment data

A complete data set is obtained for each secondary experiment. Flow rate, depth profiles, bed geometry, etc., are all measured exactly as they were for the primary experiment. Secondary experiments only involved colloid exchange; lithium was never added for a secondary experiment.

The secondary portion of Experiment #9 involved decreasing the flow rate in the flume from 9.7 to 6.9 L/s. Sediment transport decreased, but bed motion still occurred at the lower velocity. The decline in kaolinite concentration in the stream shown in Figure 5.4 was caused by increased bed exchange due to pumping at the lower bedform velocity. While it is not useful to present the entire data set, the summary data describing the hydraulic conditions of the secondary portion of Experiment #9 are presented in Table 5.10. The chemical conditions remained unchanged from the main part of the experiment.

Table 5.10: Summary hydraulic and bedform parameters for secondary experiment #9a. Numbers with * are constrained to be the same as the main part of the experiment.

Flow Rate (L/s)	Stream Velocity V (cm/s)	Shear Vel. U* (cm/s)	Froude Number F	Stream Depth d (cm)	Water Column Depth d' (cm)	Bed Depth d_b (cm)	Surface Slope	E.G.L. Slope S	Friction Factor f	Bedform Height H (cm)	Bedform Wave-length λ (cm)	Bedform Velocity U_b (cm/min)
6.9	27.5	2.77	0.28	9.4*	17.0*	8.2*	0.0011	0.0011	0.082	2.0	22	0.3

5.1.2.6 Comparison of exchange results with model predictions

The bed-exchange data are presented in a different fashion for comparison with model predictions. The time axis is $\sqrt{t^*/\theta}$, based on the typical pumping time scale t^*/θ

$= k^2 K h_m t/\theta$, where $k = 2\pi/\lambda = 0.29$ cm^{-1}, K = permeability = 9.0 cm/min, h_m = amplitude of piezometric head variation at the bed surface = 0.17 cm, and θ = porosity = 0.33. This results in $t^*/\theta = 10.8$ t when t is in hours. θ is included to convert from D'Arcy velocity to pore-water (seepage) velocity. The square-root of t^*/θ is used in order to allow better comparison at early times when exchange is high. In addition, $1\text{-}C/C_0$ (the fraction of tracer in the bed, instead of the fraction in the stream) is used for the concentration scale simply for graphing convenience and model comparisons.

Data from secondary experiments are renormalized for inclusion on the same graph as primary data. The concentration at the start of the secondary experiment, C_{02}, is used to nondimensionalize the secondary experiment data. These renormalized concentrations are then plotted against the time since the start of the secondary experiment, t_2. In other words, C_{02} and t_2 define the initial condition for the secondary experiment.

Results and model predictions for Experiment #9 and #9a are given in Figure 5.6. Concentration data from very early times are omitted because high scatter due to incomplete initial mixing tends to obscure early trends. All data are included after the initial mixing period, typically starting with t = 15 minutes. Model input data for Experiment #9 and #9a are given below Figure 5.6 in Tables 5.11 and 5.12.

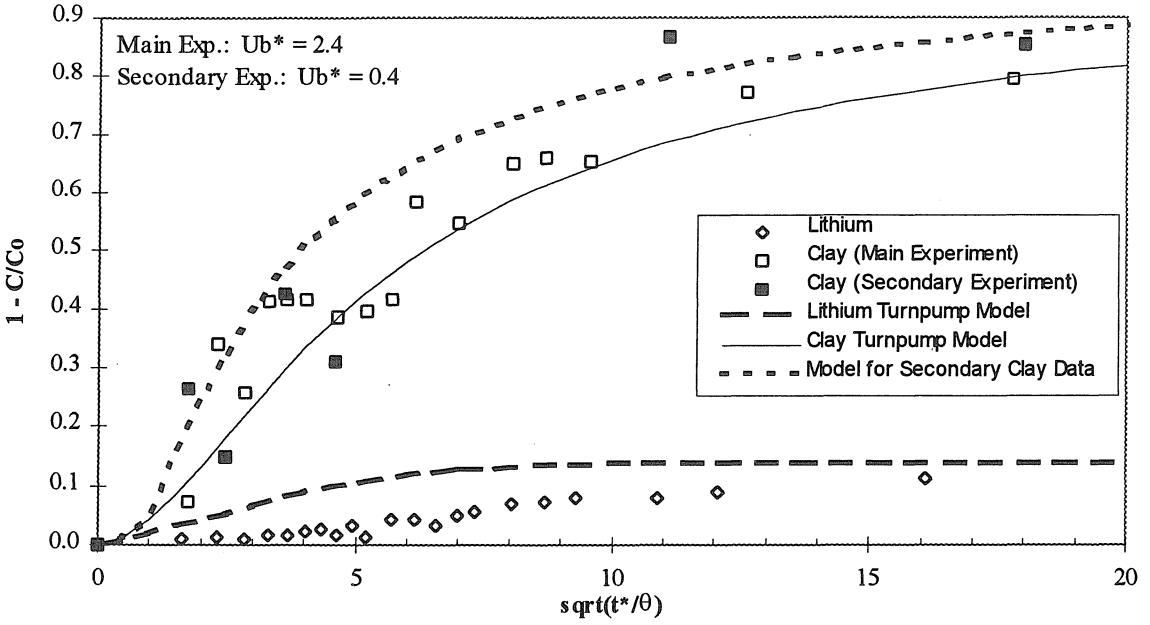

Figure 5.6: Experimental results and model predictions for both lithium and kaolinite exchange for Experiment #9, including secondary experiment.

Table 5.11: Model inputs for Experiment #9.

V (cm/s)	d (cm)	d' (cm)	d_b (cm)	λ (cm)	H (cm)	U_b (cm/min)	K (cm/min)	θ	u_u (cm/min)	v_s (cm/min)	λ_f (1/cm)
39.0	9.4	17.0	8.2	32	1.7	2.2	9.0	0.33	0.013	0.26	0.6

Table 5.12: Model inputs for secondary Experiment #9a. Numbers with * are constrained to be the same as the main part of the experiment.

V (cm/s)	d (cm)	d' (cm)	d_b (cm)	λ (cm)	H (cm)	U_b (cm/min)	K (cm/min)	θ	u_u (cm/min)	v_s (cm/min)	λ_f (1/cm)
27.5	9.4*	17.0*	8.2*	22	2.0	0.3	9.0*	0.33*	0.011	0.26*	0.6*

Model predictions were developed by running the numerical implementations of the appropriate exchange models (described in Section 3.1) with input values taken from the parameters for this experiment. The turnpump model was used to model the exchange due to moving bedforms in Experiment #9. The relationship between

experimental parameters, model predictions, and experimental results is depicted graphically in Figure 5.7. Model predictions are based entirely on the actual experimental parameters--no fitting parameters are used. The model predictions can then be thought of as the exchange that would occur in an ideal system with the bedform geometry, stream velocity, etc., of the actual system. Discrepancies between the experimental data and the model predictions are the result of: deficiencies in the physics of the model, numerical errors introduced during model implementation, poor estimation of experimental variables, natural variability of experimental data, or mismeasurement of experimental data.

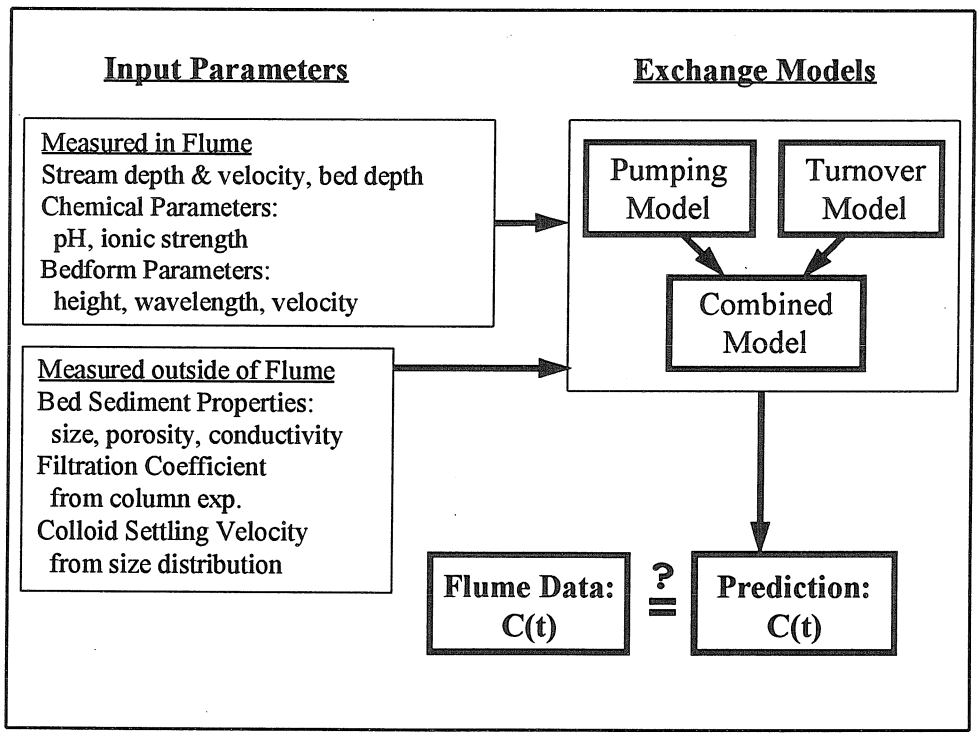

Figure 5.7: Relationship between model input parameters, exchange models, model predictions, and flume concentration data. An appropriate exchange model (e.g. pumping only, turnpump, etc.) is selected based on the conditions of the experiment.

The model predictions for Experiment #9 show fairly good agreement with experimental results for the exchange of kaolinite, for both the primary and secondary parts of the experiment. It is especially significant that the model prediction is good for the secondary data, since this clearly shows that the model correctly predicts the impact of the decrease in flow rate. The model prediction for lithium has the correct trend, but is off somewhat in magnitude. It appears in this case that the lithium data is somewhat low, probably due to an analysis error as discussed above. In other experiments, lithium data generally agreed very well with model experiments.

5.1.3 Nonmoving bedform experiments

Runs 6, 7, 10, 12, 13, 14, 15, and 17 were conducted with stationary bedforms. In these experiments, the bedforms were formed naturally by sediment transport at higher velocities, and then the flume was slowed down so that sediment transport no longer occurred. In addition, secondary experiments 11a, 14a, and 15a also involved nonmoving bedforms. The main portion of experiment 11 had moving bedforms; for the secondary portion, 11a, the flume flow was slowed down and so that transport of the remaining stream-borne clay to the bed could be observed; this experiment will be discussed in the section on moving bedform experiments. Experiments 14 and 15 were conducted primarily to examine the effect of the initial stream concentration (C_0) on transport. The secondary portion of each of these experiments involved adding additional clay to the surface water and observing its disappearance under the same hydraulic conditions as the primary experiment. Experimental results and model predictions for all nonmoving bedform experiments are presented in Figures 5.8 through 5.15.

The finite-bed pumping model described in Section 3.1.1.2 was used to predict lithium exchange in these experiments. This model assumes that bedform-induced pumping is the only exchange mechanism, and that the tracer mixes conservatively. This model predicts lithium exchange very well, except for Experiment #7 (Figure 5.9). This one exception appears to be the result of measurement errors, primarily those induced by uncorrected ICP-MS drift.

The maxpump model described in Section 3.3.1a was used to predict colloid exchange. This model also assumes that pumping is the only exchange mechanism, but

assumes that all tracer is captured by the bed. That is, the rate of tracer exchange is equal to the rate of tracer pumping into the bed. This assumption will be good for colloid transport as long as particle filtration or settling is sufficiently high ($\lambda_f * > 1$ or $v_s * > 0.3$). Model predictions generally agree well with experimental data, indicating that complete trapping did in fact occur. For Experiments #6 and #17, where the colloidal tracer was not as well defined, there was poorer agreement between model predictions and experimental results, probably due to misestimate of the average particle size and settling velocity. The first nonmoving bedform experiment, #6 shown in Figure 5.8, did not include the full clay preparation procedure. Experiment #17, shown in Figure 5.15, used glass beads which were not prepared as carefully as kaolinite was. Maxpump model predictions are compared with predictions from a more complex particle-exchange model (which explicitly includes both filtration and particle settling) in Section 5.1.5a.

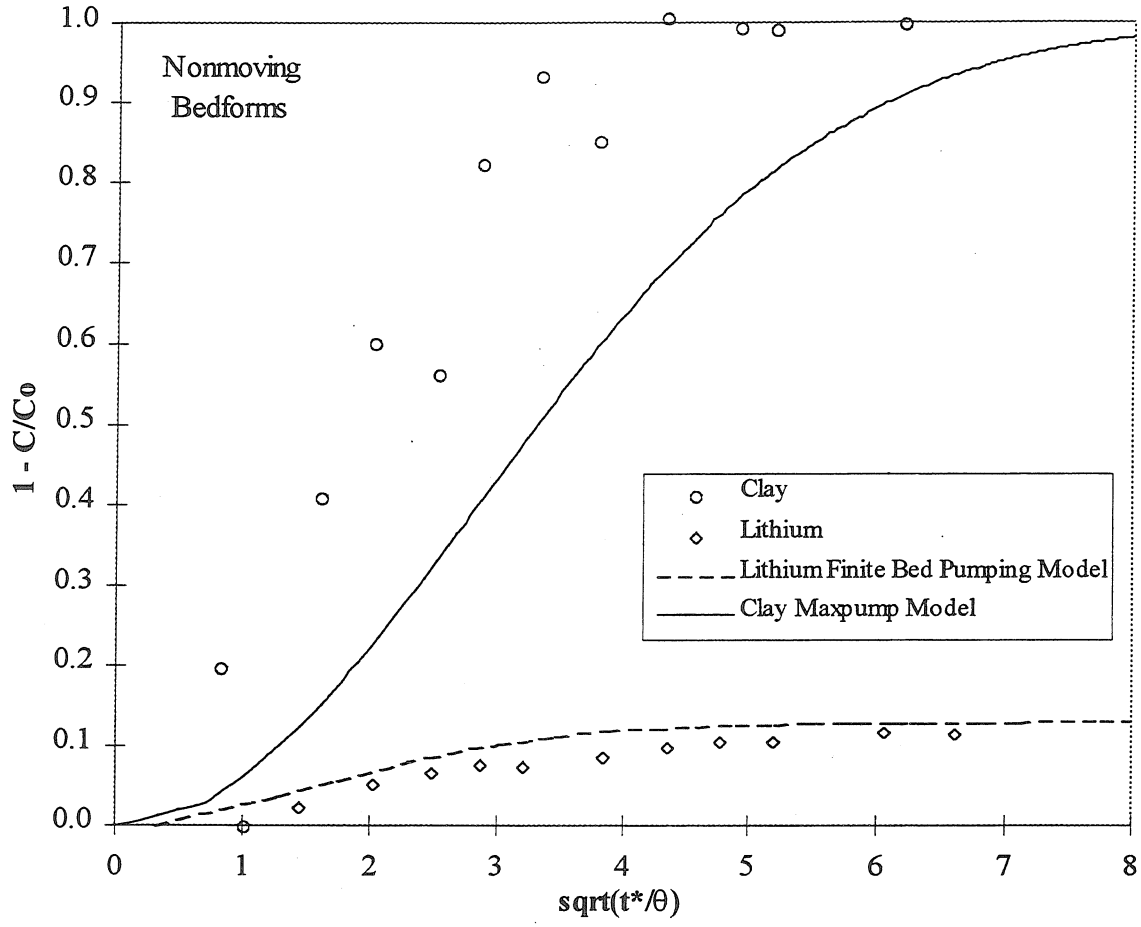

Figure 5.8: Comparison of experiment results and model predictions for Experiment #6.

Stream Parameters:	V = 16.5 cm/s	d = 6.9 cm	
Bed Parameters:	H = 1.0 cm	λ = 21 cm	$U_b = 0$
Chemical Parameters:	pH = 6.8	I = 5.0 mM	

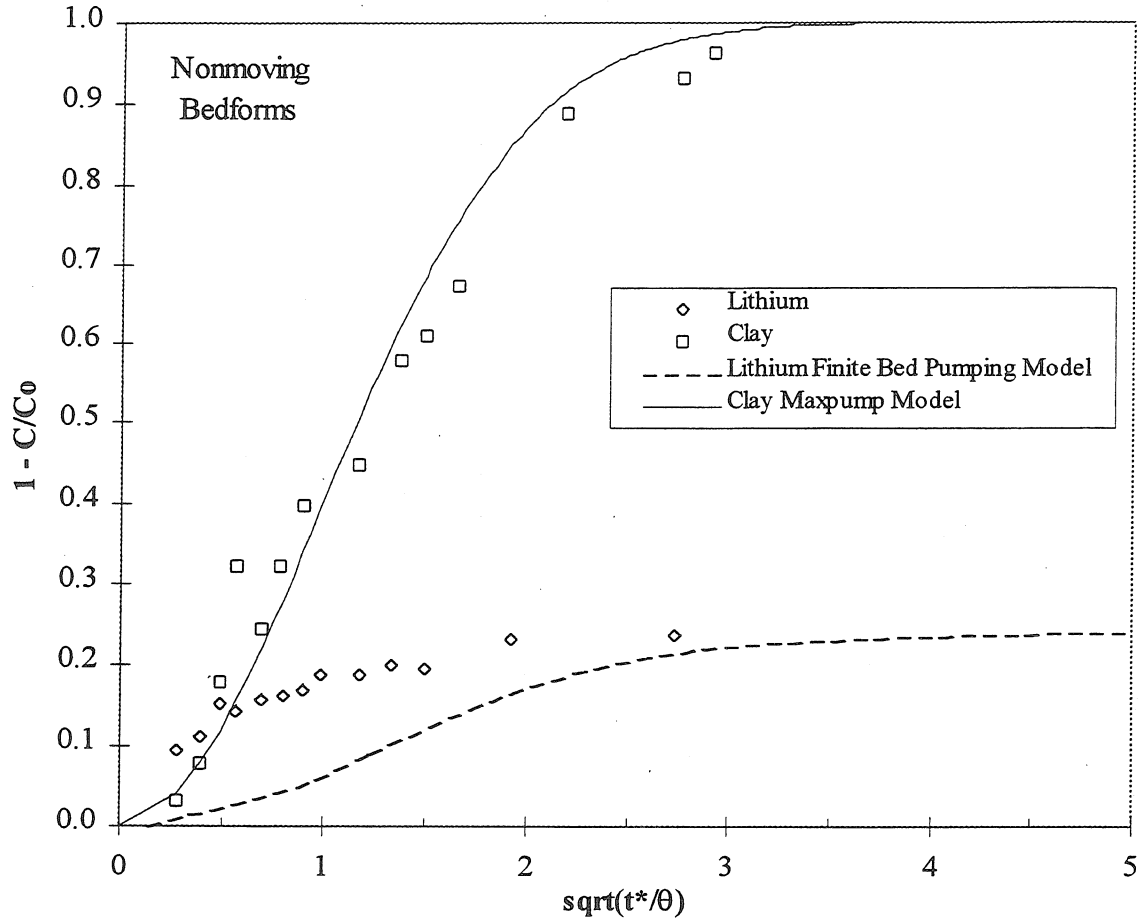

Figure 5.9: Comparison of experiment results and model predictions for Experiment #7.

Stream Parameters:	V = 15.2 cm/s	d = 12.7 cm	
Bed Parameters:	H = 1.9 cm	λ = 70 cm	$U_b = 0$
Chemical Parameters:	pH = 7.1	I = 5.0 mM	

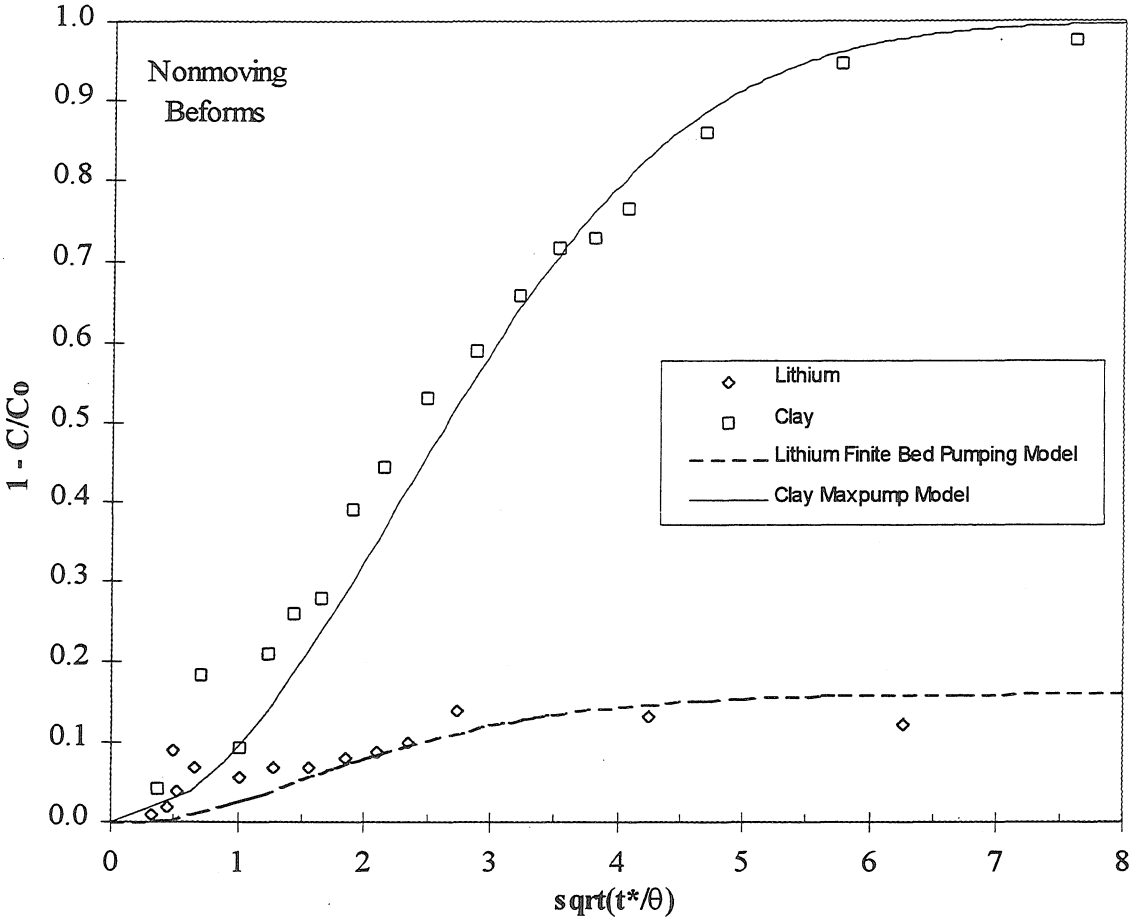

Figure 5.10: Comparison of experiment results and model predictions for Experiment #10.

Stream Parameters:	V = 15.7 cm/s	d = 9.8 cm	
Bed Parameters:	H = 1.5 cm	λ = 29 cm	$U_b = 0$
Chemical Parameters:	pH = 7.1	I = 5.0 mM	

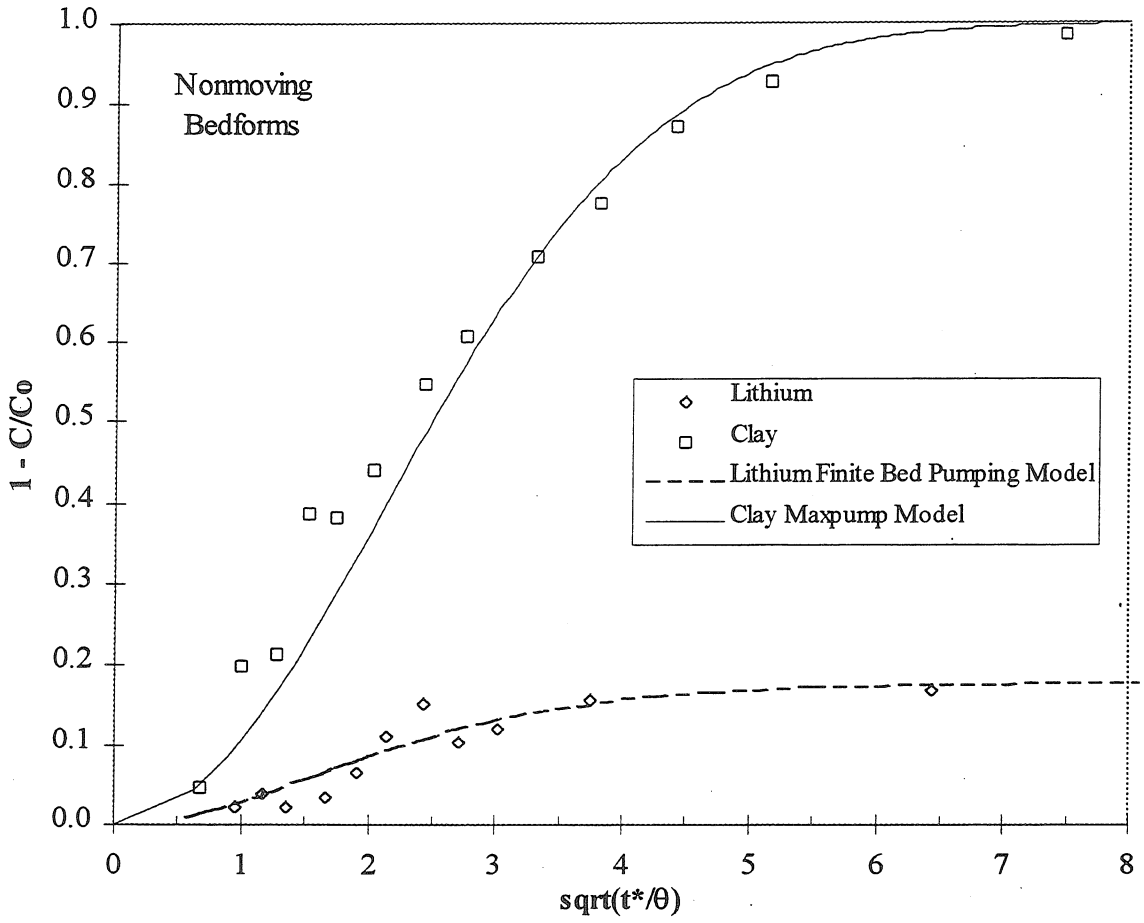

Figure 5.11: Comparison of experiment results and model predictions for Experiment #12.

Stream Parameters:	V = 15.7 cm/s	d = 9.6 cm	
Bed Parameters:	H = 1.5 cm	λ = 31 cm	$U_b = 0$
Chemical Parameters:	pH = 8.0	I = 5.3 mM	

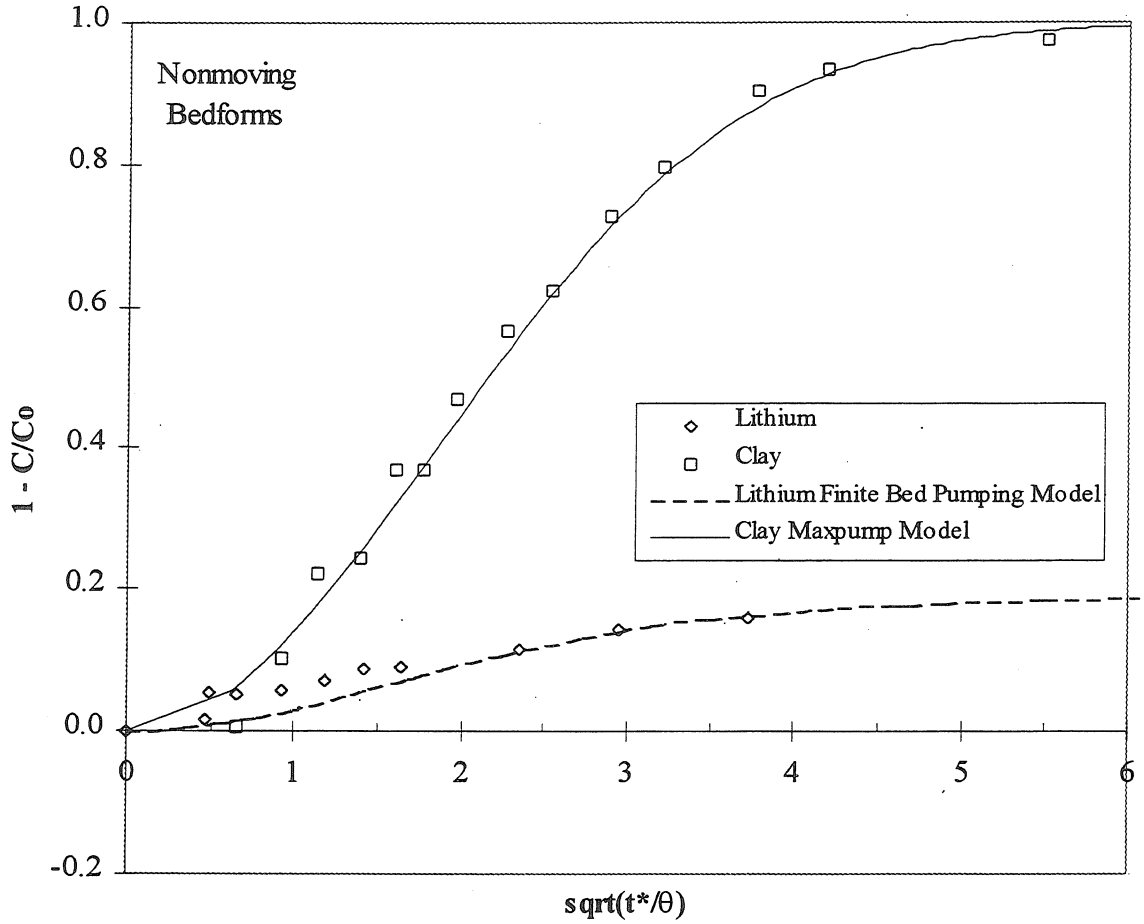

Figure 5.12: Comparison of experiment results and model predictions for Experiment #13.

Stream Parameters:	V = 14.4 cm/s	d = 9.0 cm	
Bed Parameters:	H = 1.4 cm	λ = 33 cm	$U_b = 0$
Chemical Parameters:	pH = 7.9	I = 0.5 mM	

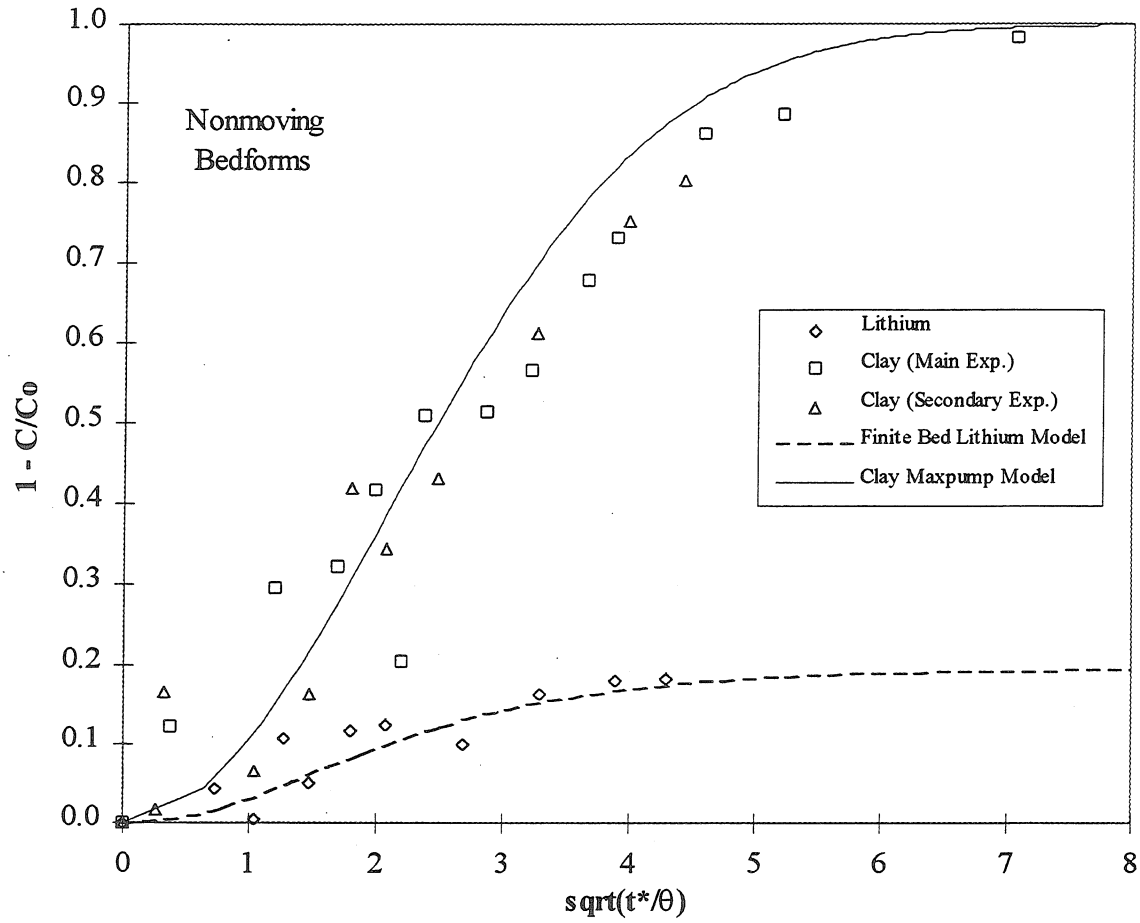

Figure 5.13: Comparison of experiment results and model predictions for Experiment #14. The secondary experiment involved adding more clay to the recirculating water without changing any other parameters.

Stream Parameters:	V = 15.9 cm/s	d = 9.4 cm	
Bed Parameters:	H = 1.6 cm	λ = 29 cm	$U_b = 0$
Chemical Parameters:	pH = 7.4	I = 0.6 mM	

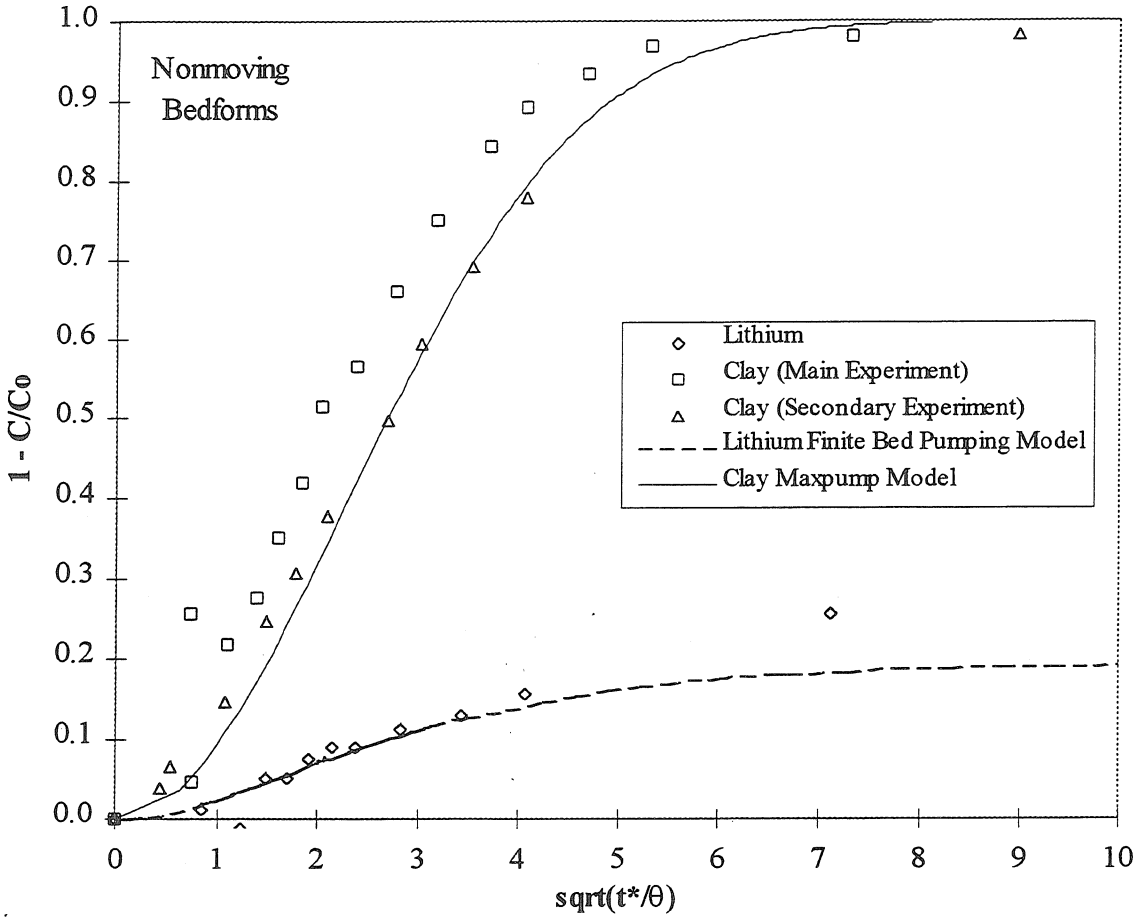

Figure 5.14: Comparison of experiment results and model predictions for Experiment #15. The secondary experiment involved adding more clay to the recirculating water without changing any other parameters.

Stream Parameters:	V = 12.6 cm/s	d = 7.9 cm	
Bed Parameters:	H = 1.5 cm	λ = 23 cm	$U_b = 0$
Chemical Parameters:	pH = 7.3	I = 5.0 mM	

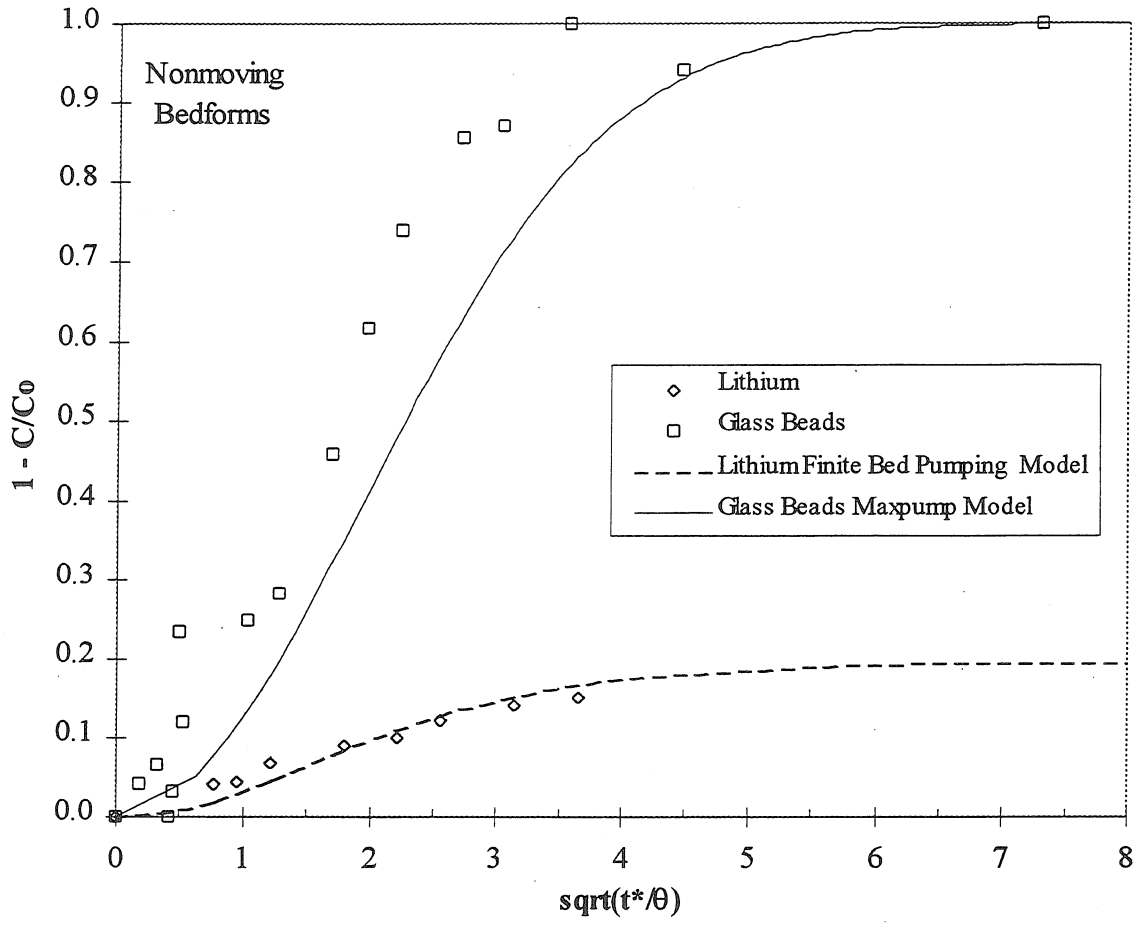

Figure 5.15: Comparison of experiment results and model predictions for Experiment #17. In this experiment, the colloidal tracer was glass beads.

Stream Parameters:	V = 16.7 cm/s	d = 9.8 cm	
Bed Parameters:	H = 1.4 cm	λ = 34 cm	$U_b = 0$
Chemical Parameters:	pH = 7.3	I = 5.0 mM	

5.1.4 Moving bedform experiments

Experiments 1-5, 8, 9, 11, and 16 were conducted with moving bedforms. Experiment 3 was conducted at the highest stream velocity (65 cm/s), which caused the production of silica fines that made colloid concentration data impossible to interpret. Secondary experiments 4a, 5a, 8a, 9a, and 15b also involved moving bedforms. Of these, experiments 4a and 5a included replacing the clay-bearing stream water with clean water, and the rest involved changing the flow rate. The secondary portion of experiment #11, with moving bedforms, involved reducing the stream velocity so that the secondary experiment, 11a, had nonmoving bedforms. Results from all primary experiments will be presented in this section, along with secondary experiments 8a, 9a, and 11a, in Figures 5.16-5.24. Secondary experiments 4a, 5a, and 15b had a release of kaolinite from the bed, which will be discussed in Section 5.1.7.1.

The turnpump model described in Sections 3.1.4.2 and 3.3.2 was used to predict lithium and colloid exchange in these experiments. Lithium was assumed to be a conservative tracer, while clay was assumed to be completely trapped by the deep bed (below the maximum scour depth). Most model predictions for lithium exchange are excellent; the exceptions are Experiments #8 and #9. Model predictions for colloid exchange with fast turnover ($U_b^* > 1$) are generally good as well, with the notable exception of Experiment #4 (Figure 5.19). Turnpump model predictions for colloid exchange with slow turnover ($U_b^* < 1$) are very good at short times, but underpredict the exchange at later times. This indicates the limited applicability of the turnpump model to cases with slowly-moving bedforms. For these experiments, maxpump model predictions

are included in the graphs for comparison. The maxpump model includes pumping with complete trapping, but assumes bedforms are stationary and thus neglects the effect of turnover. The maxpump model provided reasonably good predictions for the exchange due to very-slowly-moving bedforms ($U_b^* < 0.4$). These results indicate that turnover can be neglected when it is extremely slow. In all cases with $U_b^* < 1$, the results are observed to be between the predictions of the turnpump and maxpump models.

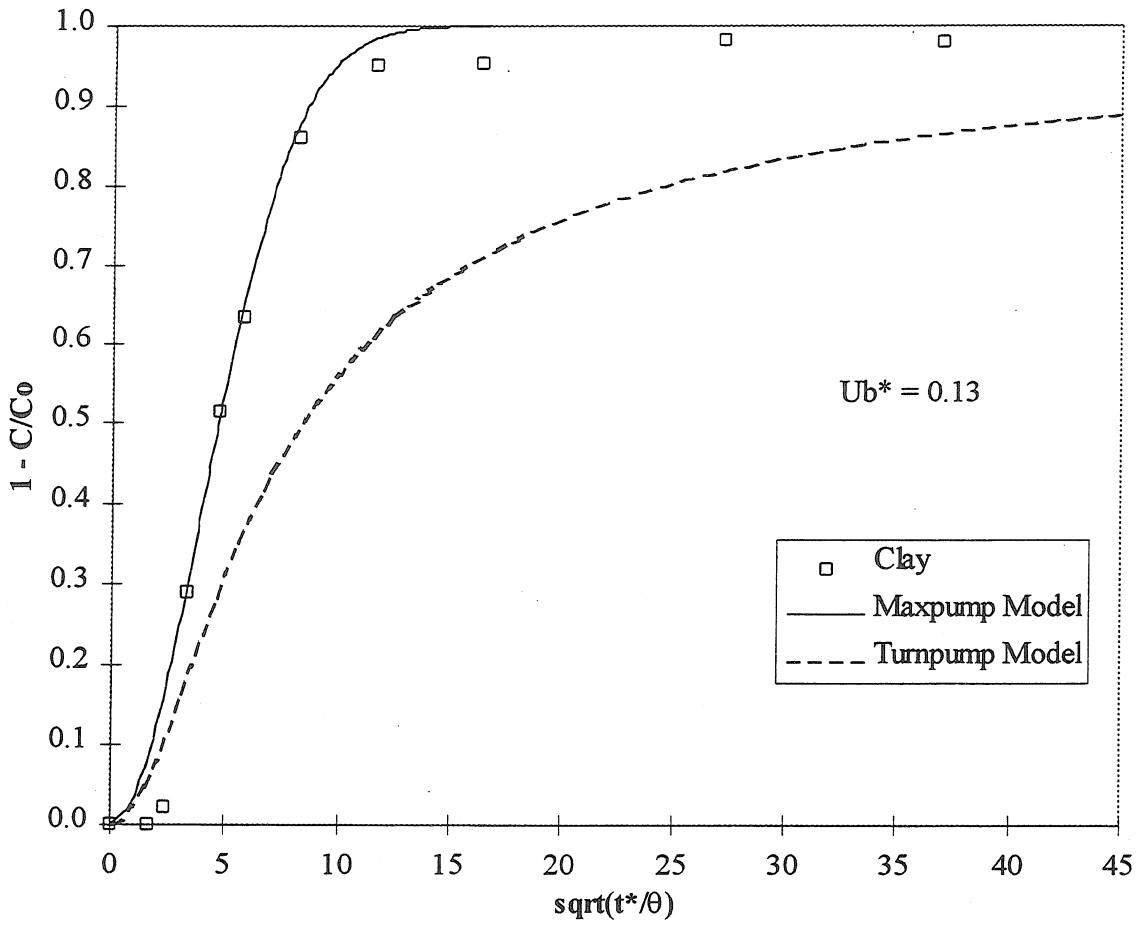

Figure 5.16: Comparison of experiment results and model predictions for Experiment #1. A lithium tracer was not used in this experiment.

Stream Parameters:	V = 15.0 cm/s	d = 3.5 cm	
Bed Parameters:	H = 3.3 cm	λ = 17 cm	U_b = 0.2 cm/min
Chemical Parameters:	tap water	pH ~ 8.2	I ~ 15 mM

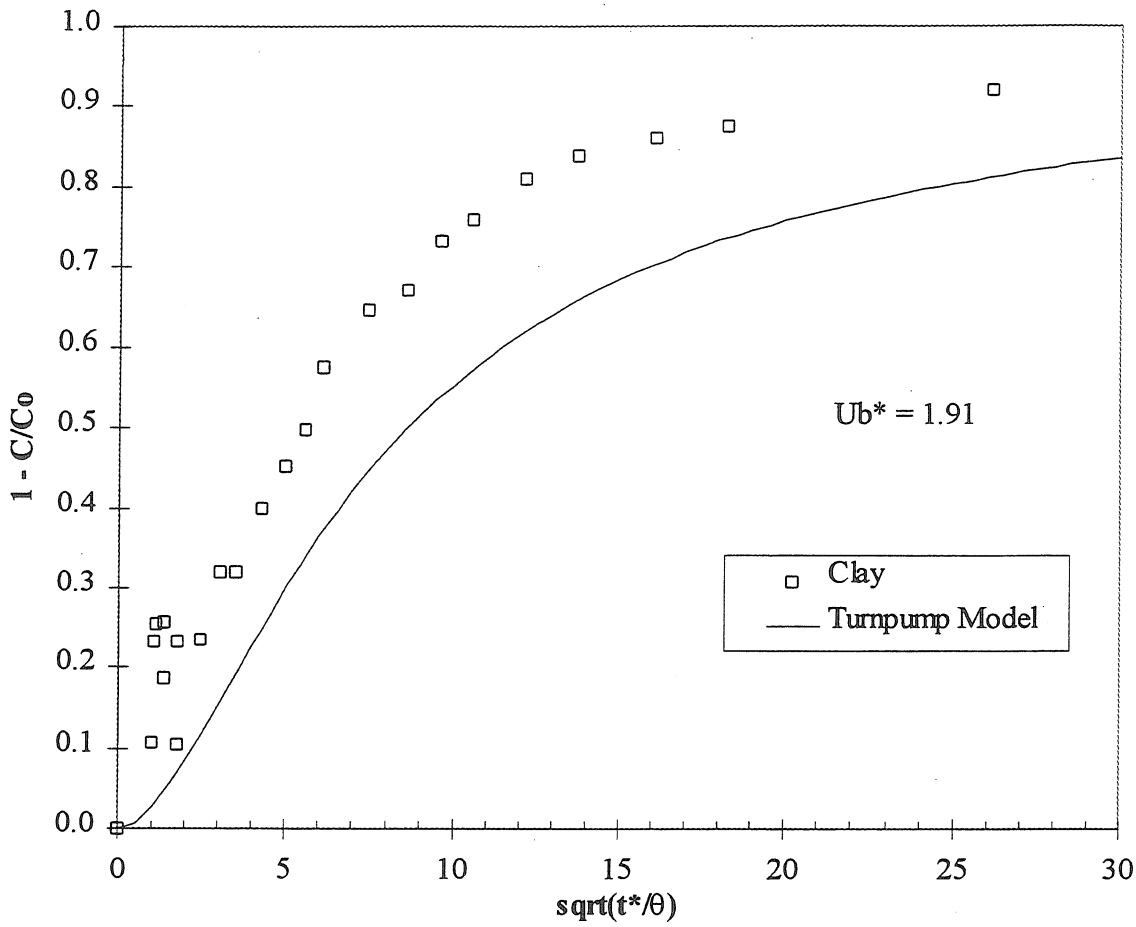

Figure 5.17: Comparison of experiment results and model predictions for Experiment #2. A lithium tracer was not used in this experiment.

Stream Parameters:	V = 36.2 cm/s	d = 6.2 cm	
Bed Parameters:	H = 1.5 cm	λ = 17 cm	U_b = 3.2 cm/min
Chemical Parameters:	tap water	pH ~ 8.2	I ~ 15 mM

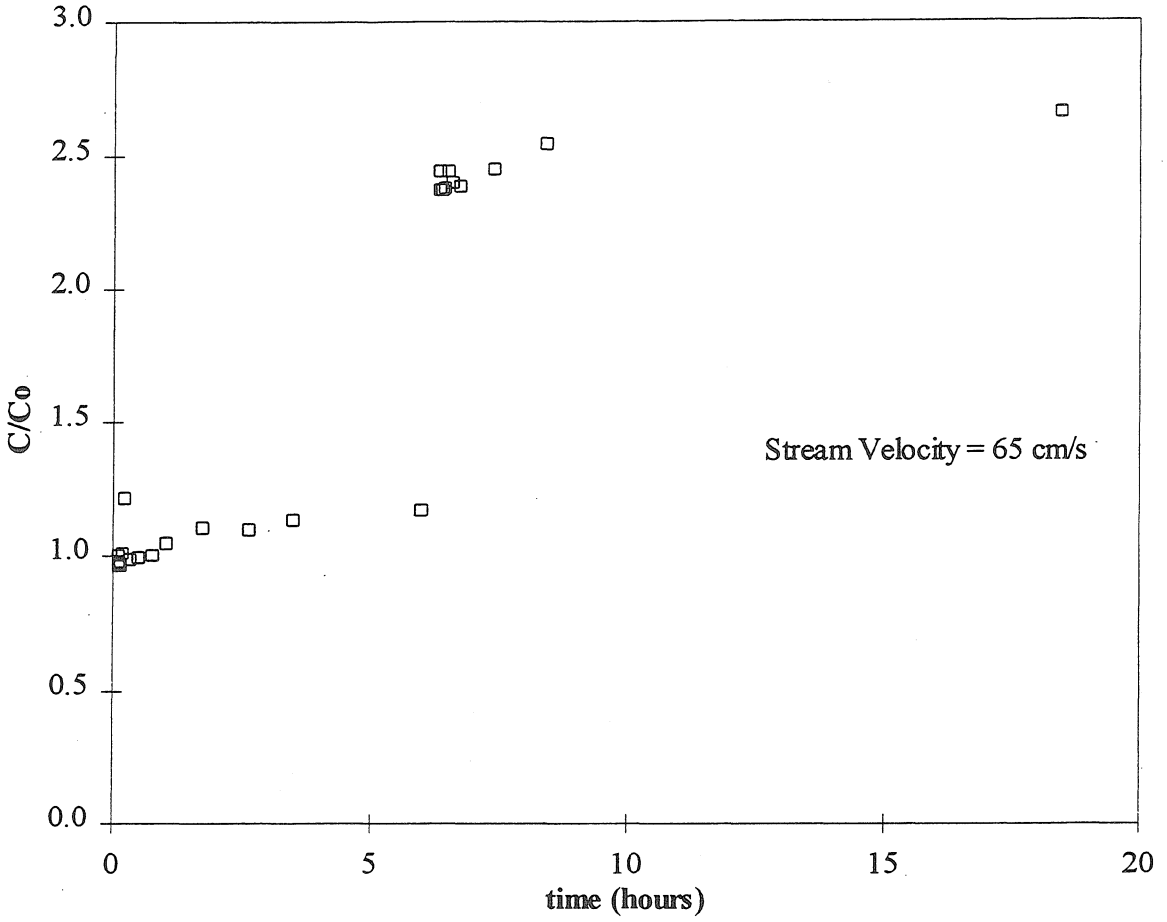

Figure 5.18: Results for the primary and secondary portions of Experiment #3. The high rate of sediment transport caused production of silica fines, which caused the colloid concentration to increase over time and thus invalidated the results. The secondary experiment simply involved adding more clay to the stream at t ~ 6 hours. No models were applied to this experiment.

Stream Parameters:	V = 64.9 cm/s	d = 9.0 cm	
Bed Parameters:	H = 2.3 cm	λ = 73 cm	U_b = 10.0 cm/min
Chemical Parameters:	tap water	pH ~ 8.2	I ~ 15 mM

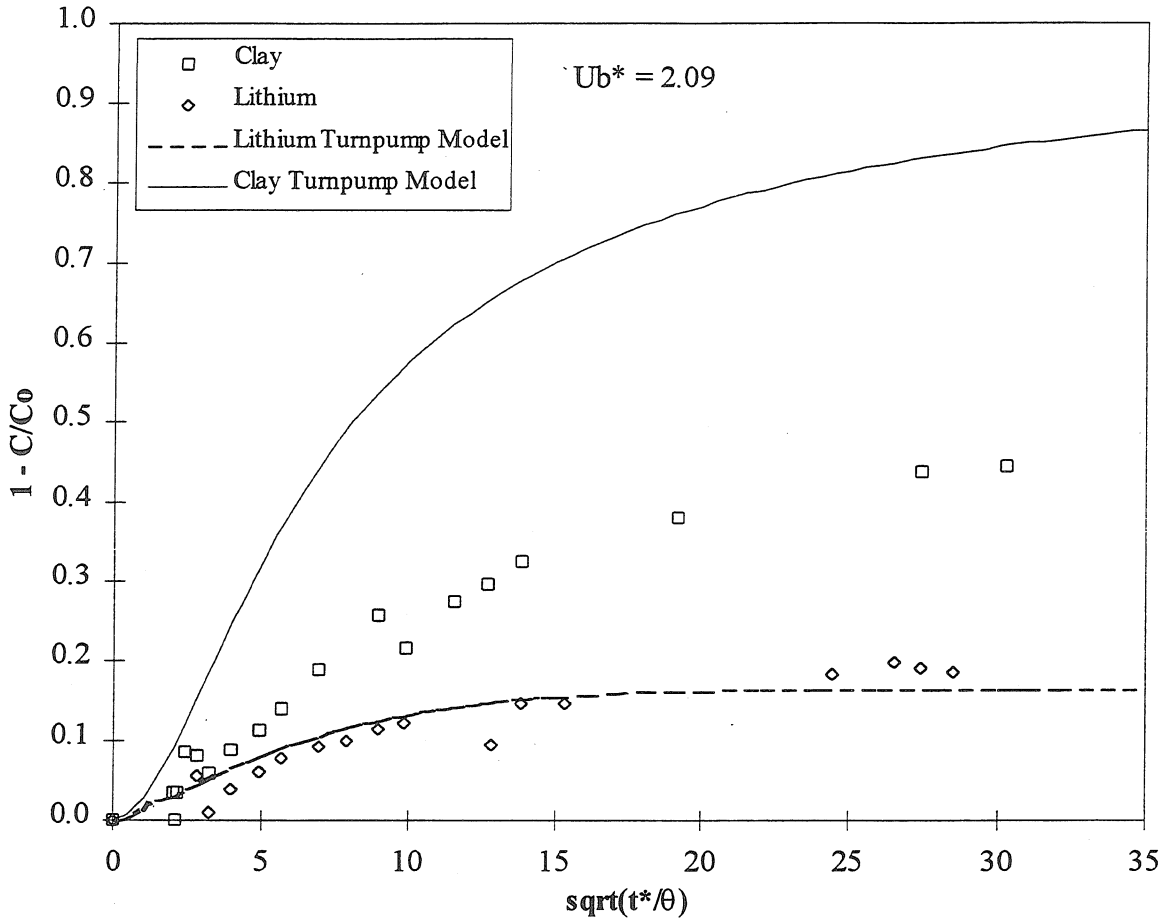

Figure 5.19: Comparison of experiment results and model predictions for Experiment #4.

Stream Parameters:	V = 42.7 cm/s	d = 7.3 cm	
Bed Parameters:	H = 1.1 cm	λ = 20 cm	U_b = 3.5 cm/min
Chemical Parameters:	tap water	pH ~ 8.2	I ~ 15 mM

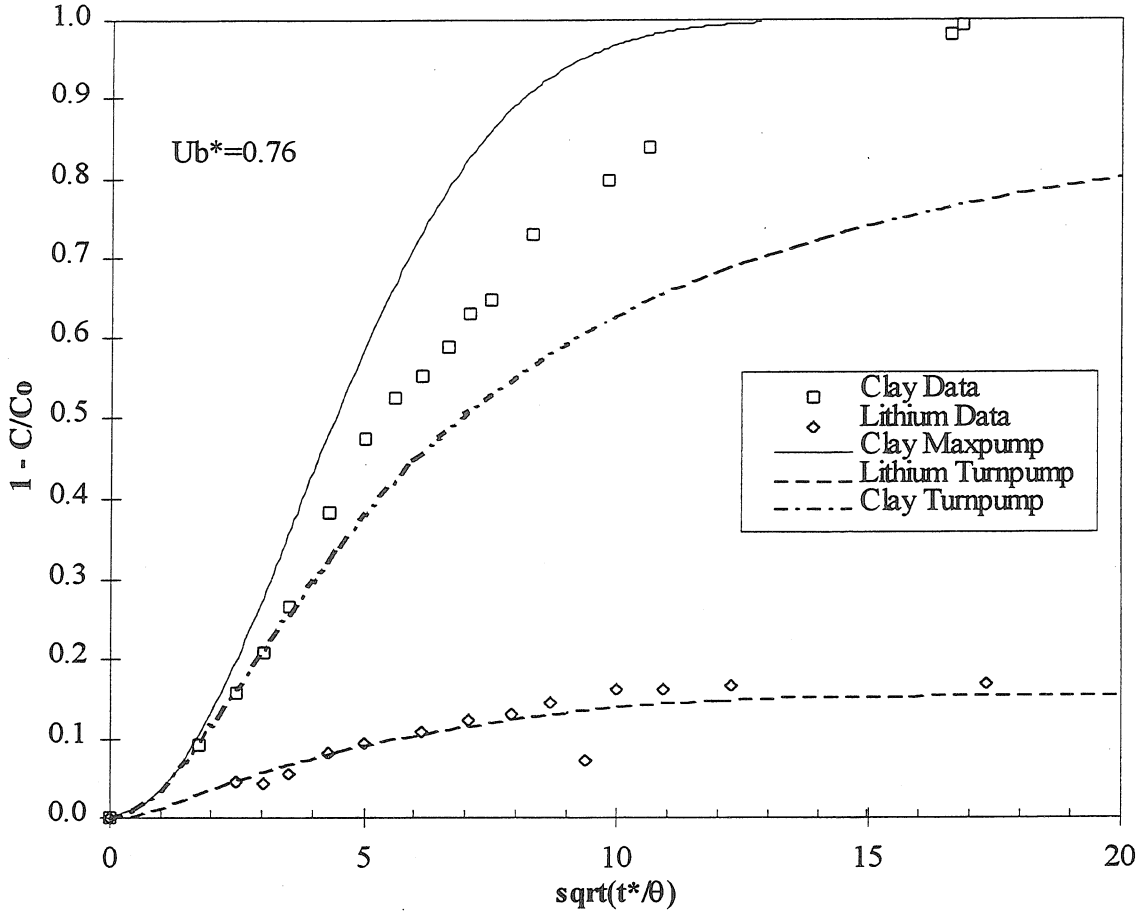

Figure 5.20: Comparison of experiment results and model predictions for Experiment #5.

Stream Parameters:	V = 28.8 cm/s	d = 8.0 cm	
Bed Parameters:	H = 2.0 cm	λ = 23 cm	U_b = 0.6 cm/min
Chemical Parameters:	tap water	pH ~ 8.2	I ~ 15 mM

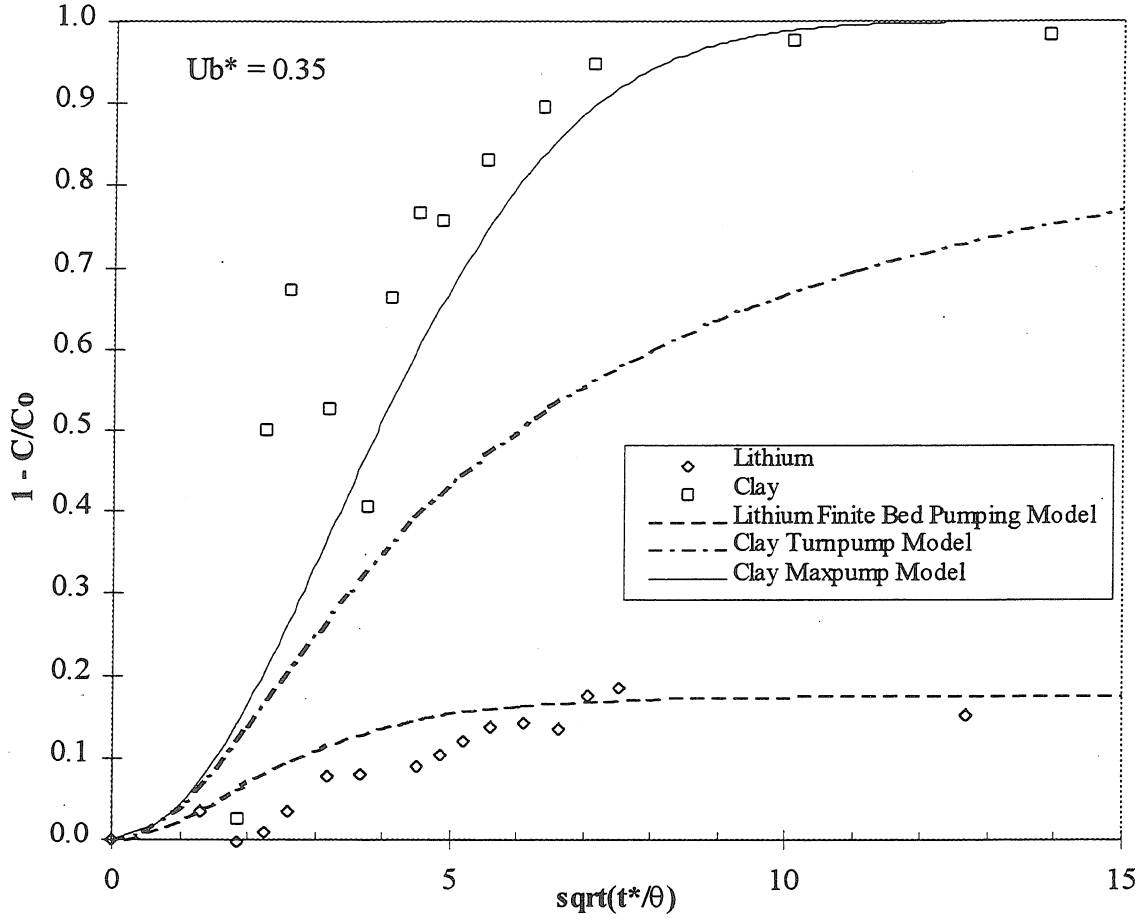

Figure 5.21: Comparison of experiment results and model predictions for Experiment #8.

Stream Parameters:	V = 22.1 cm/s	d = 11.0 cm	
Bed Parameters:	H = 2.4 cm	λ = 24 cm	U_b = 0.2 cm/min
Chemical Parameters:	pH = 7.0	I = 5.0 mM	

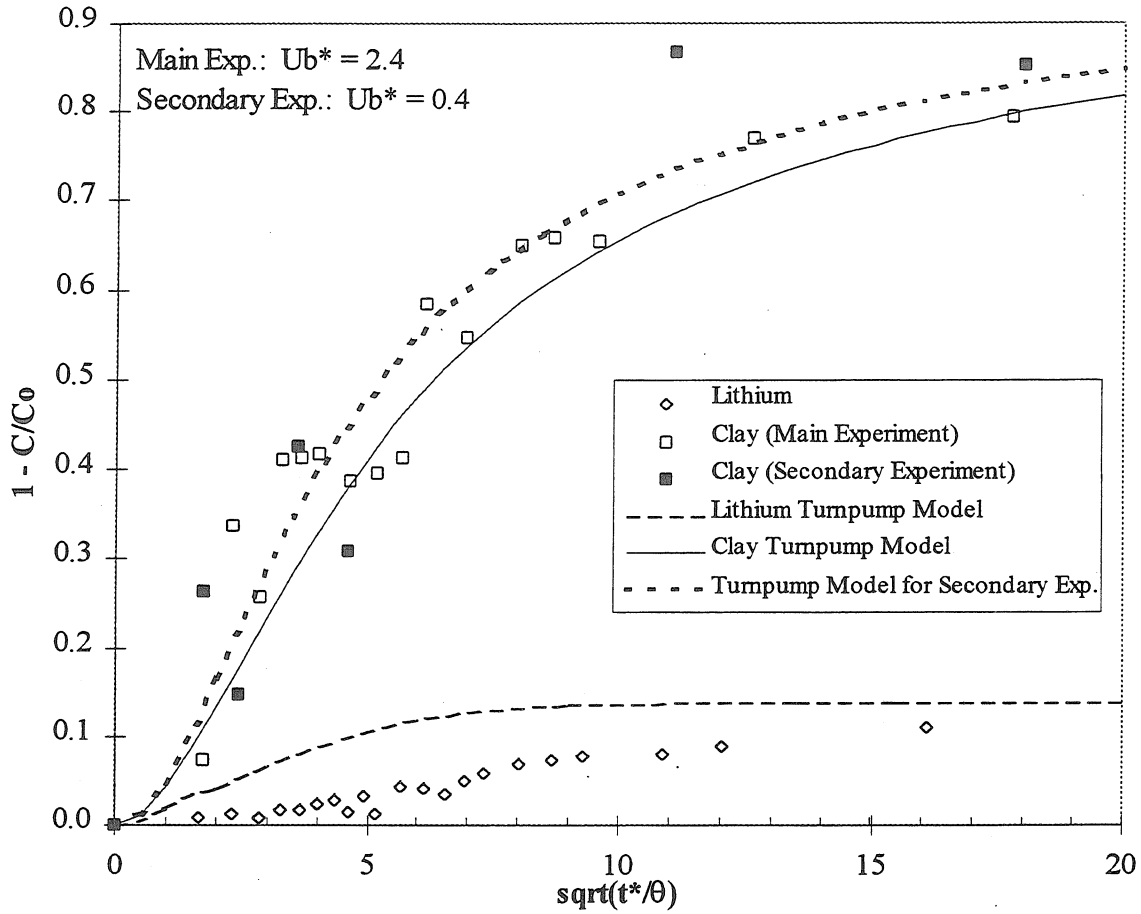

Figure 5.22: Comparison of experiment results and model predictions for Experiment #9, including secondary experiment.

Stream Parameters:	V = 39.0 cm/s	d = 9.4 cm	
Bed Parameters:	H = 1.7 cm	λ = 32 cm	U_b = 2.2 cm/min
Chemical Parameters:	pH = 7.1	I = 5.0 mM	

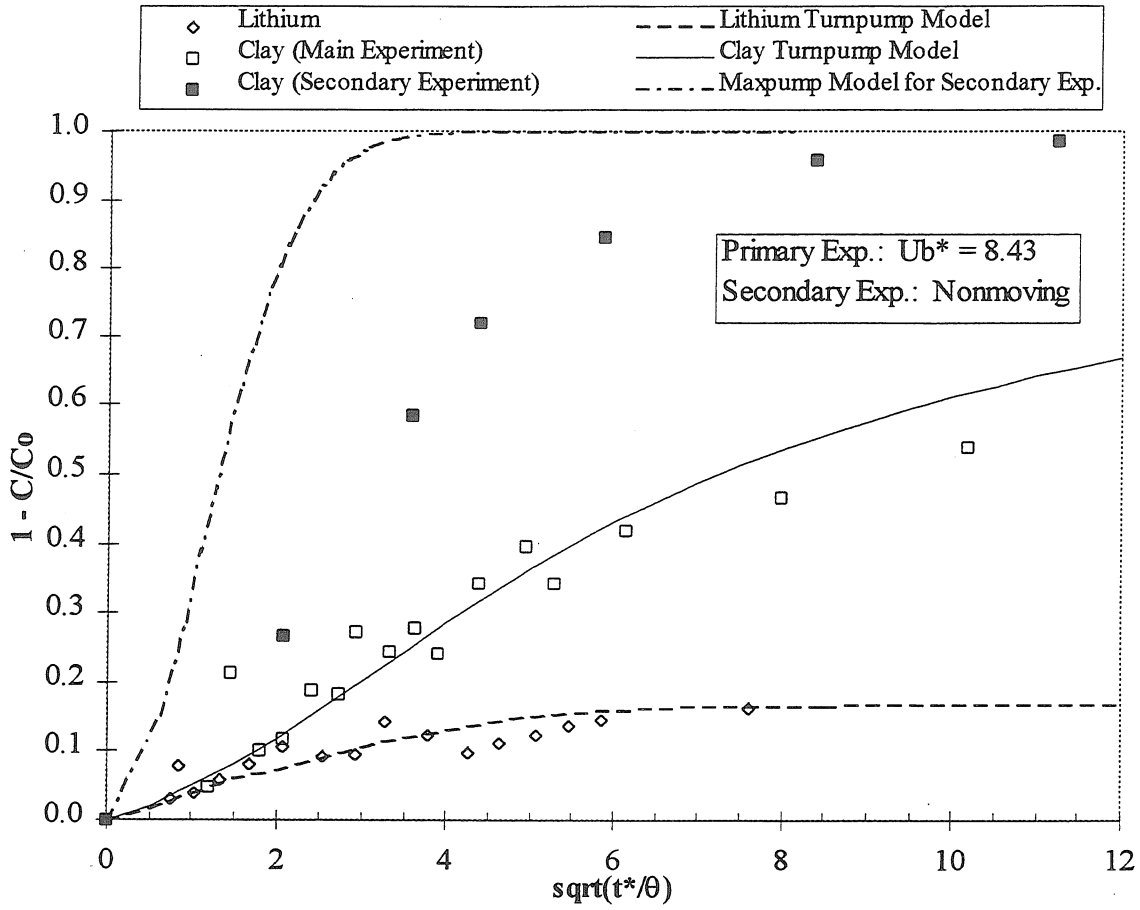

Figure 5.23: Comparison of experiment results and model predictions for Experiment #11, including secondary experiment.

Stream Parameters:	V = 45.2 cm/s	d = 9.4 cm	
Bed Parameters:	H = 2.7 cm	λ = 64 cm	U_b = 6.1 cm/min
Chemical Parameters:	pH = 7.1	I = 5.0 mM	

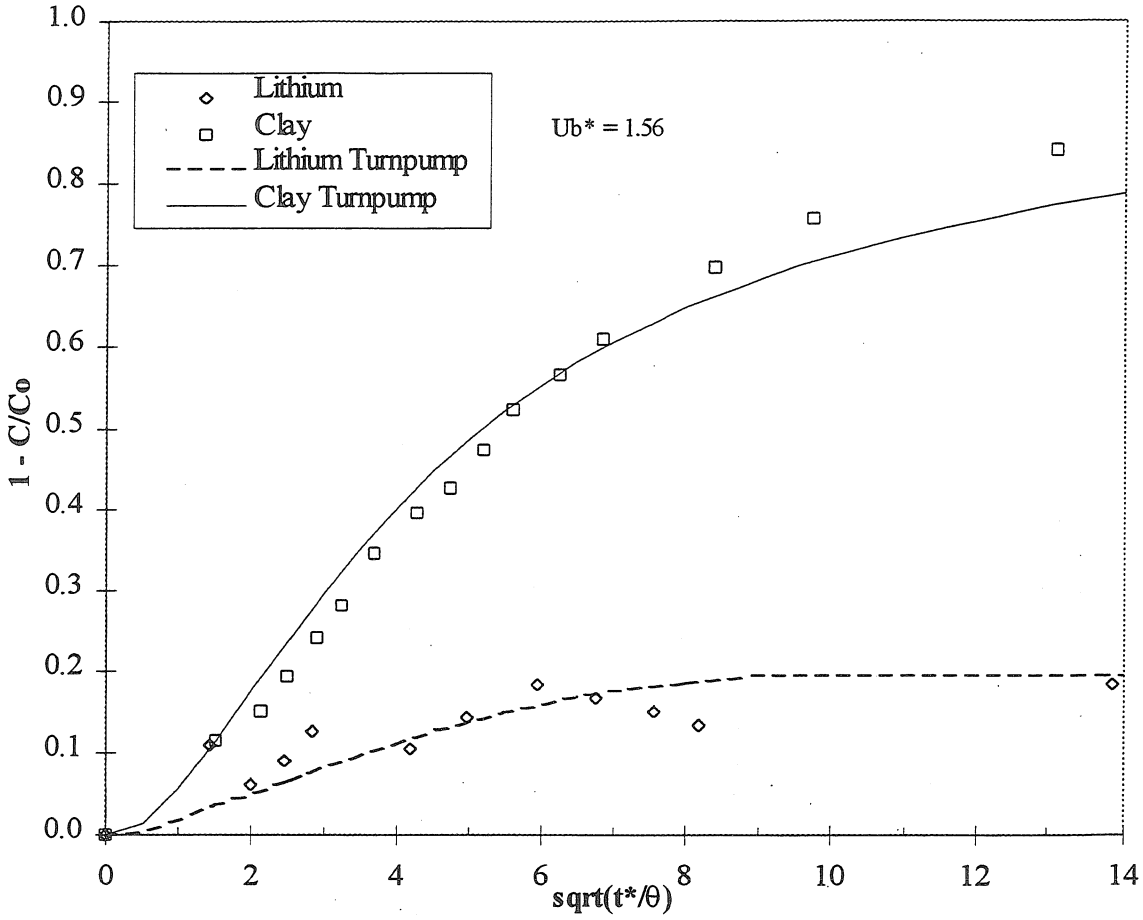

Figure 5.24: Comparison of experiment results and model predictions for Experiment #16.

Stream Parameters:	V = 34.3 cm/s	d = 8.9 cm	
Bed Parameters:	H = 1.7 cm	λ = 33 cm	U_b = 1.1 cm/min
Chemical Parameters:	pH = 7.9	I = 5.0 mM	

5.1.5 Experiments with different chemical conditions

Experiments 1-5 were done with Pasadena tap water, which typically has a pH near 8.2 and an ionic strength around 15 mM. Experiments 6-17 used deionized water with appropriate chemicals added to control the pH and ionic strength. Most of these were performed at the 'baseline' chemical condition of pH ~7 (range 6.8-7.3) and 5 mM NaCl. Experiments 13 and 14 had low ionic strength (~0.5 mM), and pH's of 7.9 and 7.4, respectively. Experiment 16 had the baseline ionic strength with pH 7.9.

For all of these chemical conditions, filtration was high enough to justify use of the complete trapping assumption. Column results showed that the filtration coefficient was always greater than 0.1 cm^{-1} (these results are presented in Section 5.2). All flume experiments had λ_f* of one or greater (see Table 5.3 for values of λ_f and λ_f* for each experiment). The results displayed in the previous two sections also show the validity of the complete trapping assumption. Model predictions for colloid exchange were good over all ranges of pH and ionic strength.

5.1.5a Comparison of maxpump model and clay pumping model

The complete clay pumping model with particle filtration and settling was initially used to predict colloid exchange. However, predictions from the clay pumping model were identical to those of the maxpump model for the range of filtration coefficients present in the experiments. This is shown in Figure 5.25 which has both clay pumping and maxpump model results for Experiment #13, which had λ_f* = 1.05. Essentially, these models give the same results. They differ only in the exchange at very

early times, due to the use of a different numerical approach for the different models. The maxpump model was calculated with larger time steps (in this case, $t^*/\theta = 0.4$), and so has poorer resolution at early times compared to the turnpump model. This effect is enhanced dramatically due to the use of the square root of t^*/θ as the abscissa. Both models give the same results after the first maxpump time step.

Clay pumping model runs for ranges of filtration coefficient and particle settling velocity can be found in Chapter 6.

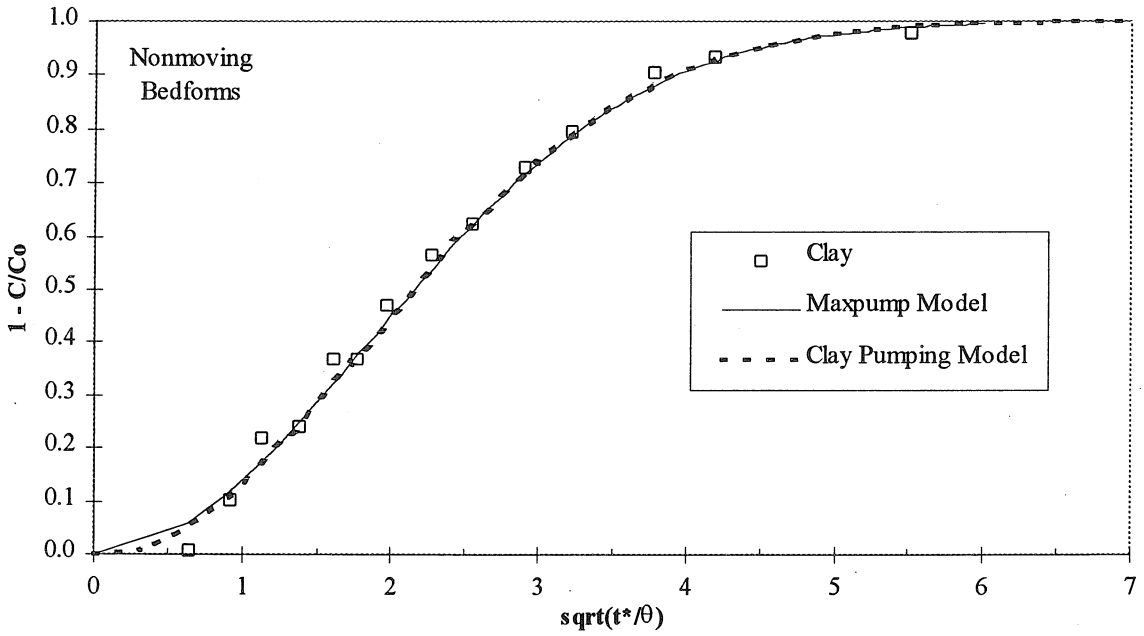

Figure 5.25: Comparison of clay maxpump model and complete pumping model with filtration and settling. Model runs were done using parameters from Experiment #13. Experimental data are included for comparison.

5.1.6 Lithium results: comparison of infinite bed, finite bed, and turnpump models

Previous work in the Keck Labs on bed exchange used a 20 cm deep sediment bed, and models applied to this system assumed that the bed was infinitely deep (Elliott, 1990; Elliott and Brooks, 1997ab; Eylers, 1990). The flume used in the experiments of this work was shallower and only allowed a bed of 8-10 cm, which necessitated the development of models based on a finite bed. The finite bed model for pumping was very successful in predicting the exchange due to nonmoving bedforms. The main effect of the finite bed is to bound the exchange at long times, as shown in Figure 5.26 Additional illustrations of how the bed depth affects the model results are given in Sections 6.1 and 6.2.

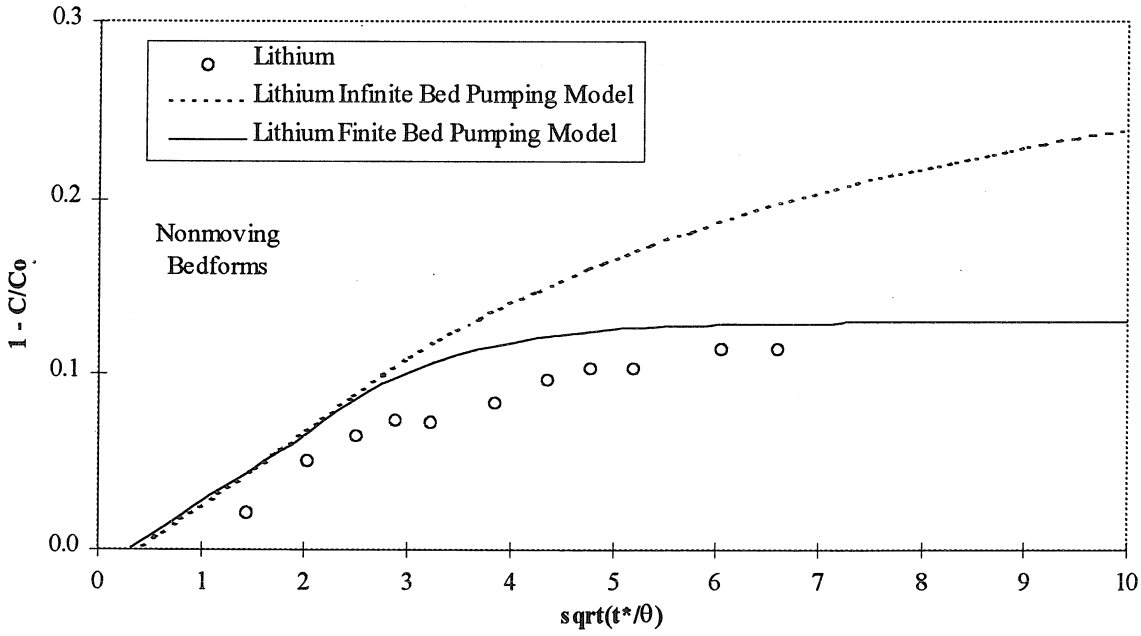

Figure 5.26: Comparison of finite bed and infinite bed pumping models for lithium. Model runs were done using parameters from Experiment #6, with nonmoving bedforms. Experimental data are included for comparison.

Previous modeling for cases with moving bedforms (Elliott, 1990) employed a modified, Lagrangian pumping model. For the present work, the finite bed pumping model was combined with the turnover model in the turnpump model. The turnpump model was very successful in predicting the exchange due to fast-moving bedforms. Turnover tends to continually mix the upper part of the bed, but hinders penetration to the deeper bed, resulting in slower exchange compared to the nonmoving bedform case. This can clearly be seen in Figure 5.27 The final lithium concentration is not affected by turnover, since ultimate dilution of a conservative tracer is controlled by the volumes of the different reservoirs of water in the system.

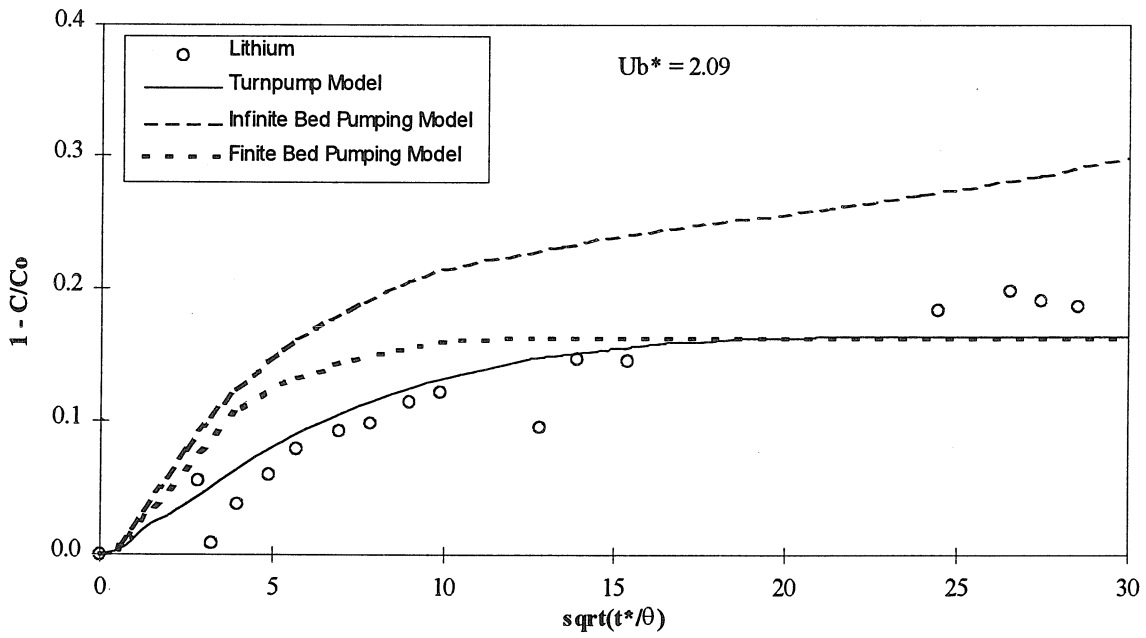

Figure 5.27: Comparison of turnpump model with finite bed and infinite bed pumping models for lithium. Model runs were done using parameters from Experiment #4, with fast-moving bedforms. Experimental data are included for comparison.

In the case of slowly-moving bedforms, the turnpump model predicts the exchange well at early times, but underpredicts exchange at later times. It appears that in this case, initial transport is strongly influenced by turnover, but later transport is controlled more by pumping. This is shown in Figure 5.28 where the experimental data is seen to roughly follow the turnpump prediction initially (sqrt(t*/θ) < 3), go through a transition period where it lies between the turnpump and finite bed predictions (3 < sqrt(t*/θ) < 7), and then reach the ultimate dilution as predicted by the finite bed model (sqrt(t*/θ) > 7). The ultimate dilution for the two models is the same, though the finite bed model predicts the ultimate dilution will be reached at an earlier time.

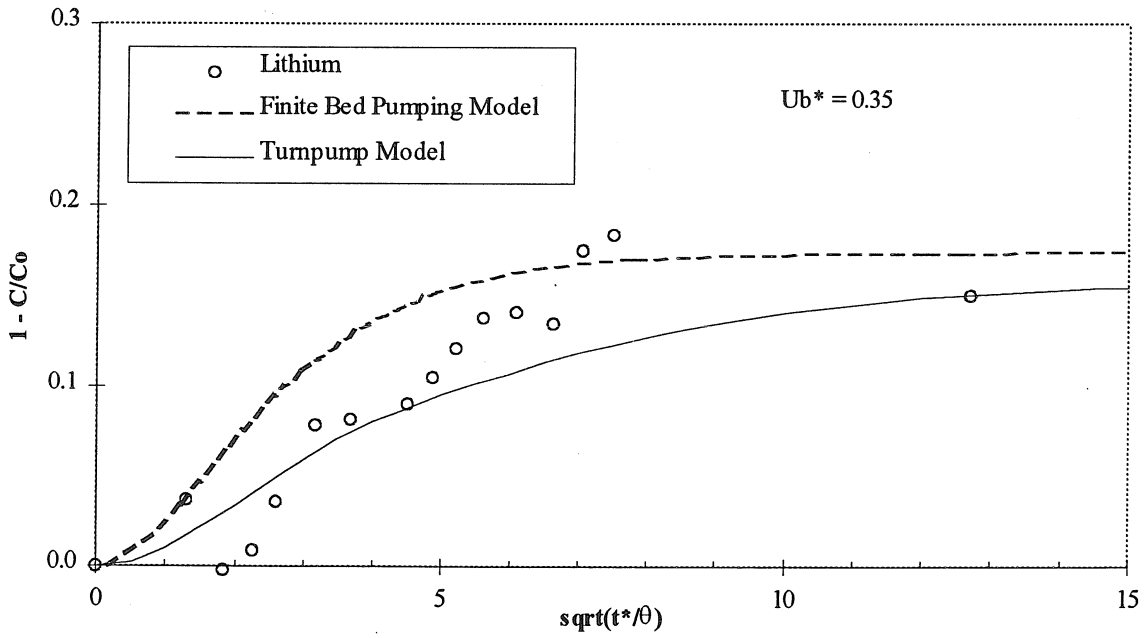

Figure 5.28: Comparison of turnpump and finite bed models for lithium. Model runs were done using parameters from Experiment #8, with slow-moving bedforms. Experimental data are included for comparison.

5.1.7 Secondary experiments

Seven experiments included successful secondary experiments. One of these secondary experiments had two separate parts. In addition, one secondary experiment was performed which did not yield meaningful results. The successful secondary experiments can be divided into two categories: those that involved changing the recirculation flow rate, and those that involved changing the colloid concentration in the recirculating water.

5.1.7.1 Decreases and increases in flow rate

Secondary experiments 9a and 11a involved reducing the recirculation flow rate. Results of these secondary experiments were renormalized so they could be presented in the same graphs as the primary results, Figures 5.22 and 5.23 in Section 5.1.4. Renormalization means that concentration data for the secondary experiments were nondimensionalized by the concentration at the time of the start of the secondary experiment, and plotted against the elapsed time since the start of the secondary experiment. In other words, the time at which the flow rate was reduced was taken as a new t_0, and the concentration at this time was taken as a new C_0. These were also taken as the initial conditions for the model prediction. The model prediction agreed fairly well with the renormalized secondary data for Experiment #9a, but did not agree with the secondary data for Experiment #11a.

Secondary experiments 8a and 15b involved increasing the recirculation flow rate. In both experiments, clay was released from the bed immediately after the flow increase,

as shown below in Figures 5.29 and 5.30. Presumably, additional turnover at the higher stream velocity resulted in the release of trapped clay. In Experiment #8, Figure 5.29, the primary experiment had slowly-moving bedforms, while the secondary experiment developed fast-moving bedforms which caused the release of a small amount of clay (13% of C_0). In Experiment #15b, Figure 5.30, the primary experiment had nonmoving bedforms, and the flow increase resulted in fast-moving bedforms and released a large amount of clay (75% of the *total* clay added, $C_{01} + C_{02}$). This supports the idea that clay is trapped mostly in the deeper bed in the case of moving bedforms (turnover and pumping), but is trapped in the upper portion of the bed in the case of nonmoving bedforms (pumping only). This also validates the turnpump model assumption that clay is not permanently stored (attached to sand grains) in the turnover region.

The release of clay was not modeled. The models of Section 3 are equally applicable to transport into or out of the bed. However, in order to calculate the exchange of a particular tracer, the initial distribution of that tracer in the system must be known. The initial condition for the clay release is not well-defined because clay has an unknown, heterogeneous distribution in the bed at the time of the flow increase. If the models were implemented in a finite-element or similar numerical scheme, then the distribution of tracer in the bed would be known at all times, and problems involving successive clay trapping and release could be solved.

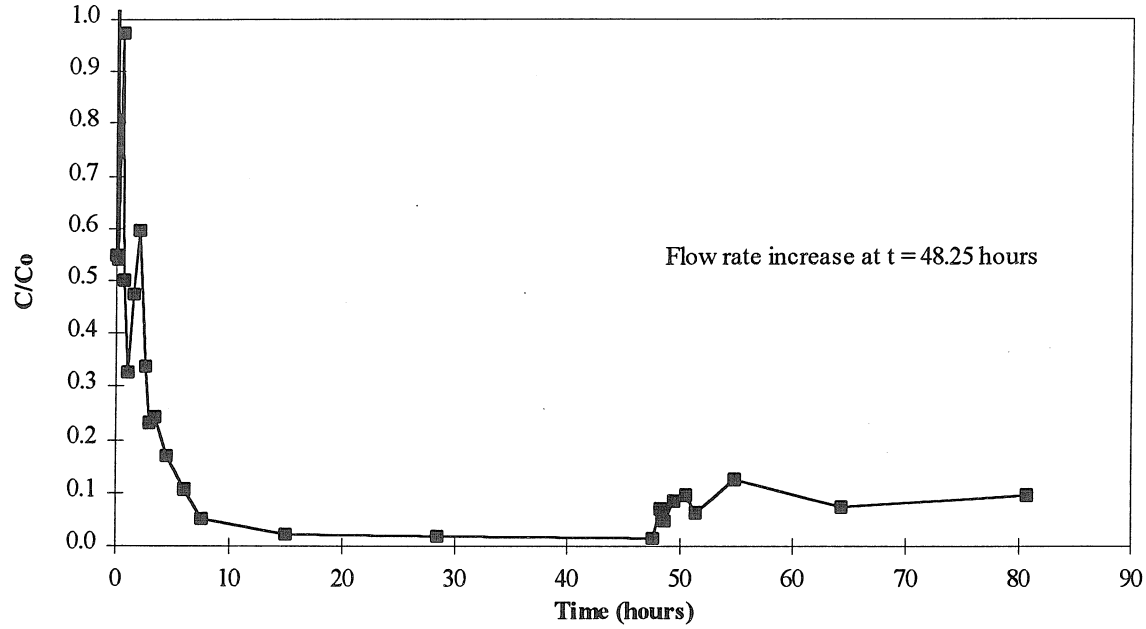

Figure 5.29: Complete clay bed-exchange data for Experiment #8, including secondary data. The primary experiment had slowly-moving bedforms ($U_b^* = 0.35$), while the secondary experiment had fast-moving bedforms ($U_b^* = 1.51$).

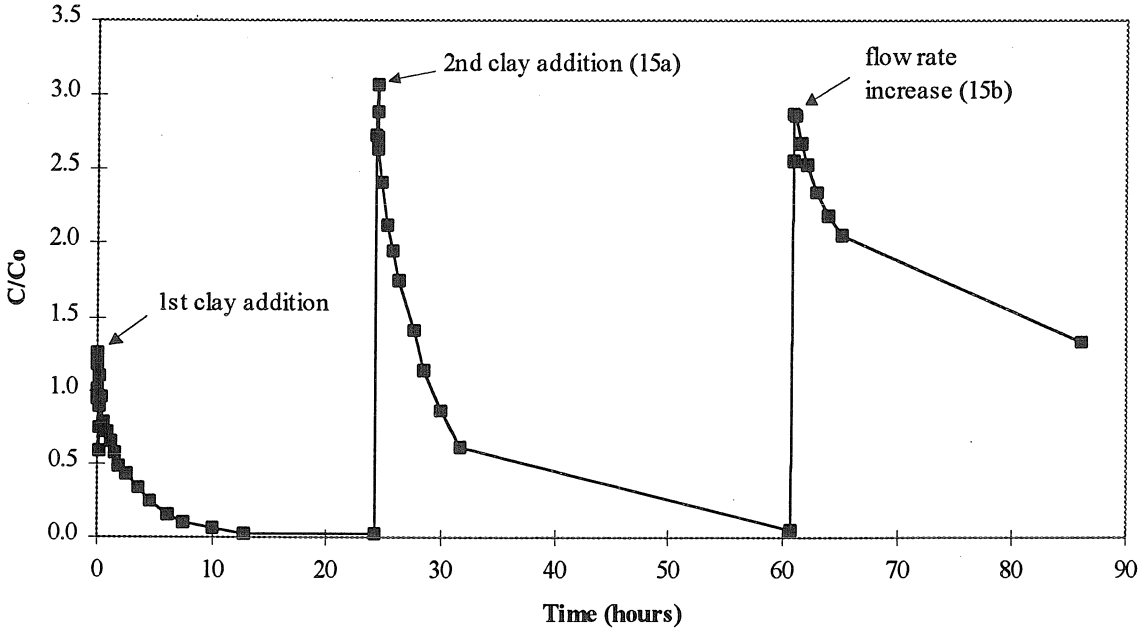

Figure 5.30: Complete clay bed-exchange data for Experiment #15, including data from two secondary experiments. The primary experiment and second clay addition (15a) had nonmoving bedforms, while 15b had fast-moving bedforms (U_b not measured).

5.1.7.2 Changes in colloid concentration of surface water

Secondary experiments 4a and 5a involved reducing the concentration of colloids in the recirculating water. This was accomplished by stopping the flume, drawing off most of the stream water, refilling the flume with colloid-free water, and then restarting the flume. Stopping and restarting the flume has no impact on the hydraulic conditions or the bedforms. At the start of the secondary experiment, almost clay-free stream water is flowing over a bed containing trapped clay. The results of these secondary experiments are presented in Figures 5.31 and 5.32, below.

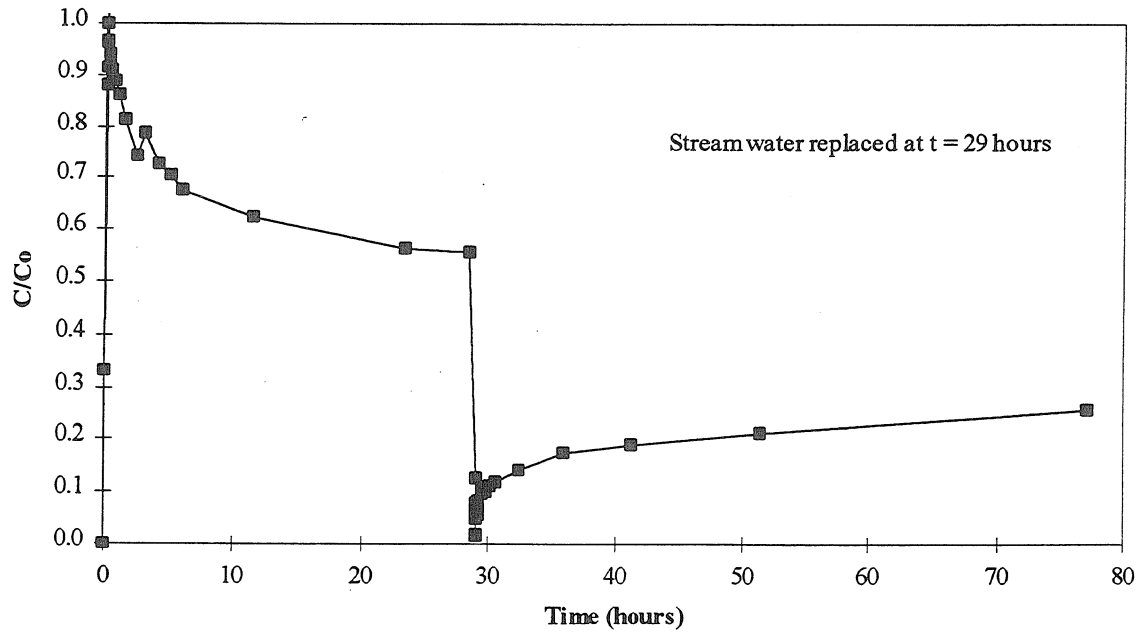

Figure 5.31: Complete clay bed-exchange data for Experiment #4, including secondary data. The entire experiment had fast-moving bedforms ($U_b^* = 2.09$).

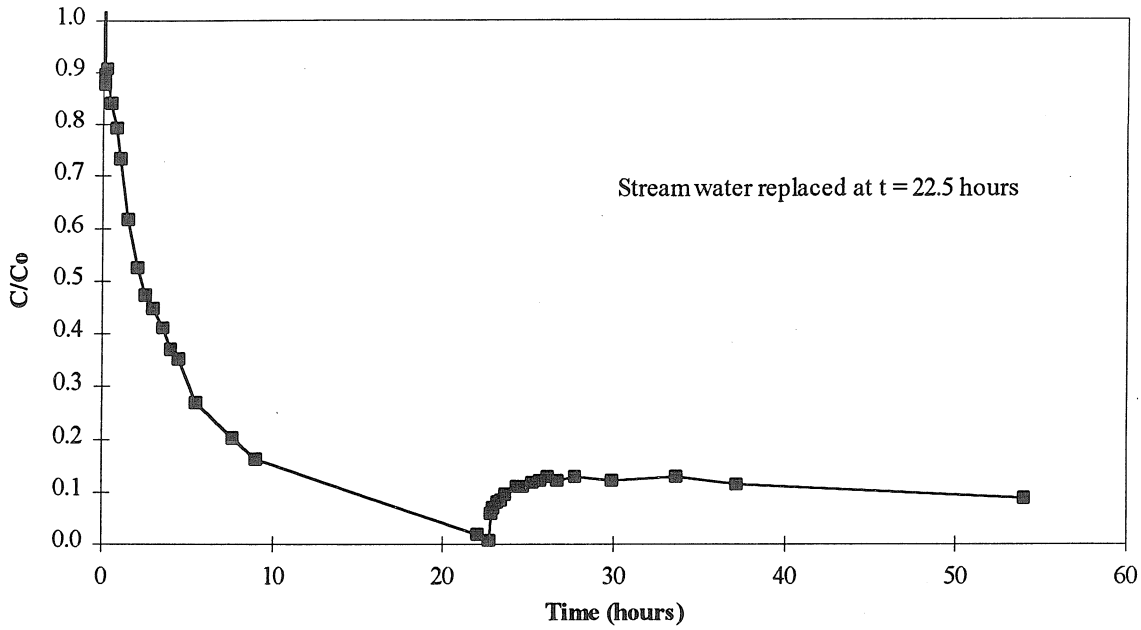

Figure 5.32: Complete clay bed-exchange data for Experiment #5, including secondary data. The entire experiment had moderately-moving bedforms ($U_b^* = 0.77$).

Secondary experiments 14a and 15a involved increasing the concentration of colloids in the stream. For both of these experiments, the first clay addition was done at a relatively low concentration (~ 40 mg/L), and the second addition was done at a higher concentration (~200 mg/L). The new clay was added to the recirculating water in exactly the same manner as for the initial clay addition. Results of these secondary experiments were presented along with primary results in Figures 5.13 and 5.14. The exchange data for experiment 14a exactly followed that of its primary experiment. The exchange data for experiment 15a was very similar to that of its primary experiment, but not exactly the same. These secondary experiments demonstrate the repeatability of the flume experiment results, and indicate that initial concentration does not affect the normalized mass exchange over the range of 40-200 mg/L.

5.1.7.3 Other types of secondary experiments

As a secondary experiment for run #10 (with nonmoving bedforms), the pH of the recirculating water was increased in order to attempt to chemically detach clay from bed sediment grains. The pH increase was accomplished by adding base (100 mL of 2N NaOH diluted in 1 L of flume water) to the stream over one recirculation period. This caused the stream pH to immediately jump to 9.5. However, this addition of base also caused flocculation of the stream-borne clay. Within 30 minutes, the clay in the stream became visibly flocculated with a floc size on the order of a few tenths of a millimeter. Clay flocs accumulated at the surface of the stream bed on the upstream side of bedforms. It appeared that the flocs were carried into the bed surface where they were immediately strained. Flocs were also observed to be transported as bed load (rolling along the bed surface). This was deemed an unacceptable perturbation of the colloidal tracer, and the experiment was stopped.

5.1.8 Pore-water profiles

Pore-water profiles of clay concentration were obtained for most flume experiments. These profiles were developed by collecting samples of pore water through a vertical series of sampling ports. Pore-water profiles thus show the penetration of a tracer at a specific location in the bed. Profiles of clay concentration were obtained for moving bedform experiments 5, 8, 9, 11, and 16, and nonmoving bedform experiments 7, 10, 12, 14, and 15. Profiles of lithium concentration were also obtained for experiments 5, 7, and 16. Much better profiles for transport of solutes into the bed can be found in other work (Eylers, 1994, Elliott, 1990). The profiles for experiments 7 and 10 were incomplete and erratic, so they are not included here. Profiles for all other experiments are shown in Figures 5.32 through 5.41. Note that the concentration scale varies from figure to figure.

It is difficult to draw general conclusions from pore-water profiles. The fact that the profiles were obtained at a single location means that they are highly dependent on the local bed geometry at that point. This is not as problematic for moving-bedform experiments, since many bedforms will pass by the sampling station during the course of the experiment. Sampling difficulties also make profiles difficult to interpret. It is difficult to get a good profile because pore-water samples tend to be drawn from a relatively large volume of the bed. To obtain a 1 mL sample of pore-water, the water must be drawn from a sphere of bed 1.8 cm in diameter (for the Ottawa sand with porosity 0.33). As a result, a staggered profile was obtained, with alternating samples being drawn from locations 3 cm and 6 cm from the flume wall. The limited sample size

also necessitated the dilution of pore-water samples to 5 times their initial volume for analysis, which increased the uncertainty of the data. Pore-water profiles for moving bedform experiments are sometimes difficult to interpret because the bed elevation at the sampling location varies by a few centimeters as bedforms pass by, so that the highest point in the profile varies with time. In this case, the deep-bed profiles are comparable, but the upper-bed profiles are strongly influenced by the local geometry at the time of sampling. Despite these difficulties, for the most part the profiles show internal consistency, and pore-water data can be used to support qualitative conclusions about the exchange of colloids.

The lithium pore-water profiles in Figures 5.33 and 5.41 show the behavior of a conservative tracer in the bed. At early times, a front of lithium is driven into the bed. Later, the bed becomes completely mixed and the entire volume of water, in both the stream and bed, attains the same lithium concentration. Again, the ultimate lithium concentration is controlled by the dilution of the stream water by the bed water. Typically, the final lithium concentration is 75-85% of C_0.

Clay pore-water profiles (Figures 5.34-5.40, 5.42) show that the colloidal tracer behaves very differently than the conservative tracer. At early times, clay also passes into the bed as a front driven in through the bed surface. However, the clay concentration in the bed drops dramatically with time, indicating that clay is being removed from suspension (the concentrations below are for clay *suspended* in the pore water). Late in the experiment, only a small fraction of clay is still in suspension.

The clay concentration for the uppermost sample in each profile is generally fairly well-mixed with the stream. Thus the concentration of the highest sample tends to decrease as the stream concentration decreases. However, lower samples are not well-mixed with the stream, but instead show the history of tracer transport and trapping. This can lead to the interesting situation where there is a concentration maximum in the middle of the bed, most clearly shown in the moving-bedform experiments 8, 9, and 11, shown in Figures 5.35 - 5.37. The presence of a deep-bed concentration maximum at later times supports the idea that the upper part of the bed stays well-mixed with the stream due to turnover, while pumping from the turnover region to the deeper bed results in the bulk of the clay being irreversibly trapped.

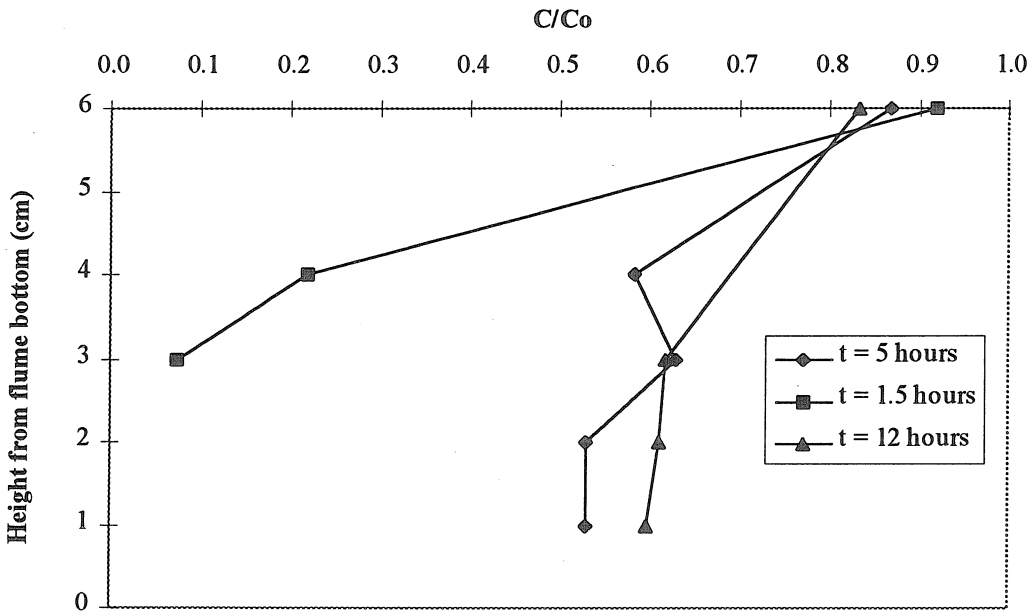

Figure 5.33: Lithium pore-water profiles for Experiment #5. $U_b^* = 0.77$.

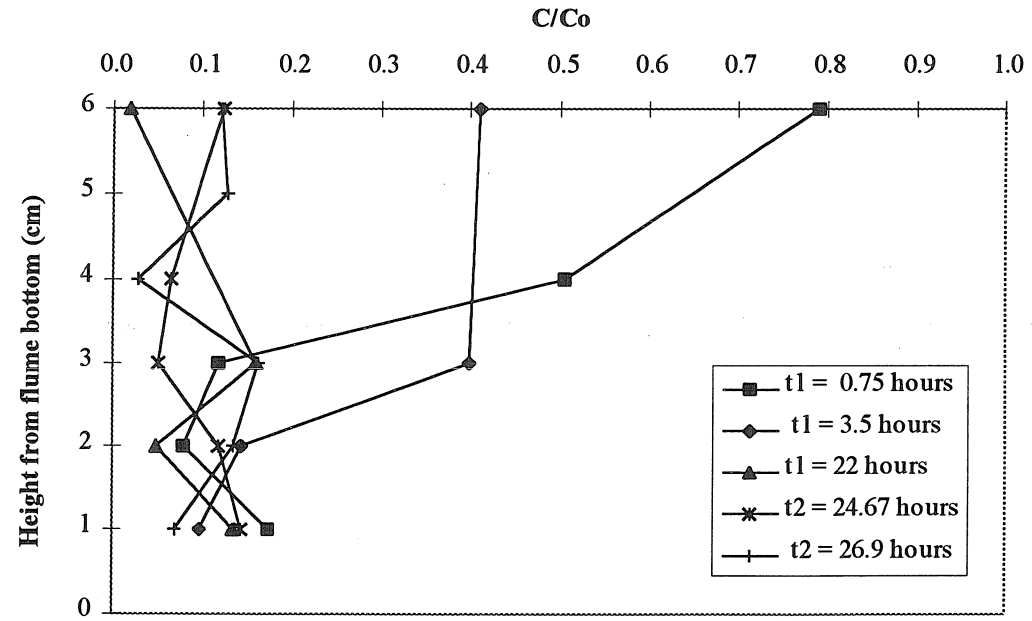

Figure 5.34: Kaolinite pore-water profiles for Experiment #5, including secondary experiment (replace stream with colloid-free water). $U_b^* = 0.77$.

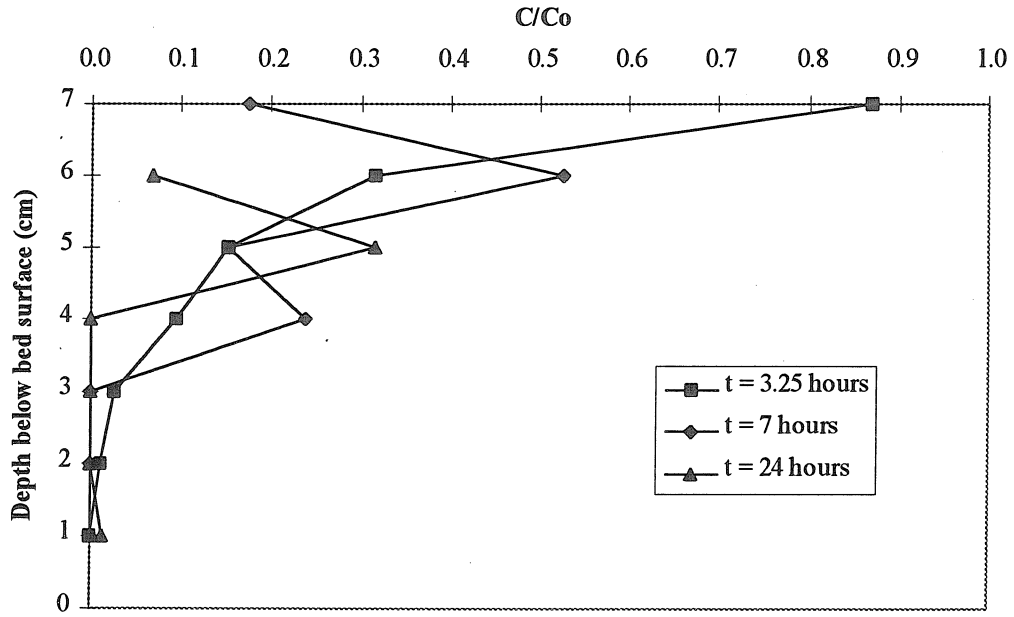

Figure 5.35: Kaolinite pore-water profiles for Experiment #8. $U_b^* = 0.35$.

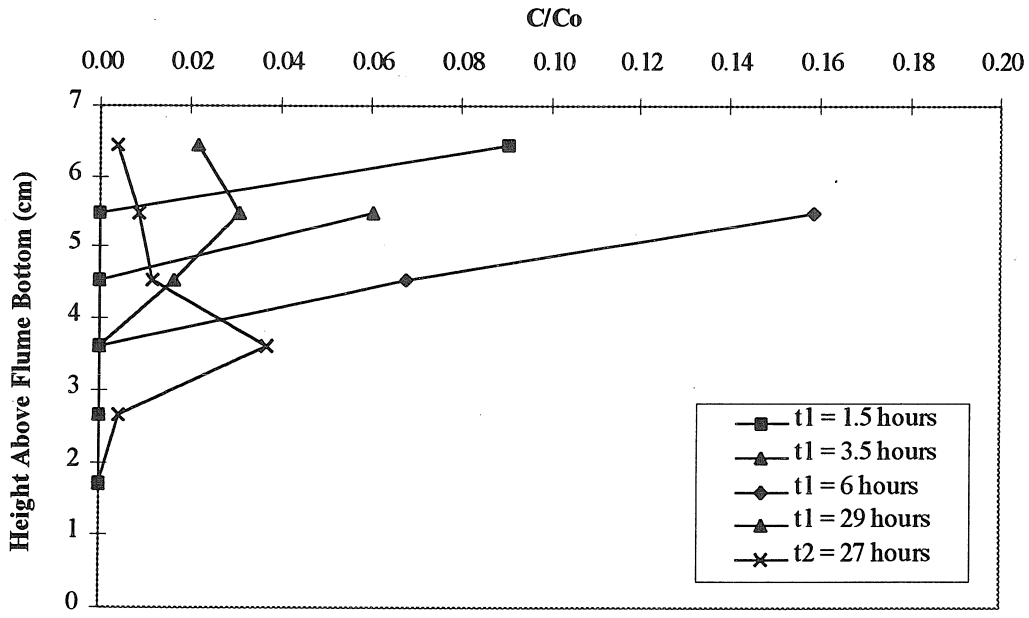

Figure 5.36: Kaolinite pore-water profiles for Experiment #9, including secondary experiment (reduce recirculation flow rate). Primary experiment $U_b^* = 2.40$. Secondary experiment had nonmoving bedforms.

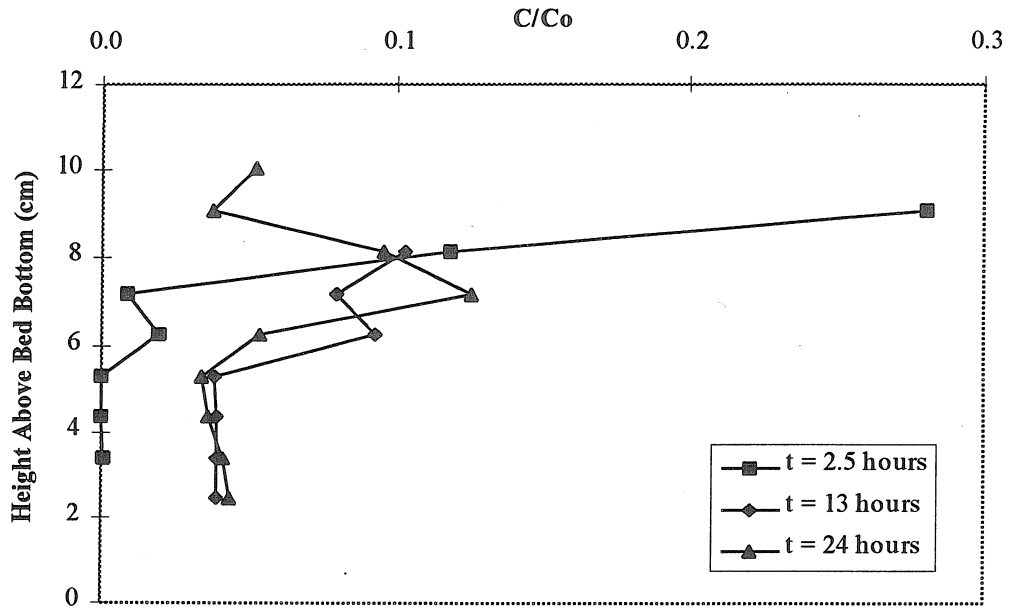

Figure 5.37: Kaolinite pore-water profiles for Experiment #11. $U_b^* = 8.43$.

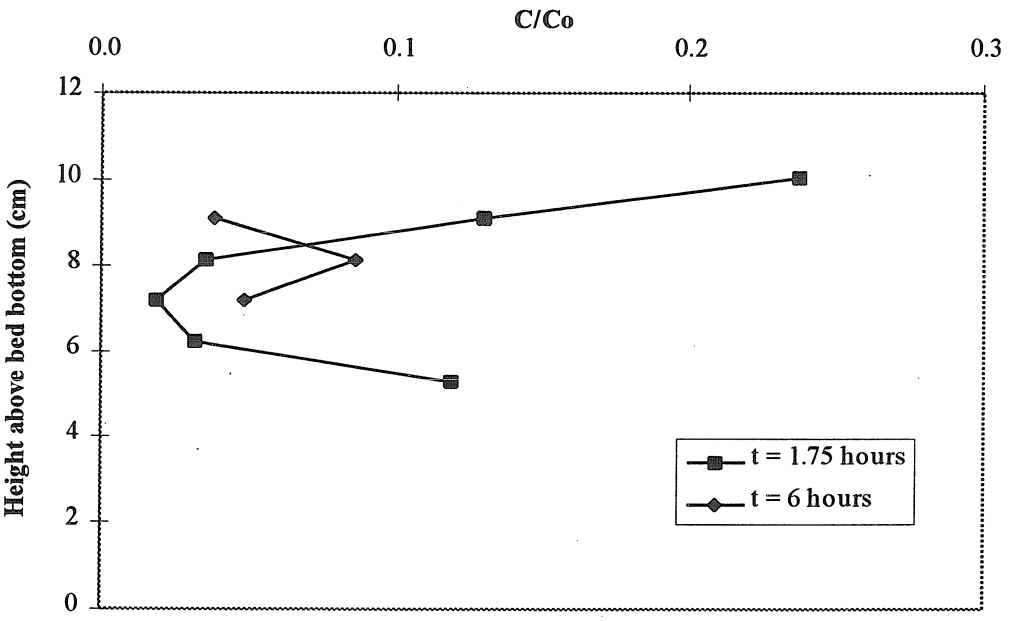

Figure 5.38: Kaolinite pore-water profiles for Experiment #12. Nonmoving Bedforms.

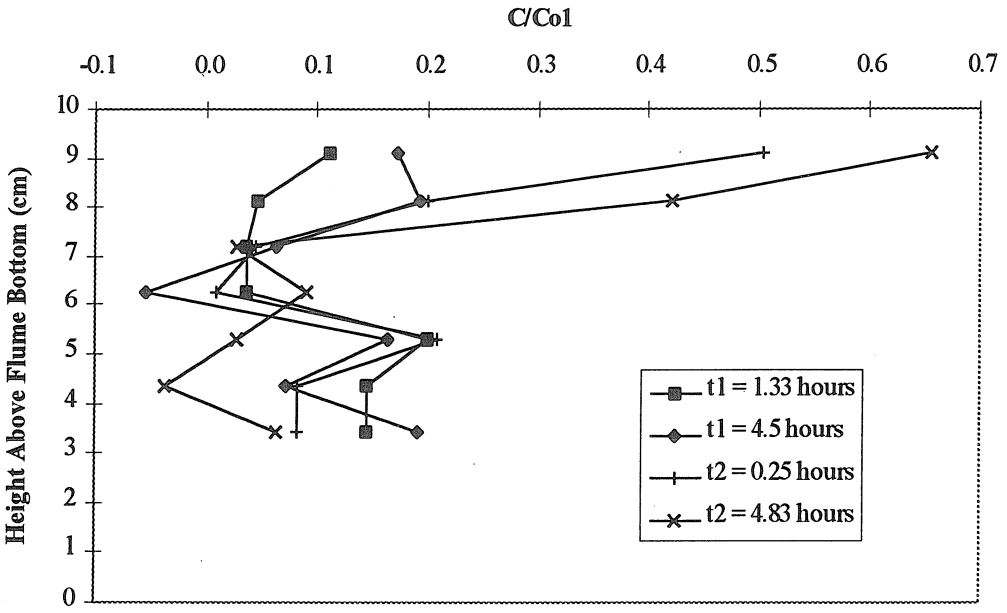

Figure 5.39: Kaolinite pore-water profiles for Experiment #14, including secondary experiment (add more clay with same hydraulic conditions). Nonmoving bedforms.

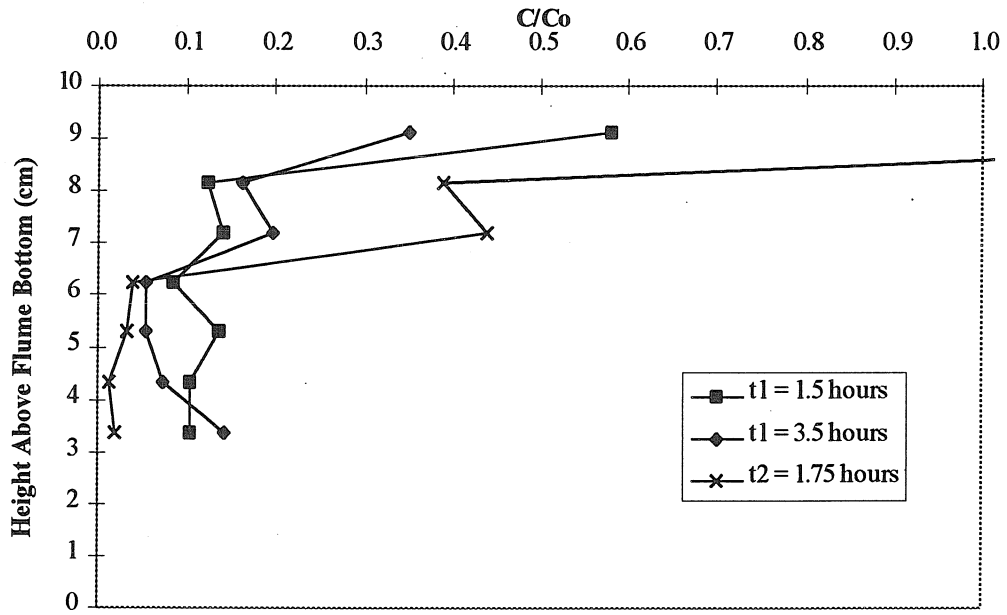

Figure 5.40: Kaolinite pore-water profiles for Experiment #15, including secondary experiment (add more clay with same hydraulic conditions). Nonmoving bedforms. The secondary experiment involved adding additional clay to the surface water, resulting in high clay concentrations in the upper bed (higher than C_0 at the uppermost sampling location).

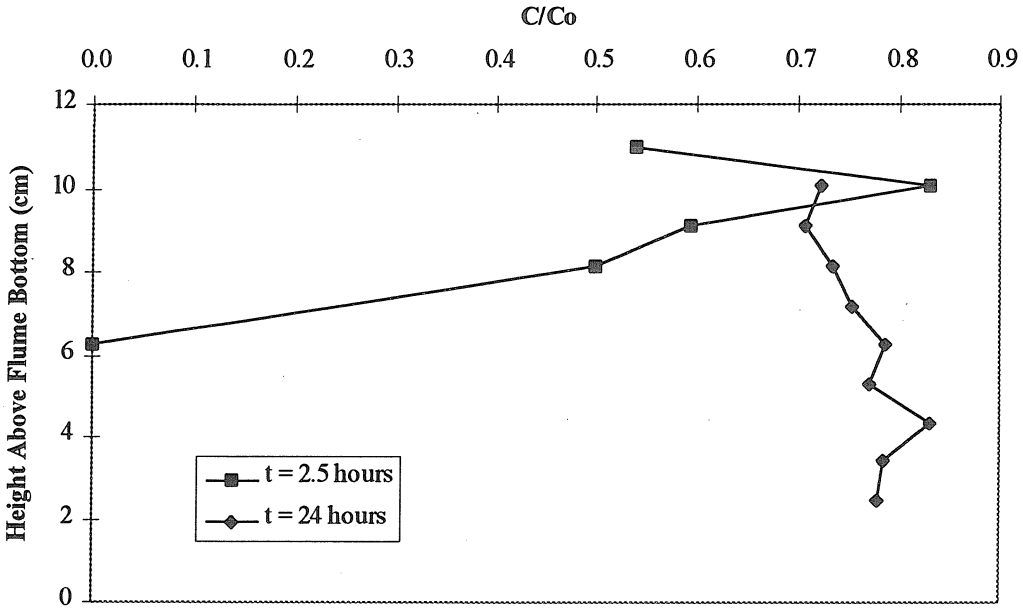

Figure 5.41: Lithium pore-water profiles for Experiment #16. $U_b^* = 1.56$.

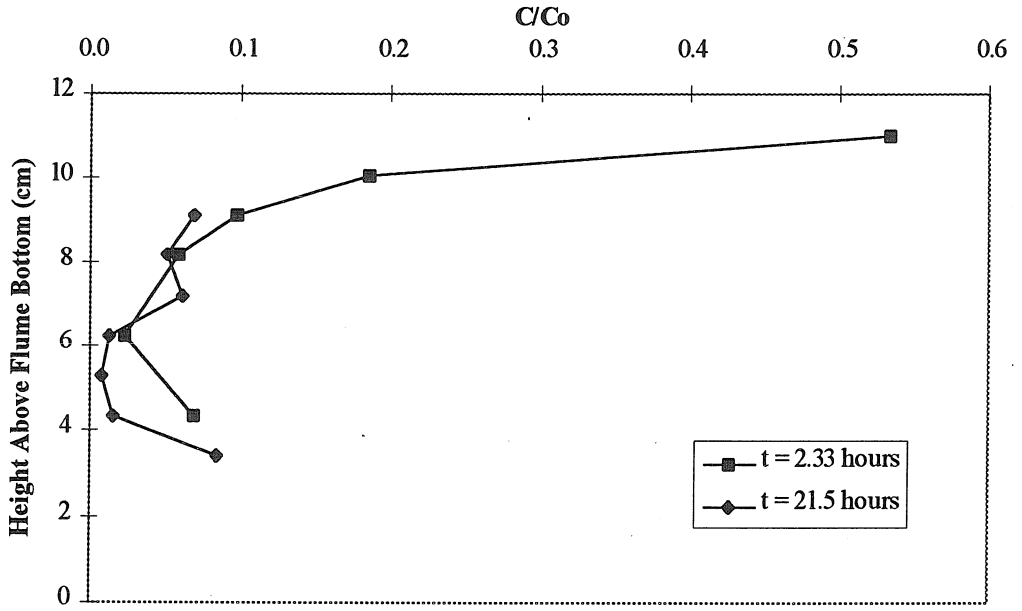

Figure 5.42: Kaolinite pore-water profiles for Experiment #16. $U_b^* = 1.56$.

5.2 Column experiment results

Column experiments were performed in several series to investigate the effects of pH, ionic strength, and initial concentration on the filtration of kaolinite by the sand used for the sediment bed in the flume. Additional experiments were performed to determine the filtration of glass beads. The complete data set for one experiment will be discussed in detail in Section 5.2.1. Then the results of each series of experiments will be presented separately in Sections 5.2.2-5.2.5.

5.2.1 Typical experimental results

To demonstrate how the filtration coefficient was determined from column experiment results, the complete data set of one experiment will be presented and discussed. The experimental procedure and materials are described in Sections 4.2 and 4.4. The data that follow are for column experiment 7/26/96-1, which was part of the experiment series examining variation of the input kaolinite concentration.

The basic data set from column experiment 7/26/96-1 is presented in Table 5.13. The absorbance of the column effluent vs. time is measured in order to obtain a breakthrough curve. In addition, the flow rate through the column and the absorbance of the input solution are each measured several times during the course of the experiment. The breakthough curve, given in Figure 5.43, is plotted based on the derived parameters of C/C_0 and the number of pore volumes that have passed through the column.

Table 5.13: Data set for column experiment 7/26/96-1. The sample time, measured flow rate, and absorbance are measured data; the other parameters are calculated. The input absorbance is the average of several measurements made over the course of the experiment. C/C_0 is calculated as the ratio of absorbance at the current time to the absorbance of the input suspension.

sample time (min)	Q measured (mL/min)	Q for pore vol. calc. (mL/min)	number of pore volumes	absorbance at 500 nm	C/C_0
input				0.031	
0	14.1	14.1	0.00	0.000	0.00
0.22		14.1	0.16	0.000	0.00
0.97		14.6	0.73	0.004	0.13
1.78	15.2	15.2	1.38	0.005	0.16
3.00		15.7	2.38	0.005	0.16
4.25	16.2	16.2	3.44	0.005	0.16
5.25		16.2	4.28	0.005	0.18
6.58	16.2	16.2	5.41	0.005	0.15

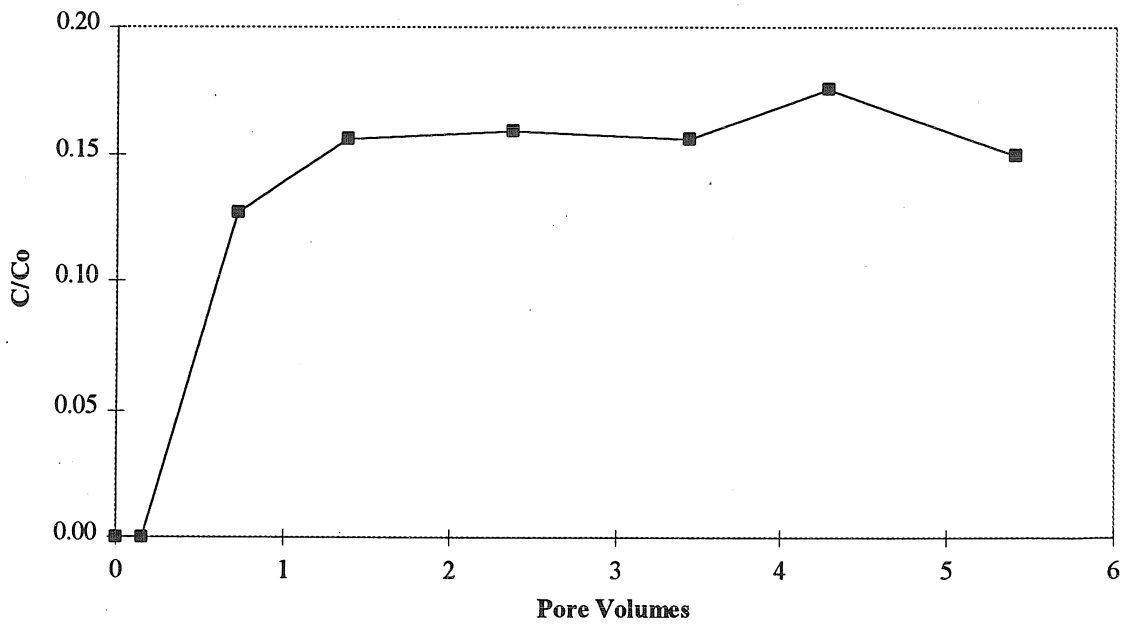

Figure 5.43: Results of column experiment 7/26/96-1.

The filtration coefficient, λ_f, is calculated using the filtration equation, presented in Section 3.2, based on C/C_0 for the plateau of the breakthrough curve. The length of the column of porous media is also required as an input to determine λ_f. In some experiments, the effluent concentration came to a plateau and then decreased, indicating that the filter was becoming plugged due to filtration. In this case, the filtration coefficient was still calculated based on the plateau C/C_0.

The results of experiment 7/26/96-1 are summarized in Table 5.14. The D'Arcy velocity is calculated based on the average flow rate through the column over the course of the experiment.

Table 5.14: Summary parameters for column experiment 7/26/96-1.

Sand column height (cm)	D'Arcy velocity (cm/min)	pH	I (mM)	Clay C_0 (mg/L)	λ_f (cm^{-1})
3.0	0.77	7.84	5.0	20	0.61

5.2.2 Experiments with different pH's

Column experiments on the filtration of kaolinite by Ottawa 30 sand were conducted over a pH range of 4-9. The results of experiments conducted to investigate the effect of changing pH (while maintaining I = 5 mM) are presented in Table 5.15. The experimental and theoretical collision efficiencies, η_{exp} and η_0, and the experimental attachment efficiency, α_{exp}, were defined in Section 3.2. Recall that the observed η_{exp} is

derived from the filtration coefficient, while the calculated η_0 is based on a microscopic model of colloid transport through porous media. α_{exp} is the ratio of η_{exp} to η_0.

Table 5.15: Results of column experiments for the filtration of kaolinite by Ottawa 30 sand over a range of pH from 4 to 9.5 with I = 5 mM.

Experiment Date	Experiment Purpose	Column Height (cm)	pH	I (mM)	D' Arcy Velocity (cm/min)	Clay C_0 (mg/L)	λ_f exp. (cm^{-1})	η exp.	η_0 calc.	α exp.
4/17/96	pH var.	2.60	5.9	5.0	1.61	~200	0.67	0.03	0.08	0.39
4/18/96	pH var.	3.00	5.8	5.0	1.14	~200	0.64	0.03	0.12	0.25
4/30/96	pH var.	3.00	7.0	5.0	1.12	~200	0.62	0.03	0.12	0.24
5/8/96	pH var.	3.65	7.7	5.0	0.94	~200	0.34	0.02	0.15	0.11
5/24/96-1	pH var.	3.20	8.0	5.0	1.45	216	0.16	0.01	0.09	0.08
5/24/96-2	pH var.	4.15	4.3	5.0	0.89	216	0.55	0.03	0.16	0.16
5/29/96-1	pH var.	3.30	4.7	5.0	0.97	216	0.36	0.02	0.15	0.12
5/29/96-2	pH var.	3.45	9.6	5.0	0.97	216	0.19	0.01	0.15	0.06
6/11/96	pH var.	3.10	8.9	5.0	1.36	216	0.21	0.01	0.10	0.10
7/11/96-1	pH var.	2.90	4.7	5.0	1.69	178	0.41	0.02	0.08	0.25
7/11/96-2	pH var.	3.10	5.9	5.0	0.92	178	0.70	0.03	0.16	0.21
7/15/96-1	pH var.	3.10	5.1	5.0	1.26	178	0.44	0.02	0.11	0.19
7/15/96-2	pH var.	3.00	4.1	5.0	1.21	178	0.74	0.04	0.11	0.31
7/18/96	pH var.	3.20	5.6	5.0	1.17	178	0.71	0.03	0.12	0.29

The variation of λ_f with pH at an ionic strength of 5 mM is shown in Figure 5.44. The data shows a reasonably consistent value of λ_f for pH 5.5 - 7, and again for 8 - 9.5. The transition from a higher λ_f at pH 5.5 - 7 to a lower one at 8 - 9.5 can be attributed to the charge reversal of pH-dependent edge surfaces between pH 7 and 8. Below pH 7, the kaolinite edges are positively charged, and the faces are negatively charged. While the net charge of the kaolinite particle is negative, there can be a local favorable interaction between the positive kaolinite edges and the negative silica surface. That is, the mode of

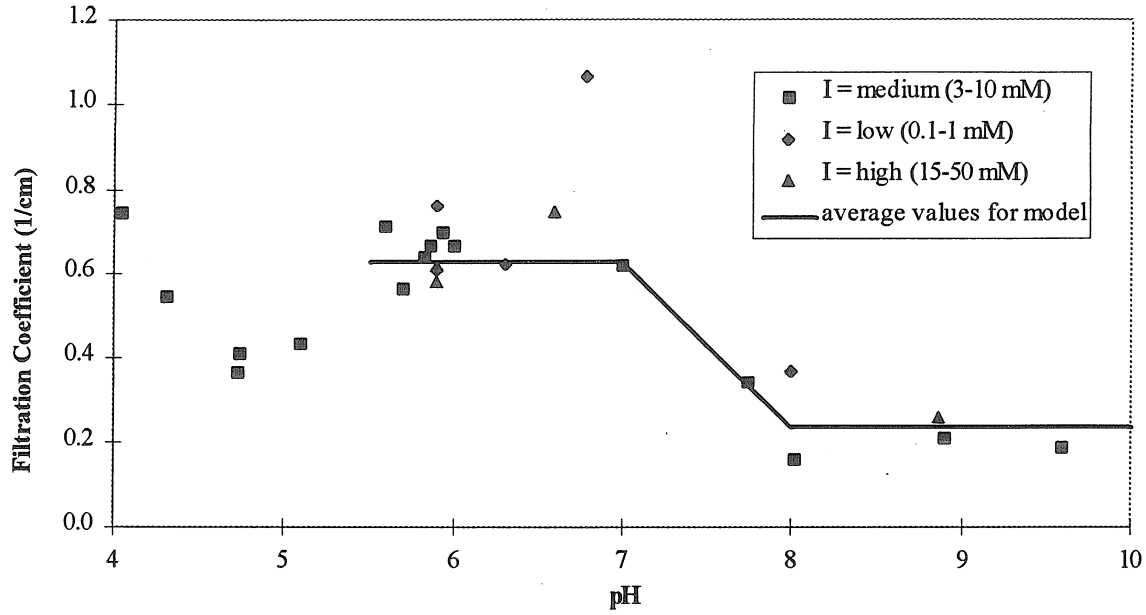

Figure 5.44: Variation of filtration coefficient with pH for column experiments with input kaolinite concentration in the range 178-216 mg/L.

interaction where a kaolinite edge becomes attached to the silica surface is favored relative to all other attachment geometries. Above pH 8, the edges and the faces will both have negative charges, and all kaolinite-silica electrostatic interactions will be unfavorable. The filtration coefficient is still very high in this region because settling of these relatively-large kaolinite colloids provides a strong physical mechanism for filtration.

The filtration behavior of this kaolinite at pH < 5.5 is somewhat unclear, and was not investigated further since flume experiments were only conducted with pH in the range 6.8 - 8.2.

5.2.3 Experiments with different ionic strengths

Column experiments were conducted over a range of ionic strength from 0.1 to 50 mM, all from NaCl. The results of experiments conducted to investigate the effect of varying ionic strength with pH < 7 are presented in Table 5.16.

Table 5.16: Results of column experiments for filtration of kaolinite by Ottawa 30 sand over a range of ionic strength from 0.1 to 50 mM with pH between 5.7 and 6.8.

Experiment Date	Experiment Purpose	Column Height (cm)	pH	I (mM)	D' Arcy Velocity (cm/min)	Clay C_0 (mg/L)	λ_f exp. (cm^{-1})	η exp.	η calc.	α exp.
5/30/96-1	I var.	2.60	6.8	0.5	1.06	216	1.06	0.05	0.13	0.38
5/30/96-2	I var.	3.00	5.9	50	1.39	216	0.58	0.03	0.10	0.28
6/25/96	I var.	3.00	6.3	1.0	1.03	216	0.62	0.03	0.14	0.22
6/27/96	I var.	3.60	5.7	3.0	1.51	200	0.56	0.03	0.09	0.30
7/13/96	I var.	3.00	5.9	15	1.32	178	0.62	0.03	0.10	0.29
7/19/96	I var.	2.90	6.0	10	1.25	178	0.66	0.03	0.11	0.29
7/20/96	I var.	3.15	6.6	25	1.38	178	0.75	0.04	0.10	0.36
7/21/96	I var.	3.00	5.9	0.1	1.04	178	0.61	0.03	0.14	0.21
7/22/96	I var.	3.00	5.9	0.3	1.21	178	0.76	0.04	0.11	0.32
6/12/96	pH + I var.	3.00	8.9	50	1.45	216	0.26	0.01	0.09	0.13
6/14/96	pH + I var.	3.20	8.0	0.5	1.08	216	0.37	0.02	0.13	0.14

The variation of λ_f with an ionic strength at pH between 5.5 and 7 is summarized in Figure 5.45. It appears that ionic strength is not an important variable over the range investigated. This was not expected, since there is a net electrostatic repulsion between the kaolinite and silica particles, and this repulsion should be inversely proportional to ionic strength. Two factors can explain the non-dependence on ionic strength. First, the high settling velocity of the clay particles could have dominated filtration to the extent that ionic-strength-induced variations in the repulsive electrostatic force were not significant. Second, the importance of ionic-strength effects could been mitigated because of the dual (edge-face) nature of the kaolinite particles.

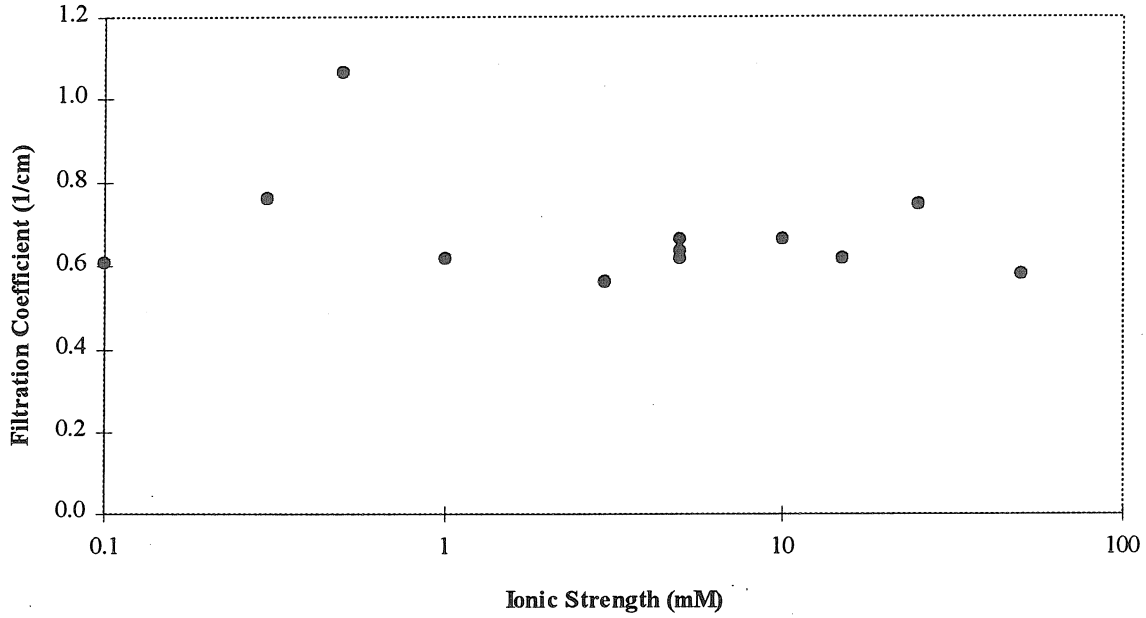

Figure 5.45: Variation of filtration coefficient with ionic strength for column experiments with pH in the range 5.8-7.0 and input kaolinite concentration 178-216 mg/L. The single high data point can be attributed to experimental error.

5.2.4 Experiments with different initial concentrations

Experiments conducted with an initial clay concentration less than 200 mg/L are presented in Table 5.17. No consistent trend between input concentration and filtration coefficient was observed. It is difficult to compare filtration coefficients for these experiments directly because of the different pH's and D'arcy velocities. Comparison of α's seems to indicate some variation with C_0. However, in all cases filtration is still high, and so that complete trapping would still be expected in the flume.

Table 5.17: Results of column experiments for filtration of kaolinite by Ottawa 30 sand with input kaolinite concentration less than 200 mg/L.

Experiment Date	Experiment purpose	Column Height (cm)	pH	I (mM)	D' Arcy Velocity (cm/min)	Clay C_0 (mg/L)	λ_f (cm^{-1})	η exp.	η calc.	α exp.
6/20/96	C_0 var.	3.00	7.1	0.5	1.09	43	0.11	0.01	0.13	0.04
6/24/96	C_0 var.	3.00	7.6	0.5	1.04	43	0.10	0.00	0.14	0.03
7/26/96	C_0 var.	3.00	5.8	5.0	0.77	20	0.61	0.03	0.19	0.15
7/27/96	C_0 var.	3.00	5.8	5.0	0.74	70	0.94	0.04	0.20	0.22
7/29/96	C_0 var.	3.10	6.1	5.0	0.50	140	1.24	0.06	0.32	0.18
9/18/96-2	C_0 var.	3.20	5.8	5.0	0.57	45	0.60	0.03	0.27	0.10
9/18/96-3	C_0 var.	3.10	5.8	5.0	0.63	70	1.19	0.06	0.24	0.23

5.2.5 Experiments with colloids other than kaolinite

Three column experiments were conducted to observe the filtration of glass beads by the Ottawa 30 sand. The results of these experiments are presented in Table 5.18. Column experiments were conducted with glass beads specifically to determine an input value of λ_f for modeling the results of flume experiment #17. The properties of the glass beads are described in Section 4.4.4.1.

Table 5.18: Results of column experiments for filtration of soda-lime glass beads by Ottawa 30 sand.

Experiment Date	Experiment Purpose	Column Height (cm)	pH	I (mM)	D' Arcy Velocity (cm/min)	C_0 (mg/L)	λ_f exp. (cm^{-1})	η exp.	η calc.	α exp.
9/11/96-1	glass beads	3.00	~7	5.0	0.40	60 - 100	0.70	0.03	0.41	0.08
9/11/96-2	glass beads	3.00	~7	5.0	0.41	60 - 100	0.59	0.03	0.41	0.07
9/12/96	glass beads	3.30	~7	5.0	0.65	14-20	0.47	0.02	0.23	0.10

6. DISCUSSION AND ADDITIONAL MODEL SIMULATIONS

This chapter presents a discussion of the more general results and implications of this work. The first part of the chapter (Sections 6.1-6.3) features model simulations for a range of stream, bed, and tracer parameters. These simulations show both the predicted exchange in cases not covered by flume experiment runs and the sensitivity of the model to the various input parameters. The importance of major variables will be discussed and compared. In addition, the accuracy of model predictions will be discussed specifically in the context of their application to flume experiments. This accuracy analysis will consider both model sensitivity and the errors in estimating model inputs from experimental data.

The second part of the chapter (Sections 6.4-6.5) presents a discussion of the extension of the exchange models to natural systems, and the implications of this work for particle transport in rivers. The increased physical and chemical complexity of real streams are considered. In addition, model simulations involving natural materials and stream conditions are presented.

Finally, some suggestions are given for future research on this topic.

6.1 Effect of major variables on solute exchange with finite beds

In order to demonstrate the impact of various model inputs, a series of figures are presented where one input is varied while all others are held constant. The constant input values for these model simulations are typical values from the flume experiment data set.

Collectively, these typical values represent a baseline case for sensitivity analysis, given in Table 6.1.

Table 6.1: The baseline case for model simulations.

Bed Parameters						Stream Parameters			Derived Parameters					
λ (cm)	H (cm)	d_b (cm)	θ	K (cm/min)	U_b (cm/min)	d (cm)	d' (cm)	U (cm/s)	h_m (cm)	u_m (cm/min)	U_b*	u_u*	d'/λ	d_b/λ
30	1.5	9	0.33	9.0	0	10	18	15	0.02	0.04	0	0.05	0.6	0.3

Variation of all hydraulic parameters (H, U, U_b*, etc.) will have a similar effect on the exchange of all tracers. Parameters of special importance to the exchange of conservative solutes are considered in this section. Other parameters will be discussed in the next section on colloid exchange.

Figures 6.1 and 6.2 present simulations for the exchange of a conservative solute with a range of bed depths and effective stream depths. Both of these variables control the ultimate stream-water solute concentration, C_f, which is given by

$$\frac{C_f}{C_0} = \frac{d'}{d' + \theta d_b} \tag{6.1}$$

Thus, d_b and d' both have a major impact on solute exchange at long times. They have a very different impact at shorter times, however. The stream concentration is related to the penetration depth by

$$\frac{C(t)}{C_0} = \frac{d'}{d' + \theta M(t)} \tag{6.2}$$

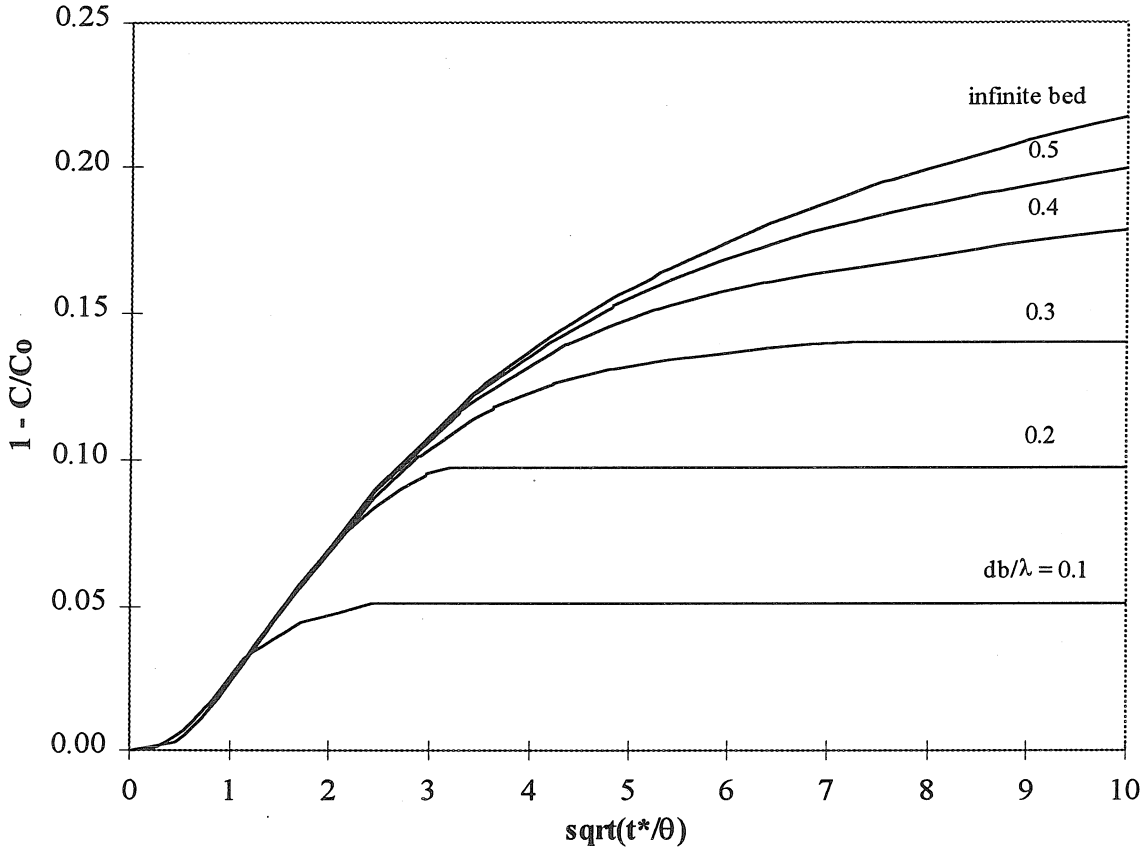

Figure 6.1: Pumping model predictions for the exchange of conservative solutes with beds of different depths. Shallower beds deviate from the infinite-bed curve at shorter times and result in a lower ultimate dilution of stream water. Input parameters other than d_b/λ are given in Table 6.1

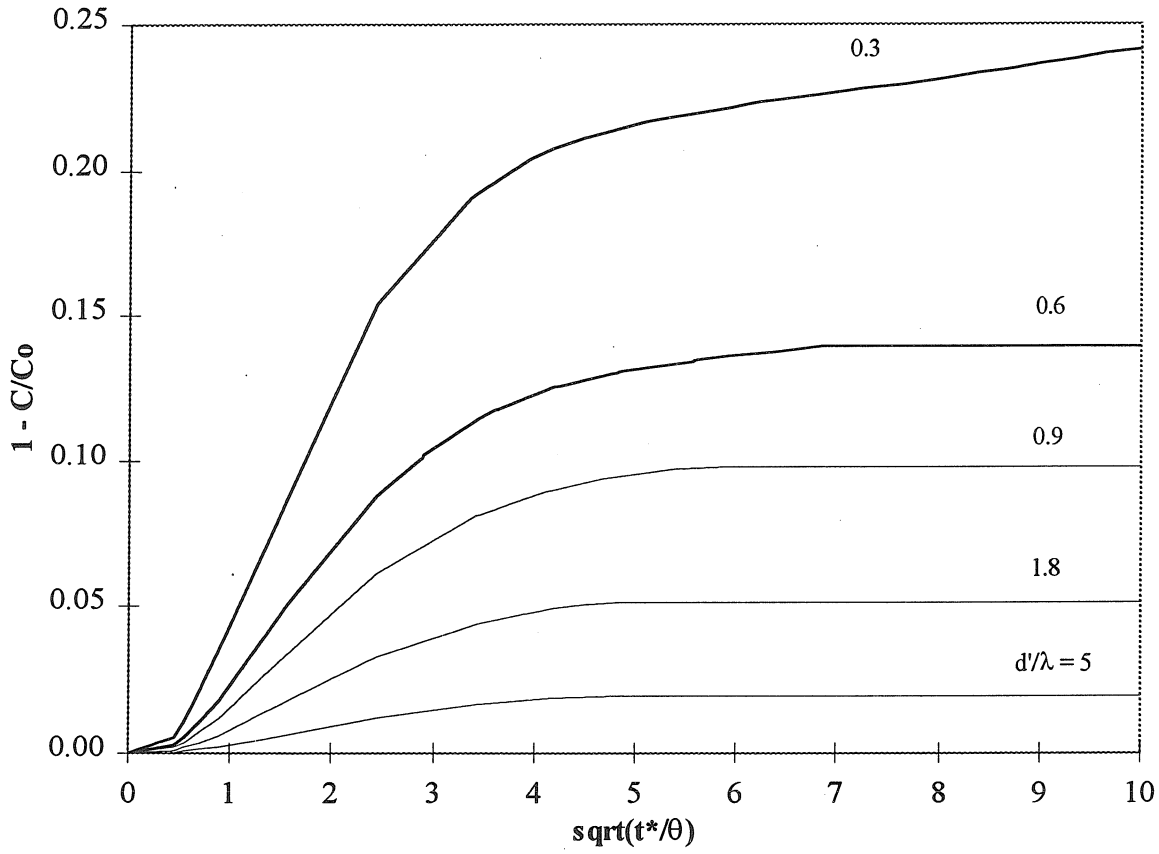

Figure 6.2: Pumping model predictions for the exchange of conservative solutes with different effective stream depths (d'). Larger d' means that the volume in the water in the stream is larger, and there is a lower ultimate dilution due to exchange with the bed. Input parameters other than d'/λ are given in Table 6.1

Since d' represents the size of the stream reservoir which is being diluted by exchange with the bed, it has a large effect on the change in concentration at all times. However, d_b is important only when it causes M(t) to deviate from the value predicted for an infinitely deep bed. This will occur at later times, when the exchange is limited by the bottom of the bed. Essentially, at early times mixing occurs in the upper portion of the bed where the pumping streamlines closely resemble those of an infinite bed. At later times, the tracer is pumped to deeper parts of the bed where the streamlines are increasingly deflected by the bottom. So, in Figure 6.1, the exchange curves for the finite and infinite beds coincide at early times, but deviate at later times. The time at which this deviation occurs is inversely proportional to the bed depth.

The effective depth, d', also has an effect on M(t) that is not apparent in the model simulations presented in Figure 6.2. An increase in stream depth (d, less than d' by a constant) reduces the amplitude of the pressure disturbance over the bedforms (h_m, given by Equation 3.2). In turn, h_m is used in the nondimensionalization of time (Equation 3.9). Thus, larger stream depths result in lower h_m and slower pumping in addition to lower ultimate dilution. The effect of d on M(t) is included in the dimensionless variable t*: it takes a longer real time, t, to reach a given value of t*.

Figure 6.3 shows the variation in exchange due to different underflow velocities, for both the finite bed and infinite bed cases. Elliott showed that underflow is important in the infinite bed case because it limits the penetration of pumping streamlines. At some depth in the bed, the pumping head becomes extremely small, and there is a separation between the pumping streamlines and the underflow streamlines. Thus, underflow

restricts the pumping streamlines to some finite region even though the bed has infinite depth. As a result, underflow causes a significant reduction in the exchange at long times. However, in the finite bed case, the exchange at long times is already limited by the finite bed. Underflow will still cause some deflection of the pumping streamlines, but the effect will be minor for relatively shallow beds. Essentially, unless the bed is quite deep, pumping dominates the flow pattern in the bed to the extent that underflow is restricted to a very small layer near the bottom.

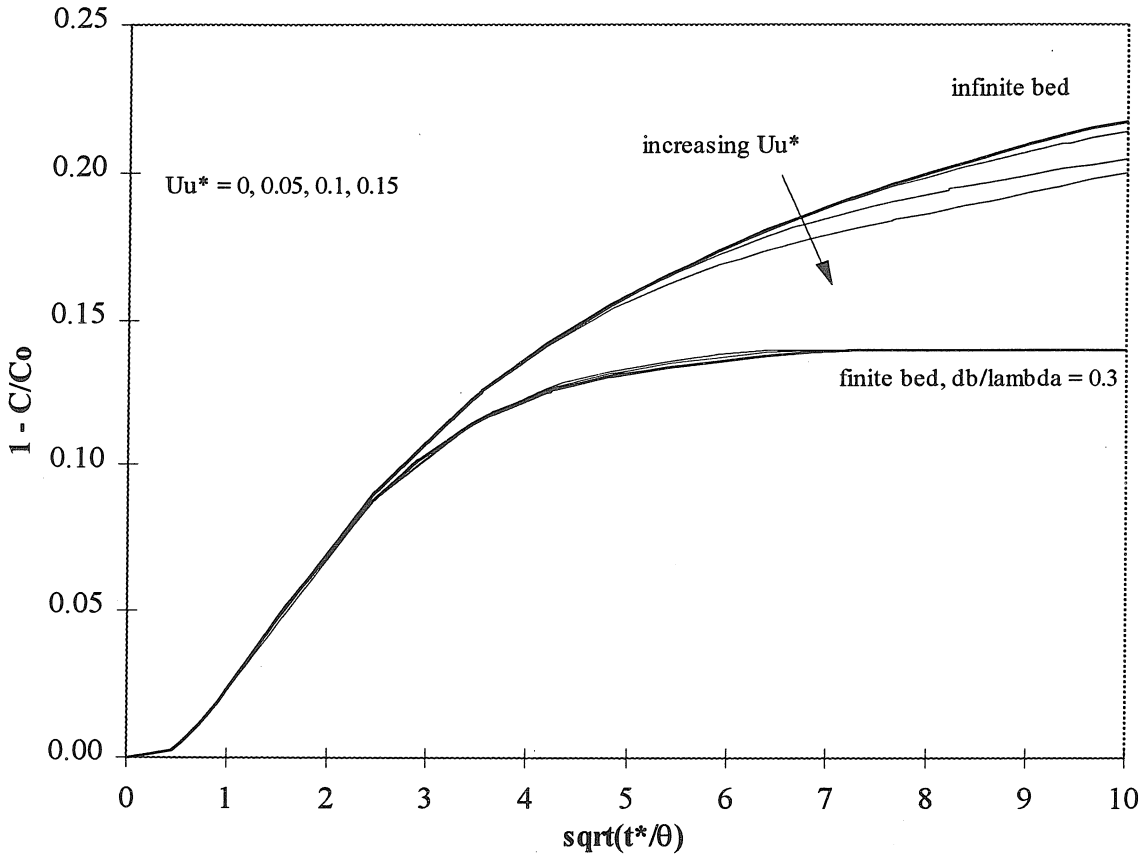

Figure 6.3: Pumping model predictions for the exchange of conservative solutes with a finite and infinite bed for different underflow velocities. Underflow has a significant impact on exchange with infinite beds because it limits the pumping penetration at long times. However, underflow has little impact on exchange with finite beds because the ultimate pumping penetration is determined by the bed depth. Input parameters other than u_u^* are given in Table 6.1.

6.2 Effect of major variables on colloid exchange

The impact of various model inputs on colloid exchange will be demonstrated through a series of figures showing variation of exchange due to changes in these variables. The constant input values for these model simulations are taken from the same baseline case given in Table 6.1, with additional particle parameters given in Table 6.2

Table 6.2: Baseline particle parameters for model simulation of colloid exchange. Filtration is sufficiently high to justify use of the complete trapping assumption.

particle diameter (μm)	v_s (cm/min)	v_s*	λ_f (cm^{-1})	λ_f^*
7.0	0.26	1.9	0.6	2.9

Most of the following simulations were done using the maxpump model which employs the complete trapping assumption for exchange with finite, stationary beds. The complete particle pumping model (based on the residence time function) was used to investigate exchange with finite, stationary beds for a range of λ_f and v_s*. The turnpump model was used for cases with complete trapping and moving bedforms. The baseline moving bedform case is defined by the same parameters for the nonmoving case (Tables 6.1 and 6.2) with new values for the stream and bedform velocity given in Table 6.3.

Table 6.3: Baseline parameters for model simulation of colloid exchange with moving bedforms.

Bed Parameters						Stream Parameters			Derived Parameters					
λ (cm)	H (cm)	d_b (cm)	θ	K (cm/min)	U_b (cm/min)	d (cm)	d' (cm)	U (cm/s)	h_m (cm)	u_m (cm/min)	U_b*	u_u*	d'/λ	d_b/λ
30	1.5	9	0.33	9.0	1.0	10	18	30	0.09	0.18	1.85	0	0.6	0.3

6.2.1 Stream parameters

Figures 6.4 and 6.5 present maxpump model simulations for colloid exchange with a stationary bed for a range of stream velocities. Figure 6.4 is plotted in the typical manner for model results, the fraction of colloid transferred to the bed ($1-C/C_0$) versus $\sqrt{t^*/\theta}$. Figure 6.5 presents the same model results plotted against dimensional time, t.

Higher stream velocities result in an increase in the amplitude of the head variation over bedforms, h_m, and a corresponding increase in the pore-water velocity distribution (via u_m). The higher pore-water velocity has two effects: it increases the overall pumping exchange rate, and it makes it more difficult for particles to settle in the bed. The higher pumping rate is included in the model through the nondimensional-ization of time (given by Equation 3.9). Thus this effect does not show up directly in Figure 6.4, but is implicit in $t^* = k^2Kh_mt = ku_mt$. The reduced importance of settling is included in the model through the nondimensionalization of the settling velocity, $v_s^* = v_s\theta/u_m$. The ratio of the settling velocity to the characteristic pumping velocity determines the importance of settling as an exchange and trapping mechanism. This effect is reflected in Figure 6.4 by the decrease in the dimensionless exchange with increasing stream velocity.

The complete effect of changing the stream velocity can only be seen in the dimensional plot. Figure 6.5 clearly shows that the overall effect of an increase in the stream velocity is an increase in exchange. In future figures, when some variable changes the nondimensionalization of t*, model predictions for changes in that variable will be

plotted against t instead of t*. This will avoid the confusion that otherwise results due to the influence of u_m on t* and v_s*.

It is useful to note that the dimensionless model predictions for different stream velocities differed solely because of particle settling. Thus, changing stream velocity has no effect on the dimensionless model predictions for solutes. Model runs for solutes with different stream velocities would all produce the same curve when plotted against t*. However, the calculation of t* would still be affected by the change in stream velocity, and an increase in exchange would be apparent if the model predictions were plotted dimensionally. In fact, changes in the stream velocity will have a proportionally bigger impact on the exchange of solutes (compared to colloids), because solutes do not have the offsetting effect of a decrease in the importance of particle settling.

Figure 6.6 presents simulations for colloid exchange with a stationary bed for a range of effective stream depths. As for solute transport, d' represents the reservoir of water in the stream. A given exchange rate will cause a smaller decrease in stream concentration at higher d'. However, d' does not have as big an impact on colloid transport as it does for conservative solutes (compare with Figure 6.2). The ultimate exchange of colloids is not limited by dilution, and thus is not influenced by d'.

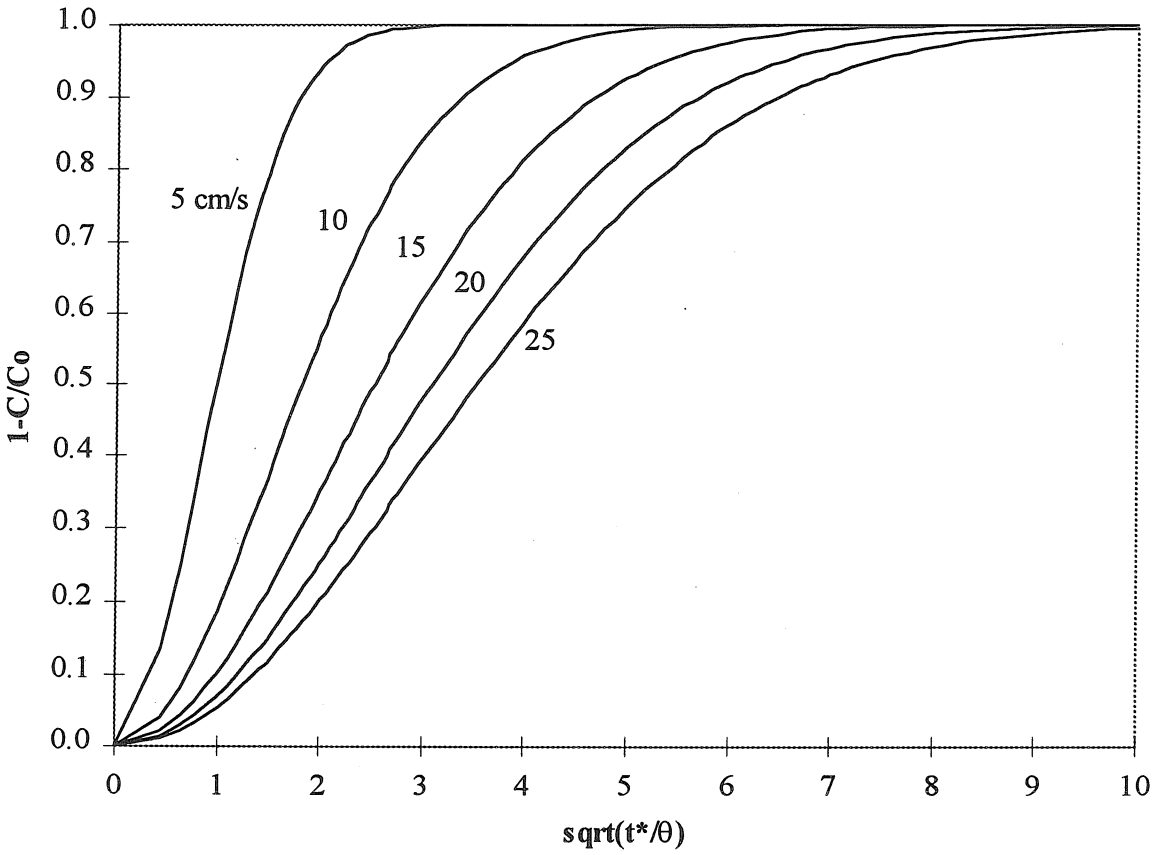

Figure 6.4: Maxpump model predictions for colloid exchange with different stream velocities. Higher U decreases exchange by keeping particles from settling in the pore spaces. U also changes the nondimensionalization of t* through its effect on h_m. Compare with Figure 6.5 plotted in real time. Input parameters other than U are given in Tables 6.1 and 6.2.

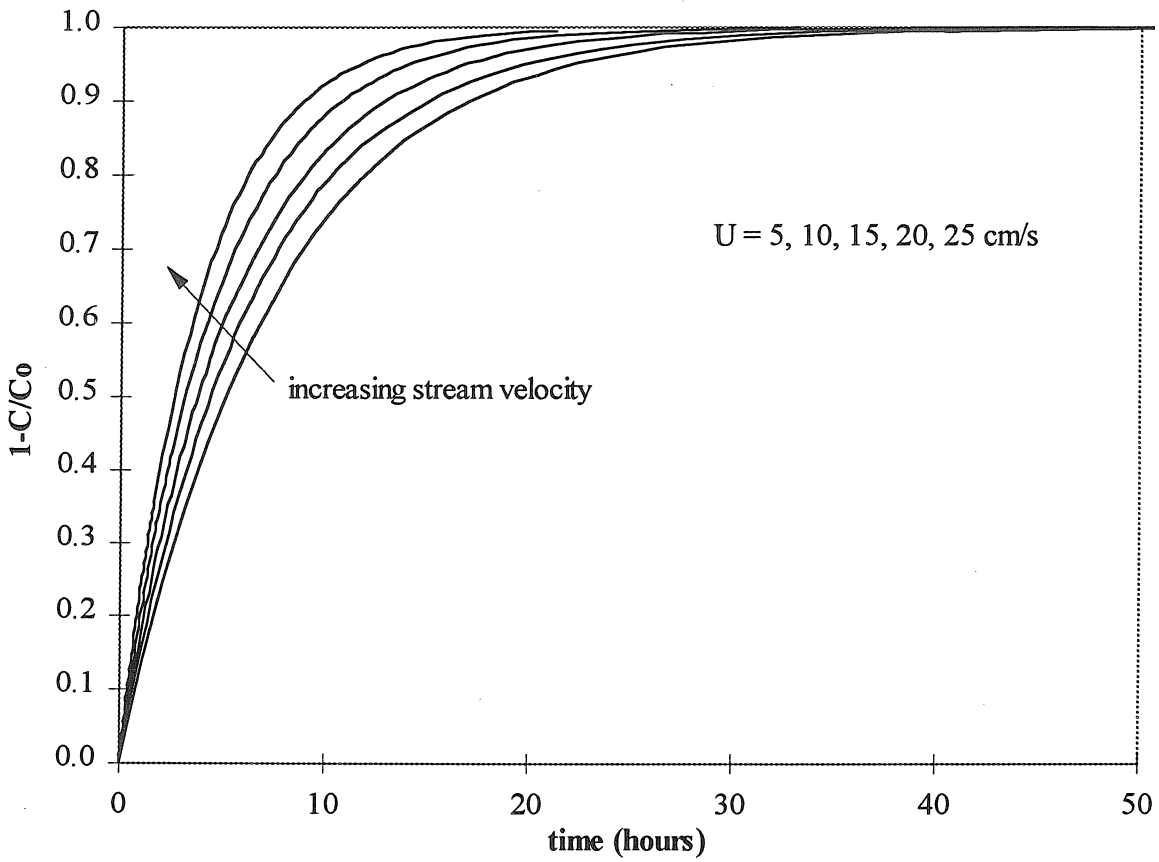

Figure 6.5: Maxpump model predictions plotted vs. real time for colloid exchange with different stream velocities. Higher U results in faster exchange due to higher form drag and a larger pressure disturbance due to bedforms. Compare with Figure 6.4 plotted in dimensionless time. Input parameters other than U are given in Tables 6.1 and 6.2.

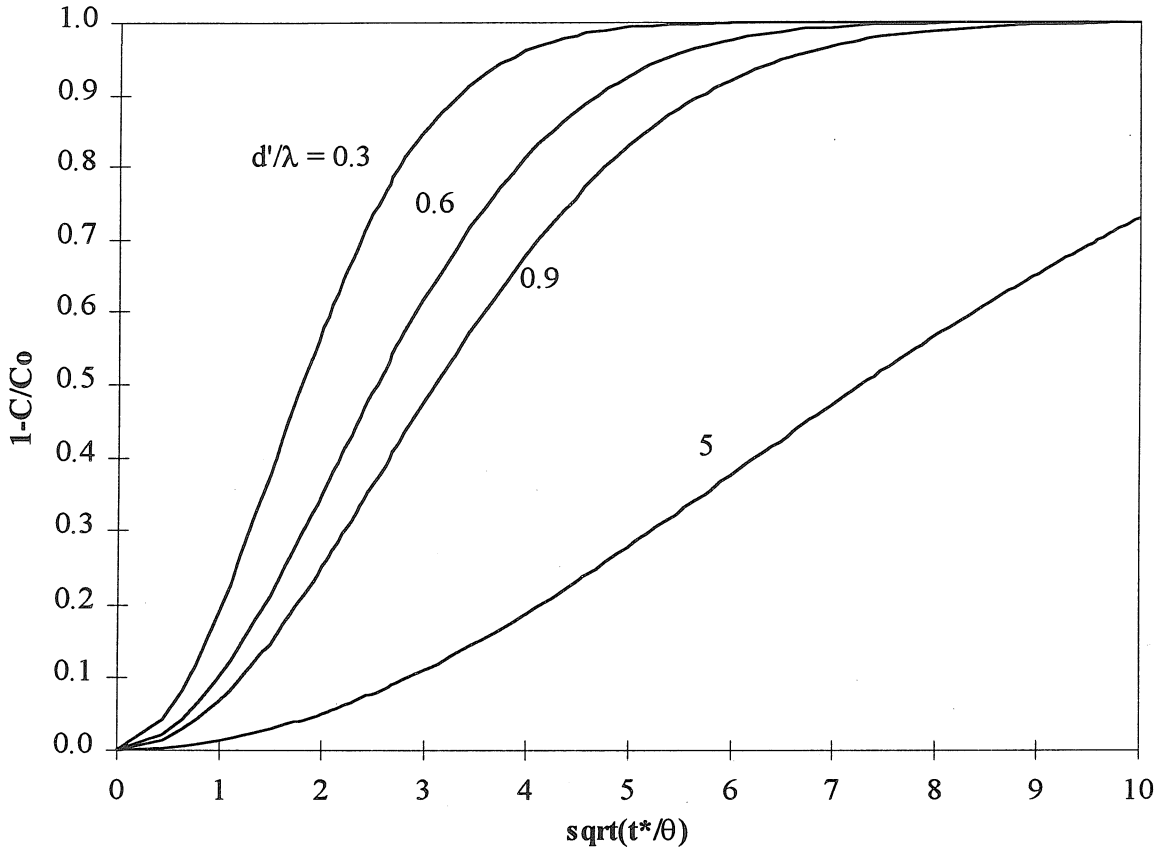

Figure 6.6: Maxpump model predictions for colloid exchange with different effective stream depths. Larger d' results in a smaller reduction in C for the same exchange with the bed. Input parameters other than d' are given in Tables 6.1 and 6.2.

6.2.2 Bedform parameters

Figure 6.7 presents model results for colloid exchange with stationary bedforms of different wavelength, λ. The bedform wavelength is an extremely important modeling parameter, as it is used to scale all other lengths. Since each bedform induces a pressure disturbance at the bed surface, pumping streamlines have a periodicity of λ. However, λ does not affect the magnitude of the pressure disturbance over a bedform. With otherwise equal conditions, longer bedforms have the same pressure disturbance applied over a greater distance, resulting in lower pumping velocities and slower exchange.

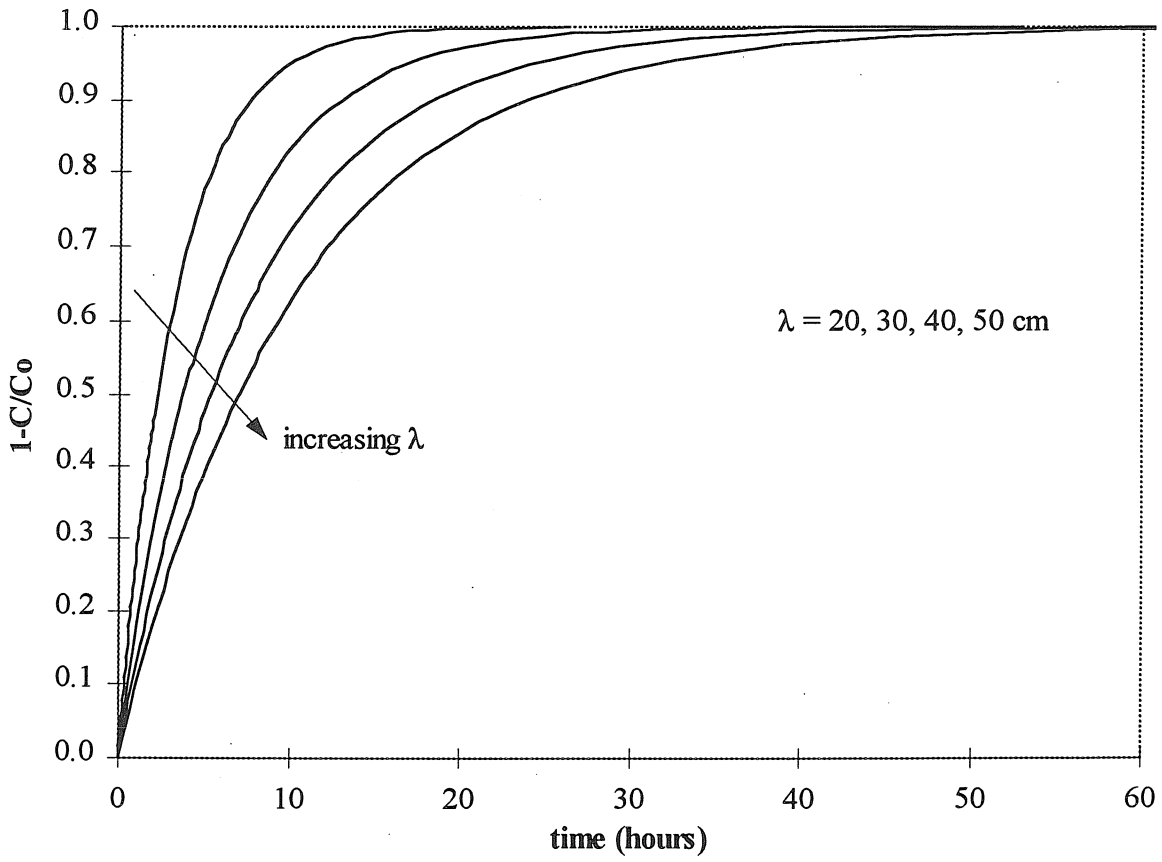

Figure 6.7: Maxpump model predictions for colloid exchange with different bedform wavelengths. Larger λ results in a lower exchange since the pressure disturbance at the bed surface has the same magnitude but pumping occurs over a larger scale. Input parameters other than λ are given in Tables 6.1 and 6.2.

Figures 6.8 and 6.9 show the variation in exchange over a range of bedform heights for both stationary and moving bedforms. Bedforms with larger H protrude farther into the stream, have a higher drag, and cause a greater pressure disturbance at the bed surface. Thus, a larger bedform height directly increases the pumping velocity and exchange. This effect will occur for both moving and nonmoving bedforms.

There are additional effects unique to the fast-moving bedform case which are reflected in the turnpump model predictions. Motion of larger bedforms will scour deeper portions of the bed. Since turnover dominates the initial exchange, larger bedforms cause considerably more exchange at early times. However, in this case, larger bedforms also reduce the effect of pumping because pumping exchange is only important below the turnover region. Larger bedforms mean that exchange due to pumping occurs at deeper levels in the bed where pore water velocities are lower. Thus, the dimensionless pumping velocity will be lower for larger bedforms in the fast-moving case.

These effects can be seen in Figure 6.9. The curves for different H begin with different slopes, deviate still more at early times, and then become close to parallel. The early behavior is dominated by turnover, with larger bedforms clearly having higher rates of exchange. However, the later behavior is controlled by pumping, and similar rates of pumping occur for all heights. Increased pumping exchange due to the larger pressure disturbance was counterbalanced by the decrease in pumping exchange due to the thicker turnover zone.

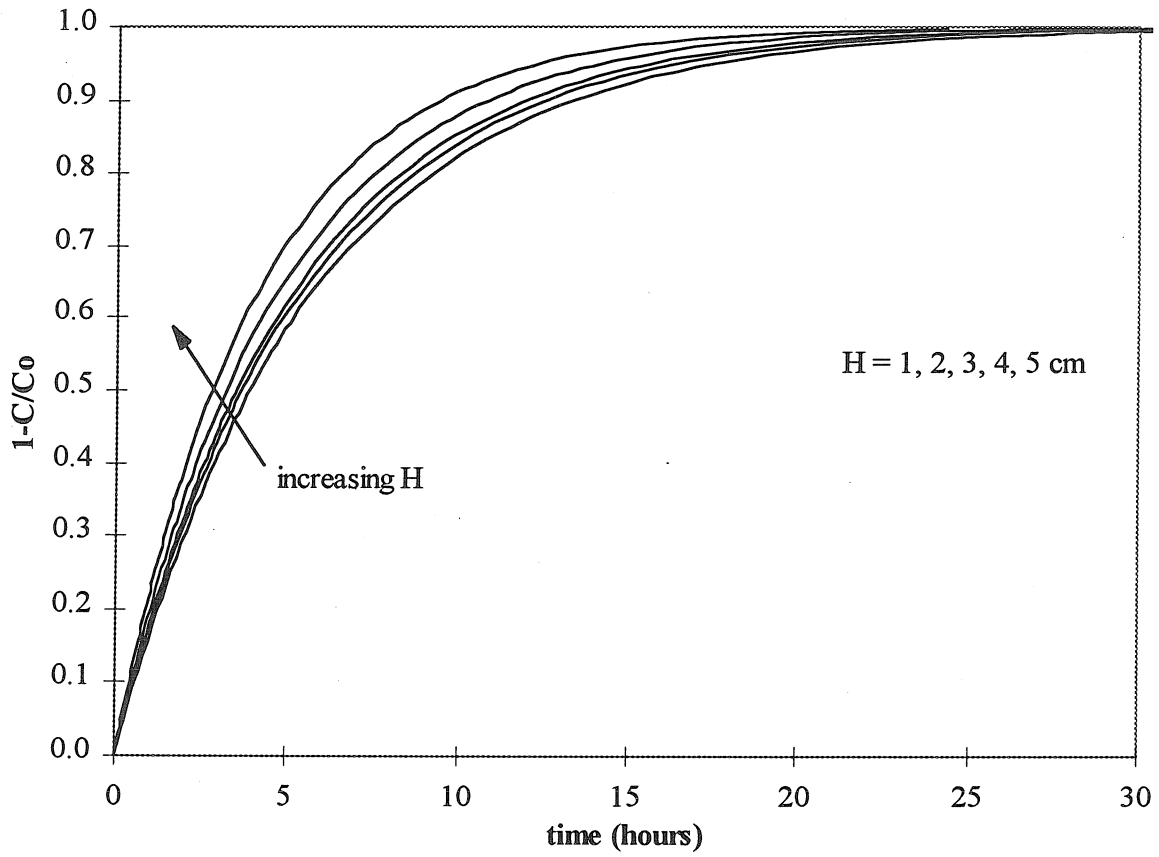

Figure 6.8: Maxpump model predictions for colloid exchange with different bedform heights for stationary bedforms. Larger H results in a larger pressure disturbance due to the bedform and a higher rate of pumping. Input parameters other than H are given in Tables 6.1 and 6.2.

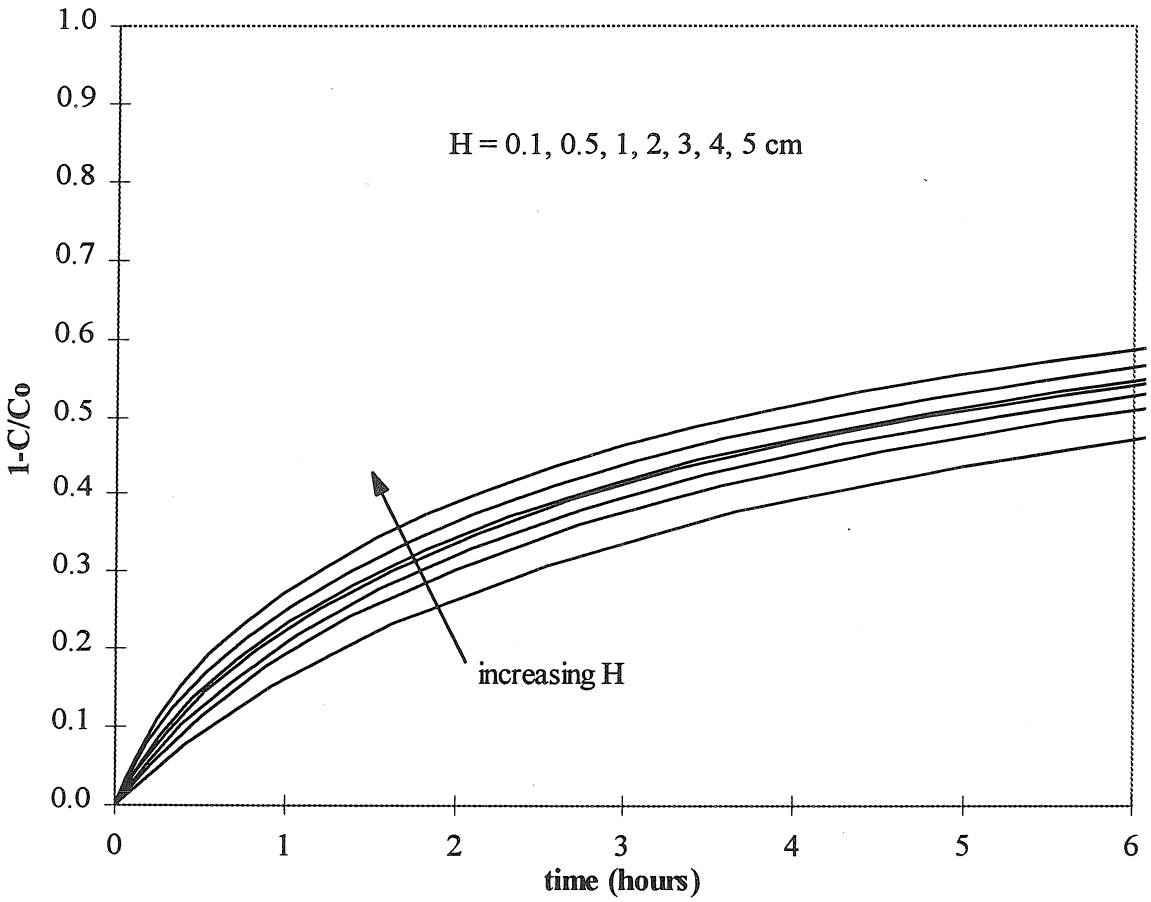

Figure 6.9: Turnpump model predictions for colloid exchange with different bedform heights for fast-moving bedforms ($U_b^* = 1.9$). Larger H corresponds to a larger turnover region and higher exchange at early times. Larger H also results in higher pumping velocities, but this effect is offset by the larger turnover region which causes pumping to be an important exchange mechanism at a deeper level in the bed. Input parameters other than H are given in Tables 6.2-6.3.

Figure 6.10 shows turnpump model predictions for a range of bedform velocities. This model is not sensitive to values of U_b^* because it explicitly assumes that turnover dominates pumping in the turnover region. In the model, the only effect of the bedform velocity is to change the rate at which turnover occurs. This can be seen in Figure 6.10 as the deviation of the predictions up to around $\mathrm{sqrt}(t^*/\theta) = 4$. Higher U_b^* results in slightly higher exchange at early times. This deviation does not persist at later times because the ultimate extent of turnover is given by the maximum scour depth, which is independent of U_b^* in the model. The exchange at later times is controlled by pumping, which is also independent of U_b^*.

The independence of turnpump model predictions from U_b^* indicates the limitations of this model. The turnpump model was developed for the asymptotic case of high bedform velocity where the magnitude of U_b^* is no longer an important variable. Strictly speaking, this should be true only for $U_b^* >> 1$. However, this model was applied with some success to experiments with lower bedform velocities (see Section 5.1.4 for specific comparisons).

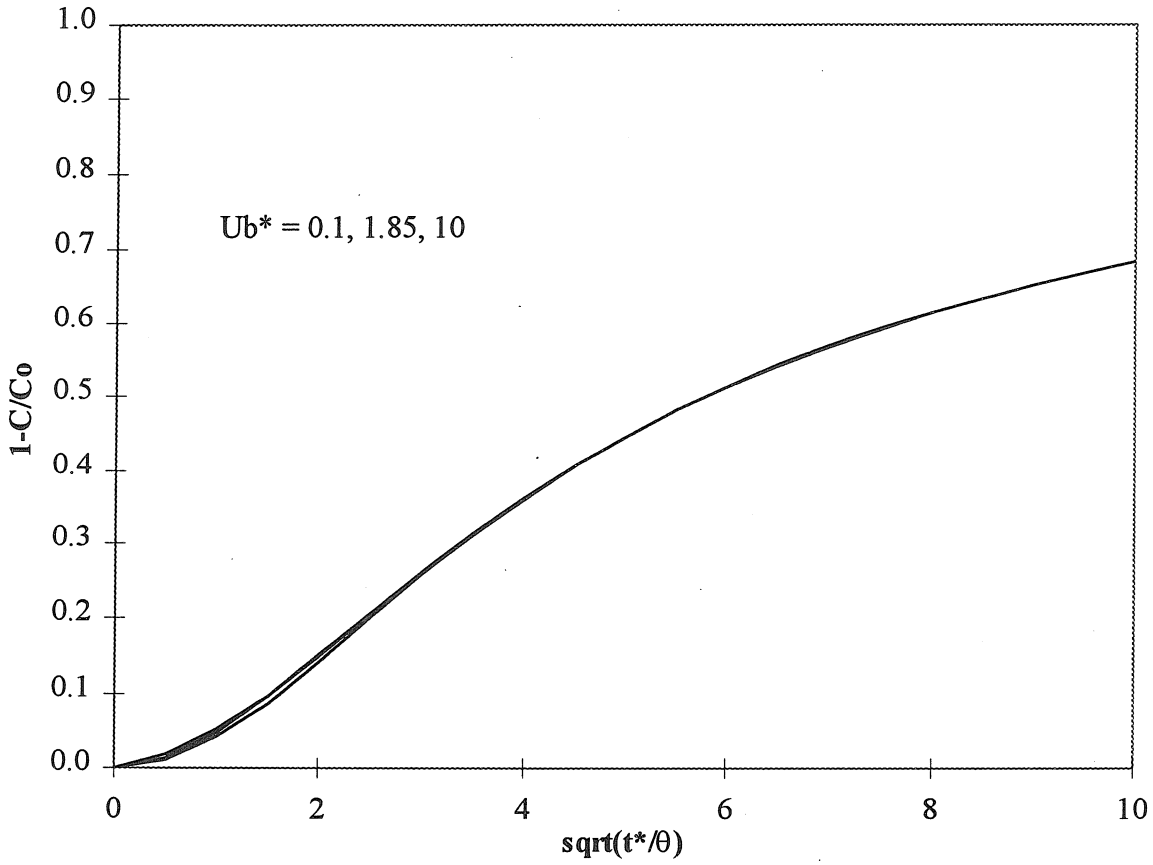

Figure 6.10: Turnpump model predictions for colloid exchange with different bedform velocities. U_b* has little effect on turnpump model predictions because the model assumes that turnover is sufficiently fast to dominate pumping. Input parameters other than U_b* are given in Tables 6.2 and 6.3.

6.2.3 Other bed parameters

Figure 6.11 presents maxpump model predictions for several bed depths for stationary bedforms. The only effect of d_b in the maxpump model is to change the flux through the surface of the bed. Equation 3.38 shows that the pumping flux through the surface goes like $\tanh(d_b^*)$. As a result, the bed depth has little impact on model predictions because the surface flux will be significantly reduced only for very shallow beds. Changing bed depth has much less impact on colloid exchange than it does on the exchange of a conservative solute (compare Figure 6.11 with Figure 6.1). This is true because the exchange of conservative tracers is limited by dilution, while colloid exchange is unlimited at low inputs. (Continual colloid trapping by the bed will eventually lead to pore spaces becoming plugged with colloid deposits. Thus, ultimate colloid exchange is limited by changes in bed parameters due to colloid accumulation in the upper layers of the bed.) It is important to note that pumping path lengths will also be shorter for shallower beds, and a higher filtration coefficient may be required to justify use of the maxpump model.

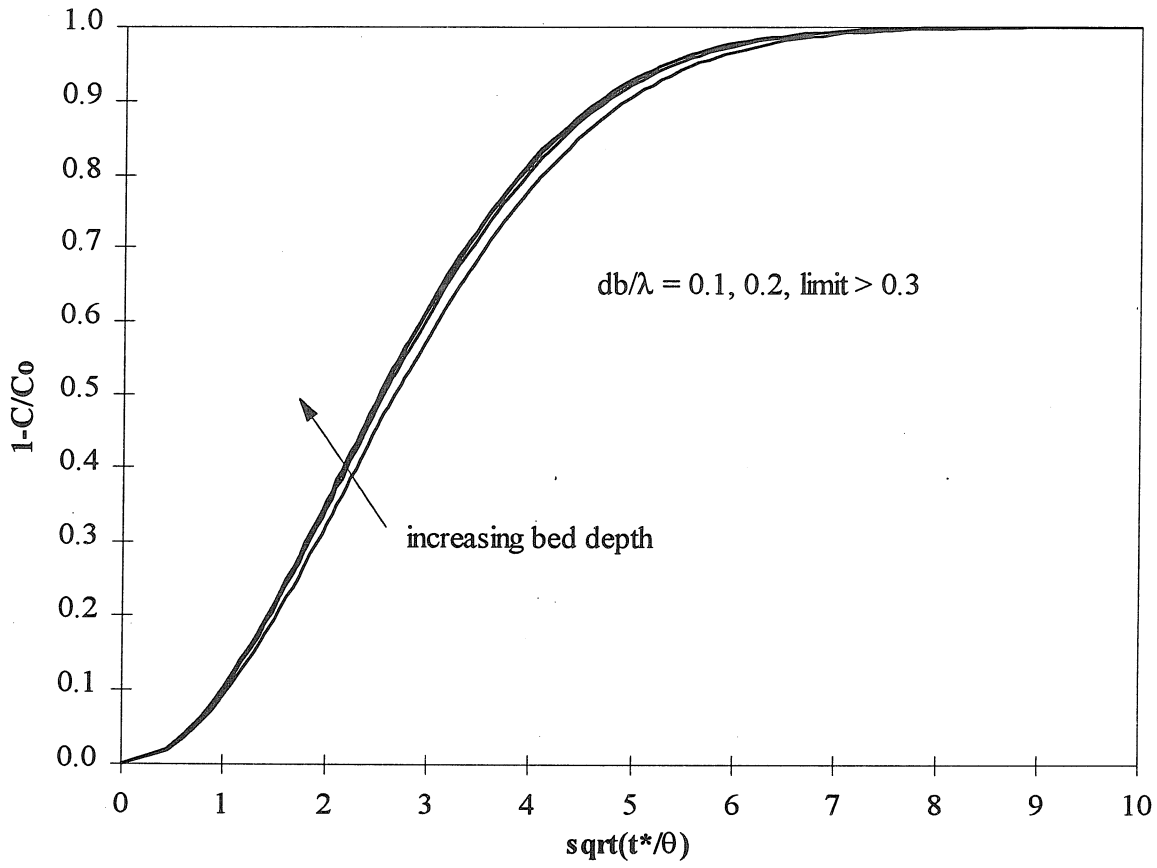

Figure 6.11: Maxpump model predictions for colloid exchange with beds of different depths with stationary bedforms. Bed depth has little impact on maxpump model predictions because this model calculates exchange based on flux through the bed surface, which is only affected by bed depth for extremely shallow beds. Input parameters other than d_b/λ are given in Table 6.1 and 6.2.

Figure 6.12 shows the change in maxpump model predictions for colloid exchange due to different sand sizes and hydraulic conductivities with stationary bedforms. The bed sediment properties are included in all of the exchange models through the porosity and hydraulic conductivity. However, bed sediment size is a more intuitive parameter for comparative purposes. Hydraulic conductivity was related to sediment grain diameter for the simulations in Figure 6.12 by starting from the measured value of K = 9.0 cm/min for the sand used for this work (geometric mean diameter of 0.480 mm) and using the similarity relation that K is proportional to D^2. Larger sand with higher conductivity allows higher pore-water velocities in the bed, and correspondingly higher exchange rates.

It should be noted that this simulation ignores any dependence of filtration on the bed sediment size. In reality, for a given type of colloid and collector, there will often be an inverse relationship between the filtration coefficient and the filter grain diameter (for example, see Yoshimura's data on kaolinite filtration by sand in Tien, 1989). Consequently, the complete-trapping assumption could become invalid for larger grain sizes, in which case the maxpump model would no longer provide a good prediction for the exchange, although this prediction would still be a valid upper limit.

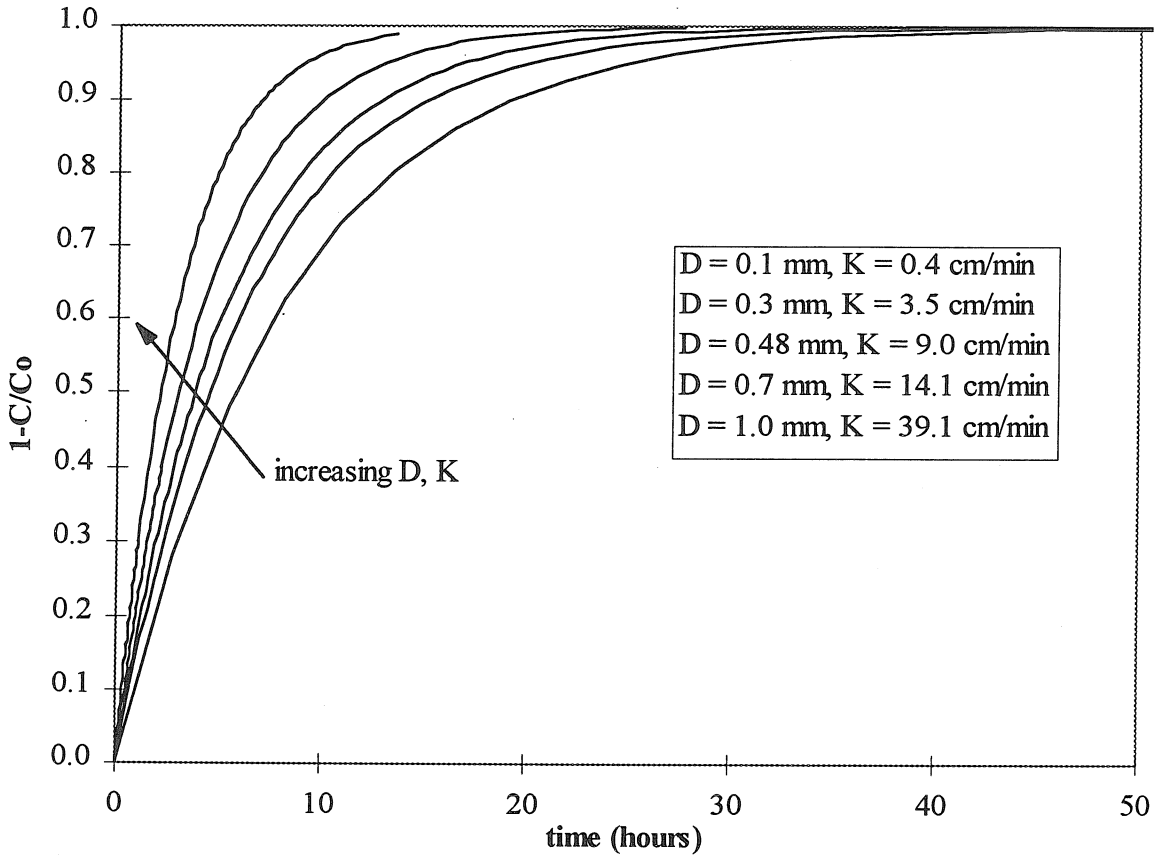

Figure 6.12: Maxpump model predictions for colloid exchange with different average sand diameters and hydraulic conductivities with stationary bedforms. K is assumed to be proportional to D^2. Larger K results in higher flow through the bed for the same bedform-induced pressure disturbance. Input parameters other than K are given in Tables 6.1 and 6.2.

6.2.4 Particle parameters

The particle-specific transport processes of filtration and settling control the extent of particle trapping by the stream bed. The filtration coefficient, λ_f, and settling velocity, v_s, are thus of primary importance in determining the overall exchange. Indeed, the results of Chapter 5 show that only these two parameters are needed to distinguish the exchange of colloids from that of conservative solutes.

Figures 6.13 and 6.14 show the variation in colloid pumping model predictions for a range of filtration coefficient for no settling ($v_s^* = 0$) and slow settling ($v_s^* = 0.1$). In the case of non-settling colloids, the lower limit for no filtration ($\lambda_f = 0$) represents the exchange of a conservative solute. Higher filtration results in more net exchange up to another limit value for complete trapping given by $\lambda_f^* > 1$. (The dimensionless filtration coefficient is scaled by the bedform size as represented by the average bedform wavenumber, $\lambda_f^* = \lambda_f/k$.) When the filtration coefficient is large, its magnitude is no longer important and the colloid pumping model gives results identical to those of the maxpump model. In the case of slowly-settling colloids, the lower limit of no filtration shows the trapping and exchange simply due to particle settling. Filtration causes additional trapping and exchange, again up to the limit for complete trapping. In general, the value of λ_f^* needed to produce complete trapping will be less when v_s^* is higher, and the exchange for complete trapping will be higher when v_s^* is higher. However, these effects are not obvious in Figures 6.13 and 6.14 since the results of Figure 6.14 include only a small degree of particle settling.

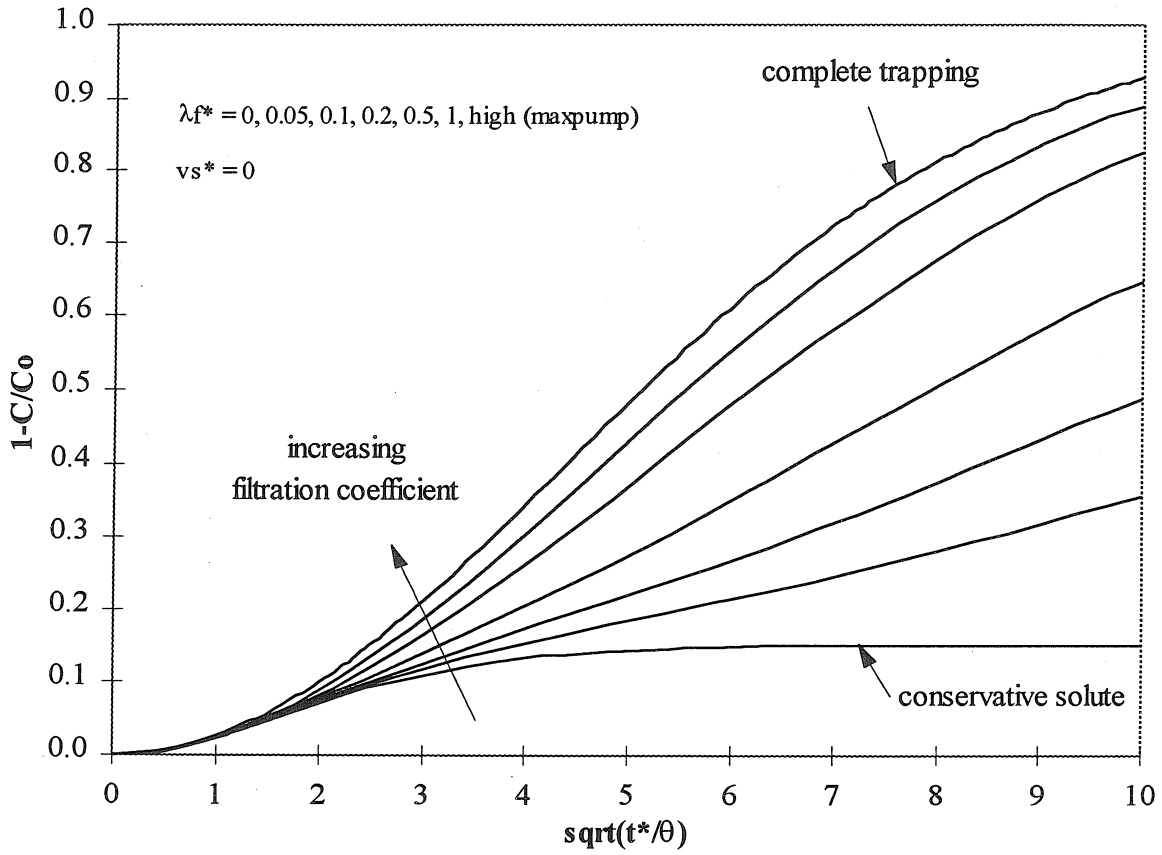

Figure 6.13: Particle pumping model predictions for exchange of non-settling colloids with different filtration coefficients with stationary bedforms. The curve for $\lambda_f * = 0$ represents a prediction for conservative solutes. For high values of the filtration coefficient, all colloids that enter the bed will be filtered and the predictions of the clay pumping and maxpump models are identical. Input parameters other than λ_f^* and v_s^* are given in Table 6.1. Note: for this simulation $\lambda_f^* = \lambda_f/k = 4.8\ \lambda_f$.

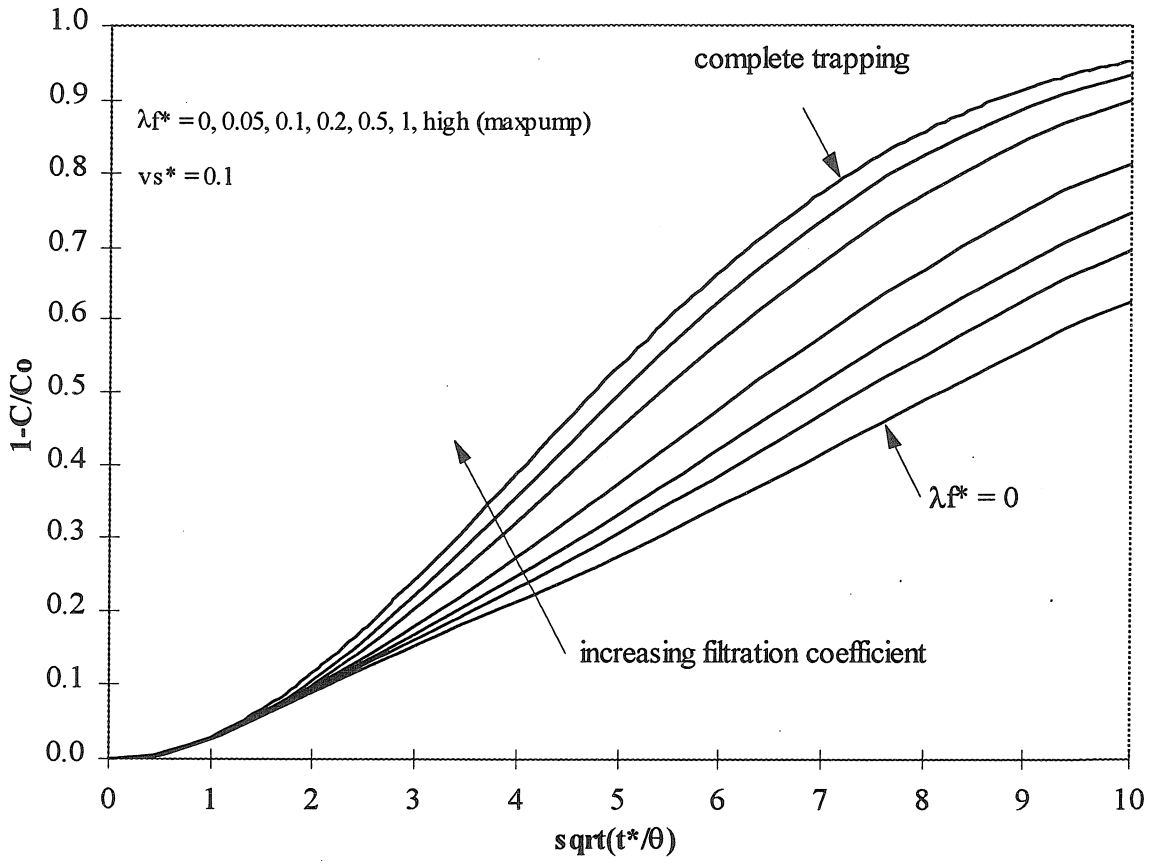

Figure 6.14: Particle pumping model predictions for slowly-settling colloids with different filtration coefficients with stationary bedforms. All model predictions fall in an envelope defined by the exchange due to settling with no filtration, and the exchange due to settling with complete filtration. Input parameters other than λ_f and v_s^* are given in Table 6.1. Note: for this simulation $\lambda_f^* = \lambda_f/k = 4.8\ \lambda_f$.

Figure 6.15 shows colloid pumping model predictions for various settling velocities and no filtration. Again, the prediction for $v_s^* = 0$ represents the exchange of a conservative solute; this curve is identical to the one for $\lambda_f = 0$ in Figure 6.13. Increased settling causes additional trapping and higher exchange, just as higher filtration does. Settling with $v_s^* > 1$ causes complete trapping because particles cannot be advected upward in the bed. Higher settling velocities also result in higher flux of particles through the bed surface, and thus higher exchange.

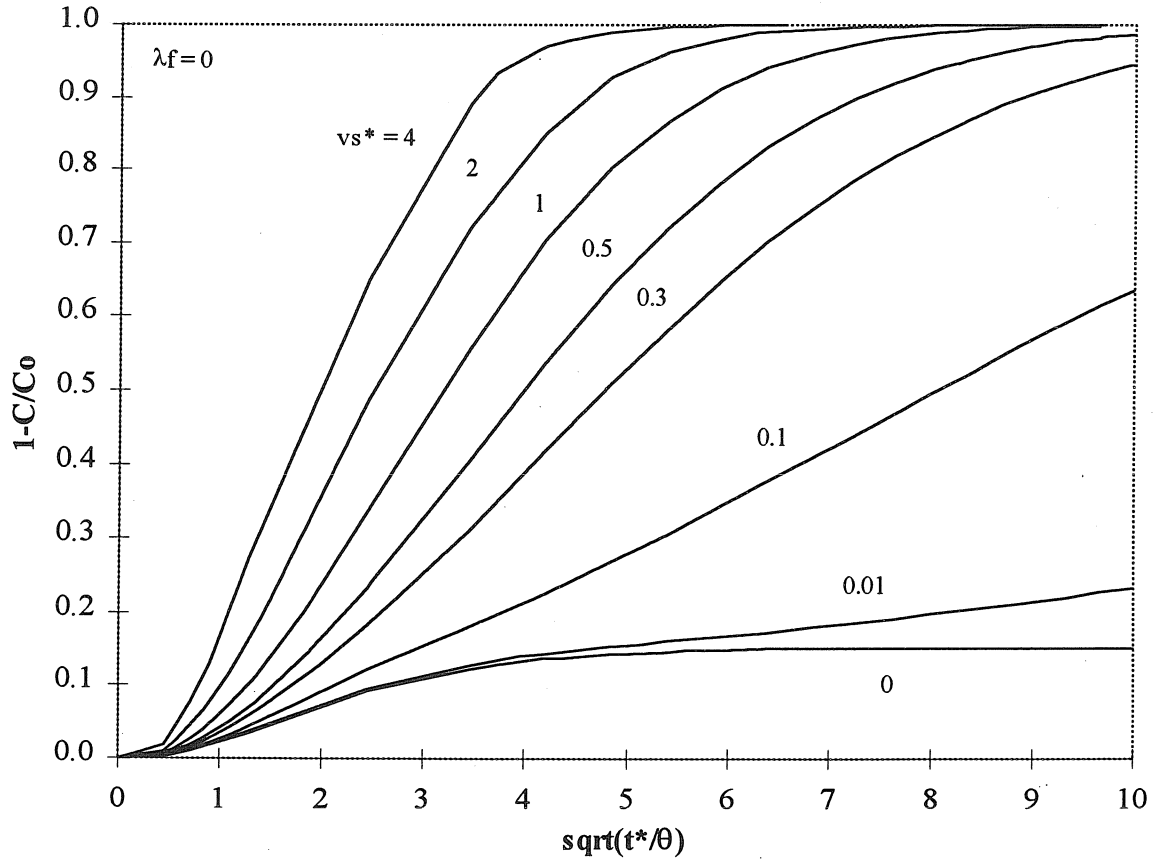

Figure 6.15: Particle pumping model predictions for colloids with no filtration and different settling velocities with stationary bedforms. The curve for $v_s^* = 0$ represents a prediction for conservative solutes. Higher settling velocity increases the flux of particles through the bed surface. Input parameters other than λ_f and v_s^* are given in Table 6.1.

Figure 6.16 shows maxpump model predictions for colloids of different sizes and settling velocities. These results differ from those of Figure 6.15 in that complete trapping (due to high filtration) is assumed for all values of v_s*. In addition, the curves in Figure 6.16 were generated for colloids of different sizes. To apply the model to a colloid of a particular size, the particle settling velocity is nondimensionalized by the pore water velocity, u_m/θ. By comparing Figures 6.15 and 6.16, it can be seen that filtration causes additional trapping and exchange of small colloids (with $v_s^* < 1$), but has no effect on larger colloids ($v_s^* > 1$) that are already completely trapped due to settling.

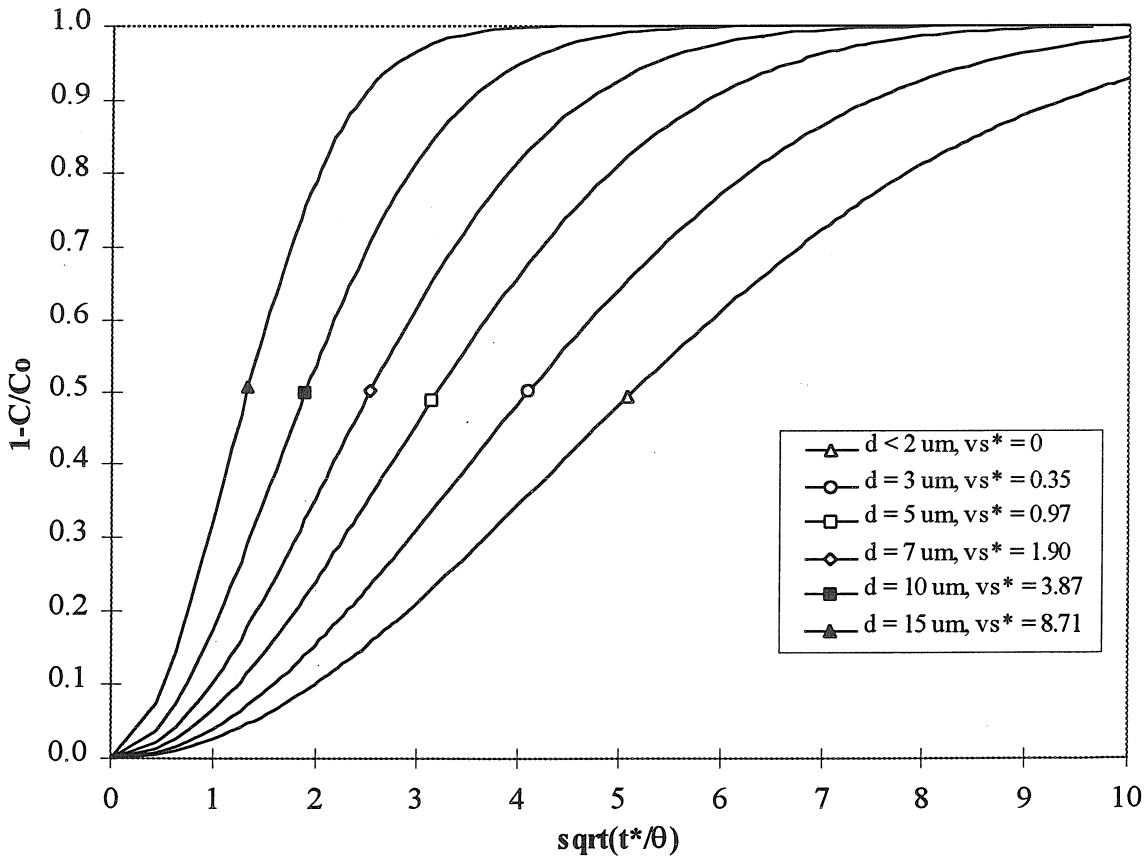

Figure 6.16: Maxpump model predictions for exchange of colloids of different sizes and settling velocities with stationary bedforms. The maxpump model assumes that complete trapping occurs (e.g., due to filtration), so these predictions specifically show the additional contribution due to increased settling. Input parameters other than v_s* are given in Table 6.1.

Figure 6.17 gives turnpump model results for colloids of different sizes and settling velocities. Figure 6.17 differs from Figure 6.16 in that the stream velocity is higher so that the bedforms are fast-moving. Changing the particle size will generally have a smaller effect with fast-moving bedforms because the stream and pore-water velocities are higher. That is, the particle settling velocity will change just as much, but $v_s^* = v_s\theta/u_m$ will change less due to the higher u_m.

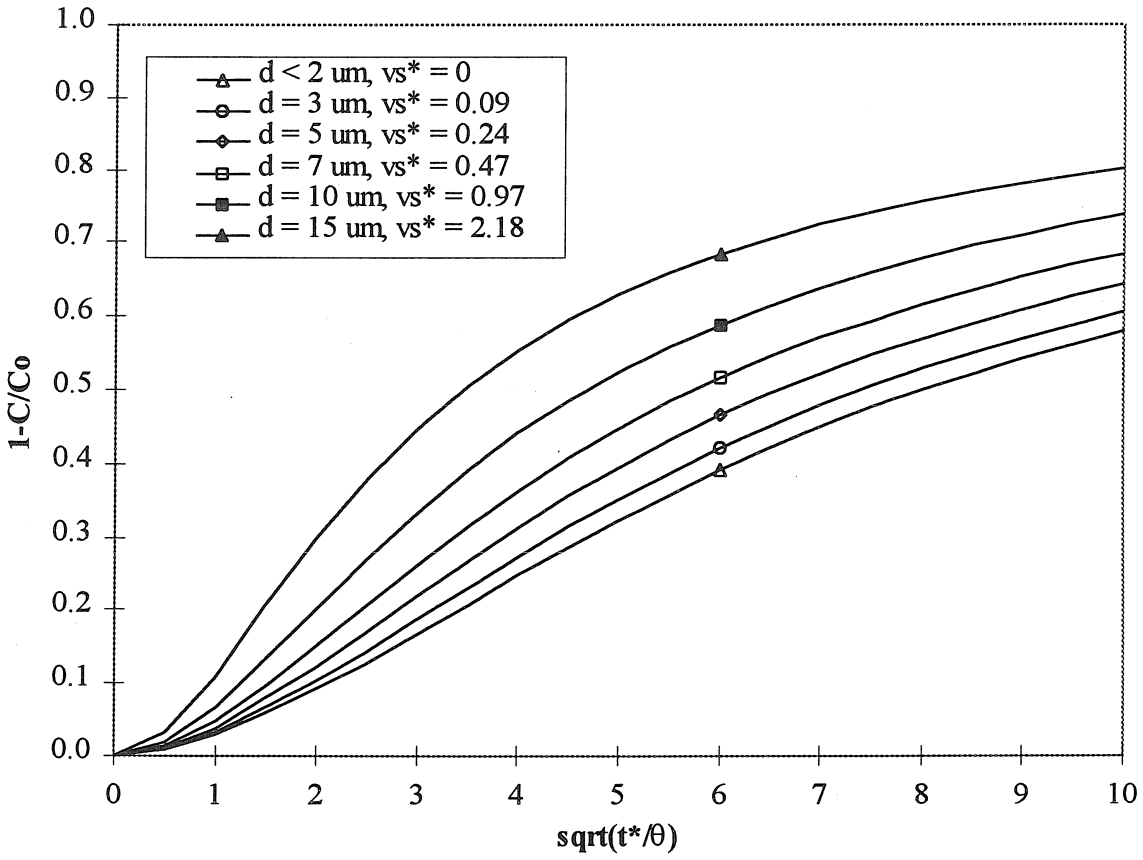

Figure 6.17: Turnpump model predictions for exchange of colloids of different sizes and settling velocities with rapidly-moving bedforms ($U_b^* = 1.9$). The turnpump model assumes complete trapping in the pumping region, so these predictions show the additional contribution from increased settling. Turnover reduces the impact of increased particle settling (compare with Figure 6.16). Input parameters other than v_s^* are given in Tables 6.2-6.3.

6.2.5 Stream chemistry -- example of hematite filtration by sand

Stream chemistry is not described explicitly in the exchange models, but is included through the filtration coefficient and to a lesser extent through the particle settling velocity (via the size distribution). Stream chemistry and the composition of the particles involved will control the filtration coefficient as described in Section 3.2.3. In general, chemical effects can be expected to have a large impact on the exchange behavior of colloids. In the particular experiments on kaolinite exchange described herein, however, the stream chemistry was not observed to have much impact because all experiments had sufficiently high filtration ($\lambda_f * > 1$) to lie in the asymptotic region of complete trapping. Also, because the kaolinite colloids were relatively large, with a mean diameter of 7 μm, particle settling dominated trapping.

An example of hematite filtration by sand will be used to demonstrate the effect of stream chemistry on colloid exchange. The chemical inputs for this example are taken from the unpublished data of Noelte, who conducted experiments at Caltech on the filtration of hematite by Ottawa-30 silica sand (Noelte and Morgan, 1995). The pristine hematite colloids used in these experiments were spherical with a diameter of 60 nm, and had a pristine point of zero net proton charge (PPZNPC) at pH 8.5. These colloids are in the Brownian range and have a settling velocity of zero. Filtration of these hematite particles by silica is expected to be favorable at pH < 8.5 when the hematite surface is positively charged, and unfavorable at pH > 8.5 when the hematite surface is negatively charged. Phosphate ions are known to specifically interact with hematite, and the surface

charge of the hematite particles could be made negative at pH's below the PPZNPC by the addition of phosphate (as NaH_2PO_4) to the suspension.

The results of four of Noelte's experiments are given in Table 6.4. These experiments were performed in a column of length 25 cm and diameter 5.1 cm. All experiments were conducted with a background of 1 mM NaCl. Filtration behavior was explained by the hematite surface charge. All hematite was filtered (C = 0 in the effluent) in the experiment in which hematite had positive surface charge. Experiments with negative hematite surface charge had a small degree of filtration. In addition, the filtration coefficient was inversely related to the phosphate concentration.

Table 6.4: Conditions and results of column experiments on the filtration of hematite by sand (after Noelte and Morgan, 1995).

Exp. #	pH	I (mM)	Phosphate (μM)	Hematite Surface Charge	C/Co	λ_f (1/cm)
1	5.6	1.0	0	positive	0	>0.3
2	10.0	1.0	0	negative	0.31	0.047
3	7.0	1.0	5.0	negative	0.42	0.035
4	7.0	1.0	10.0	negative	0.70	0.014

Figure 6.18 shows pumping model runs for the four hematite/sand filtration experiments described above. Hydraulic data for these model runs were taken from the baseline case used in previous simulations (defined in Table 6.1). These curves should be thought of as predictions for the exchange of this hematite in flume experiments where the stream has the given chemical composition. For this combination of colloid and bed material, stream pH and phosphate concentration have a substantial impact on the degree of particle trapping by the bed.

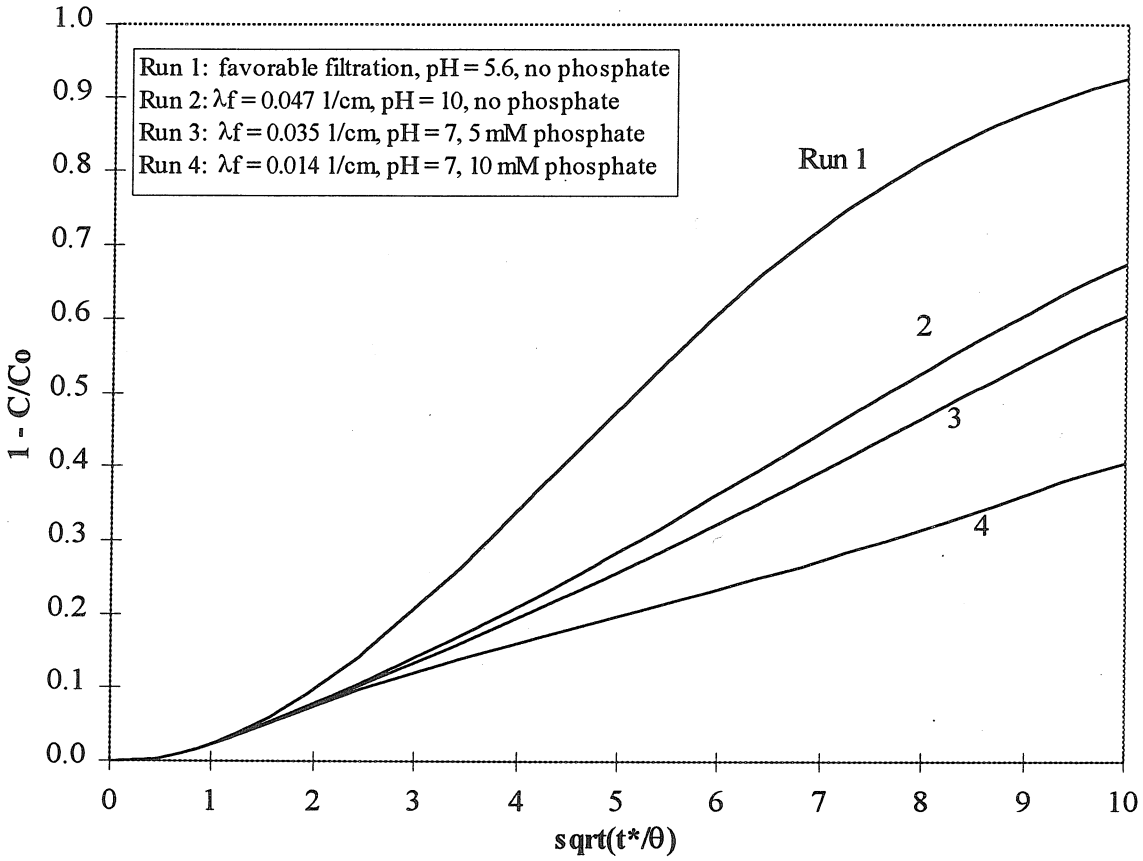

Figure 6.18: Particle pumping model predictions of hematite exchange with different stream pH's and phosphate concentrations with stationary bedforms. Stream hydraulic conditions are given in Table 6.1. I = 1 mM for all runs.

6.3 Analysis of the accuracy of model predictions for experimental results

Discrepancies between experimental and modeling results are the result of three sources of error: difficulties in measuring experimental data, failure to provide good model inputs, and deviation of actual conditions from model assumptions. Specific sources of error will be discussed within these three categories.

Hydraulic data were measured very accurately and precisely in the flume. Heights, slopes, and flow rates were all measured sufficiently well that their errors are insignificant. As a result, the stream parameters such as depth and velocity were known within 3%.

However, it was difficult to determine average bedform parameters from basic measurements. Bedforms were generally irregular, showed wall-effects, and, in the case of moving bedforms, often changed shape. This made it difficult to define a unique height, wavelength, and celerity for each bedform. Also, some bedforms were only partially formed (i.e., covered half the width of the flume), and others were ripples much smaller than the typical dune. It was an arbitrary decision whether to include ripples in the overall average. Finally, measurements of 20-50 bedforms were used to define the average bedform geometry, and 10-20 were used to define the average velocity. Some deviation of the actual average from the average of these measurements is expected. Since bedform data are used to predict pumping and turnover exchange, misestimation of average bedform parameters contributes to the disagreement between model predictions and experimental results. The estimated errors in the bedform parameters are: H ±20%,

$\lambda \pm 10\%$, and $U_b \pm 30\%$. The simulations of Chapter 6 show the sensitivity of exchange predictions to changes in these variables.

Accuracy of concentration measurements was also very good. Lithium concentrations were always far above the detection limit on the ICP-MS, so lithium data are expected to be accurate within a few percent. Clay concentrations were also generally sufficiently high to limit errors from spectrophotometer accuracy to <1%. (However, pore-water profiles often had large analysis error, up to ~50%, because these samples were diluted. Some analysis problems were also encountered at the end of flume experiments when most clay had been trapped by the bed.) On the other hand, drift of ICP-MS measurements was sometimes a problem and caused some bad lithium data sets. This was corrected in later experiments by the use of a reference solution which was remeasured after every 3-5 samples.

It was also difficult to define an average stream-water concentration from the basic data early in the experiment. Ideally, the entire body of recirculating water always has the same tracer concentration. In reality, however, the initial tracer distribution was fairly non-uniform (typically varied from the mean by ±20%), and this non-uniformity persisted for some time (typically ~15 minutes). Grab samples taken later in the experiments still showed some scatter, on the order of a few percent. The wide scatter in early samples made it difficult to determine the initial concentration, C_0. This causes significant error in all dimensionless concentration data, since C_0 is used to scale all other concentrations. Misestimation of the initial concentration was probably a major source of the disagreement between model predictions and experimental results.

The simulations presented in Sections 6.2 can be used as a sensitivity analysis to identify inputs that have a large impact on model predictions and could be major sources of error in model predictions. For colloid transport, model predictions are very sensitive to filtration coefficient and settling velocity. For the kaolinite experiments, the filtration coefficient was always asymptotically high, so errors in measuring filtration are not reflected in model predictions. However, the model is very sensitive to settling velocity for particles of the size used. The problem is compounded by the fact that settling velocity is actually calculated from the average particle diameter, and the settling velocity is proportional to the square of diameter. Error in determining the average particle diameter results from the use of polydisperse kaolinite suspensions and analysis instrument error. Misestimation of the particle settling velocity was probably a major source of disagreement between model predictions and experimental results for colloids. This is especially true for the first six experiments, because the preparation procedure for kaolinite described in Section 4.4.3 was not used for these early experiments. As a result, experiments #1-6 show poorer agreement between model predictions and exchange data.

The general agreement between model predictions and experimental results demonstrates that the model describes the essential exchange processes correctly. However, the model assumes a simplified geometry that does not exactly match actual conditions. In particular, the model assumption of regular 2D bedforms is not representative of naturally-formed bedforms, which have some 3D features. This assumption is true to first order, however, and is thus a useful approximation which captures most of the actual exchange behavior. Failure to account for actual bedform geometries results in

some error in the model predictions. Based on the sensitivity analysis of Section 6.2.2, these errors are expected to be relatively minor, on the order of 1-10%.

To summarize, the discrepancies between model predictions and experimental results are attributed to (in rough order):

1. Misestimation of particle settling velocity.
2. Misestimation of average bedform parameters (including the related second-order effect: the inability of model to handle irregular bedform shape/sizes/velocities).
3. Misestimation of initial tracer concentration in the stream, C_0.
4. Scatter of data due to nonrepresentative flume samples, measurement errors, and analytical instrument errors.

In addition, ICP-MS drift resulted in poor lithium data for a few experiments.

Experiment #6 will be used as an example to demonstrate the magnitude of errors which can be responsible for disagreement between model predictions and experimental results. In general, the colloid exchange in nonmoving bedform experiments was predicted very well by the maxpump model. Experiment #6 is the one exception, as shown in Figure 6.19. However, for this experiment, the finite bed pumping model for conservative solutes predicted the lithium exchange reasonably well. This indicates that the hydraulic inputs were probably correct and the exchange hydraulics were modeled well, but the inputs that determine colloid behavior in the model were incorrect so that the kaolinite exchange was misestimated. Since it is assumed that filtration is very high, it is most likely that an error in the particle settling velocity was responsible for the relatively poor agreement between experimental results and model prediction.

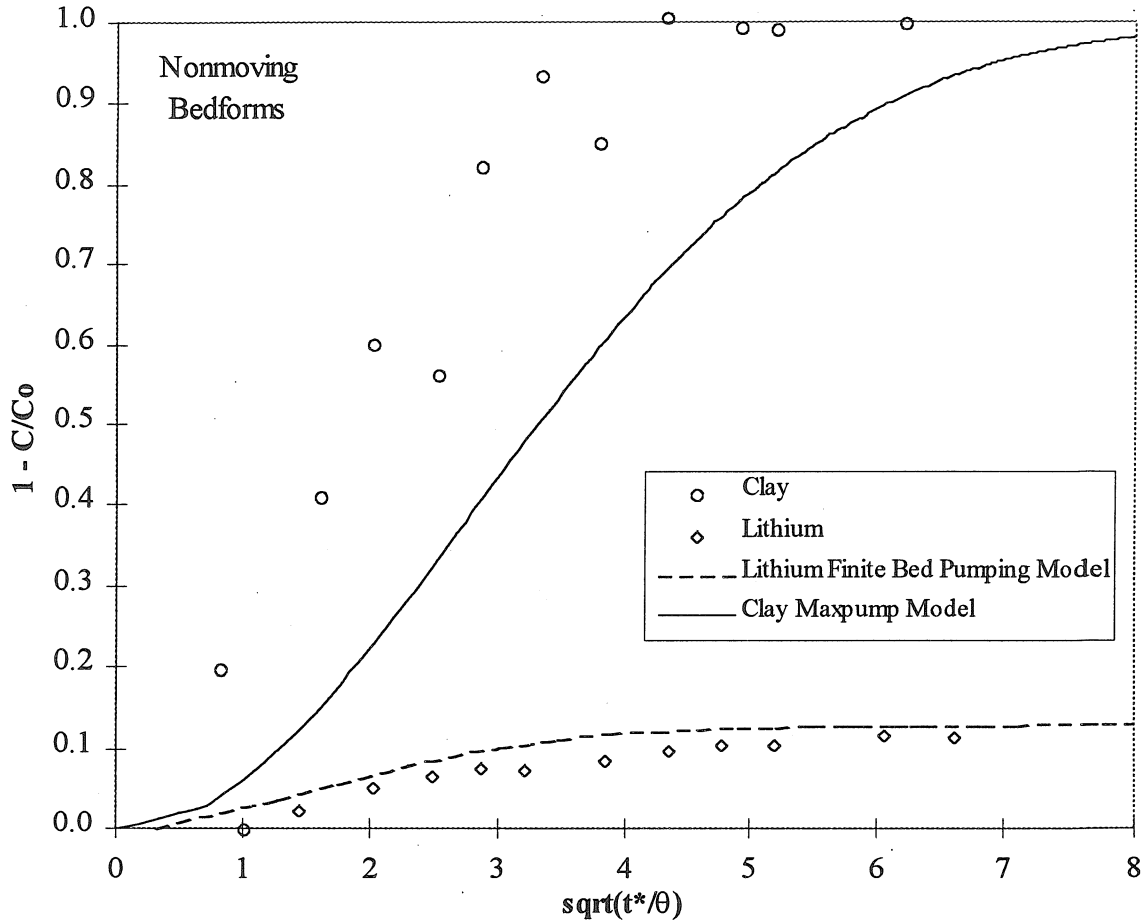

Figure 6.19: Comparison of experiment results and model predictions for Experiment #6. Particles were assumed to be 7 μm in diameter.

This experiment was the first one which used deionized water (instead of tap water), but it did not employ the complete kaolinite preparation procedure described in Section 4.4.3. As a result, the clay size distribution was not well-defined. The simple grinding-and-washing preparation method used for this experiment could have produced kaolinite particles that were larger than those produced by the complete procedure. The input value of the particle settling velocity is taken from the size distribution measured

for the clay prepared with the complete method, so deviation of the size distribution in the flume from this expected value causes error in the model prediction.

The model prediction can be fit to the experimental data using the settling velocity, as shown in Figure 6.20. Good agreement between experimental results and model predictions for experiment #6 can be obtained by assuming that the kaolinite present in the flume had a mean diameter of 13 μm (instead of 7 μm). This causes the particle settling velocity to increase by a factor of $(13/7)^2 = 3.45$, and increases the colloid exchange with the bed. This example demonstrates that care must be taken to ensure that model input values are representative of the conditions in the flume.

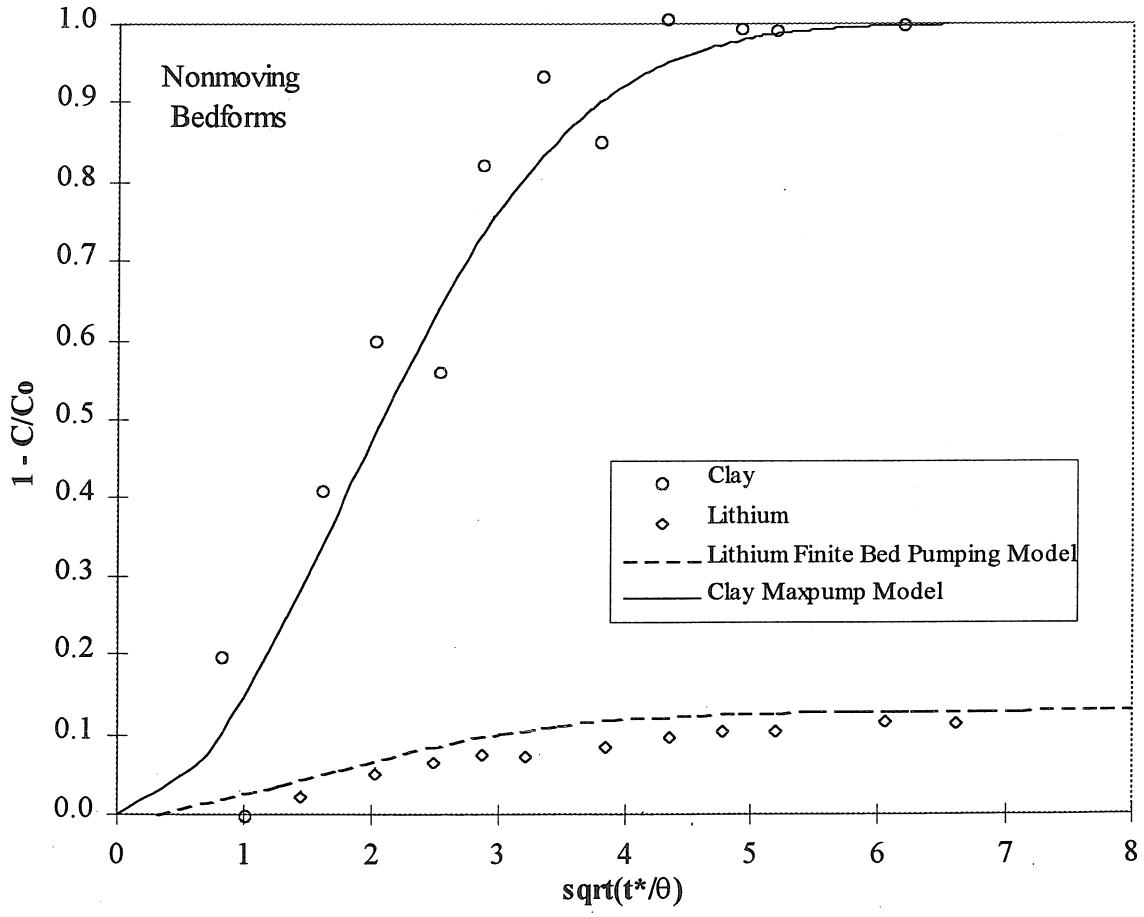

Figure 6.20: Comparison of experiment results and model predictions for Experiment #6. Particles were assumed to be 13 μm in diameter.

6.4 Implications for colloidal particle transport in real rivers

The exchange models developed in this work can be used to draw conclusions about colloid transport in natural sand-bed streams. Most importantly, this work identified the ways in which the behavior of colloids differs from that of conservative solutes. Filtration and settling of colloids causes them to become trapped in stable sand beds. As a result, fine particles traveling down a natural stream are expected to disappear from the stream over time due to trapping in the stream bed. That is, for steady stream conditions with only a small amount of bed sediment transport, there will generally be some flux of colloids to the bed. However, trapped colloids can be released when the stream velocity rises so that previously stationary regions of the bed are scoured.

It is useful to consider the factors that could control the bulk concentration of colloids in natural sand beds. When the supply of colloids is relatively small, as in the flume experiments, colloid accumulation in the bed will be controlled by the input. The frequency at which the bed experiences significant scour will also control the extent of accumulation. When the bed is stationary for a long period of time, colloids will accumulate in the bed until the pore spaces become plugged with deposited colloids. However, the colloids will never be able to fill all the pore space in the bed. Instead, colloids will accumulate near the bed surface in areas of high inflow. As these areas become plugged, the hydraulic conductivity of the surface layer will decrease and exchange between the stream and bed will essentially end. Thus, even when the bed is stable for a long time and the colloid supply is high, the bulk concentration of colloids in

the bed is not expected to be high. This expectation is confirmed by observations in sand-bed rivers, in which the clay fraction is typically 2-5%.

Use of dimensionless models and correct parameterization of the various inputs provides for application to systems of different scales without the need for additional experiments. The bedform wavelength is used to scale all other lengths. In nature, dune dimensions all scale with the wavelength as well (i.e., all dunes have a roughly similar shape). Thus, the overall size of the bedforms in a natural stream determines the relative importance of various processes. For example, the dimensionless filtration coefficient scales directly with bedform wavelength, so larger bedforms have a higher λ_f^* for the same dimensional λ_f. This means that, for a given λ_f, trapping will be higher for pumping through larger bedforms. This is very intuitive as well, since filtration is an exponential decay of transported particle concentration with distance, and the pathlines over which filtration occurs will be longer through larger bedforms.

The results of this work can be applied directly to natural materials. The use of the filtration coefficient, λ_f, and settling velocity, v_s, to parameterize particle transport allows modeling of exchange even in cases where the chemical behavior of the system is not well-understood. Detailed knowledge of the particle composition and chemistry is not required to apply the model. Instead, these factors are all implicit in the filtration coefficient and particle size distribution, which can be measured for any system of interest. Care must be taken, however, to ensure that values of these parameters input in the model actually reflect the conditions of the natural system.

6.5 Future research

Extensions of this work lie primarily in four areas: developing a better understanding of the hydraulics of bedforms and bedforms-driven exchange, conducting flume experiments on colloid exchange with a wider range of trapping behavior, conducting laboratory experiments and developing analytical models for the exchange of additional reactive substances, and extending existing models for bed-exchange to natural streams.

The models presented in this thesis calculate exchange due to idealized bedforms. Better exchange predictions could be made if the hydraulics of flow over and through bedforms was better understood. The pressure variation at the bed surface, an important exchange parameter, is estimated from an empirical formula originally determined for a bedform of fixed triangular geometry. The effect of irregular 2D and 3D bedform shapes on the pressure distribution should be investigated. In addition, the hydraulics of exchange with flat sand beds has been studied but not successfully modeled.

The exchange due to slowly-moving bedforms could not be modeled well because competing effects of pumping and turnover could not be resolved when they were of the same magnitude. Current models are based on asymptotic assumptions for either stationary or fast-moving bedforms. Development of a finite-element model for bed exchange would be useful in resolving actual tracer distributions in the bed. This would provide considerable generality to the application of the model. The slowly-moving bedform case could be modeled, along with other problems such as ones with an arbitrary initial distribution of tracer in the bed.

Work done to date has involved steady, uniform flow. Nonuniform and nonsteady flow conditions should be investigated. In particular, the trapping and release of pollutants due to aggradation and degradation of the bed should be studied. Current models are limited in application because the boundary conditions of the stream will change over time. Inclusion of these changing boundary conditions in the model would allow modeling of natural streams over much longer time periods.

In the experiments of this work, the colloidal tracer used always showed a very high degree of trapping by the stream bed sediment. As a result, the maxpump model for complete trapping always applied, and the trapping due to filtration could not be distinguished from that due to settling. Additional experiments should be performed to verify model predictions for weakly-trapped colloids. Experiments on Brownian colloids can be used to examine the effect of filtration alone. Experiments with non-Brownian colloids and very unfavorable filtration can be used to examine the effect of settling.

The exchange of reactive tracers merits further study. Different types of pollutants will have different chemical behavior in the stream bed. Current understanding is limited to conservative solutes, solutes that sorb to the bed sediment in the equilibrium case, and colloids. Some other interesting problems are: simultaneous transport of reactive solutes and colloids, exchange of tracers that interact with the bed sediment with kinetic effects, exchange of heterogeneous tracers, and exchange with beds of heterogeneous sediment. Additional chemical effects should be added to the exchange models so that systems of full natural complexity can be analyzed.

The ultimate goal of this research is to model the transport and fate of pollutants in natural streams. In order to do this, current bed-exchange models will have to be incorporated into larger models which include additional transport and exchange processes not present in the flume. The analytical descriptions of bed-exchange developed in this thesis should be used to describe exchange with the bed due to bedforms. Additional work will have to be done to model other processes that drive exchange between the stream and hyporheic zone. The methodology developed here for the parameterization of chemical processes for inclusion in exchange models should be a useful tool to predict the behavior of reactive substances in natural streams. In particular, the use of relatively simple batch and column experiments to quantify chemical processes provides an excellent method for predicting how chemistry will affect overall transport in hydrodynamically complex systems.

7. SUMMARY AND CONCLUSIONS

7.1 Summary of experiments, models, and results

Experiments were conducted in a recirculating flume to determine the important parameters and processes controlling the exchange of colloids between a stream and sand bed. Kaolinite was used as the colloidal tracer in 16 experiments; glass beads were used in the remaining experiment. Lithium was also used in 14 experiments as a conservative tracer to determine hydraulic exchange with the bed. A high-purity silica sand with a geometric mean diameter of 480 μm was used as the bed sediment in all experiments.

Stream hydraulic conditions were controlled by choosing the bed and stream depths, the channel slope, and flow rate. All experiments were run with uniform flow and fully-developed bedforms. Stream velocity varied from 13.5 to 64.9 cm/s, flow depth from 5.7 to 11.0 cm, average bedform height from 1.1 to 3.3 cm, average bedform wavelength from 17 to 73 cm, and average bedform velocity from 0 to 10 cm/min.

The chemical conditions of the water, bed sediment, and tracers were controlled for most experiments. The first five experiments used tap water and no special preparation or cleaning procedures. The last 12 experiments used deionized water with salt (NaCl), acid (HCl), and base (NaOH) added to control the ionic strength and pH, and sand that had been cleaned by acid- and base-washing. Starting with the seventh experiment, the colloids were prepared using a defined procedure. Flume experiments were conducted over a range of pH from 7.0 - 8.0 and ionic strength from 0.5 - 5.3 mM.

The exchange of tracer between the stream and stream bed was determined by establishing a uniform tracer concentration in the stream water at the start of an

experiment and then monitoring the decrease in the stream-water concentration over time. Profiles of tracer concentration in the bed were also obtained by sampling pore water. Lithium exhibited conservative behavior in this system: lithium exchange was controlled by the dilution of stream water with pore water over time. Kaolinite and glass beads behaved very nonconservatively: these colloids became irreversibly trapped by the bed over time. In most cases with nonmoving bedforms, all colloids added to the stream were removed by the bed during the course of the experiment. Cases with moving bedforms generally showed less trapping, though complete colloid removal was sometimes observed. In cases where some colloid remained in the stream at the end of the experiment, the system was not in equilibrium and there was a continuing net flux of particles to the bed. Even though this exchange was generally small, it would eventually cause all colloids to be trapped by the bed.

Column experiments were conducted to examine colloid filtration by the bed sand in a simpler hydrodynamic environment. Materials used in column experiments were prepared in exactly the same manner as for flume experiments. Column experiments were conducted on kaolinite filtration over a range of pH from 4.1 - 9.6 and ionic strength from 0.1 - 50 mM. Column experiments were conducted on glass beads at a pH of 7 and ionic strength of 5 mM. In general, filtration coefficients determined from column experiment results can be used as inputs in the colloid exchange models applied to experimental results. However, for the present flume experiments, the filtration coefficients were always sufficiently high so that complete trapping could be assumed.

Previous models (by Elliott) for solute exchange from a stream to a sand bed were extended, and new models were developed for colloid exchange. All models calculate the exchange due to the mechanisms of pumping and turnover, but differ in their assumptions of the relative importance of these mechanisms. Models were developed to predict solute and colloid transport to finite-depth beds with stationary bedforms, and to beds of any depth with fast-moving bedforms. A catalog of the exchange models, including those developed previously by other researchers at Caltech, is presented in Table 7.1.

Table 7.1: Catalog of models for the exchange of solutes and colloids between a stream and stream bed. See the notation section of the introduction for definition of symbols.

Model Name	Source	Hydraulic Conditions	Tracer(s)	Required Inputs
infinite bed pumping	Elliott (1990)	deep bed, stationary bedforms	conservative solutes	U, d, d', λ, H, K, θ, u_u
turnover	Elliott (1990)	fast-moving bedforms	conservative solutes	λ, U_b, H, θ, d'
combined	Elliott (1990)	slowly-moving bedforms	conservative solutes	U, d, d', k, H, K, θ, u_u, U_b
pumping with sorption	Eylers (1994)	deep bed, stationary bedforms	reactive solutes with fast sorption	U, d, d', λ, H, K, θ, u_u, R
finite bed pumping	this work	stationary bedforms	conservative solutes	U, d, d', λ, H, K, θ, u_u, d_b
colloid pumping	this work	stationary bedforms	colloids	U, d, d', λ, H, K, θ, u_u, d_b, λ_f, v_s
maxpump	this work	stationary bedforms	tracers that are completely trapped	U, d, d', λ, H, K, θ, d_b, v_s
turnpump	this work	fast-moving bedforms	conservative solutes	U, d, d', λ, H, K, θ, d_b, U_b
turnpump for colloids	this work	fast-moving bedforms	colloids that are completely trapped	U, d, d', λ, H, K, θ, d_b, U_b, v_s

Models for colloid exchange require the input of stream, bed, and particle parameters. The inputs required for each model are also detailed in Table 7.1. The effect

of stream hydraulics is included through the stream and bed geometry, the stream velocity, and the bedform velocity. Colloid transport processes are included through the filtration coefficient and settling velocity. Chemical effects are not modeled explicitly, but are included through the filtration coefficient (and to a lesser extent in the settling velocity). The colloid exchange models can be used to predict the exchange of a conservative tracer by setting the filtration coefficient and settling velocity to zero.

To model a flume experiment, most stream and bed parameters are obtained by direct measurement in the flume, and the remaining parameters are measured in smaller experiments. Of the hydraulic inputs, only the bed porosity and hydraulic conductivity cannot be measured in the flume. These properties of the bed sediment are easily obtained by standard methods. The filtration coefficient is determined by conducting a column experiment with materials, chemical conditions, and pore-water velocity identical to those in the flume. The settling velocity is determined by measurement of the size distribution of the colloidal tracer.

The pumping and turnpump models were quite successful in reproducing experimental results for the cases of nonmoving and fast-moving bedforms, respectively. In addition, the maxpump model (a simplified version of the pumping model which assumes that all colloids that enter the bed are irreversibly trapped) was successful in predicting the exchange due to nonmoving bedforms because colloid filtration and settling were very high in all flume experiments. The results of experiments with slow-moving bedforms could not be modeled well, but always fell between the pumping and turnpump model predictions. The results of experiments with very-slowly-moving

bedforms were predicted reasonably well by the pumping model. All inputs for these models were measured parameters, and no fitting of any sort was used.

Some deviation of model predictions from experimental results was observed, but this was almost always within 10%. This level of discrepancy between model predictions and experimental results is expected due to the difficulty in collecting data and estimating average values to use as model inputs. In particular, the following quantities were identified as important sources of error: the average instantaneous tracer concentration in the stream water, the average particle settling velocity, and the average bedform height, wavelength, and velocity.

Additional model simulations were run in order to investigate the effect of major variables on exchange of the solutes and colloids. These simulations covered a wider range of conditions than were investigated in flume experiments. For example, simulations were run for the entire range of filtration and settling behavior, while the flume experiments always had very high filtration and settling. These simulations provide an easy method to determine the most important variables which control exchange and the sensitivity of the models to changes in those parameters..

The models developed in this work should be directly applicable to natural streams. Stream and bed parameters can be measured in the field to determine the hydraulic exchange with the bed. Particle parameters can be determined outside of the stream by the same methods used for flume experiments. It is especially important that the use of the filtration coefficient to summarize chemical interactions allows complex natural materials to easily be included in the exchange models. However, the models

developed in this work specifically predict the bedform-induced exchange with the stream bed, and additional stream processes will have to be considered in order to determine the total exchange between the stream and hyporheic zone.

7.2 Conclusions about experimental techniques

1. This work demonstrated that the transport of a reactive tracer such as kaolinite can be studied in a recirculating flume provided that the water, sand, and tracer are all prepared so that all relevant chemical parameters are well-defined. In designing these experiments, it is important to determine the appropriate level of control of chemical variables in order to avoid either spending excessive effort on unnecessary preparation or obtaining meaningless data.

2. Smaller-scale experiments such as column experiments can be used in conjunction with flume experiments to quantify chemical interactions that are not directly measurable in the flume. In this work, results of column experiments were included in a model which predicted exchange in the flume. Use of supporting small-scale chemistry experiments can be a powerful tool to interpret the behavior of reactive substances in systems with complex hydrodynamics.

7.3 Conclusions about experimental results

1. Flume experiments demonstrated that sand beds can trap large amounts of clay. In runs with stationary bedforms, all clay was usually removed from the stream by the end of the experiment (24-48 hours). Bedform motion caused clay to be trapped less rapidly. However, in all cases more than 50% of the clay added to the stream was trapped by the

bed. Where some clay remained in the stream water at the end of the experiment, the system was not in equilibrium and trapping still continued at a low rate. These results indicate that all clay would have been trapped by the bed if the experiment were continued for a sufficiently long period of time.

2. Trapping of clay by the stream bed is the result of two irreversible mechanisms: filtration of clay by the bed sediment and settling of clay to the deepest part of the bed. Column experiments indicated that filtration of kaolinite by sand was always very high in this system ($\lambda_f = 0.2$ to 0.6 cm^{-1}). In addition, the settling velocity of the kaolinite particles was on the same order of magnitude as the maximum pore water velocity (generally between 0.1 and 0.5 cm/min).

7.4 Conclusions about models of exchange between the stream and stream bed

1. The models described in Table 7.1 were developed to predict the exchange of solutes and colloids between the stream and stream bed based on measured hydraulic and chemical parameters. These models were quite successful in reproducing experimental results without resorting to the use of any fitting parameters.

2. These models include the exchange mechanisms of pumping, an advective flow in the bed resulting from the bedform-induced pressure variation at the bed surface, and turnover, the trapping and release of pore water due to bedform motion.

3. The behavior of colloids was parameterized in the models by the filtration coefficient and particle settling velocity. These parameters include the effects of surface and solution chemistry. The use of these parameters to summarize complex physicochemical phenomena allows application of the model to situations where the interaction behavior is not understood in detail.

4. Since the models presented here include the fundamental hydraulics of exchange due to bedforms, they can be applied to an arbitrary tracer by including additional terms to account for processes unique to that tracer. The models for colloid exchange were identical to those for solute exchange except for the functions which calculate the effect of filtration and settling. Conversely, the exchange of a conservative solute could be modeled as a limiting case of colloid exchange, i.e., where the "particles" have no filtration or settling.

7.5 Conclusions about the modeling of experimental results

1. The finite-bed pumping model successfully reproduced experimental data for the exchange of a conservative solute with a finite bed due to stationary bedforms. In this case, the finite bed depth reduces exchange by compressing pumping streamlines and imposing a finite dilution.

2. The turnpump model successfully predicted exchange of a conservative solute due to fast-moving bedforms. In this case, turnover dominates the exchange to the upper part of the bed, and the net exchange at early times. Pumping is the only process that causes exchange with the deeper bed, and dominates exchange at long times. Turnover tends to reduce the net exchange by causing a periodic unsteadiness in the pressure distribution at the surface of the bed which hinders advective pumping to the deep regions of the bed.

3. The colloid pumping model successfully predicted colloid exchange due to nonmoving bedforms. High filtration coefficients allowed use of the simplified maxpump model which assumed that pumping would result in complete trapping by the stationary portions of the bed. In this case, colloid exchange was modeled simply by summing the flux into the bed.

4. The turnpump model for colloids successfully predicted colloid exchange due to fast-moving bedforms. This model assumes that all colloids pumped from the turnover region to deeper portions of the bed are permanently trapped. Colloid exchange was modeled by calculating turnover in the upper portion of the bed and adding the exchange due to the flux to the deeper bed. No model was developed to predict colloid exchange due to fast-moving bedforms when trapping in the lower bed is incomplete.

5. The models could not successfully predict solute or colloid exchange for the case of slowly-moving bedforms. In this regime, the distribution of tracer in the upper portion of

the bed is very complex because pumping and turnover have competing effects of the same magnitude. However, the pumping model (for nonmoving bedforms) and turnpump model (for fast-moving bedforms) can be used to bound the exchange in the case of slowly-moving bedforms. Experimental results for slowly-moving bedforms always fell between these model predictions. Experimental results for very-slowly-moving bedforms fell very close to the predictions of the pumping model, indicating that turnover can be ignored if it is extremely slow.

7.6 Conclusions about the effect of specific parameters on colloid exchange

1. The rate of colloid exchange is fundamentally controlled by the hydraulics of pumping exchange. The basic rate of exchange between the stream and stream bed is controlled by the stream depth and velocity, bedform size and velocity, and the hydraulic properties of the bed sediment.

2. Filtration and settling cause colloids to behave much differently than conservative solutes. These mechanisms both result in irreversible trapping by the deep bed, which causes colloids to be removed from the stream much more rapidly and completely than conservative tracers. Once filtration becomes sufficiently high that nearly complete trapping occurs over the course of a pumping pathline ($\lambda_f^* > 1$), the magnitude of the filtration coefficient is no longer an important variable. On the other hand, the magnitude

of settling is always important because the settling velocity influences the downward flux of particles.

3. Bedform motion also has a major impact on colloid exchange. Motion of bed grains and rapid release of pore water prevents colloids from being irreversibly trapped in the turnover region. Thus, bedform motion results in the formation of a separation layer between the stream and the deeper bed region where irreversible trapping occurs, and a decrease in the overall rate of trapping. In experiments with nonmoving bedforms, complete removal of clay from the stream was almost always observed within 24 hours. In experiments with moving bedforms, 50-80% of the clay added to the stream was typically removed after 24 hours, and 20-50% remained in the stream. Faster bedform velocities resulted in slower trapping.

8. APPENDICES

8.1 Variation of residence time function with λ_f, v_s

The residence time function, R(t), represents the fraction of the tracer that entered the bed that still remains there at time (t). Figures 8.1 and 8.2 show the variation in R(t) due to changes in filtration (λ_f) and settling (v_s). These curves were generated in a subroutine of the colloid pumping model computer program (i.e. they were actually used to generate model predictions).

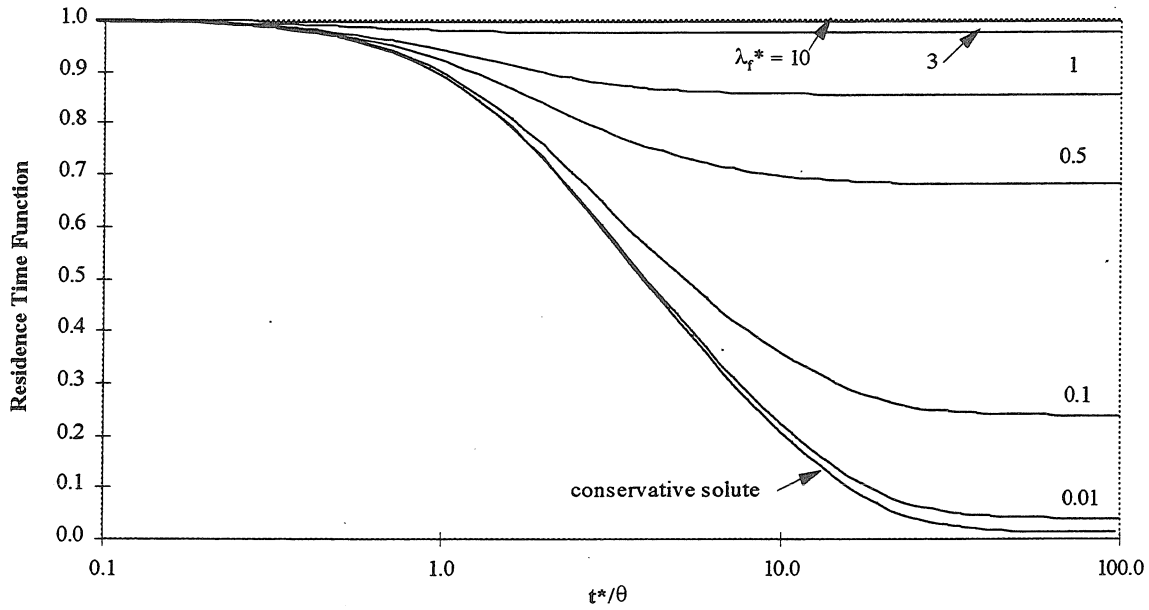

Figure 8.1: Variation of residence time function of colloids with filtration coefficient, for exchange to a finite bed with $d_b/\lambda = 0.3$.

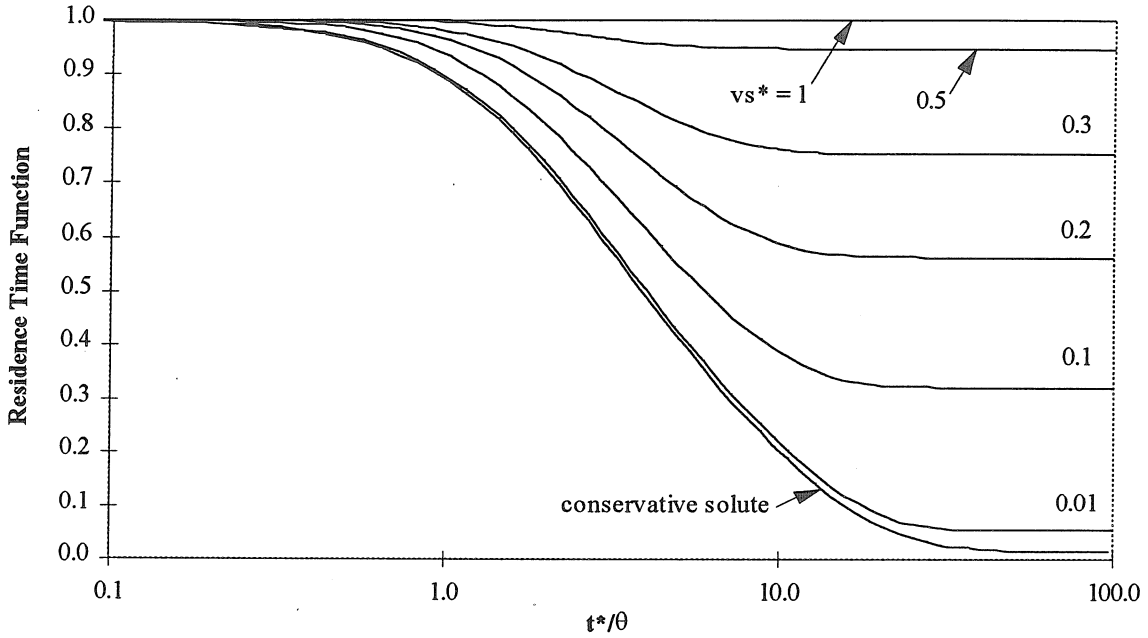

Figure 8.2: Variation of residence time function of colloids with particle settling velocity, for exchange to a finite bed with $d_b/\lambda = 0.3$.

The shape of the residence time function reflects the flow of tracer through the bed and any processes that trap tracer in the bed. At early times, R = 1 because tracer that entered the bed has not had time to leave. The decrease in R occurs because tracer is carried through and then out of the bed by the advective pore water flow. The shape of R(t) for conservative solutes is determined entirely by the advective flow pattern in the bed. For conservative solutes, $R \rightarrow 0$ as $t \rightarrow \infty$, indicating that no tracer is permanently retained in the bed.

Both filtration and settling cause the residence time function for colloids to be higher than the curve for conservative solutes. The residence time function asymptotes to

some non-zero value at $t = \infty$ when filtration or settling is included. The value of R at $t = \infty$ is the fraction of tracer that has been permanently trapped by the bed.

The mechanism of trapping is different for filtration and settling. Filtration causes some of the colloids which entered the bed to become attached to stationary bed sediment grains. Thus, in Figure 8.1, the value of R at $t = \infty$ is the average fraction of colloids that have become filtered over all flow paths (or, the filtration over the average path length). On the other hand, settling causes particle paths to differ from the pore water streamlines, so that particles that enter through certain regions of the bed surface will be carried deep into the bed and never advected out. In Figure 8.2, the value of R at $t = \infty$ is the fraction of particles that are irreversibly settled to deep regions of the bed.

Complete trapping by the bed occurs when $R = 1$ for all times. High filtration coefficients cause complete trapping by causing all colloids which enter the bed to be attached to the bed sediment. However, since filtration is an exponential-decay process, filtration only asymptotically approaches complete trapping at $\lambda_f^* \rightarrow \infty$. In practice, $\lambda_f^* > 1$ is enough to justify use of the complete trapping assumption. High settling velocities cause complete trapping by preventing particles from moving upward in the bed. This can also be thought of in terms of forces: complete trapping will occur when the downward gravitational force on the particles is greater than the forces induced by pore water flow. Since the settling velocity is made dimensionless with the maximum seepage velocity of the pore water ($v_s^* = \theta v_s / u_m$), complete trapping occurs for $v_s^* \geq 1$.

8.2 Comparison of bedform parameter estimation methods

For most experiments, visual and point gauge measurements were used to measure bedform parameters. For the last two experiments, a laser position measuring device was used to obtain a profile of the bed surface elevation on a line down the flume. The details of both methods are described in Section 4.1.3.1. The estimations for average bedform parameters from each of these methods agree well, but the laser profiler gives additional data on smaller-scale variations in the bed surface.

Figure 8.3 shows laser profiler results and visually-identified crest positions from experiment #17. The crest positions from the visual method agree well with the major peaks from the laser profiler. Some discrepancies are expected because the visual observation identified the average crest position, while the laser provides a profile on a line down the flume. Thus, deviation of the crest position from the laser-derived peak can occur when the bedform has a three-dimensional shape and the crest is not exactly perpendicular to the flume walls. Height measurements for individual bedforms were not compared, but the laser results in Figure 8.3 can be seen to agree reasonably well with the average bedform height from point gauge measurements: 1.4 cm.

Laser profiler data provide a lot of information that was not obtained in visual measurements. While visual observations identified every major peak in the laser profile, they failed to capture the additional detail of the surface between peaks. For the experiments on bed exchange, the simpler method was sufficient because the major bed features (dunes) will drive exchange. However, for other applications, the ability to resolve smaller-scale features (ripples) and actual bedform shapes makes the laser profiler

an excellent choice for data acquisition. The profiler can also be used to get three-dimensional profiles of the bed surface by simply making multiple passes down the flume on parallel lines across the channel.

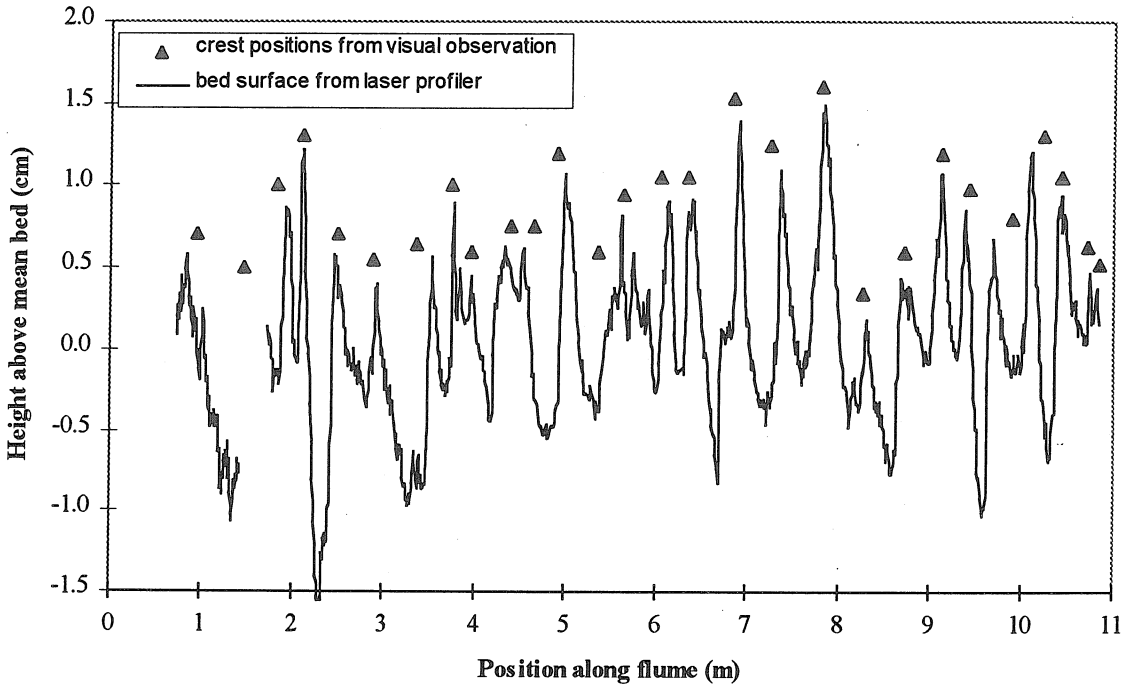

Figure 8.3: Comparison of laser profiler results for variations in the bed surface with visual observations of the position of bedform crests from experiment #17. The visual data are for the downstream position of the crest only, not the bedform height.

References

Avanzino, R.J., Zellweger, G.W., Kennedy, V.C., Zand, S.M., and Bencala, K.E., 1984, *Results of a Solute Transport Experiment at Uvas Creek, September 1972,* U.S. Geological Survey Open-File Report 84-236

Bencala, K.E., 1983, "Simulation of solute transport in a mountain pool-and-riffle stream with a kinetic mass transfer model for sorption," *Water Resources Research*, 19(3), 732-738

Bencala, K.E., 1984, "Interactions of solutes and streambed sediment 2., A dynamic analysis of coupled hydrologic and chemical processes that determine solute transport," *Water Resources Research*, 20(12), 1804-1814

Bencala, K.E., Duff, J.H., Harvey, J.W., Jackman, A.P., and Triska, F.J., 1993, "Modeling within the stream-catchment continuum," *Modeling Change in Environmental Systems,* A.J., Jakeman, M.B., Beck and M.J., McAleer, Eds., John Wiley & Sons, Ltd, New York, 163-187

Bencala, K.E., Jackman, A.P., Kennedy, V.C., Avanzino, R.J., and Zellweger, G.W., 1983, "Kinetic analysis of strontium and potassium sorption onto sands and gravels in a natural channel," *Water Resources Research*, 19(3), 725-731

Bencala, K.E., Kennedy, V.C., Zellweger, G.W., Jackman, A.P., and Avanzino, R.J., 1984, "Interactions of solutes and streambed sediment 1., An experimental analysis of cation and anion transport in a mountain stream," *Water Resources Research*, 20(12), 1797-1803

Bencala, K.E., McKnight, D.M., and Zellweger, G.W., 1990, "Characterization of transport in an acidic and metal-rich mountain stream based on a lithium tracer injection and simulations of transient storage," *Water Resources Research*, 26(5), 989-1000

Bencala, K.E., and Walters, R.A., 1983, "Simulation of solute transport in a mountain pool-and-riffle stream: a transient storage model," *Water Resources Research*, 19(3), 718-724

Brady, P.V., Cygan, R.T., and Nagy, K.L., 1996, "Molecular controls on kaolinite surface charge," *Journal of Colloid and Interface Science*, 183 (Article No. 0557), 356-364

Broshears, R.E., Runkel, R.L., Kimball, B.A., McKnight, D.M., and Bencala, K.E., 1996, "Reactive solute transport in an acidic stream: experimental pH increase and simulation of controls on pH, aluminum, and iron," *Environmental Science and Technology*, 30, 3016-3024

Castro, N.M., and Hornberger, G.M., 1991, "Surface-subsurface water interactions in an alluviated mountain stream channel," *Water Resources Research*, 27(7), 1613-1621

Cushing, C.E., Minshall, G.W., and Newbold, J.D., 1993, "Transport dynamics of fine particulate organic matter in two Idaho streams," *Limnology and Oceanography*, 38(6), 1101-1115

Einstein, H.A., 1968, "Deposition of suspended particles in a gravel bed," *Journal of the Hydraulics Division, Proceedings of the American Society of Civil Engineers* (94), 1197-1205

Elimelech, M., Gregory, J., Jia, X., and Williams, R.A., 1995, *Particle Deposition and Aggregation: Measurement, Modeling, and Simulation,* Butterworth-Heinemann Ltd, Oxford

Elliott, A.H., 1990, *Transfer of Solutes into and out of Streambeds*, Ph.D. Thesis, Caltech (available as report KH-R-52, W.M. Keck Laboratory of Hydraulics and Water Resources, Mail Code 138-78, Caltech, Pasadena, 91125)

Elliott, A.H., and Brooks, N.H., 1997, "Transfer of nonsorbing solutes to a streambed with bed forms: Laboratory experiments," *Water Resources Research*, 33(1), 137-151

Elliott, A.H., and Brooks, N.H., 1997, "Transfer of nonsorbing solutes to a streambed with bed forms: Theory," *Water Resources Research*, 33(1), 123-136

Eylers, H., 1994, *Transport of Adsorbing Metal Ions between Stream Water and Sediment Bed in a Laboratory Flume*, Ph.D. Thesis, Caltech (available as report KH-R-56, W.M. Keck Laboratory of Hydraulics and Water Resources, Mail Code 138-78, Caltech, Pasadena, 91125)

Eylers, H., Brooks, N.H., and Morgan, J.J, 1995, "Transport of adsorbing metals from stream water to a stationary sand-bed in a laboratory flume," *Marine and Freshwater Research*, 46, 209-214

Happel, J., 1958, "Viscous flow in multiparticle systems: slow motion of fluids relative to beds of spherical particles," *AIChE Journal*, 4, 197-201

Harvey, J.W., and Bencala, K.E., 1993, "The effect of streambed topography on surface-subsurface water exchange in mountain catchments," *Water Resources Research*, 29(1), 89-98

Harvey, J.W., Wagner, B.J., and Bencala, K.E., 1996, "Evaluating the reliability of the stream tracer approach to characterize stream-subsurface water exchange," *Water Resources Research*, 32(8), 2441-2451

Herrington, T.M., Clarke, A.Q., and Watts, J.C., 1992, "The surface charge of kaolin," *Colloids and Surfaces*, 68, 161-169

Huettel, M., Ziebis, W., and Forster, S., 1996, "Flow-induced uptake of particulate matter in permeable sediments," *Limnology and Oceanography*, 41(2), 309-322

Hunt, J.R., 1980, *Coagulation in Continuous Particle Size Distributions, Theory and Experimental Verification*, Ph.D. Thesis, Caltech

Hunter, R.J., and Alexander, A.E., 1963a, "Surface properties and flow behavior of kaolinite, part II: electrophoretic studies of anion adsorption," *Journal of Colloid Science*, 18, 833-845

Hunter, R.J., and Alexander, A.E., 1963b, "Surface properties and flow behavior of kaolinite, Part I: electrophoretic mobility and stability of kaolinite sols," *Journal of Colloid Science*, 18, 820-832

Hunter, R.J., and Alexander, A.E., 1963c, "Surface properties and flow behavior of kaolinite, part III: flow of kaolinite sols through a silica column," *Journal of Colloid Science*, 18, 846-862

Hunter, R.J., and James, M., 1992, "Charge reversal of kaolinite by hydrolyzable metal ions: an electroacoustic study," *Clays and Clay Minerals*, 6, 644-649

Ives, K.J., 1987, "Filtration of clay suspensions through sand," *Clay Minerals*, 22, 49-61

Jepson, W.B., and Rowse, J.B., 1975, "The composition of kaolinite--an electron microscope microprobe study," *Clays and Clay Mineralogy*, 23, 310-317

Jobson, H.E., and Carey, W.P., 1989, "Interaction of fine sediment with alluvial streambeds," *Water Resources Research*, 25(1), 135-140

Litton, G.M., and Olson, T.M., 1993, "Colloid deposition rates on silica bed media and artifacts related to collector surface preparation methods," *Environmental Science & Technology*, 27(1), 185-193

McDowell-Boyer, L.M., Hunt, J.R., and Sitar, N., 1986, "Particle transport through porous media," *Water Resources Research*, 22(13), 1901-1921

McKnight, D.M., and Bencala, K.E., 1990, "The chemistry of iron, aluminum, and dissolved organic material in three acidic, metal-enriched, mountain streams, as controlled by watershed and in-stream processes," *Water Resources Research*, 26(12), 3087-3100

Mau, R.E., 1992, *Particle Transport in Flow through Porous Media: Advection, Longitudinal Dispersion, and Filtration,* Ph.D. Thesis, Caltech

Melton, I.E., and Rand, B., 1977a, "Particle interactions in aqueous kaolinite suspensions, II., comparison of some laboratory and commercial kaolinite samples," *Journal of Colloid and Interface Science*, 60(2), 321-330

Melton, I.E., and Rand, B., 1977b, "Particle interactions in aqueous kaolinite suspensions, III., Sedimentation Volumes," *Journal of Colloid and Interface Science*, 60(2), 331-336

Newman, A.C.D., ed., 1987, *Chemistry of Clays and Clay Minerals*, Longman, Essex

Newman, A.C.D., and Brown, G., 1997, "The Chemical Constitution of Clays," *Chemistry of Clays and Clay Minerals.*, A.C.D., Newman, Ed., John Wiley & Sons, Inc., New York, 1-128

Noelte, J.L., and Morgan, J.J., 1995, unpublished data, abstract "The effects of surface chemistry on colloid deposition rates in flow through porous media," *Abstracts of the division of Environmental Chemistry, American Chemical Society*, Anaheim, California, April 2-7, 1995, 484-487

O'Melia, C.R., 1987, "Particle-Particle Interactions," *Aquatic Surface Chemistry*, W., Stumm, Ed., Wiley-Interscience, 386-403

O'Melia, C.R., 1989, "Particle-particle interactions in aquatic systems," *Colloids and Surfaces*, 39, 255-271

Rajagopalan, R., and Tien, C., 1976, "Trajectory analysis of deep bed filtration with the sphere-in-cell porous media model," *AIChE Journal*, 22, 523-533

Rand, B., and Melton, I.E., 1977, "Particle interactions in aqueous kaolinite suspensions, I., Effect of pH and electrolyte upon the mode of particle interaction in homoionic sodium kaolinite suspensions," *Journal of Colloid and Interface Science*, 60(2), 308-320

Raudkivi, A.J., 1990, *Loose Boundary Hydaulics*, 3rd edition, Pergamon Press, New York

Reible, D.D., and Savant-Malhiet, S.A., 1993, "Comparison of physical transport processes in noncohesive river sediments," *Journal of Environmental Engineering*, 119 (1), 90-103

Runkel, R.L., Bencala, K.E., and Broshears, R.E., 1996, "Reactive solute transport in streams 1., Development of an equilibrium-based model," *Water Resources Research*, 32 (2), 409-418

Runkel, R.L., McKnight, D.M., and Bencala, K.E., 1996, "Reactive solute transport in streams 2., Simulation of a pH modification experiment," *Water Resources Research*, 32 (2), 419-430

Ryan, J.N., and Elimelech, M., 1996, "Colloid mobilization and transport in groundwater," *Colloids and Surfaces A: Physicochemical and Engineering Aspects*, 107, 1-56

Savant, S.A., Reible, D.D., and Thibodeax, L.J., 1987, "Convective transport within stable river sediments," *Water Resources Research*, 23(9), 1763-1768

Shen, H.W., Fehlman, H.M., and Mendoza, C., 1990, "Bed form resistances in open channel flows," *Journal of Hydraulic Engineering*, 116(6), 799-815

Shimizu, Y., Tsujimoto, T., and Nakagawa, H., 1990, "Experiment and macroscopic modeling of flow in highly permeable porous medium under free-surface flow," *Journal of Hydrosciences and Hydrological Engineering*, 8, 69-78

Sojitra, I., Valsaraj, K.T., Reible, D.D., and Thibodeax, L.J., 1995, "Transport of hydrophobic organics by colloids through porous media 1. Experimental results," *Colloids and Surfaces A*, 94, 197-211

Stumm, W., 1992, *Chemistry of the Solid-Water Interface*, Wiley-Interscience

Stumm, W., and Morgan, J.J., 1996, *Aquatic Chemistry*, 3rd Edition, Wiley-Interscience

Thibodeax, L.J., and Boyle, J.D., 1987, "Bedform-generated convective transport in bottom sediment," *Nature*, 325(22), 341-343

Tien, C., 1989, *Granular Filtration of Aerosols and Hydrosols*, Butterworths,

Tobiason, J.E., 1989, "Chemical effects on the deposition of non-Brownian particles," *Colloids and Surfaces*, 39, 53-77

Tobiason, J.E., and O'Melia, C.R., 1988, "Physicochemical aspects of particle removal in depth filtration," *American Water Works Association, Journal*, 80, 54-64

Valsaraj, K.T., Verma, S., Sojitra, I., Reible, D.D., and Thibodeax, L.J., 1996, "Diffusive transport of organic colloids from sediment beds," *Journal of Environmental Engineering*, 122(8), 722-727

van Olphen, H., 1977, *An Introduction to Clay Colloid Chemistry*, 3rd Edition, Wiley-Interscience

van Olphen, H., 1987, "Dispersion and Flocculation," *Chemistry of Clays and Clay Minerals.*, Newman, A.C.D., Ed., John Wiley and Sons, Inc., New York, 203-224

Vanoni, V.A., ed., 1975, *Sedimentation Engineering*, ASCE, New York

Vittal, N., Ranga Raju, K.G., and Garde, R.J., 1977, "Resistance of two-dimensional triangular roughness," *Journal of Hydraulic Research*, 15(1), 19-36

Yoshimura, Y., 1980, *Initial particle collection mechanism in clean deep bed filtration*, D. Eng. Thesis, Kyoto University

Zellweger, G.W, et al., 1986, "Data on the solute concentrations within the subsurface flows of Little Lost Man Creek in response to a transport experiment, Redwood National Park, Northwest California," *U.S. Geological Survey Open File Report 86-403W*

Zhou, D., and Mendoza, C., 1995, "Pollutant transport beneath porous stream beds," American Society of Civil Engineers, *Proceedings of the First International Conference on Water Resources Engineering*, 219-223